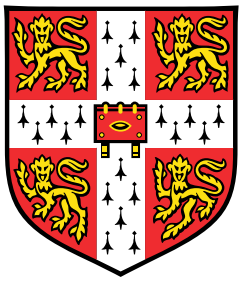

Oncogene-induced remodelling of cellular networks

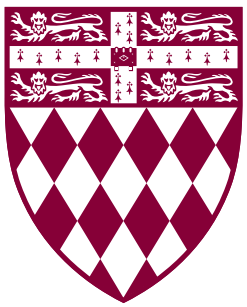

Pablo Oriol Valls

Supervisor: Dr. A. Esposito
Prof. A. Venkitaraman

MRC Cancer Unit
University of Cambridge

This dissertation is submitted for the degree of
Doctor of Philosophy

Fitzwilliam College

March 2021

I would like to dedicate this thesis to: María, Andrea, Mamá y Papá

Declaration

This thesis is the result of my own work and includes nothing which is the outcome of work done in collaboration except as declared in the Preface and specified in the text. I further state that no substantial part of my thesis has already been submitted, or, is being concurrently submitted for any such degree, diploma or other qualification at the University of Cambridge or any other University or similar institution except as declared in the Preface and specified in the text. It does not exceed the prescribed word limit for the relevant Degree Committee.

Pablo Oriol Valls
March 2021

Oncogene-induced remodelling of cellular networks

Pablo Oriol Valls

Abstract

Biochemical networks maintain cellular homeostasis by processing information from the intra- and extra-cellular environments and coordinating appropriate responses to stimuli and stressors. During carcinogenesis, cells accrue genetic alterations that rewire signalling pathways, eventually leading to the partial loss of homeostatic control and cancer- related phenotypes. Cancer is a very heterogeneous disease with genetic alterations that exhibit vast variability within a tumour, between tumours of different tissues, and patients. Despite the enormous advances the community has achieved in understanding the molecular causes of cancer, the mechanisms of pathogenicity of specific mutations are often unclear, severely limiting the efficacy of the therapeutic intervention and disease management. Moreover, we are recognizing that *driver* mutations once considered sufficient to induce initiation and promotion of cancer are more frequent than originally expected also in healthy tissues. In addition to genetic variability, cell-to-cell variability of non-genetic origin is increasingly recognized – yet poorly understood – as a fundamental force fuelling carcinogenesis and resistance to therapies. We therefore develop biochemical imaging techniques to investigate aspects of cancer heterogeneity that are currently challenging – if not impossible – to study.

KRAS is a *driver* gene significantly involved in lung, colorectal and pancreatic carcinogenesis. Various types of KRAS mutations respond differently to therapy, and some have been linked to the emergence of resistance. However, the mutation-specific mechanisms leading to these phenotypes is not well understood. We used KRAS as a clinically relevant model to study the effects of mutations at codon G12 on signalling dynamics and phenotypic changes, including cell-to-cell variability.

In this thesis, first I introduce the concepts of evolution-driven oncogenesis, genetic and non-genetic heterogeneity and signal transduction pathways. In Chapter 2, I describe the characterisation of *KRAS* mutation-specific MAPK signalling. To do this, I generated an isogenic panel of cells stably expressing a FRET sensor and developed an experimental pipeline including automated biochemical imaging, microfluidic-based stimulation, and custom image analysis. Using these tools, I have identified differential signalling dynamics and heterogeneity in response to epidermal growth factor (EGF). Taken together with other results, we hypothesise the presence of a weakened negative feedback loop in cells with a G12D mutation in *KRAS*. In Chapter 3, I report on methodological developments aimed at drastically improving our capability to characterise biochemical networks in single living cells. I have optimized novel pairs of fluorescent proteins dedicated to biochemical multiplexing and capable of simultaneously monitoring three biochemical reactions. Moreover, I developed an expandable software pipeline that yields single-cell ERK signalling data and several types of analyses from microscopy FRET imaging. Finally, I further develop optogenetic systems designed to dynamically and optically activate KRAS in single cells.

In conclusion, I show the effects of *KRAS* mutations on signalling dynamics and cell-to-cell variability, a first step towards a deeper understanding of how genetic and non-genetic heterogeneity may cooperate to make of cancer the terrible disease we know. At the same time, I have improved methodologies designed for the novel study of biochemical networks, laying down the foundations of system-level investigation in single living cells.

Acknowledgements

First and foremost I would like to thank Dr. Alessandro Esposito for his stellar mentorship. He has provided me with the best support and advice available at all stages of my PhD, and is a continual source of inspiration. I am highly grateful of his unwavering leadership from which I benefited and learned from. I would also like to thank all members of the Esposito group, past or present, as they have also shaped me as a scientist and provided – both scientific and social – support.

I would like to acknowledge Prof. Ashok Venkitaraman for supporting me in his laboratory and co-supervising my thesis. I will always fondly appreciate his omnipresent and inspiring enthusiasm, his sense of humour and ~~hard~~ smart work ethic. Thank you to all members of the Venkitaraman laboratory for creating a friendly and supportive atmosphere.

I would also like to thank all my friends in Cambridge for being part of my PhD journey and making it a very enriching experience. I would like to acknowldege Fitzwilliam College for their dedication to students, as shown by the many events and sports societes it funds but also by accommodation flexibility.

Last but not least, I would like to thank my parents for their continued support over all years since my very inception. I am infinitely grateful to have them and my sisters as my family – without whom I wouldn't stand where I am today. Gracias familia!

Table of contents

List of figures

List of tables

Acronyms

B/C/G/Y/R FP Blue/Cyan/Green/Yellow/Red Fluorescent Protein

CRC Colorectal Cancer

DDR DNA Damage Repair

DNA Deoxyribonucleic Acid

EGF Epidermal Growth Factor

EGFR Epidermal Growth Factor Receptor

ERK Extracellular signal-Regulated Kinase

ERKi ERK inhibitor/inhibition

FLIM Fluorescence Lifetime Imaging Microscopy

FLT Fluorescence Lifetime

FOV Field Of View

FRET Förster Resonance Energy Transfer

GAP GTPase Activating Protein

GDP Guanosine Diphosphate

GEF Guanine nucleotide Exchange Factor

GRN Gene Regulatory Network

GTP Guanosine-5'-Triphosphate

GUI Graphical User Interface

HPNE Human Pancreatic Nestin-Expressing

HR Homologous Recombination

HVR Hyper Variable Region

hTERT human Telomerase Reverse Transcriptase

ITH Intra-Tumour Heterogeneity

MAPK Mitogen Activated Protein Kinase

NGF Neuronal Growth Factor

NHEJ Non Homologous End-Joining

NLS Nuclear Localisation Signal

OS Overall Survival

PCB Phycocyanobilin

PCR Polymerase Chain Reaction

PFS Progression Free Survival

PI3K Phosphoinositide 3-kinase

PTM Post Translational Modification

RBD Ras Binding Domain

ROS Reactive Oxygen Species

RTK Receptor Tyrosine Kinase

seFRET sensitised emission FRET

SOS Son of Sevenless

STN Signal Transduction Network

TCI Time Course Inspector

UT Untreated

UV Ultra Violet

Chapter 1

General Introduction Heterogeneity & Cell Signalling

To our knowledge, cancer has been a disease that has afflicted the human species for a significant period of time, given that the first descriptions of the disease date back from the egyptian civilisation (Faguet, 2015). It is only in the last century that we have invested a copious amount of work into understanding this disease. Such investment has allowed us to not only define its pathological features, but also grasp, for the first time in History, the fundamental origin of cancer. Tumorigenesis is intricately and directly linked to genetic aberrations (Vogelstein et al., 2013). To this date however, due to the high-order complexity of such disease, we still struggle to manage - let alone cure - most tumours. Genetic information is carried by each of the 30 trillion cells (Sender et al., 2016) that make up the human organism. Thus, the physical outgrowth of tissue that we come to know as cancer is, in fact, a disease of homeostatis. In addition to metastasis and drug resistance, another major challenge we face today is understanding tumourigenesis at its earliest steps.

At the micro-scale world, just as in the perceived world, genetics – although important – are not the only factor contributing to life. How early genetic aberrations affect cellular function has been thoroughly studied. Although single-cell research approaches are not recent (Novick and Weiner, 1957), it is only in the last decade that major efforts have been directed towards understanding cellular function and gene regulation at the single cell level. Contextual single-cell approaches (i.e. the question on how cell-to-cell interactions affect cellular function) as well as the inherent and natural variability existing in biological systems are fields that have been studied rather separately in cancer research. Through the coupling of these aspects we expect to gain a thorough understanding that

will place us in a significantly better position to describe in detail the earlier stages of tumourigenesis.

1.1 Evolution: Driver of Oncogenesis & Tumour Progression

Early Concepts

Two centuries ago, Jean-Baptiste Lamarck proposed a first theory of evolution of the species that emphasised the environmental influence on species' development (Lamarck, 1802, 1809). Lamarck argued that the use and disuse of body parts would result in their enhancement or disappearance over time (Lamarck 1809). Half a century later, Charles Darwin proposed the theory of evolution by natural selection arguing that natural selection favours physical or behavorial changes across generations through inheritance of characteristics that make individuals fitter in a given environment (Darwin and Kebler, 1859; Wallace, 1867). Natural selection is nowadays the established model for the evolution of the species but the debate and controversies regarding evolutionary models might still be valuable in cancer evolution. Lamarck implied that evolution is driven by behaviour, Darwin stipulated that nature itself selects traits from a population that exhibits pre-existing variation.

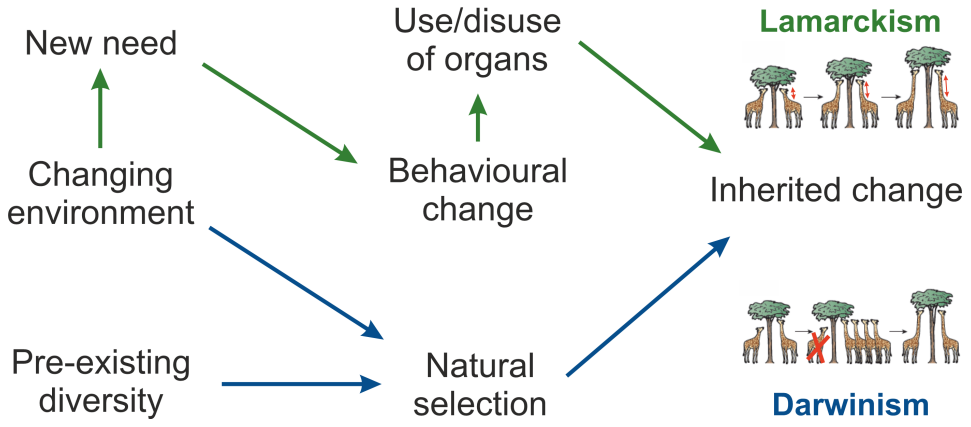

Fig. 1.1 The concept of evolution was outlined by both Charles Darwin and Jean-Baptiste Lamarck in the 19^{th} century. The latter suggested that evolution is species-driven through the use (or disuse) of organs involved in a specific behaviour. Darwin stipulated that both (existing) variation and a changing environment (exerting natural selection on a diverse population) are required for a species to evolve.

Besides the mechanistic explanation of evolution there are certain universal implications - of which not all will be outlined in the interest of sustaining the reader's attention. First, the traits that species develop across generations provide enhanced adaptation to their environment. In other words, evolution fosters characteristics that increase the likelihood for survival. Moreover, access to resources and the presence of predators (other species) threatening a species' safety are important factors (or selection forces in Darwinian terms) affecting its evolution. Not to mention, the rare but possible shock that natural disasters may cause. In absence of these - which are essentially depictions of a changing environment - there would be no reason for biological adaptation - and thus evolution - to occur.

In Cancer

Much like species in the visible world, such concepts have been theorised in the context of oncogenesis (Nagy, 2004; Nowell, 1976) and observed at the cellular level (Reid, 1996). Evolutionary theory of tumour development has been widely accepted and further elaborated (Greaves, 2015; Vogelstein et al., 2013).

The very material that acts as the vehicle for generational transmission of traits (i.e. DNA) can acquire 'defects' or 'faults' – anomalies such as mutations are osberved in tumours. A cell's survival depends on its fitness, which is regulated by mutational burden – caused by cellular population evolution and DNA damage – and subjected to tissue-specific natural selection predispositions (Ostrow et al., 2016). Thus some tumour types are known to display particular genetic anomalies whereas others show very few or different genetic aberrations (Vogelstein et al., 2013). Of important note though, over millennia mammalian cells have developed robust DNA mechanisms (low error-rate replication and damage repair) that minimise somatic (non-heritable) evolution (Ostrow and Hershberg, 2016). Thus each human individual is equally likely to experience similar somatic evolution. Moreover, interactivity between different cell populations is another aspect of tumour development gaining investigational traction due to the likely influence it may have on existing populations (Tabassum and Polyak, 2015).

Thus, tumorigenesis is shaped by the eventual accumulation of fitness-enhancing genetic mutations that are selected for by contextual selection forces.

The Genetic Basis

Tumorigenesis is a phenomenon that arises from an iterative combination of a whole range of complex biological events. The most well known contributor to evolutionary

trajectories of tumour potential are DNA defects. A genetic aberration has the potential to completely disrupt cellular life (Vogelstein and Kinzler, 2004). On most occasions, mutations and other genetic aberrations are events effectively dealt with by cellular DNA damage repair (DDR) mechanisms. These have evolved over millennia to correct the various types of damage DNA can succumb to. To name a few, single nucleotide damage (ROS-induced) is resolved by Base Excision Repair (Wilson and Bohr, 2007), whereas homologous recombination (HR) and non-homologous end-joining (NHEJ) deal with double strand breaks (Sung and Klein, 2006). Repair mechanisms and other DNA processes such as replication are not fail-safe (Rodgers and Mcvey, 2016) and on a span of human lifetime a minuscule error rate is sufficient for cells to acquire mutations (Chatterjee and Walker, 2017) (see (a,b) in Fig. 1.2) - some of which may bypass cellular homeostatic controls and be inherited by progeny. Mutations can be functionally beneficial, neutral or deleterious, altough the latter two are most common. Thus, the appearance of genetic alterations is a crucial first 'ingredient' to develop evolutionary trajectories ultimately leading to cancer.

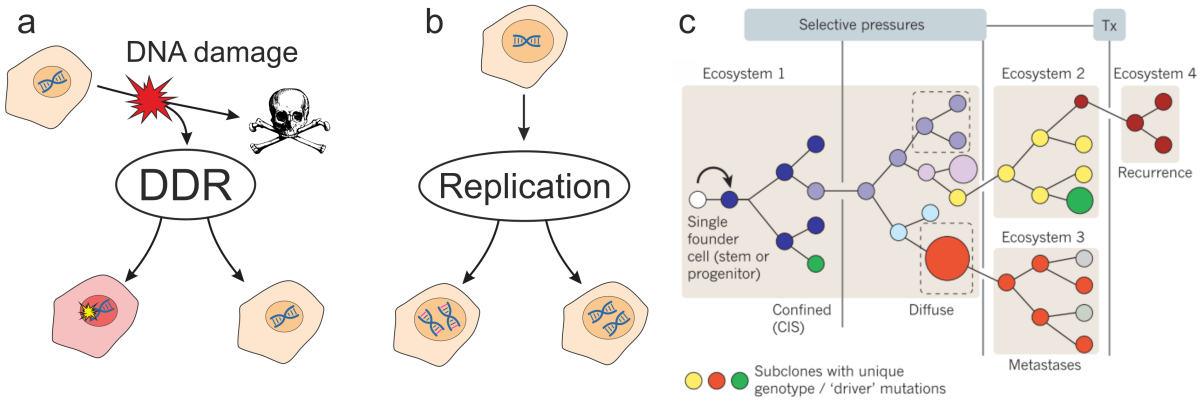

Fig. 1.2 Genetic processes such as DNA damage repair (DDR) mechanisms (a) and even DNA replication (b) can lead to cells acquiring new mutations. Over many iterations, cells become genetically distinct and are thus classified as different subclones (derived from a common clone). Heterogeneous populations with genetically distinct subclones are more likely to survive under the selective pressures of different environments (c, from Greaves and Maley (2012))

Variation

As cells continue to live on and divide, they inevitably and constantly experience events of genetic as well as non-genetic nature. This results in the accumulation of (cell-specific) alterations over time. However, if the cumulative combination of these become

homeostatically deleterious or unbearable, cell death is triggered and said alterations disappear. Importantly, it is reasonable to assume that not one cell is physically identical to another nor does it experience the exact same sequence of environmental events as any other cell. Therefore, every 'daughter' cell that survives lasting changes provides the evolutionary framework to enable tumour-forming cell candidates, each presenting a unique combination of genetic and functional features. This process results in the appearance of clones and over time greatly fosters diversification of clonal populations. This variability is crucial, as without it one's 'luck' (probability of survival) is much diminished in face of environmental changes (see (c) in Fig. 1.2). The lower the number of different 'options' (clones) the lesser the likelihood of any of these being viable and selected for.

1.2 Genetic Mutations Rewire Cells

The appearance of mutations that stand the test of time is what drives opportunistic evolutionary trajectories that may result in oncogenesis. However, a single gene mutation is not sufficient to induce oncogenesis (Knudson, 1971). To this end, we have formulated the concept of cancer onset as the result of the sequential acquisition of a particular number and set of mutations affecting select genes (Fearon and Vogelstein, 1990; Nowell, 1976). Such genes - commonly known as driver genes - have gained particular attention due to 1) their high mutation frequency in tumours and 2) the mutation-induced effect on their respective functional role in cellular homeostasis (see Fig. 1.3). It is important to emphasize that it is fairly common to observe *passenger* mutations that have a 'neutral' effect in highly mutated genes (scenario 1). Yet, there are other mutations at specific gene loci that induce significant protein biochemical changes resulting in a survival advantage (Vogelstein et al., 2013) – driver gene mutations. Driver genes contain such mutations, granting cells a fitness advantage through gain of function means (eg. constantly active *KRAS* or *EGFR*) or inactivation of tumour suppressor genes such as *BRCA2* or *TP53*. The latter was discovered over four decades ago (Lane and Crawford, 1979) and found to be mutated in 42% of cases across 12 different tumour types (Kandoth et al., 2013). *TP53* has an important role in monitoring DNA damage (Maki and Howley, 1997) and regulating cell cycle progression (El-Deiry et al., 1993) and aptoptosis (Toshiyuki and Reed, 1995). Thus, it is evident that driver *TP53* mutations have profound & irreversible molecular effects that corrupt the functional systems maintaining cellular homeostasis.

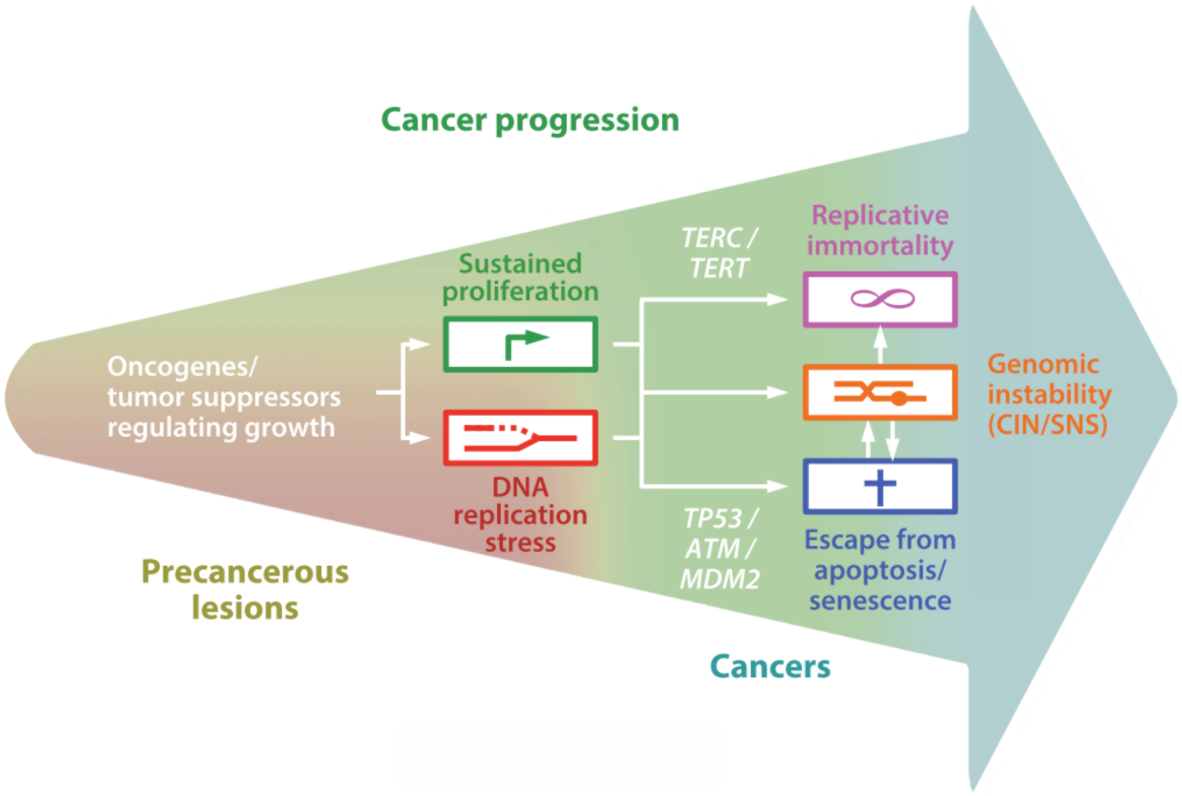

Fig. 1.3 Mutations in driver genes fundamentally change cellular wiring resulting in anomalous and unregulated behaviour. Such genetic change can result in 'fitter' cells owing to their sustained proliferation, for example. Further DNA damage induced by replication (stress) promotes the accumulation of genetic aberrations in pre-malignant cells. Commonly found to be mutated are the *TERT* and *TP53* genes, resulting in replicative immortality and escape from apoptosis, respectively. Figure from Macheret and Halazonetis (2015).

An explanation as to why driver gene mutations are observed in a select number of tumours may be due to their dependency on other *hitchhiker* gene mutations that may not have a direct effect, but are necessary for the driver gene to reach its full oncogenic potential (Maley et al., 2004; Maynard and Haigh, 1974). *Hitchhiker* mutations may be more frequently mutated in certain tissues due to tissue-specific microenvironment which itself may be shaped by tissue function and its required homeostatic activities.

Driver gene mutation-induced *rewiring* is the target of molecular therapies to selectively eradicate cancer cells (Chapman et al., 2011; Cobleigh et al., 1999; Paez et al., 2004). Although these have had resounding success, it is not uncommon to observe a mid-to-low response rate in a cohort of patients with the same cancer type. Often, lack of response to treatment is attributed to the high level of variability among cells of a tumour - a characteristic that has been greatly scrutinized in the last decades with the advent of single-cell assays.

1.3 Diversity – the 'Gift' that Keeps on Giving

In Darwinian evolutionary theory, diversity is a necessity for species to increase their chances of survival via acquisition of new traits. In other words, in the absence of heterogeneity, species threatened by a change in environment or event are much more likely to become extinct, since there would be no other (advantageous) traits to select for.

In the cellular context, the terms *heterogeneity*, *diversity* or *variability* are used to describe the different phenotypes present in a cell population. A phenotype is the combination of observed characteristics of an organism – here a cell – known to derive from its genome and epigenome resulting from its interaction with the surrounding environment. Phenotypic heterogeneity implies the presence of non-genetic variability (such as dissimilar protein levels among cells, for example) or genetic diversity (via genome instability), or – most likely – both (see (c) in Fig. 1.4).

The most basic and obvious observation of variability in cancer is that of the range of tissues in which tumours can arise (see (a) in Fig. 1.4), demonstrating that oncogenesis cannot be attributed to a particular tissue, even though tissue context is involved in the process (Haigis et al., 2019; Schneider et al., 2017). In fact, cancer can either arise locally as a solid mass or develop systemically in liquid form (such as leukemia). Therapy may vary depending on tissue of origin, since accessibility will impact on the possibility of

performing the preferred strategy – surgery – for solid tumours. Thus, this 'first grade' of variability in cancer – form and location – already greatly influences treatment strategies.

The picture is unfortunately much more complex. In addition to the aforementioned, a tumour's aberrant cells can display various kinds and degrees of variability (see (b) in Fig. 1.4), of which genetic heterogeneity has been well documented (Reiter et al., 2019; Vogelstein et al., 2013). Such heterogeneity can be broadly categorised as follows:

- *inter-patient*: among cancer patients with the same tissue of origin
- *inter-tumour*: across (a patient's own) tumour sites (Curtis et al., 2012; Nakamura et al., 2015)
- *intra-tumour* (ITH): within the primary tumour site itself (Gerlinger et al., 2012; Karaayvaz et al., 2018)

Less documented although potentially equally important are the contributions made by the microenvironment (Lloyd et al., 2016), epigenetic regulation (You and Jones, 2012), state transitions (Hoek and Goding, 2010) - to name but a few of the non-genetic factors involved in ITH.

Oncogenesis entails the development of abnormal cells that may reach malignancy – described as the result of a step-wise acquisition of aberrations in specific genes (Fearon and Vogelstein, 1990). However, it is important to consider 1) the potentially infinite number of cellular evolutionary trajectories, some of which result in malignancy and 2) that oncogenic development does not halt once malignancy is reached. The extent of and means leading to a tumour's heterogeneity has been well-documented in the genetic context. In fact, genetic profiling has enabled the deciphering of a tumour's overall evolutionary trajectory (Alexandrov et al., 2013; Govindan et al., 2012; Nik-Zainal et al., 2012), as well as revealed the high number of dissimilar mutational profiles present in tumours (Stephens et al., 2012). Tumour cells preserve an 'active layer' of (genetic) heterogeneity (due to genomic instability) enabling development under selection forces. Malignant cells display frequently observed oncogenic features such as uncontrolled growth and evasion of cellular death programmes, among others (Hanahan and Weinberg, 2011). Malignant phenotypes can result from various evolutionary trajectories (and not just specific trajectories), be it through parallel (same clone of origin) or convergent (different ancestral clone) evolution (Francis et al., 2014; Venkatesan et al., 2017). The 'end' (malignancy) can be reached through different means (trajectories) (Radhakrishna et al., 2016), resulting in a genetically diverse cell population.

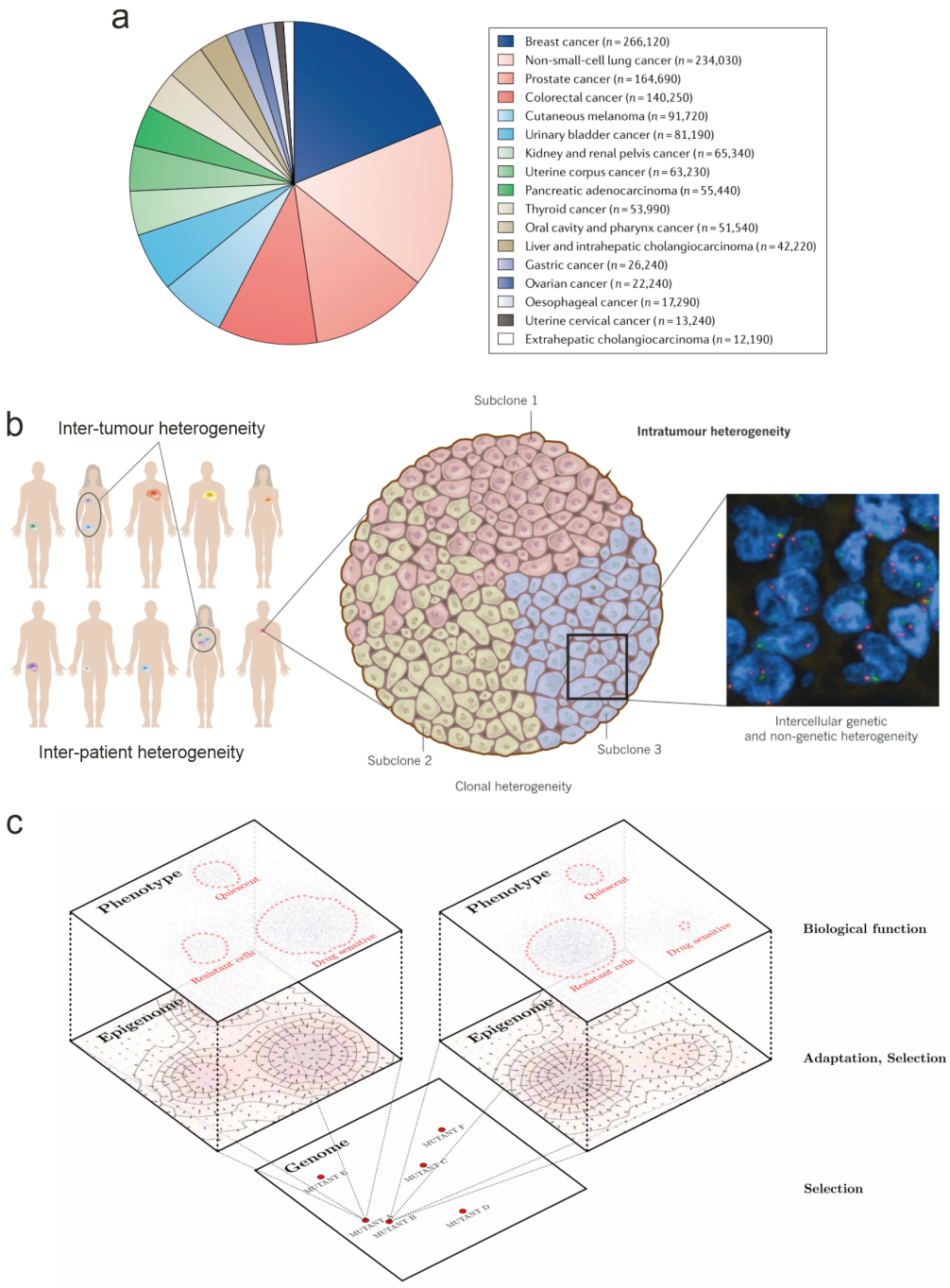

Fig. 1.4 Cancer does not develop in specific tissues; an even and broad distribution of (solid) tumour types were observed in the USA in 2018 (a, from Reiter et al. (2019)). Heterogeneity can be observed at different levels; across patients, between a patient's own tumours and within tumours as well (b, adapted from Burrell et al. (2013)) Non-genetic factors such as the epigenome acts as an additional player (and inducer of diversity) involved in shaping the cellular phenotypes (c, from Wooten and Quaranta (2017))

All these considerations taken, cancer is far from a disease recognised as being reproducible. More on the contrary and as a matter of fact, irreproducibility effectively impinges on success rates of many therapies. Heterogeneity – which increases in time, emphasizing the value of early detection – is the main cause of resistance to therapy and relapse (Pribluda et al., 2015; Shi et al., 2014). These are the current major clinical challenges for disease management. Personalised medicine is the best solution to address clinical bottlenecks and more effectively treat cancer patients. Although much progress has been made, to enlighten our insight we need to significantly deepen our understanding of how heterogeneity arises in the first place and – most importantly – how it contributes to a tumour's development. Armed with the relevant answers to such questions will put us in a better position to *prevent* and *manage* cancer. The following sections will summarise known causes (and effects) of genetic and non-genetic variability contributing to phenotypic diversity and tumour behaviour.

1.3.1 Genome Instability Induces Genetic Heterogeneity

The driving force of genetic heterogeneity derives from genome instability (Burrell et al., 2013). It creates opportunistic genetic aberrations that are then subjected to selection pressures, potentially resulting in the acquisition of fitness-enhancing mutations. The vast array of DNA stressors result in a whole range of types of aberrations. For example, errors in DNA repair mechanisms, replication and chromosomal segregation contribute to genome instability. This genetic imbalance induces specific alterations that jeopardise genomic integrity. Some modifications, though, are more commonly observed than others.

Single nucleotide damage can be the result of either endogenous or exogenous chemical events. In a recent analysis of a large dataset of somatic mutations representative of most cancer types, the authors characterised up to 49 mutational signatures (Alexandrov et al., 2020) - the 'marks' left behind by specific genome instability processes (see (a,c) in Fig. 1.5) - displaying the breadth of events causing genetic alterations. In another analysis of over 30 cancers, Alexandrov & colleagues found 20 characteristic mutational signatures (Alexandrov et al., 2013). Of these, cytosine (C) to thymin (T) transitions at CpG sites (age-related) and C to T and cytosine to guanine (G) mutations at TpC sites (APOBEC-related) were observed in numerous tumour types whereas other signatures were only tumour-type specific (Alexandrov et al., 2013). The cause of many of these mutational signatures however is still unknown (Helleday et al., 2014). Exogenous sources of genomic instability are easier to identify. When comparing non-small-cell lung cancer (NSCLC) from heavy cigarette smokers vs non-smokers, it was found that the former

displayed a tendency towards C to A transversions as well as amplified copy numbers and mutations (Govindan et al., 2012). Inconveniently and paradoxically, chemotherapy treatment - used with the purpose of eradicating or managing cancerous tissue - such as the use of platinum compounds - also contribute to genomic instability (Johnson et al., 2014).

Intratumour heterogeneity is also dependent on and fueled by chromosomal instability (Lengauer et al., 1997). Deficiency in DNA repair mechanisms such as in homologous recombination (HR) are known to induce a particular set of copy number aberrations. This results in a specific genetic profile of prognostic value, as suggested from a study where HR-induced signatures predicted response to cisplatin treatment (Birkbak et al., 2012). Other genetic single events such as chromothripsis - localised chromosomal rearrangements - result in catastrophic effects of varied magnitude and have the potential of seeding cancer-driving lesions (Stephens et al., 2011). Such aberrations can be quantified and used as a surrogate marker of chromosomal instability (Birkbak et al., 2011) - typically associated with poor prognosis (McGranahan et al., 2012).

The described insults (among others not mentioned) result in a particular genetic imprint (signature) (see (c) in Fig. 1.5), thus reflecting the process or damage encountered. This provides insight into oncogenesis and tumour evolution but there are still mutational signatures that are yet to be fully harnessed as a useful tool for the design of personalized therapies. Intratumoural heterogeneity observations thus provide vital developmental insight and can inform on disease prognosis (Andor et al., 2016; Maley et al., 2017).

Particular sets of mutated genes and genome instability mechanisms found in tumours tend to be tissue-specific (Ciriello et al., 2013; Graham et al., 2018). Thus, much of the cancer research carried out until the present day focuses on understanding tissue-specific tumour behaviour, with the objective of finding treatments that impinge or ultimately eliminate (tissue-specific) cancer cells. Successful pre-clinical treatments validated *in vitro* and *in vivo* further progress onto cancer clinical trials which, by convention, enroll patients with tumours of the same tissue of origin. However, in cases where the tested therapy is proven to be clinically effective, it is common to observe lower and various levels of efficacy and even lack of it in certain patients. Thus cancer originating from a specific tissue does not guarantee response to targeted therapy. This is a clear indicator that each patient's tumour is unique and that tissue-specific tumours could be considered as collective of diseases of the same type - emphasizing individuality - rather than a single disease characterised only by its origin.

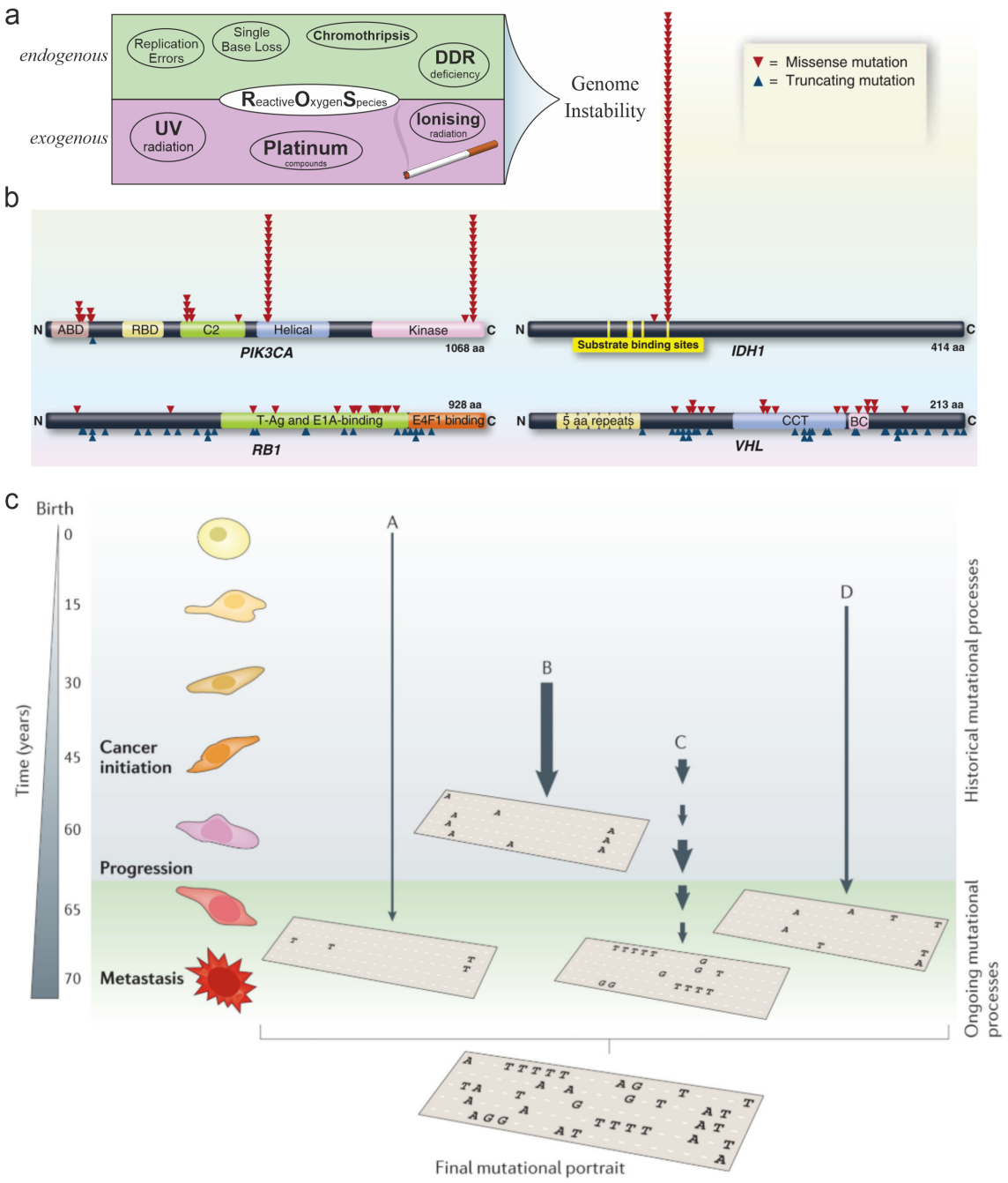

Fig. 1.5 The multitude of events resulting in genome instability arise from within a cell and its environment (a). Certain molecules such reactive oxygen species (ROS) can derive from both milieus via metabolism (endogenous) or ionising radiation (exogenous). Driver genes such as oncogenes *PIK3CA* and *IDH1* and tumour suppressors *RB1* and *VHL* are frequently mutated in tumours (b, from Vogelstein et al. (2013)). However, aberrations can greatly vary in type and gene locus as seen with the tumour suppressors. Genetic events such as those shown in (a) are known to 'imprint' specific patterns in the gene. Over time, the cumulative imprint of all these processes result in a mutational 'signature' representative of a cell's history (c, from Helleday et al. (2014))

Because many solid tumours take a long time to develop, they are deemed to result from complex evolutionary trajectories, themselves defined and differentiated by fitness-inducing genetic alterations (Scott and Marusyk, 2017) inherited or acquired through somatic mutations. Therefore, a substantial contributor to a tumour's 'uniqueness' is its genetic makeup. This results in inter-patient heterogeneity. For example, two patients of similar age with colorectal cancer (CRC) are likely to share aberrations in known colorectal driver genes, namely *APC* and *KRAS*. However, those aberrations are likely not identical (see (b) in Fig. 1.5) and the additional set of non-driver gene (passenger) mutations in each patient will further differentiate them from one another. Thus, commonality may be found in a small subset of genes crucial for oncogenesis, but the diversity derives from the combination of mutations encountered in each tumour (Stephens et al., 2012; Wood et al., 2007). The aberrations found in driver genes can vary by mutation type and gene location, and it is not uncommon to observe differences in these across patients. Such subtle differences have the potential to affect protein function in different ways and to different extents.

In fact, it is well documented that for certain crucial genes such as KRAS, clinical outcome has shown to be dependent on mutations' location and substitution type. In a study involving CRC patients treated with cetuximab and chemotherapy, those with *KRAS* G13D mutations had better overall survival (OS) and progression free survival (PFS) than those with other *KRAS* mutations (De Roock et al., 2010). In another study looking at metastatic CRC with the same treatment regime, depending on the KRAS mutation, tumours had superior (G13D) or worse (G12V) response and PFS when compared to chemotherapy treatment only (Tejpar et al., 2012). Molecular features such as transcriptional activity and anchorage independent growth has been shown to be mutation-location dependent (Stolze et al., 2014). Moreover, specific substitution type mutations within the same *KRAS* codon 12 can differentially activate downstream signalling pathways (Ihle et al., 2012).

Thus, tumours derived from the same tissue should not necessarily be treated equally. Although two tumours are considered similar enough to be categorised as part of a group (tissue-specific category) they can be distinct enough from one another to be considered different (molecular-specific category). If said tissue-specific tumours are considered dissimilar diseases, it begs the question as to how they have come to differ from one another across patients. What's more, one can make the reasonable speculation that these tumours have developed in dissimilar ways resulting in small yet significant differences of clinical relevance.

1.3.2 Non-Genetic Forces – The Ace Up a Tumour's Sleeve

Heterogeneity has often been considered and described exclusively at the genetic level, due to the well-corroborated fact that genetic aberrations contribute to oncogenesis and the rise of characteristic cancer hallmarks (Hanahan and Weinberg, 2011). In the last decade however, the field of cancer research has seen a rise of evidence describing various forms of non-genetic heterogeneity (Brock et al., 2009; Marine et al., 2020; Pisco and Huang, 2015; Tabassum and Polyak, 2015) - a concept traditionally thought of as noise, randomness or stochasticity having little or no effect on population fitness and seen as a byproduct of evolution (Via, 1993) rather than a contributor.

Growing Evidence

Variability of this nature was first observed and more thoroughly studied in bacterial (Golding et al., 2005; Losick and Desplan, 2008; Norman et al., 2015; Spudich and Koshland, 1976) and yeast research (Van Heerden et al., 2014). Such studies challenge the view that the genome and epigenome only determine a (static) phenotype. For example, sister bacteria from the same mother cell can co-exist in different molecular states, even in the context of a static environment. This is thought to be caused by stochastic events – such as RNA partitioning during cell division or transcriptional 'bursts' (Golding et al., 2005) – that enable phenotypic diversification. Variability of this type results in increased resilience (in an adverse environment) but at the expense of decreased overall population fitness (in a non-adverse environment) – a phenomenon termed as bet-hedging (Balaban et al., 2004; Solopova et al., 2014). Essentially, bet-hedging is an alternate strategy for maximising a species' survival.

Non-genetic diversity has also been observed in multicellular organisms, including plants (Nicotra et al., 2010), animals (Lyon, 1961; Nussey et al., 2005; Vogt, 2015) and humans (Zwijnenburg et al., 2010). A population of cells can be diverse at the genetic level; certain mutations have the potential to induce profound functional effects on a cell, for as long as the cell (and its progeny) that hosts them survive. For a cell to survive it needs to generate the relevant gene-coded functional units (proteins); it is these that determine a cell's molecular state (i.e. what it can or cannot do). One can infer that it is rather unlikely that cells may have the exact same types and amounts of proteins, even in the case of 'genetically identical' cells. Hence, the term 'non-genetic heterogeneity'; variation in cellular function. This variability can originate from the (seemingly) random changes or fluctuations – in part influenced by the exposure to changing environments – of the units responsible for the determination of a cell state.

These can include the intermediaries of the central dogma (such as mRNA transcripts) and the functional proteins themselves (e.g. p53) – of which variability is known as gene and protein expression, respectively. One might reason that cells differing from one another by the quantity of protein X may not function in the same way. Indeed, Spencer et al. (2009) showed that cell-to-cell variability in levels of proteins mediating apoptosis was the main determinant of probability and time of death. Another example is the significantly different transcription profiles encountered in haematopoietic progenitor derived subpopulations with low or high expression of stem cell marker Sca-1 (Chang et al., 2008). As such, protein and gene expression are the more known and distinguishable characteristics resulting from inter-cellular variability.

In addition to random fluctuations, functional states are also dictated by long-lasting events – e.g. different cell cycle stages (Buettner et al., 2015; Loewer et al., 2010) and microenvironmental effects – cell density, for example, can impact cells' endocytic capability (Snijder et al., 2009). The described evidence offers but a succinct representation of the non-genetic factors in cell populations and how these may impact cellular decisions (Balázsi et al., 2011) through regulation (or lack thereof) of molecular states. Before delving deeper into the question of non-genetic heterogeneity in cancer, it is useful to first understand its fundamental structure and how time may be a vital factor in the equation.

Structure

There are various non-genetic factors involved in generating the diversity present in cell populations. Such factors can be categorised into two broad groups (see Fig. 1.6). The first involves the (micro-)environment which may be heterogeneous itself (nutrient gradients, for example), and this is often reflected in the observed phenotypic diversity of a cell population (Huang, 2009). Thus, micro-environmental factors can be considered as a trivial and *extrinsic* cause of variability, whereas the more subtle population-driven (ie originating within cells) diversity is categorised as *intrinsic* non-genetic heterogeneity. The latter can be further broken down into macro- and micro- heterogeneity which can be represented as two distinct populations (multi-modality) or as a spectrum (uni-modality), respectively, in the distribution of a trait X in a given isogenic population (see Fig. 1.6). These distinctions allow for a clearer depiction of heterogeneity and a representation of the potentially existing stable network (defined by gene expression levels) states towards which cells evolve, ie attractor states. The presence or absence of subpopulations (macro-heterogeneity) may indicate attractor states, whereas the width of a distribution

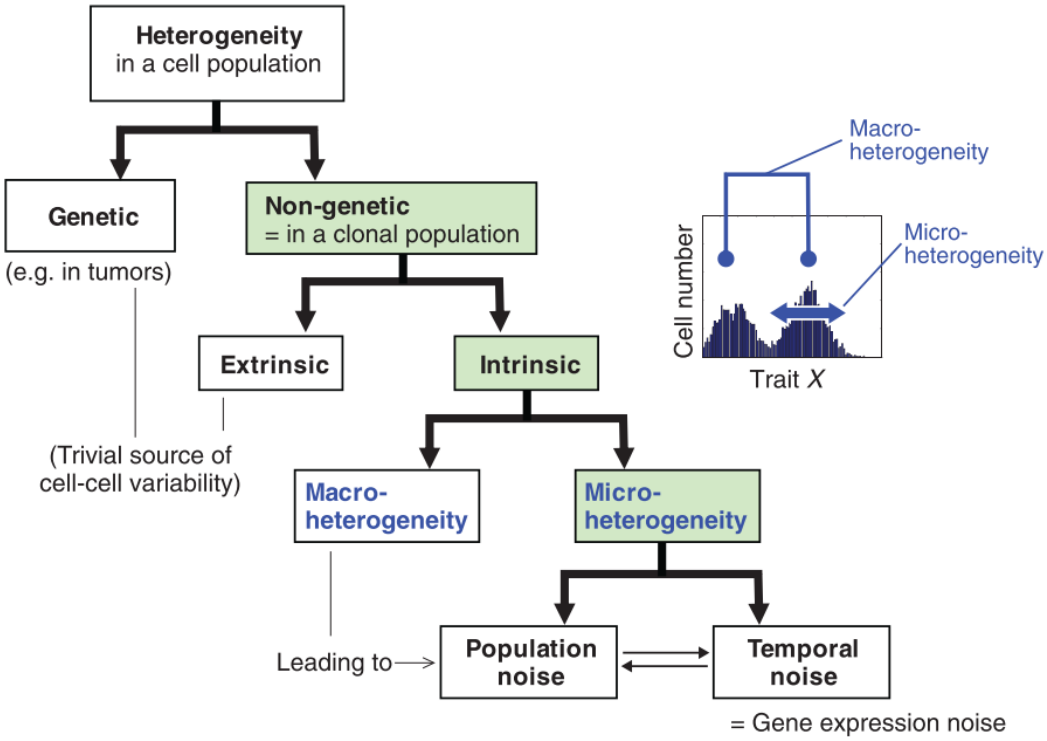

Fig. 1.6 To better understand non-genetic heterogeneity, one can devise categories according to the diversity-inducing causes and their effects. At the most basic level, isogenic cells may be different due to variable environmental conditions or internal composition (extrinsic vs intrinsic). The latter can distinguish two types of heterogeneity depending on the modality (macro-heterogeneity) and spread (micro-heterogeneity) of the distributon of a trait X across an isogenic cell population. Figure from Huang (2009)

(micro-heterogeneity) may inform on the breadth of phenotypic plasticity of a population. However, since these are descriptions derived from a single point in time, one might ask how 'stable' or 'unstable' these phenotypes are (ie is time a influential and defining factor?). If there is such a dichotomy, what determines a phenotype's stability?

Deterministic & Stochastic Heterogeneity

Living systems are not static; homeostasis and potential for cellular adaptation are dynamic features that can shape phenotypic landscapes over time. Thus, time is a necessary variable in determining the stability (or lack thereof) of cellular phenotypes and behaviour - characterised by (potential fluctuations in) molecular elements and network states. The terms *determinism* and *stochasticity* are used to relate to a phenotype as a function of time or its stability (see Fig. 1.7). In the context of variability, *deterministic* heterogeneity posits the presence of multiple stable phenotypic states in a cellular population (Huang, 2009). An oversimplified example is the cell type; groups of cells categorised by their specific gene regulatory network (GRN) and resulting phenotype – more likely to appear as *macro*-heterogeneity.

On the other hand, *stochastic* heterogeneity designates cellular phenotypes of deterministic (stable) state that show unstable phenotypes (see Fig. 1.7). Such concept is associated (and used interchangeably) with *noise* – a term classically used to designate random cellular biochemical reactions (ie probabilistic molecular events) contributing to the variability usually observed when measuring gene and protein expression in a 'uniform' population (Elowitz et al., 2002; Raser and O'Shea, 2004). Thus stochasticity mainly involves so-called random events that occur in cellular life. These events are understood to be the probabilistic reactions resulting in the generation or degradation of individual molecules (such as proteins or mRNA), but these can also occur at a larger scale such as mitosis – where equal partitioning of molecules is only guaranteed for DNA (Huh and Paulsson, 2011). Stochastic effects in bacteria have been shown to give rise to *persistency* – the concept of entering a state of dormancy (or reduced homeostatic activity) to sustain species-threatening conditions (such as lack of nutrients) (Balaban et al., 2004). In this case, survival is warranted through stochasticity-induced phenotypic diversification (Norman et al., 2015). However, such diversification may alter biological circuitry regulating important homeostatic activities such as signalling, metabolism, movement and stress-responsive networks (Van Boxtel et al., 2017), essentially resulting in information corruption and maladaptation. As such, stochasticity has the potential to be either benefitial or detrimental to a population's survival.

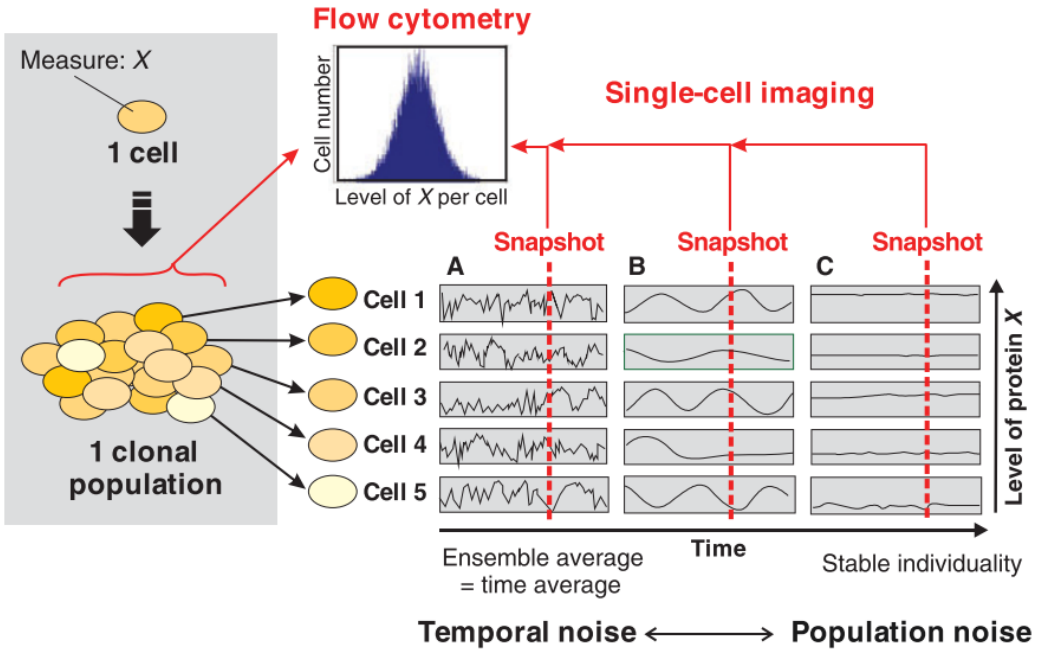

Fig. 1.7 A clonal population of cells differentially express a trait X; its measurement with flow cytometry is displayed as a gaussian distribution. If we were to take a sample from this clonal population, we would find that expression levels of X fluctuate in the short term (stochasticity). However, with time, eventually we can observe that X remains at a particular level of expression (determinism). The latter contributes to population noise, whereas the former is known as temporal noise. Both of these make up the distribution of the level of X. Figure from Huang (2009)

When it comes to single-cell measurements, snapshot-type assays provide us a glimpse of the variability at a single point in time (see Fig. 1.7) and the *micro*-heterogeneity we observe may be associated with *noise*. But unimodal distributions may well also be consisting of cells that host slightly different but more 'durable' phenotypes, ie not caused by random events resulting in temporal fluctuations (Huang, 2009). Subtle deterministic factors such as cell volume (Kempe et al., 2015), cell cycle stage (Zopf et al., 2013), metabolic state (Kiviet et al., 2014) and signalling (Iwamoto et al., 2016) prime cells in particular functional or molecular states contributing to a 'spectrum-like' variability. Thus, we can conceive *micro*-heterogeneity as being driven by either *stochastic* or *deterministic* effects (Zopf et al., 2013), resulting in observable traits generated by noise or by stable (yet subtle) differences among cells, respectively, or both (Eling et al., 2019).

These concepts have been formulated to explain the observed non-genetic variability and to gain a more structured insight on their causes and effects. Because of the non-triviality of some of its aspects and the lack of technologies available to gather the necessary high resolution data, non-genetic heterogeneity has been off the active spotlight of cancer research, until approximately a decade ago. The conceptualisations of *determinism* and *stochasticity* – derived from observations in developmental biology – and their potential implication in survival raises a few eyebrows as to what role these might play in oncogenesis and/or tumour behaviour, if at all.

In Cancer

The somatic mutation theory of cancer initially proposed in 1914 (Boveri, 1914) is the long-standing and most accepted view on cancer genesis. The current take posits that fitness-inducing DNA mutations in *driver* genes (cf. 1.2) are acquired by cells which then are capable of expanding as a clonal population. As time goes on, these cells evolve - via Darwinian-like selection - by accumulating further mutations, eventually leading to cancer onset and malignancy; it is a multistep process (Vogelstein and Kinzler, 1993). Another prominent and debated model is that of cancer stem cells (CSCs) - a small fraction of undifferentiated cells in a clonal population which are capable of self-renewal and generating multiple differentiation lineages (Medema, 2013; Vermeulen et al., 2008). The full picture of the process seems much more complex and is unlikely to be explained by a single paradigm nor universally.

The literature is relatively scarce on how non-genetic forces contribute to cancer onset. Noteworthy observations showing that presence and frequency of specific driver genes

correlate with distinct tissues (Haigis et al., 2019; Kandoth et al., 2013; Schneider et al., 2017) are a clear indication that carcinogenesis cannot amount to genetics only. Such evidence suggests that tissue microenvironment influences genetic developments either through tissue-specific cell differentiation mechanisms (Chou et al., 2010) or due to the cell types that constitute them - which are effectively cells of different developmental lineage. Cell types do not respond equally to the same microenvironmental cues such as growth promotion (Sack et al., 2018), and they host particular epigenetic states (John et al., 2011). Related to these is the idea of phenotypic plasticity whereby cells can change their phenotype due to *stochastic* effects or in response to microenvironmental events (Marusyk et al., 2012) (see Fig. 1.8). The research community has increasingly focused on the characterisation and implications of such non-genetic phenomena in tumour maintenance and progression - especially under cancer treatment regimens - resulting in a more substantial body of work.

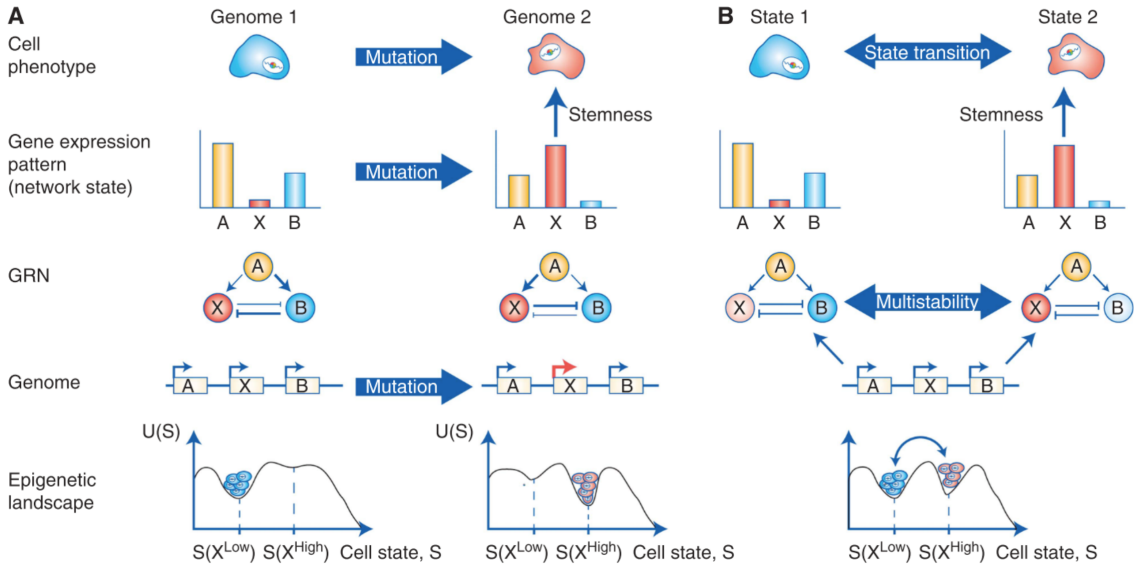

Fig. 1.8 Acquired resistance involves the Darwinian selection of a clone that has acquired a benefitial mutation (A). Said mutation results in a modification of the gene regulatory network (GRN) and higher expression of gene X, placing the mutated cell in a new single cell state $S(X^{High})$. However, therapy can also induce transitions between two different states with the same GRN and within a non-changing multistable epigenetic landscape (B). Figure from Pisco and Huang (2015)

Intra-tumour heterogeneity (ITH) contributes to the biggest bottlenecks in cancer treatment and management; resistance and relapse. We have rather successfully harnessed our genetic understanding of cancer by targeting mutation-induced vulnerabilities with molecular compounds - examples being BRAF and PARP inhibitors for patients with

$BRAF^{V600E}$ (Hyman et al., 2015) and germline *BRCA 1/2* mutations (Kaufman et al., 2015). However, on too many scenarios, we observe the rise of resistant cells able to sustain traditional - chemotherapy and radiotherapy - as well as more modern - molecularly-targeted and immunotherapy - treatments (Holohan et al., 2013; Senft et al., 2017; Sharma et al., 2017). Alas, our ability to detect and understand genetic abnormalities does not warrant sufficient insight into the high order complexity that drives cancer.

The lack of a complete response to treatment - *fractional killing* of cancer cells - may be due to pre-existing genetically resistant clones or the generation these during treatment (Hata et al., 2016; Ng et al., 2012) (see Fig. 1.8). Others postulate that CSCs are the culprits (Makena et al., 2020). In addition to these, it is also plausible that phenotypic diversity or plasticity may result in said resistant cells (Bell and Gilan, 2020; Konieczkowski et al., 2014; Paudel et al., 2018; Pisco et al., 2013; Salgia and Kulkarni, 2018). An intriguing study - where Kreso et al. (2013) and colleagues explored the functional integrity of single genetic clones - found that various single-cell tumour derived (sub-)clones displayed different behaviours over a 4-week oxaliplatin course in mouse xenografts. Behaviours such as persistency, proliferation and tolerance to chemotherapy seemed to vary within cell lineages. This study strongly suggests non-genetic mechanisms at work, since copy number alteration profiles and mutation hot spots remained mostly intact. Such plasticity entails that cells can change between drug-tolerant and sensitive states - otherwise known as *phenotypic switching* (Hoek and Goding, 2010; Sun et al., 2014). Notably, the various phenotypes present in cell populations can be inherited to the progeny (Brock et al., 2009) and may even be preferentially selected for (Anderson et al., 2006; Sharma et al., 2010), thus affecting evolutionary trajectories.

Despite the seemingly influential role of phenotypic diversity in cancer resistance, there is a need to provide a complete characterisation of its potential synergy with genetic defects. The understanding of how cell-to-cell variability influences response to oncogenic cues and therapeutic interventions is essential for a more practical understanding of how neoplastic lesions are triggered and become clinically manifest, and to improve the effectiveness of clinical intervention.

1.4 Signalling Networks: the Decision-Makers

The human body is a complex organism comprising many tissues that need to be maintained in a steady state in order to carry out their designated function. This so-called steady state, aslo known as homeostasis, is highly dependent on the equilibrium

of physical and chemical conditions not only within tissues but also within the units that constitute them, i.e. cells. Cellular homeostasis, including the capability to respond to external stimuli, is maintained by chemically active networks. These, more commonly known as signal transduction networks (STNs) (see Fig. 1.9), play a fundamental role in cellular life as they enable cells the ability to sense and process information in order to execute context-dependent decisions. The complexity of STNs is such that it supports the integration of multiple inputs and processes. These result in a specific output or cellular phenotype. Such molecular information-processing 'machines' maintain homeostasis not only at an individual, single-cell level but also at a cell-contextual, tissue level.

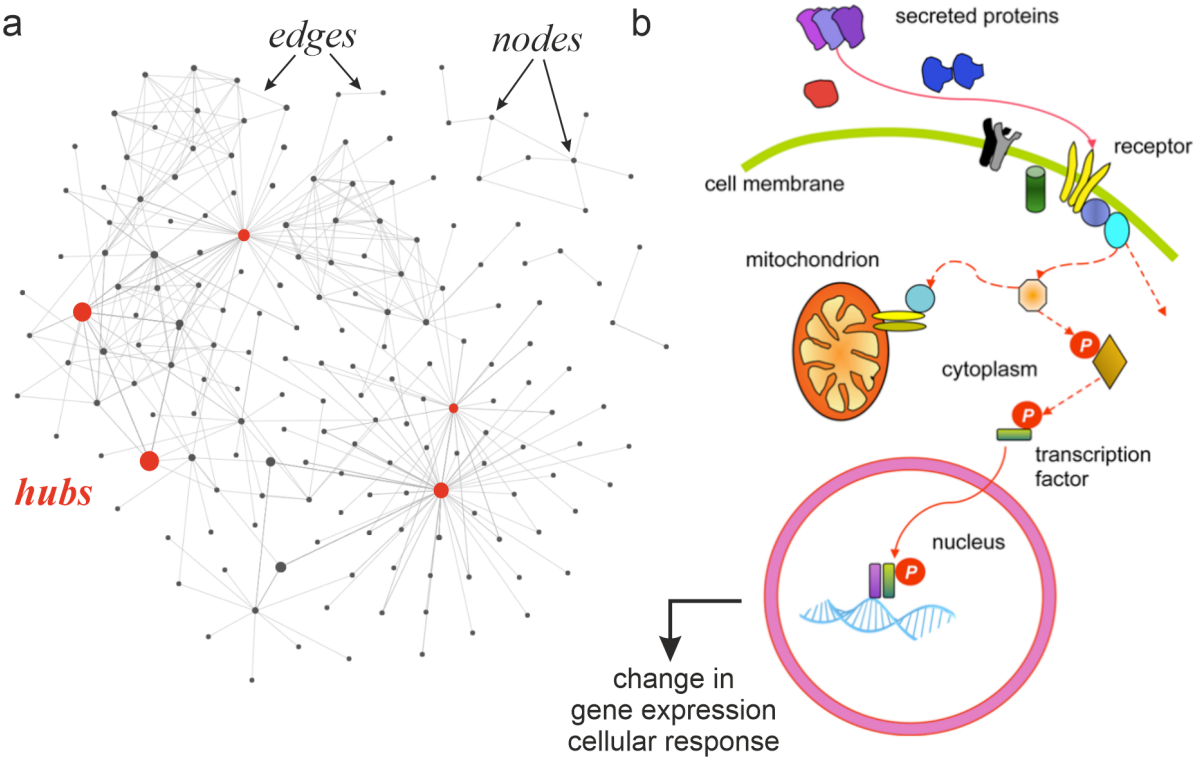

Fig. 1.9 A signal transduction networks (STN) is a group of interconnected proteins (or molecules) relaying biological information typically via chemical reactions. Here, proteins or network components (nodes) are represented as dots, and their interaction by edges (lines connecting dots) (a). Hubs (shown in (a) as red dots) are nodes with high connectivity. Biologically, a standard STN structure typically starts in the extracellular space, where ligands bind cell surface receptors. These in turn activate and kick-start a series of sequential reactions, i.e. a signalling cascade. Finally, proteins furthest 'downstream' of a cascade interact with DNA to promote gene expression and ultimately induce a specific behaviour (b, adapted from Jackson et al. (2018))

STNs are constituted of *nodes* and *edges* (see (a) in Fig. 1.9) – terms derived from graph theory, a branch of mathematics (Biggs et al., 1986). *Nodes* can be thought of as

biological units that are subject to (or induce) actionable events or *edges* (Azeloglu and Iyengar, 2015). The former are made up of proteins, microRNAs and indirectly by certain DNA sequences affecting gene expression (Csermely et al., 2016). These are connected together via *edges*; chemical reactions characterised by their type (inhibition/stimulation) and strength (Csermely et al., 2016). The way *nodes* and *edges* are structured allow for the sensing of specific information and its transmission to the relevant cellular location. For example, a cell detects an external signal through growth factor-induced activation of a receptor-tyrosine kinase (RTK), which then results in the sequential activation of a number of 'downstream' proteins and eventually the activation of a transcription factor prompting expression of select genes (see (b) in Fig. 1.9). Here, the nodes (RTK, 'downstream' proteins, transcription factor) connected by edges (chemical activation events) constitute a single signal transduction network. However, networks do not function independently, on the contrary; they are connected (see (a) in Fig. 1.9), thus enabling a higher order of cognition. This interconnectivity is achieved through *hubs* - *nodes* with many *edges* (rather than the average few) providing them with superior signalling influence (Azeloglu and Iyengar, 2015). An example of a *hub* is KRAS (thoroughly described in Chapter 2) – a protein regulating mainly growth and survival (Cox et al., 2014). Such important cellular behaviours are deregulated when a genetic mutation induces the expression of an 'anomalous' version of KRAS, ultimately leading to unwanted consequences such as oncogenesis. Therefore, it is vital to understand how cells make 'decisions' in the first place. And although network-network connectivity contributes to signal processing, the final cellular output ('decision') is determined by the various signal characteristics registered in space and time, i.e. signalling dynamics.

1.4.1 Signalling Dynamics Enables Complex Information Processing

Signalling dynamics in STNs are paramount to a cells' ability to carry out fate decisions such as proliferation, survival or apoptosis (Marshall, 1995; von Kriegsheim et al., 2009). Mechanistically speaking, the concept of dynamics has the objective to either convert a gradual signal into binary information (i.e. ON/OFF), or maintain a particular encoded message despite variable signal cues (Kholodenko et al., 2010). This way, cells can discriminate important information or signal (and decisions to make) from a noisy environment.

To clarify, the term *signal* is usually employed to refer to protein activity in response to an event. Each protein in a STN has the capability for dynamics but it is of particular

importance in so-called 'key' proteins – such as ERK – due to their ability to activate gene regulatory machinery, ultimately triggering specific transcriptional programmes (Makadia et al., 2015; Wilson et al., 2017).

Signalling dynamics are profoundly characterised by temporal features such as signal *duration* and *frequency* (see (b) in Fig. 1.10). One of the main mechanisms through which these features are regulated is the stimulation type and amount perceived by cells. For example, the signal duration-phenotype association was first elucidated in pheochromocytoma rat cells (PC-12), where observed EGF-induced transient ERK activation resulted in proliferation. Whereas NGF-induced chronic ERK activation elicited differentiation (Marshall, 1995) (see (b) in Fig. 1.10). These observations have been further replicated in subsequent studies by various researchers (Albeck et al., 2013; Ryu et al., 2015; Santos et al., 2007). Similarly, single or multiple signals in a particular window of time (ie dissimilar signal frequency) may have different consequences. This is observed in p53 activity which may be either pulsatile (γ-radiation) or sustained (UV radiation) to different extents (ie dose-dependent) depending on the type of DNA damage detected (Purvis and Lahav, 2013) (see (b) in Fig. 1.10).

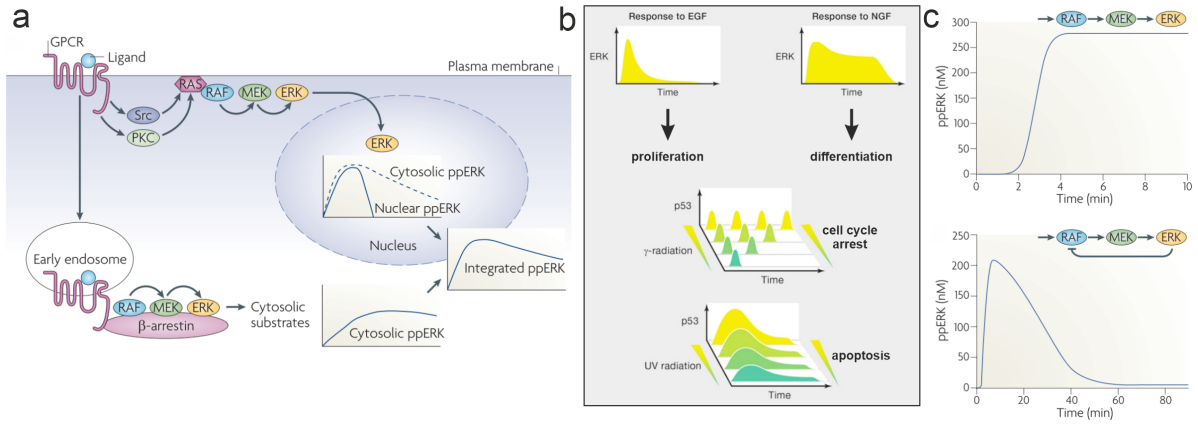

Fig. 1.10 Biological information can be modified depending on cellular location (a), input-induced differential time dynamics (b, adapted from Purvis and Lahav (2013)) and the presence of network motifs, such a negative feedback loops (c), wired within a STN. Both (a) and (c) adapted from Kholodenko et al. (2010)

The way *nodes* and their connecting *edges* are arranged constitute the topology of a network. Signalling dynamics are restrained to a higher or lesser extent by network topologies. These include modular *network motifs* - *edges* with regulatory roles, in addition to information transfer functions. *Motifs* can either stimulate (positive regulation) or inhibit (negative regulation) proteins at different stages of signal processing.

Feedback or feedforward loops affect proteins earlier or later, respectively, in a signalling cascade. Effectively, these loops significantly shape the different types of responses (Alon, 2007; Brightman and Fell, 2000; Kholodenko, 2000; Kiyatkin et al., 2006), such as the aforementioned acute or sustained protein activity (see (c) in Fig. 1.10), among others.

Frequency features such as oscillations were in fact first theoretically described (and predicted) mathematically in the MAPK signalling cascade. Negative feedback from ERK to Son of Sevenless (SOS) or RAF and ultrasensitivity of ERK activity to changes resulted in so-called oscillations (Kholodenko, 2000). This was later observed experimentally (Nakayama et al., 2008; Shankaran et al., 2009). These remarks confirm and highlight the temporal dynamics capabilities of biochemical networks.

In addition to variations in temporal aspects of a signal, another response-shaping factor is that of space (Muñoz-García et al., 2009). Biochemical networks exist within cells – biological bodies with a total volume of 400-5000 μm^3 (Moran et al., 2010; Wiederschain, 2005) hosting a wide range of function-specific structures (Golgi, nucleus, endoplasmic reticulum, membrane to name a few) and a much wider range of proteins. The latter can be as small as 1nm in size, meaning that the space dimension is vast. To put it in context, E.coli have a volume of 3 μm^3 with similar sized proteins. This results in a much reduced dimensionality, restricting signalling complexity and processing. Coming back to the example of *KRAS*, previous research has proved that it needs to be located at the plasma membrane in order to undergo efficient activation (Augsten et al., 2006) and subsequently stimulate downstream pathways (e.g. MAPK, PI3K). Moreover, key downstream targets such as ERK have differential activity depending on its cellular location and interaction with other proteins (see (a) in Fig. 1.10). Therefore, for 'normal' signalling to occur, a protein needs to have a certain activity for a certain amount of time and at a certain location.

Signalling Heterogeneity

It is clear that signalling cues are dependent on a high number of factors, of which time, location and activity of a protein play a dominant role in encoding and decoding information (Kholodenko et al., 2010). However, biological systems are not *quite* binary - variability is an omnipresent factor that affects many aspects of cellular life. Protein concentrations varying from cell to cell (potentially) differentially affect the networks they are part of. This isn't to say that all cells have differently functioning STNs, but rather highlights the fact that certain cells may not respond as expected. Such cells may

be at such 'distance' from the norm due to the effective sum of past events that have led them to a particular state (one that may be considered at the 'edge' of homeostasis).

In a relatively recent study where the authors aimed at understanding how PC-12 cells interpret different external stimulations (Ryu et al., 2015), experiments showed a high level of intercellular heterogeneity in signalling patterns when compared to the population average – an observation previously described (Marshall, 1995; von Kriegsheim et al., 2009). Interestingly, they observed a correlation between ERK 1^{st} peak amplitude and sustained activation, in addition to the EGF and NGF specific induction of ERK responses previously aforementioned (Ryu et al., 2015). Pulsed GF experiments shed light on new aspects of the MAPK network; ERK refraction behaviour (ability to respond to the same stimulus in an identical manner) occurring only once the cell has reached its basal state, and the identification of different hour-scale negative feedback loops depending on GF identity and concentration.

Therefore, in response to the same stimulus, genetically identical cells exhibit different signaling dynamics. More importantly, cell-to-cell variability in signalling responses results in variability of cellular decision. These seemingly stochastic responses are frequently observed when live single-cell imaging technologies are utilised to characterise cellular responses. However, these observations are then often neglected when we model carcinogenesis and response to clinical intervention.

1.4.2 Cancer as an ecological problem

Cell decisions are determined both by cell-autonomous and non-cell-autonomous mechanisms. Tissues are made up of millions of cells in direct physical contact with each other, and cell-to-cell communication has a fundamental role in tissue homeostasis (Tabassum and Polyak, 2015). The mechanism of signaling dynamics described so far, should indeed be considered within this context.

The secretion of cytokines by cells is a form of intercellular communication studied since the 1940's (Dinarello, 2007). Since then, we know that these chemical units are the way in which cells communicate between one another. As an example, the secretion of chemokines inform the immune system (via neutrophil recruitment among others) of the presence of non-self (i.e. foreign) material that has the potential to be threatening to the human organism. In other words, cells from the immune system attracted by chemokines migrate to the site where cells secreting said pro-inflammatory reside, i.e. the site of pathogen. This constitutes a form of positive intercellular communication –

termed *commensalism* – in that the immune cells prevent chemokine-secreting cells from death by neutralisation of the pathogenic material.

However, there are several types of cell-to-cell interactions that affect cellular life. Both positive (*mutualism*, *commensalism*) (Chiarugi and Cirri, 2016) and negative (*competition*, *predation*) (Caignard et al., 1985) interactions have been experimentally shown. Such events drive cells to increase (positive interaction) or decrease (negative interaction) their likelihood of survival, on occasion at the benefit of other cells. These are selection forces at play, which in the context of cancer become paramount factors shaping clonal evolution trajectories and promoting malignancy (see Fig. 1.11).

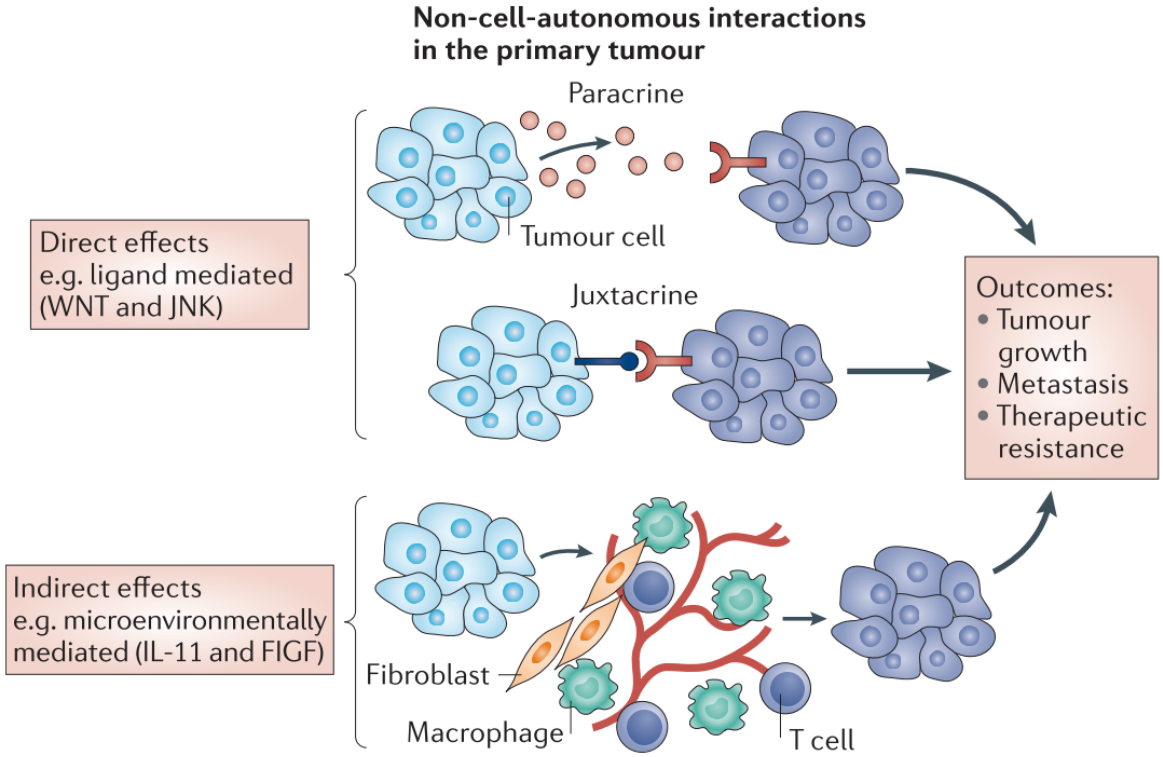

Fig. 1.11 Cells interact with one other via direct or indirect means. Intercellular interactions can promote drug resistance, malignant and metastatic behaviour, thus benefiting cell populations' survival. Figure from Tabassum and Polyak (2015)

Although intercellular communication has been described and proven with factors such as cytokines and cellular nutrients (such as glucose (Santo-Domingo et al., 2019)) it has also been osberved in the signalling context in the form of progressive MAPK activation, for example. Numerous cell migration studies have shown that ERK information 'travels' through cell populations in a wave-like pattern (Aoki et al., 2017, 2013; Gerosa et al., 2020; Hino et al., 2020). Interestingly, the state of a cell (cell cycle stage) can determine whether

it is more prone to induce an ERK pulse and subsequent activation 'wave' (Hiratsuka et al., 2015). ERK activation of a cell induces its contraction. Said contraction in turn stretches the neighbouring cell prompting it to stimulate ERK via EGFR activation (Hino et al., 2020). However, ERK activity can also be spatially transmitted via paracrine signalling. Extracellular ATP binds to P2Y receptors, resulting in the activation (and secretion) of matrix metalloproteases (MMPs) to which EGF is tethered (Aikin et al., 2019; Handly et al., 2015). Local diffusion of the secreted EGF results in the activation of EGF receptors in neighbouring cells. This signalling cascade can be triggered by an apoptotic cell as a means of temporarily protecting neighbouring cells from death (Gagliardi et al., 2021). Alternate cell fates such as growth arrest (Park et al., 2003) and dedifferentiation (Takahashi et al., 2003) can also be imposed on neighbouring cells via the ERK-induced release of Leukemia Inhibitory Factor (LIF) and epiregulin, respectively.

Thus, the state of a cell as well as its microenvironment may differentially influence the way a cell affects its neighbours' behaviour, i.e. non-self cellular decisions. Due to the unlimited number of possible scenarios, cell-to-cell communication can also significantly contribute to a cell population's heterogeneity (Davies and Albeck, 2018).

1.5 Studying Single Cells - Towards Accurate Information

Biochemical networks and quantitative controls of signal timing and strength together with quantitative monitoring of biochemical outputs and phenotypes are necessary to describe the actual mechanism by which oncogenic signalling causes cancer or failure of therapeutic interventions. Such detailed understanding of signalling requires technologies of unprecedented accuracy and precision. Classic methodologies used to study signal transduction pathways are limited by their spatial and temporal resolution (see (b) in Fig. 1.12). Only until recently, STNs have mostly been studied by measuring protein levels in whole populations - samples constituting of millions of single cells. Thus, such experiment outputs mirror the behaviour of cell populations, rather than single cells. The sample may be derived from a tissue and thus cells are considered 'the same'. However, it is not unusual to have cell populations with a large variety in protein levels (Sigal et al., 2006).Thus, potentially biologically relevant cell-to-cell differences (present in cell populations) are masked by ensemble measurements (Altschuler and Wu, 2010) (see (a) in Fig. 1.12).

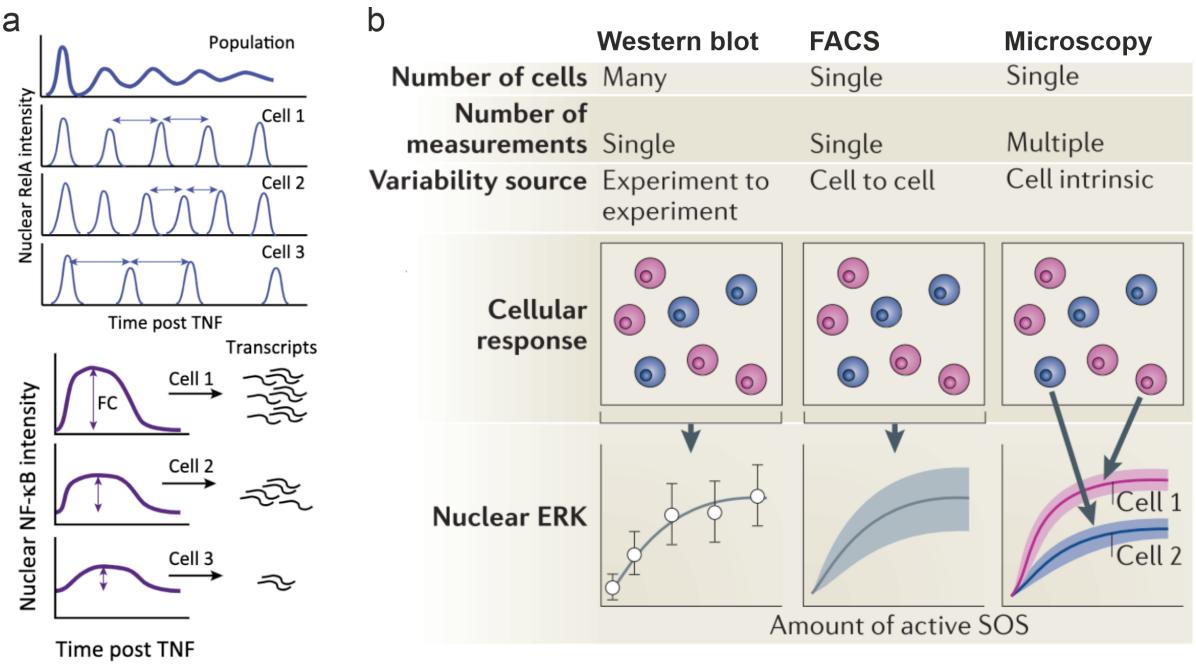

Fig. 1.12 Traditional assays (such as Western blot) provide population measurements. These, however, are far from an accurate representation at the single-cell level. Population measurements may mask asynchronous signal activity and fail to provide suitable explanations - such as fold change detection - for certain phenotypes (a, adapted from Gaudet and Miller-Jensen (2016)). With microscopy, one can not only measure single cells but also yield a very high time resolution rendering a much more accurate depiction of signalling activity (b, adapted from Tischer and Weiner (2014)).

It is important to stress that biological features such as signalling should be monitored frequently if one is to dissect the acute dynamics involved in information processing. Moreover, it is worth studying protein activity over a rather long period of time as its cumulative activity may have an effect on how cells behave.

1.5.1 Dissecting cell-to-cell variability in oncogenesis

Cell-to-cell variability in cell populations can result in the appearance of a diversity of phenotypes, some of which are conducive to a tumour's development or resistance to therapies. We hypothesise that heterogeneity in signalling dynamics and its causes are key to understand tumour maintenance, with important consequences to disease management. However, non-genetic heterogeneity is scantly studied and mechanistically not fully understood. In addition, cell-to-cell variability is often neglected or challenging, even impossible to characterise. It is therefore insufficient to probe samples at limited time points if we ought to understand dynamics and further enrich our knowledge of forces driving cellular decisions.

The development of the green fluorescent protein (GFP) in the 60's (Shimomura et al., 1962) and subsequent fluorescent proteins (FPs), combined with imaging, provided the research community a novel and innovative toolbox that enabled a whole new dimension through which to understand biological phenomena. This was especially so in the case of live cell studies, where one can track cells expressing a relevant FP-bound protein over time. Moreover, objectives with different magnifications means that one can have different levels of spatial detail – to the point where we can make out organelles and obtain subcellular spatial information on a protein of interest. Thus, the main characteristics of this general technology combinaton (imaging and fluorescent probes) are that of a superior time and space resolution, in addition to the main advantage of using microscopy; the ability to perform single-cell measurements (see (b) in Fig. 1.12).

In conclusion, the aim of this PhD project is to investigate cell-to-cell variability in signalling dynamics and how genetic and non-genetic heterogeneity may synergise to give rise to oncogenesis & shape cancer cell decision-making. To this purpose, I use isogenic cell lines with different mutations at the same codon of *KRAS* and the most advanced tools for single live cell biochemistry that are required for the study of cell-to-cell variability. Alongside the utilisation of established tools, I also develop novel optogenetic tools and monitoring methods for KRAS-dependent signal transduction pathways that

enable the study of oncogenic signalling with unprecedented spatiotemporal control and biochemical resolution.

Chapter 2

KRAS Signalling
Dissecting the subtleties

2.1 Introduction

The RAS genes were the first oncogenes identified, over 35 years ago (Der et al., 1982; Parada et al., 1982; Santos et al., 1982). There are three main genes; *HRAS* (Harvey rat sarcoma viral oncogene homolog), *KRAS* (Kirsten rat sarcoma viral oncogene homolog) and *NRAS* (neuroblastoma v-ras oncogene homolog). They encode four different proteins, namely H-Ras, N-Ras, K-Ras4A and K-Ras4B. The latter two derive from alternative RNA splicing of a pre-processed KRAS protein; however, K-Ras4B is the predominant variant (Hobbs et al., 2016). These form part of a wider RAS superfamily which affects a large range of signalling networks, ultimately regulating cellular processes such as cell migration, differentiation, proliferation, cytoskeletal modifications, apoptosis and senescence (Fernández-Medarde and Santos, 2011).

2.1.1 Role & function of RAS in the cell

RAS proteins function via chemical interactions with guanosine molecules. Just as all members of the RAS superfamily, RAS proteins are small GTPases, i.e. hydrolase enzymes. These are proteins that break down guanosine triphosphate (GTP) into guanosine diphosphate(GDP). Thus, small GTPases exist in two forms; GDP-bound, and GTP-bound conformation (see (a) in Fig. 2.1). Guanosine nucleotide exchange factors (GEFs) and GTPase activating proteins (GAPs) regulate the activity of small GTPases. GAPs catalyse the hydrolysis of the bound GTP, whereas GEFs exchange a bound GDP for a freely available GTP (Hobbs et al., 2016; Vigil et al., 2010). Thus, RAS

proteins switching between GTP-bound and GDP-bound states are considered as active ('ON' state) or inactive ('OFF' state) RAS, respectively. Active RAS (i.e. GTP-bound) interacts with proteins containing RAS Binding Domains (RBD) to stimulate effector downstream targets. This type of interaction regulates a variety of molecular networks such as the frequently studied MAPK and PI3K signaling cascades, but also RAL, RAC and RASSF pathways (Cox and Der, 2003; Pylayeva-Gupta et al., 2011; Zhou et al., 2016). These signaling networks ultimately induce the promotion of specific cellular fates.

While the developments shown in Chapter 3 are aimed to monitor multiple pathways simultaneously, due to current technical limitations, I have focused on the characterisation of MAPK signalling in cells with mutated *KRAS*.

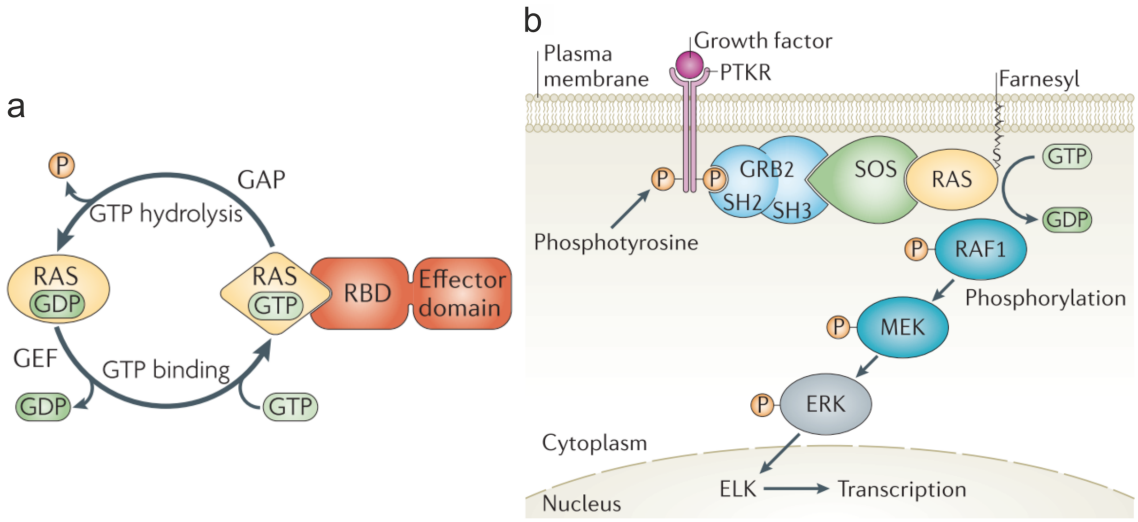

Fig. 2.1 The RAS GTP-GDP cycle (a) and the MAPK signalling cascade (b). Adapted from Ahearn et al. (2011)

The RAF-ERK or Mitogen Activated Protein Kinase (MAPK) pathway (see (b) in Fig. 2.1) – heavily involved in cellular proliferation and growth (Campbell et al., 1998; McCubrey et al., 2007; Mebratu and Tesfaigzi, 2009) – is one of the central signalling cascades that RAS proteins regulate. First active RAS binds to the RBD domain of a RAF protein (Moodie et al., 1993) at the plasma membrane. Active RAF stimulates MEK which in turn phosphorylates extracellular signal-regulated kinase (ERK). Upon activation, ERK translocates to the nucleus where it plays the instrumental role of triggering transcriptional programmes directly regulating gene expression. Signalling dynamics – tightly regulated by regulatory mechanisms such as feedback loops (see section 1.4.1 on page 23 and (c) in Fig. 1.10 on page 24) – of the RAF-ERK pathway determines the

activation of specific transcriptional programmes (Aoki et al., 2013). Pulsatile activity results in the recruitment of serum response factor (SRF) – a transcription factor involved in the transcriptional activation of immediate early genes (IEGs) – and upregulation of around a dozen genes. Sustained ERK activity however, prompts the recruitment of other transcription factors (activator protein-1 and transcription enhancer factor) resulting in the expression of a much wider range of genes. Importantly, Wilson et al. (2017) discovered that frequent ERK pulses result in efficient transcriptional activation, as opposed to sustained or infrequent ERK pulses.

Thus, the deregulation of proteins within the MAPK cascade has the potential to alter signalling dynamics resulting in alterations in the capability of a cell to trigger physiological responses and transcriptional programs.

2.1.2 Patterns in cancer

The frequency and the type of genetic aberrations affecting different isoforms varies from tissue and cancer type rather drastically. The most common point mutations occur in hotspots at codons 12 (G12), 13 (G13) and 61 (Q61) and they account for most (87-97%) mutations in all RAS isoforms (Prior et al., 2020). The mutational frequency at these codons varies on the RAS isoform (see Fig. 2.2). For example, in KRAS, mutations in G12, G13 and Q61 account for 81%, 14% and 2%, respectively (Prior et al., 2020). However, most mutations in NRAS occur at the Q61 locus, followed by G12 and G13. Also, the mutational spectrum changes between isoforms and tissues as illustrated in Figure 2.2. For example, G12D, G13D, and Q61H are the predominant mutations in KRAS overall. However, in non-small cell lung cancer (NSCLC), the predominant KRAS mutation is G12C. The transversion G:C→T:A that causes the G12C mutation is associated with a mutagen found in cigarette smoke, combustion engine gas and power plants (Seo et al., 2000).

A G12C mutation in lung tissue is an evident effect of specific carcinogens. However, there is strong evidence that the tissue-dependent prevalence of different mutations across isoforms and at specific hotspots does not depend only on tissue-dependent mutagenesis. Rather, such prevalence for mutations could be attributed to selective pressures that might favour some mutations more than others (Cook et al., 2021; Ostrow et al., 2016; Temko et al., 2018).

These observations can be explained only partly by the effect of different mutagenic processes in different tissues. It is thus possible that different, albeit similar, mutations

might trigger subtle differences in cellular states (such as differential gene expression) that might confer tissue dependent fitness. Underpinning my work is the hypothesis that mutations alter signalling dynamics triggering different transcriptional programmes.

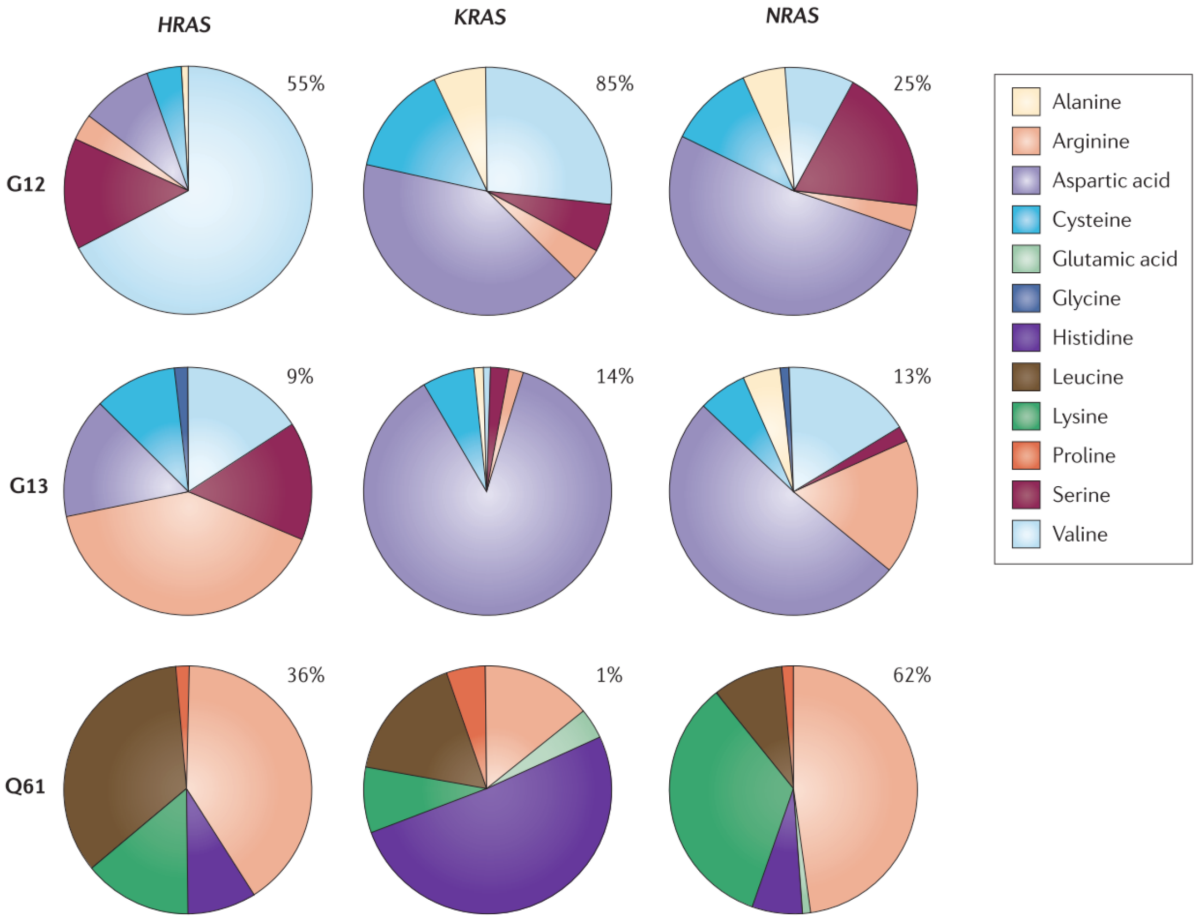

Fig. 2.2 Mutational frequencies at G12, G13 and Q61 codons of the different RAS gene isoforms. Shown percentages indicate the frequency with which the highlighted codon (left) is mutated in a given RAS isoform. Adapted from Pylayeva-Gupta et al. (2011)

2.1.3 Variable RAS Dosage

The heterogeneity in mutations in RAS isoforms across cancer types might also relate to differential expression or function. Although the isoforms' sequences closely resemble one another, what distinguishes them is the hypervariable variable (HVR) region. The HVR is subject to complex post-translational modifications (PTMs) that prime RAS proteins for organelle trafficking and membrane binding, in addition to protein level regulation (Ahearn et al., 2011). In the case of KRAS, the HVR-induced PTMs prompt it to

localise to the plasma membrane where GAPs and GEFs regulate it and where it recruits downstream RAS effectors (see (b) in 2.1). Other variables involved in the regulation of RAS protein levels include differences in promoters, splice variant expression, transcript expression (Tsai et al., 2015), translation processing (via different codon usage) (Lampson et al., 2013), untranslated regions (UTRs) (Mayr, 2017) and degradation rates (Jeong et al., 2012). All these factors contribute to the visibly wide range of RAS protein levels observed across tissues (Newlaczyl et al., 2017). Furthermore, the observed variation in the proportion of GTP-bound proteins (Killoran and Smith, 2019), as well as active RAS stability (Smith et al., 2013), are chemical factors that, together with the protein expression levels, shape the RAS 'dosage' (Li et al., 2018a; Prior et al., 2020). Different RAS-dependent signalling might then be more conducive to specific RAS-dependent functions.

2.1.4 Isoform-specific Signalling

RAS has been found to engage key effector pathways in an isoform-specific manner. In the MAPK pathway, KRAS only undergoes critical regulation by SOS2 (Sheffels et al., 2018) and preferentially binds to B-RAF over other isoforms (Terrell et al., 2019). In contrast, HRAS and NRAS are considered to more effectively activate PI3K (Voice et al., 1999; Yan et al., 1998). Haigis et al. (2008) were one of the first to demonstrate isoform-specific functions during tumorigenesis in vivo. Even with identical sequence regulation (to control for variable expression) of *HRAS* and *KRAS*, Drosten et al. (2017) and colleagues observed dissimilar oncogenic behaviour, underlining the isoform-specific functional divergence.

This distinction could be due to isoform/HVR-specific PTM-induced localisation of RAS proteins, which is instrumental for its signalling function (Willumsen et al., 1984). Moreover, there is a growing number of proteins found to interact with specific isoforms, such as calmodulin for KRAS4B (Abraham et al., 2009) and galectin 1 for oncogenic HRAS (Paz et al., 2001). However, the seemingly dispensable function of HRAS, NRAS and KRAS4a in the development of normal mice (Esteban et al., 2001; Koera et al., 1997; Plowman et al., 2003), the relatively high mRNA transcript expression levels (Newlaczyl et al., 2017) and the title of most frequently mutated isoform suggest KRAS4B may play a more prominent role in cell signalling.

2.1.5 Oncogenic KRAS Signalling

Most mutations in *KRAS* are thought to alter the rate of loading, hydrolysis and unloading of GTP to KRAS, therefore rendering KRAS active even in the absence of extracellular signals (Parker et al., 2018; Shima et al., 2010; Smith et al., 2013). Thus, the canonical interpretation of the effects of activating mutations on *KRAS* is the resulting hyperactivation of the MAPK cascade. Nevertheless, rodents and primary human cells with ectopic expression of oncogenic RAS (Bennecke et al., 2010; Serrano et al., 1997) found to have senescent phenotypes led to the idea of 'too much' oncogenic RAS signalling. Indeed, MAPK hyperactivity can be detrimental to tumour maintenance, as observed in melanoma cells with mutations in *RAS* or *RAF* (Leung et al., 2019). Multiple studies also show that mutant KRAS is, in fact, not constitutively active. In unstimulated conditions, some cell lines with mutant *KRAS* do not have particularly high levels of active KRAS (Ardito et al., 2012; Huang, 2014; Stolze et al., 2014) and downstream ERK phosphorylation (Konishi et al., 2007). However, once stimulated by upstream signals, KRAS remains active for longer periods compared to wild-type KRAS due, for example, to GAP insensitivity of the mutant form. In some cases, RAS signalling can be insufficient for tumorigenic transformation. Mice expressing *KRAS* in various tissues failed to show typical signs of cell transformation such as hyperplasia (Guerra et al., 2003).

Therefore, the depiction of oncogenic *RAS* as a simple hyper-activity of mitogenic signalling is an oversimplification and several laboratories are now trying to understand the mechanisms underpinning *RAS*-driven tumorigenesis. A new model of *RAS*-driven carcinogenesis is therefore emerging, where the mutant allele might cooperate with the wild-type, in a tissue-dependent and isoform-dependent way leading to a sweetspot (Li et al., 2018a) of oncogenic signalling. At least during early carcinogenesis, this sweetspot permits the cell to maintain high fitness in permissive tissues without triggering tumour suppressive mechanisms.

2.1.6 Mutant Specificity

In this model, the variability of hotspot mutations across tissues (i.e. G12, G13 & Q61) might be better understood. Different mutations, for example, confer KRAS with different hydrolytic and exchange rates (Smith et al., 2013). Different mutations can then result in mutation-specific phenotypes (Stolze et al., 2014) or transcriptional regulation of target genes such as doublecortin-like Kinase 1 (DCLK1) (Hammond et al., 2015), a cancer stem cell marker. More importantly, different mutations at the same codon

can provide different prognosis. For example lung tumour patients with KRAS-G12C and KRAS-G12V mutations have a worse prognosis to those with other mutants (Ihle et al., 2012). Therefore, the understanding of the pathophysiology of specific mutations is essential to improve strategies for disease management.

2.1.7 Concluding Remarks

The RAS biology covered here, although by far not an exhaustive review of all the literature, underlines the still unmet need of further defining oncogenic signalling activities that drive (or not) cancer onset and how do they maintain tumours. Different *KRAS* mutations may trigger different responses in cells.

The working hypothesis is that during carcinogenesis mutant *KRAS* alleles results in aberrant signalling dynamics corresponding to a sweetspot of oncogenesis in permissive tissues. Furthermore, as cell-to-cell variability in MAPK signalling has been widely reported (Albeck et al., 2013; Blum et al., 2019; Cohen-Saidon et al., 2009; De et al., 2020; Ryu et al., 2015), heterogeneity in MAPK signaling might also affect the plasticity and heterogenety of KRAS signalling.

Therefore, this chapter focuses on work aimed to better understand how genetic and non-genetic heterogeneity might cooperate to drive carcinogenesis in *KRAS*-driven tumours. This is an aspect of carcinogenesis that is poorly understood and often neglected despite its significant implications.

2.2 Results

To investigate cell-to-cell variability and characterise how a mutation in *KRAS* alters signaling dynamics, I set out to design an assay to yield and accurately analyse single-cell measurements of MAPK activity. After an extensive characterisation of several ERK sensors (including EKAR2G, EKAREV, EKAREN4 and EKAREN5, see suppl. Fig. 2.13), I selected EKAREN5 – a new FRET-based sensor of ERK activity that was kindly provided by Prof Hugo Snippert and Dr Bas Ponsioen (Utrecht University) (Ponsioen et al., 2021). EKAREN5's improved specificity is due to the removal of substrates targeted by CDK1 and the overall speed of response and dynamic range of the sensor is better that other sensors that had been published previously.

Therefore, with the use of transposon-mediated gene transfer, I generated stable cell lines expressing EKAREN5 (see (a) and (b) in Fig. 2.3 on the facing page). I have generated SW48 (colorectal), LIM1215 (colorectal) and HPNE (pancreatic) reporter cell lines, harbouring mutant KRAS alleles (G12A, G12C, G12D and G12V). SW48 and LIM1215 cell lines are isogenic lines of commercial origin where a single allele is mutated. HPNE cells have been engineered in-house to express doxycycline inducible KRAS mutants (also including G12R, specific to pancreatic cancer) and controls expressing inducible WT KRAS and mCherry. However, due to the complexity and ensuing long development of the experimental setup, it was decided to initially investigate two samples (out of the 30 cell lines generated); SW48 (colorectal cancer cell line) cells with ($KRAS^{wt/G12D}$) or without ($KRAS^{wt/wt}$). For simplicity, I will hereon refer to these (monoclonal) reporter cell lines as $KRAS^{G12D}$ and $KRAS^{WT}$, respectively. Of note, $KRAS^{G12D}$ cells are heterozygous and also carry a wild-type *KRAS* allele.

I also integrated a commercially available microfluidic device to our imaging platform (see (c) in Fig. 2.3) to enable computer-controlled chemical stimulation of cells. Finally, I developed a custom imaging pipeline (*PyFRET*, see Chapter 3 and (e) in Fig. 2.3) to analyse the image data generated with a widefield fluorescence microscope.

MAPK activity has previously been observed to display ligand- (EGF vs NGF) and concentration-dependent signalling activity (Ryu et al., 2015). Growth factor-based linearity and dynamics of the MAPK cascade in the context of a *KRAS* mutation was to be assessed. To do this, various physiologically-relevant concentrations of epidermal growth factor (EGF) spanning up to a 500 fold change difference between the lowest (0.1 ng/ml) and highest (50 ng/ml) concentration were used. The experimental imaging

protocol involved four separate stages; **adaptation** (6 hours), **EGF treatment** (3 hours), **ERK inhibiton** (1 hour) and **wash** (2 hours) (see (d) in Fig. 2.3).

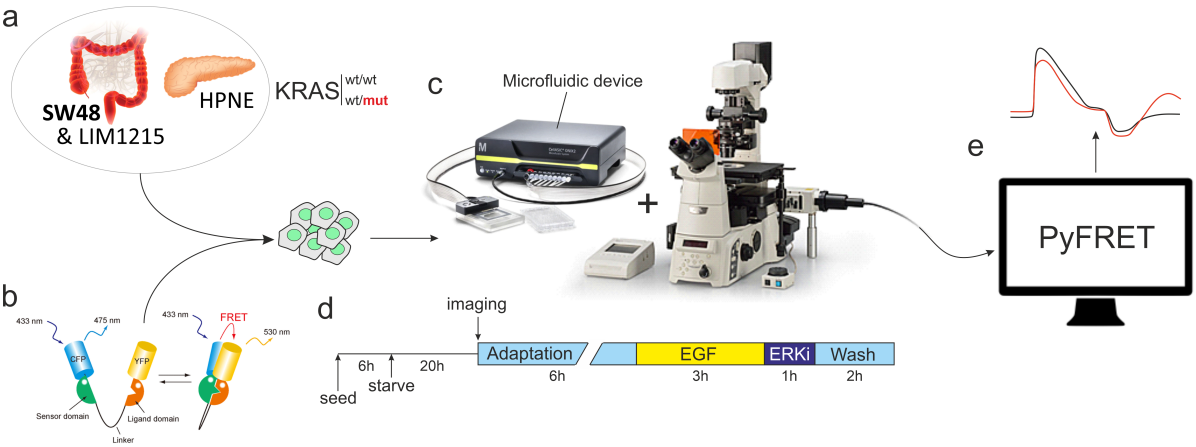

Fig. 2.3 Experimental platform for single-cell imaging assays. Three cell lines with different *KRAS* mutations (a) are used as a clinically-relevant model for studying single-cell dynamics. These cell lines stably express an ERK FRET sensor (b, illustration from Komatsu et al. (2011)). A microfluidic device and fluorescence widefield microscope (c) are used to record timelapses of cells under a dynamic protocol (d). Finally, images are processed by *PyFRET* to yield single-cell data.

Cells respond to mechanical stress induced by flow. Therefore, cells are left to adapt to flow for six hours similarly to Ryu et al. (2015). This time lag was selected through preliminary long experiments executed to exclusively assess flow-based adaptation time of cells. Once adapted, cells are then stimulated with an identical and constant flow of EGF for 3 consecutive hours to measure the EGF response and the following desensitisation. After stimulation, cells were treated with the ERK inhibitor SCH227984 (ERKi) to acquire the nominal null activity of ERK as a reference. ERKi was used at the concentration of 500 nM, determined by the manufacturer guidelines and a titration-based experiment (see suppl. Fig. 2.14 on page 68). Finally, ERKi is washed-off with fresh imaging media for a further 2 hours, again with constant flow, to assess the return to basal ERK activity as a mean to control for possible artefacts. For better representation, the first 5 hours of the adaptation phase are not shown in the figures. In this work, I present relative activity of ERK as r(t), i.e. the background-subtracted YFP/CFP intensity ratio to which the minimum ratio measured during ERKi is further subtracted (see materials and methods).

2.2.1 Mutant *KRAS* cells display specific signalling dynamics

In all EGF-treated conditions, on average, $KRAS^{WT}$ cells reach a peak relative ERK activity of approximately >1.0. After reaching peak ERK activity, cells follow a pattern that is either rather sustained or adaptive (reaching a stable activity) when treated with lower (0.1 ng/ml, 0.5 ng/ml and 1 ng/ml) or higher (10 ng/ml and 50 ng/ml) concentrations of EGF, respectively. Interestingly, in all EGF-treated conditions, intercellular $KRAS^{WT}$ variability greatly increases 1 hour after EGF treatment, as inferred from the rise of the standard variation (see Fig. 2.4 on the facing page). This variability remains relatively high until ERK inhibitor is administered, suggesting the presence of subpopulations with different ERK activity patterns.

On average, cells reach a peak ERK activity $r_{peak} = 1.008 \pm 0.003$ ($n = 3230$) for all EGF concentrations tested relative to a basal $r_{basal} = 0.166 \pm 0.002$ ($n = 4556$). After the peak, cells exposed to EGF are known to desensitise. However, at EGF concentrations higher than 1 ng/ml, cells desensitise to reach a plateau at $r_{plateau} = 0.298 \pm 0.006$ ($n = 1100$) after 1.5 hours, while at lower EGF concentrations cells exhibit a slower desensitisation thus resulting in a more sustained response. At around the same time of 1.5 hours, in all EGF-treated conditions, cell-to-cell variability in cells increases significantly as denoted from the rise of the standard deviation (see Fig. 2.4 on the next page). This variability remains relatively high until ERK inhibitor is administered, suggesting the presence of subpopulations with different ERK activity patterns. In the presence of ERKi and with the subsequent media wash, cells homogeneously exhibit an $r_{wash} = 0.179 \pm 0.004$ ($n = 3230$), similar to r_{basal}.

In contrast, mutant cells exhibit a rather homogeneous response both to EGF concentrations and over time. Unsurprisingly, mutant cells exhibit a higher basal activity $r_{basal} = 0.296 \pm 0.002$ ($n = 4785$) compared to wild-type cells, but they reach only average peak values $r_{peak} = 0.890 \pm 0.003$ ($n = 3591$). Also, cells respond with a lower peak value for the lowest EGF concentration of 0.1 ng/ml but show no differences in the speed of desensitisation, reaching an $r_{plateau} = 0.349 \pm 0.008$ ($n = 609$), similar to r_{basal}. Unexpectedly, after ERKi treatment $KRAS^{G12D}$ cells do not just reach basal level again but overshoot this value ($r_{wash} = 0.428 \pm 0.003$ ($n = 3591$)) to relative ERK activities similar to those of $r_{plateau}$ of wild-type cells. Mutant cells that have not been pre-treated with EGF (i.e. *control* cells) also exhibit this post-inhibition rebound but in a more pronounced and faster way (see Fig. 2.5 on page 44). Thus, the presence or absence of EGF prior to ERK inhibition clearly affects how cells respond during the washing sequence of the experiment. Variability in mutant cells remains relatively stable

($\sigma \approx 0.11$) during the phases where ERK inhibitor is not present. Finally, untreated cells show a minimal but visible increase in ERK activity at the start of the treatment sequence. This suggests that mutant cells are more sensitive to mechanically-induced stimulation than their WT counterpart.

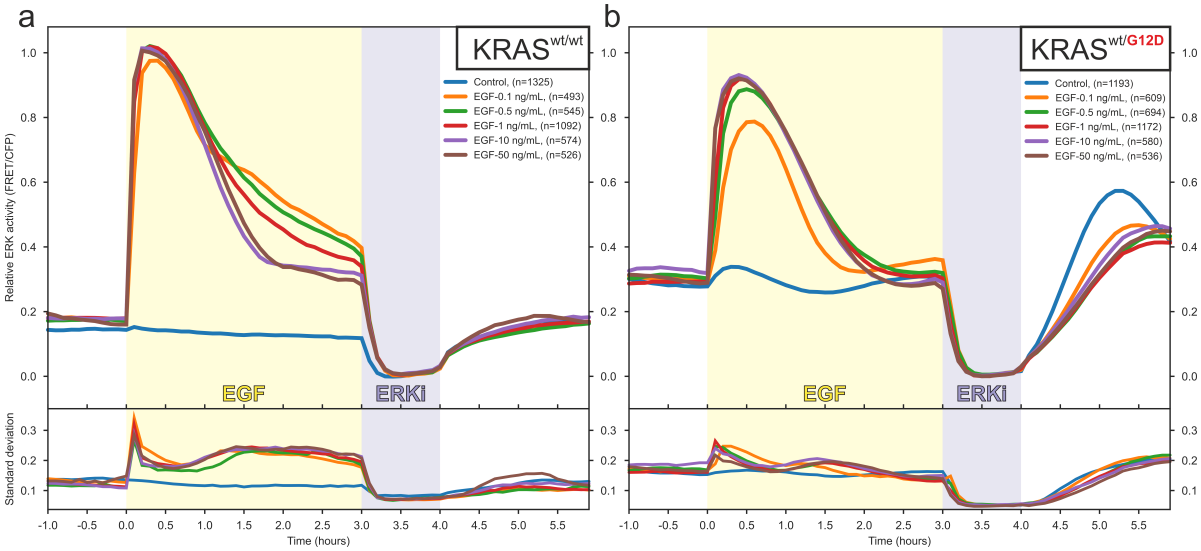

Fig. 2.4 Shown is the relative ERK activity of $KRAS^{wt}$ (a) and $KRAS^{G12D}$ (b) in response to various concentrations of EGF. Each activity curve represents mean single-cell data (cell number shown in brackets) culled from three identical repeats, except for *Control* and *EGF-1ng/mL*, of which the conditions were replicated in a total of 6 experiments. Below is the standard deviation as a measure of variability.

Figure 2.5 on the next page summarizes various statistical features of $KRAS^{WT}$ and $KRAS^{G12D}$ cells. For example, in addition to differences in peak amplitude (see (c) in Fig. 2.5), mutant cells show a concentration-dependent ERK rise to peak. Rate differences are quantified in (b) of Figure 2.5 as derivatives of r(t). $KRAS^{WT}$ cells exhibit a very similar $r'(t_{peak}) \approx 0.4$ whereas mutant cells only reach a maximal derivative of 0.3 with the top three EGF concentrations (50,10 and 1 ng/ml). Moreover, this results in delayed (>20min after EGF) maximal activity of ERK in mutant cells, whereas $KRAS^{WT}$ cells consistently reach peak ERK activity within 20 minutes from exposure to EGF (see suppl. Fig. 2.15).

The differences in concentration-dependent ERK deactivation dynamics seen in Figure 2.4 for the wild-type cells is evident from r'(t) values plotted between 30' to 3hrs post treatment (see (d) in Fig. 2.5). To high EGF concentrations correspond the highest deactivation rate reaching a value of ≈ -0.06 with quick adaptation (near-zero derivative or flat curve). To low EGF concentrations correspond slower and smaller responses with the largest r'(t) values of about ≈ -0.05, similar to $KRAS^{WT}$ cells treated with low EGF

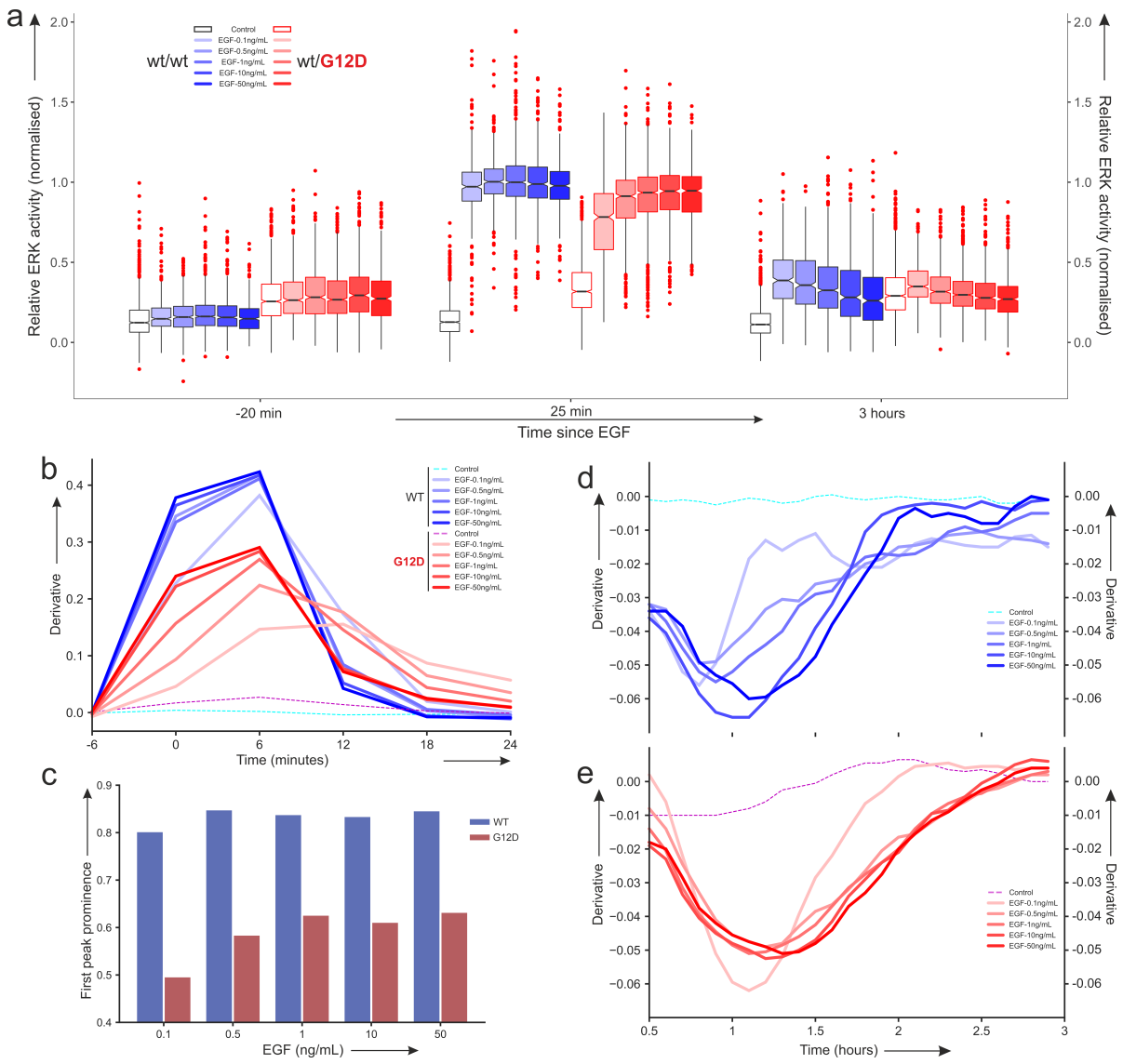

Fig. 2.5 The population distributions of ERK activity at key experimental timepoints – namely baseline, response peak and sustained activity – are shown in (a). $KRAS^{G12D}$ cells show concentration-dependent ERK activation kinetics (b) and amplitude response (c). $KRAS^{WT}$ cells show linear-type deactivation kinetics (d) but not mutant cells (e). Data shown in this figure is representative of $n = 3$ for all conditions except for control & EGF 1 ng/ml which were replicated in $n = 6$ experiments. In boxplot (a), the notch with a dark line represents the median, the top and bottom edges of the box represent the 75th and 25th percentile, the error bars represent values within 1.5 of the interquartile range (IQR) and the red dots are the outlier values above 1.5 IQR. Total cells analysed (including all EGF conditions and both $KRAS^{WT}$ and $KRAS^{G12D}$ cells) are n= 2518.

concentrations but with an overall slower decay (see (d) in Fig. 2.5). Interestingly, the deactivation kinetics of $KRAS^{G12D}$ cells treated with EGF 0.1 ng/ml (the only condition that yields a different profile) resemble most those observed in $KRAS^{WT}$ cells when treated with high EGF concentrations (10 ng/ml and 50 ng/ml) (see (d) and (e) in Fig. 2.5). The faster deactivation rate – suggesting the presence of a stronger negative feedback in mutant cells – results in a shorter ERK pulse akin to the proliferative-type of activity profile in KRAS wild-type cells induced by high EGF concentrations. This observation potentially designates mutant cells' preference for low EGF stimulation, as the signalling dynamics may lead to enhanced promotion of transcription of target genes involved in proliferation.

Correlation analysis of signalling features

A clear feature that might have clinical relevance is that the baseline KRAS activity in the presence of an oncogenic mutation is higher than the wild-type. It was hypothesized that the higher background activity seen also with the ERK sensor might induce cells to adapt to avoid detrimentally high oncogenic signalling. To test this hypothesis, the cell-to-cell variability in background signaling was exploited and checked if basal ERK activity might predict ERK responses.

The linear correlation between baseline magnitude and the cells' respective response amplitude (i.e. the difference between a cell's maximal and baseline ERK activity values) was measured. The graphs in (a) of Figure 2.6 on the following page show two examples of correlations in two EGF concentration conditions (one low, one high). In both cases, wild-type cells broadly display a larger amplitude than mutant cells – as already described in Fig. 2.5. Moreover, for both genotypes the linear correlation is negative, suggesting the higher a cell's baseline activity the smaller the peak amplitude will be. However, the correlation is stronger (i.e. more negative) in $KRAS^{G12D}$ cells. Thus, mutant cells have a more pronounced decrease in peak amplitude with increasing baseline activity, when compared to $KRAS^{WT}$ cells. This correlation is observed for all other EGF treatment conditions (see suppl. Fig. 2.16 on page 69).

To substantiate this observation with a quantitative analysis, I performed Pearson correlation analysis of signalling features. I analysed single-cell traces to describe them with the following features (see (b) in Fig. 2.6):

- Number of peaks (α): although the average responses exhibit one peak after EGF stimulation, individual traces might exhibit multiple peaks.

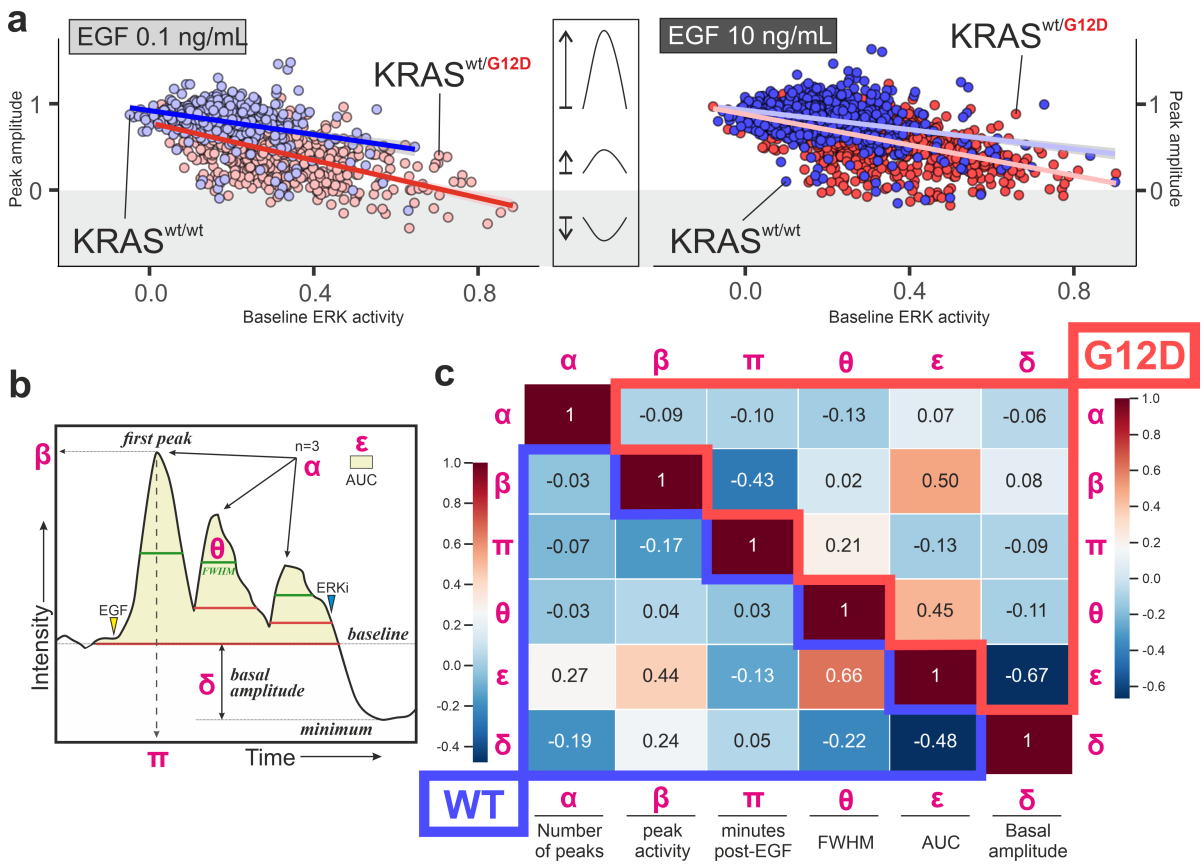

Fig. 2.6 Scatter plots of single-cell data on the relation between baseline activity and EGF response amplitude (a). Symbols illustrated between both dot plots are a schematic representation of the amplitude of a cell according to a data point's y axis position. The arrows indicate whether the amplitude of a cell is an increase (up) or decrease (down) in signal activity. Using Pearson correlation, specific signalling activity features (b) are associated with one another in $KRAS^{WT}$ and $KRAS^{G12D}$ cells (c).

- Peak activity (β): the maximal ERK activity in an EGF-induced response
- Minutes post-EGF (π): the time a cell need to reach maximal amplitude.
- Full width at half maximum (FWHM, ϕ): the width (time difference) of a response curve at half its amplitude
- Area under the curve (AUC, ϵ): the area between the response curve and the baseline level, starting from the time of EGF stimulation to the start of ERKi treatment. In other words, AUC is the cumulative ERK activity post-stimulation.
- Basal amplitude (δ): the difference between baseline activity and minimum ERK activity.

It can observed that a number of obvious correlations such as the peak activity (β) and area under the curve (AUC, ϵ) and generally correlations between features are similar across cell lines. However, there are also correlations that exhibit a different strength in different genotypes.

There is a very strong negative correlation between basal amplitude and AUC from which it can be inferred that -– irrespective of genotype -– those cells that have a higher steady-state ERK activity have more restrained dynamics after EGF stimulation resulting in a 'lower signal'. Furthermore, the peak activity (β) is negatively correlated with the time when ERK activity reaches its peak (π), particularly in mutant cells. This observation suggests that cells that exhibit a lower peak also reach it slower, and so at later times.

Taken together, the data suggest that cells with higher basal steady state ERK activity respond less and slower to extracellular stimuli. In agreement with this observation, mutant cells – exhibiting high basal activity – still respond to EGF but to a lower extent and with a lower speed.

2.2.2 Corrupt MAPK negative feedback in mutant *KRAS*

After $KRAS^{G12D}$ cells have been treated with an ERK inhibitor, their ERK activity 'overshoots' their respective baseline levels (see right panel of Fig. 2.4 on page 43). This rebound effect peaks ≈1.5 hours after the inhibitor is washed away. Control cells not treated with EGF exhibit the strongest and fastest rebound whilst EGF-treated cells showing a milder and slower rebound activity with increasing EGF concentrations (see

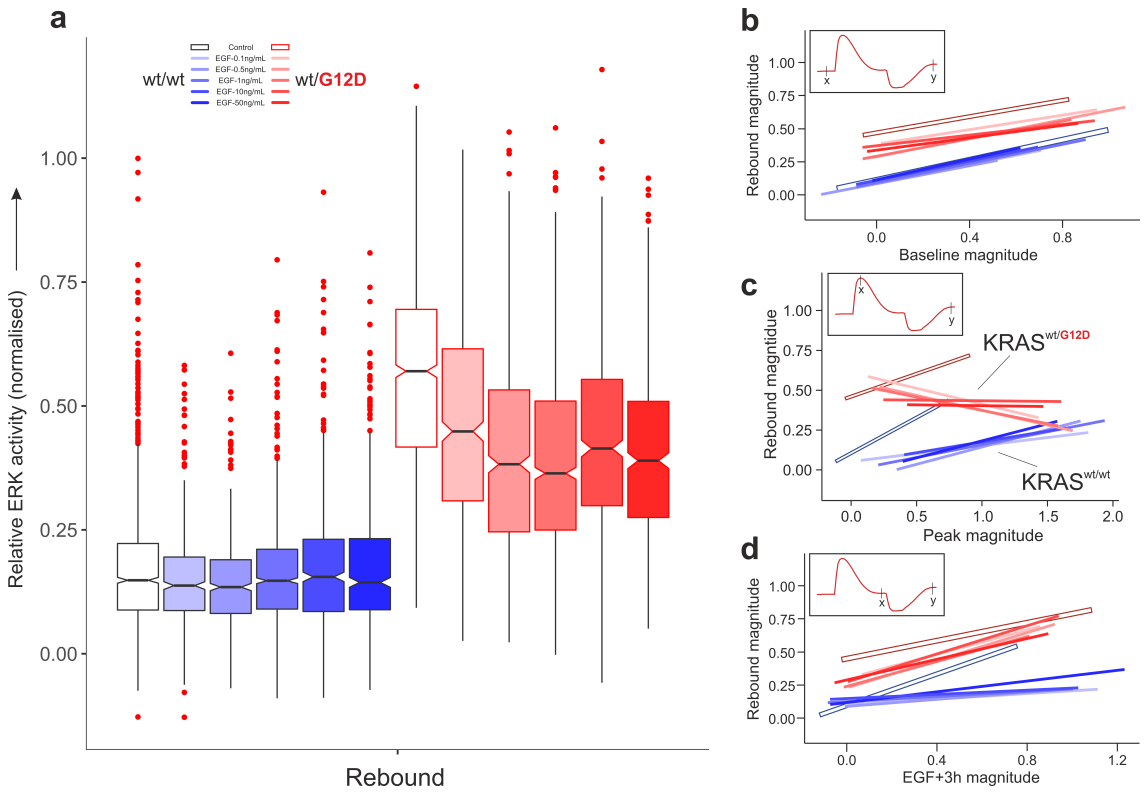

Fig. 2.7 Distribution of all conditions in both genotyopes (a) show the stark difference in ERK activity 1.5 hours after ERK inhibitor is removed – value designated as 'rebound' (normalised ratio of YFP/CFP, see section 2.4.7 for further details). The notch represents the median, the box represents the interquartile range (IQR), whiskers represent values within 1.5 IQR and red dots are outlier data points beyond 1.5 IQR. Scatter plots show differing linear correlations between baseline (b), peak (c) and sustained (EGF+3h, d) and rebound activity. Subplots in (b-d) are a representation of the activity plotted in the x axis (x) and y axis (y, rebound). Single-cell data points have been omitted for clarity.

(a) in Fig. 2.7 on the preceding page). This response is very distinctive and absent in $KRAS^{WT}$ cells that return to baseline ERK activity irrespective of EGF stimulation.

It was hypothesized that during the ERKi phase, negative feedbacks that might restrain MAPK signalling are no longer enforced and that when ERKi is removed mutant cells might temporarily overshoot baseline level until the MAPK network readapts. Evidence of desensitisation and resensitisation was tested by investigating correlations between ERK activities before and after ERKi (see (b-d) in 2.7). Positive linear correlations of the rebound magnitude with baseline and sustained (EGF+3hrs) activities (see (b) & (d) in 2.7) can be observed. However, these correlations are similar between genotypes.

Interestingly, there is a $KRAS^{G12D}$-specific EGF concentration-dependent correlation between peak magnitude and rebound magnitude. Contrarily to wild-type *KRAS* cells, mutant cells that respond strongly to low EGF concentrations exhibit a low rebound but cells that have modest responses to EGF exhibit a larger rebound effect. This negative correlation between peak response and rebound magnitude disappears when cells are treated with high EGF concentrations (see (c) in 2.7).

This was taken as evidence that mutant cells have an adaptive MAPK pathway in conditions of low extracellular stimuli that restrains activity of highly responsive (sensitive) cells and loosens regulation on moderately responsive (insensitive) cells.

To further validate the observed rebound activity, it was decided to replicate the protocol outlined in (d) of Fig. 2.3 on page 41 and read out protein activity via Western blot (see (a) in Fig. 2.8 on the next page). EGF 100 ng/ml was used in order to exaggerate the phenotype previously observed; rebound activity is high in untreated cells but much decreased when pre-treating cells with EGF (more so in high concentrations). Unexpectedly, 30 minute DMSO treatment resulted in an activation of p-/t-ERK in both genotypes. Quantification of p-/t-ERK (see (b) in Fig. 2.8) suggests there is a 'rebound' activity. However, presence or absence of pre-EGF treatment did not make a difference. Although the phenotype in this case is not significant, it remains $KRAS^{G12D}$-specific.

Because p-/t-ERK does not represent ERK activity (as does the FRET sensor) per se, but rather the pool of active ERK molecules, CDC25C was probed as a surrogate measure for ERK activity. CDC25C was specifically chosen as, in addition to being a direct target of ppERK, a specific region of its genetic sequence containing a known ERK target (Threonine 48) was integrated in the FRET sensor to act as a substrate

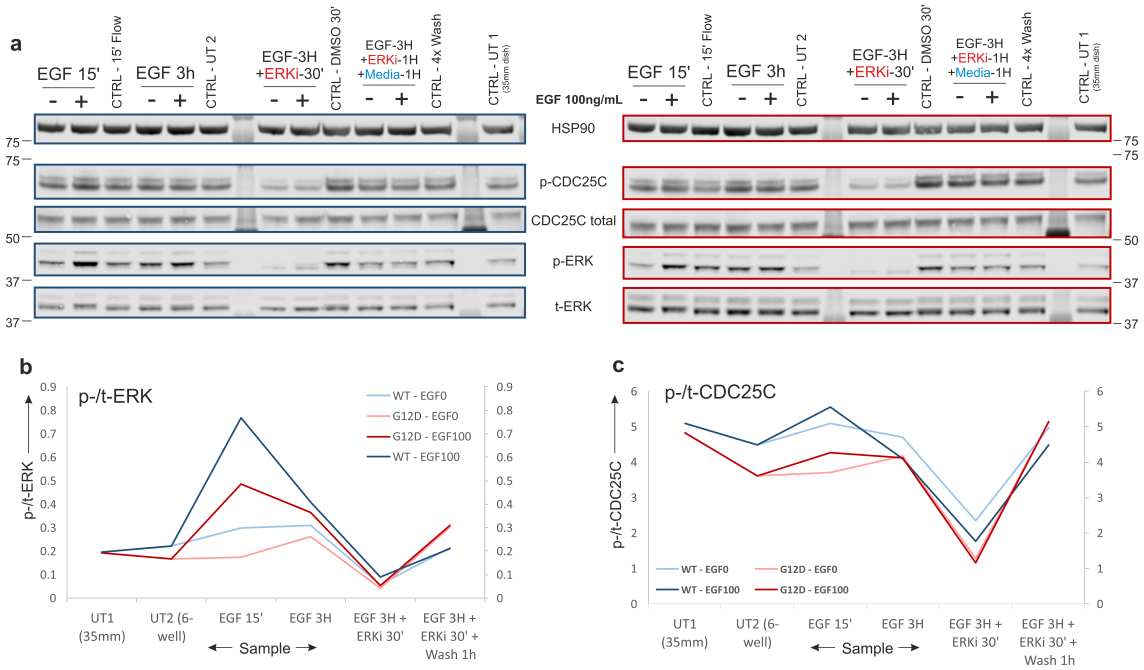

Fig. 2.8 Western blot (a) probing of relevant proteins ERK (b) and CDC25C (c) confirm the 'rebound' effect seen in previous imaging experiments, albeit not as strongly. Both $KRAS^{WT}$ (left) and $KRAS^{G12D}$ (right) cells were treated with or without EGF (100 ng/ml). $n = 1$

region. Active CDC25C levels broadly replicate those of active ERK (see (c) in Fig. 2.8). However, the levels of active CDC25C in mutant cells at the 'rebound' timepoint (i.e. 1 hour after ERK inhibition) are in fact higher than those 15 minutes after EGF treatment, contrarily to $KRAS^{WT}$ cells which do not overshoot baseline CDC25C levels. One of the control samples (UT1) does show higher active CDC25C levels than the response to EGF in mutant cells, but is still surpassed by the rebound activity levels.

As part of a wider effort to characterise the effects of mutations at the G12 codon of *KRAS*, our laboratory has carried out extensive characterisation of the isogenic panels of cells with RNA sequencing and metabolomics. To identify plausible mechanisms that might underpin the adaptive feedback previously described, RNA sequencing data was used to compare the parental (i.e. cells without the sensor) mutant and wild-type cells to perform gene enrichment and expression analysis (see Fig. 2.9 on the facing page). A number of signalling pathways are differentially regulated in mutant cells, of which a select few signalling pathways are significantly downregulated (Hippo, Wnt, and mTOR) and upregulated (MAPK and FoxO). Within the differentially regulated RNA transcripts in $KRAS^{G12D}$ cells, several of these are related to MAPK signalling regulation and

negative feedback loops. For example, dual specificity phosphatases (DUSPS) are known targets and negative regulators of ERK. Interestingly, DUSPS 6 and 19 are shown to be upregulated in mutant cells whereas DUSP8 is downregulated. Of these, DUSP6 is known to reside in the cytoplasm whereas DUSP8 is located in both cytoplasmic and nuclear compartments (Huang, 2009; Kidger and Keyse, 2016). Sprouty 4 (SPRY4) – another ERK inhibitor – is upregulated in mutant cells whereas another sprouty protein (SPRY1) is downregulated. Lastly, MAP3K1 (also known as MEKK1), a less common MEK kinase (Caunt et al., 2015) is upregulated as well.

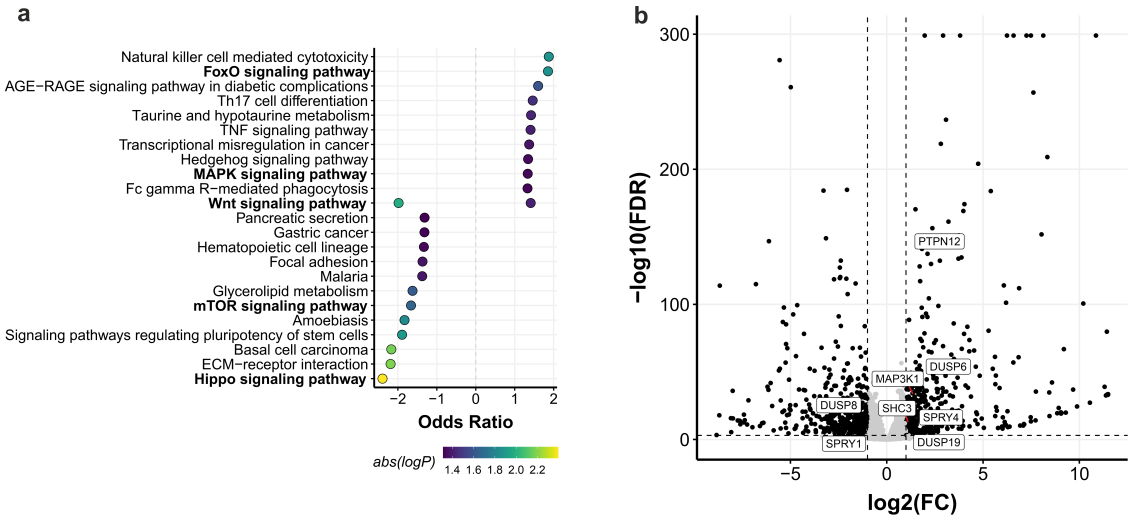

Fig. 2.9 Gene enrichment analysis from RNA sequencing data shows differential regulation of a number of genes involved in signalling pathways and tumours (a). Moreover, among the differentially regulated genes, several of these are involved in MAPK activity control (b).

Although the relevance of these genes in the observed signalling dynamics are yet to be confirmed, they pose a plausible class of proteins that will be assessed in upcoming experiments.

2.2.3 Hierarchical clustering reveals a mutant-specific phenotype

It is to be noted that the scatter of cell responses changes during different stages of the single-cell assays. Also previously highlighted is the existence of correlations between features of single-cell dynamics that are similar between genotypes or distinctive of the RAS mutant cell line. Fig. 2.10 on page 53 illustrates a density plot of all traces discussed so far that reveal the vast cell-to-cell variability in biochemical responses.

To better quantify the cell-to-cell variability of genetic and non-genetic origin affecting KRAS signaling, hierarchical clustering (see (a) in Fig. 2.10) of all single-cell signalling profiles was performed using the Time Course Inspector tool developed by Dobrzyński et al. (2019). The data seems to be best described by a total of 7 clusters representative of responses that are somewhat simple to interpret (see (b) in Fig. 2.10 on the facing page):

- Cluster 1 | non-responding cells with high baseline activity (≈0.25)
- Cluster 2 | non-responding cells with low baseline activity (≈0.10)
- Cluster 4 | transient responders with low ERK amplitude (≈0.40) and comparatively faster desensitisation (≈2hr post-treatment)
- Cluster 5 | transient responders with large peak amplitude (≈0.75) and FWHM resulting in desensitisation at ≈2.5hrs post-treatment
- Cluster 6 | transient responders with a large peak amplitude – similar to Cluster 5 – but with a smaller FWHM resulting in the return to baseline activity similar to Cluster 4.
- Cluster 3 | sustained responders – i.e. cells that cannot return to baseline activity spontaneously before the ERKi treatment – with a strong peak amplitude (≈1.2)
- Cluster 7 | sustained responders with lower amplitude (<1.0) than Cluster 3.

Panel (c) in Figure 2.10 shows how each cluster represents experiments at different EGF concentrations and different genotypes. Cluster 2 represents cells with low baseline activity and no response, which are present only in mock-treated *KRAS* wild-type cells (≈55%). Similarly, cluster 1 represents the higher baseline activity of untreated control $KRAS^{G12D}$ cells. However, it was observed that ≈40% of the wild-type phenotype exhibits also a higher baseline activity. The transient and modest response shown by Cluster 4 is visible only in $KRAS^{G12D}$ cells, with a prevalence decreasing from ≈50% to 20% at increasing EGF concentrations. The faster and more robust response depicted by Cluster 6, conversely, titrates from ≈30% to 50% with increasing EGF concentrations in cells of both genotypes. The intermediate phenotype described by Cluster 5 is also prevalent in equal proportions between wild-type and mutant cells. Finally, the sustained responders described by Clusters 3 and 7 are mostly present in wild-type cells, except for ≈20% prevalence of Cluster 7-like phenotype in treated mutant cells.

This cluster analysis shows that $KRAS^{G12D}$ cells still respond to extra-cellular signalling but in a more modest, slower, and faster to desensitise manner.

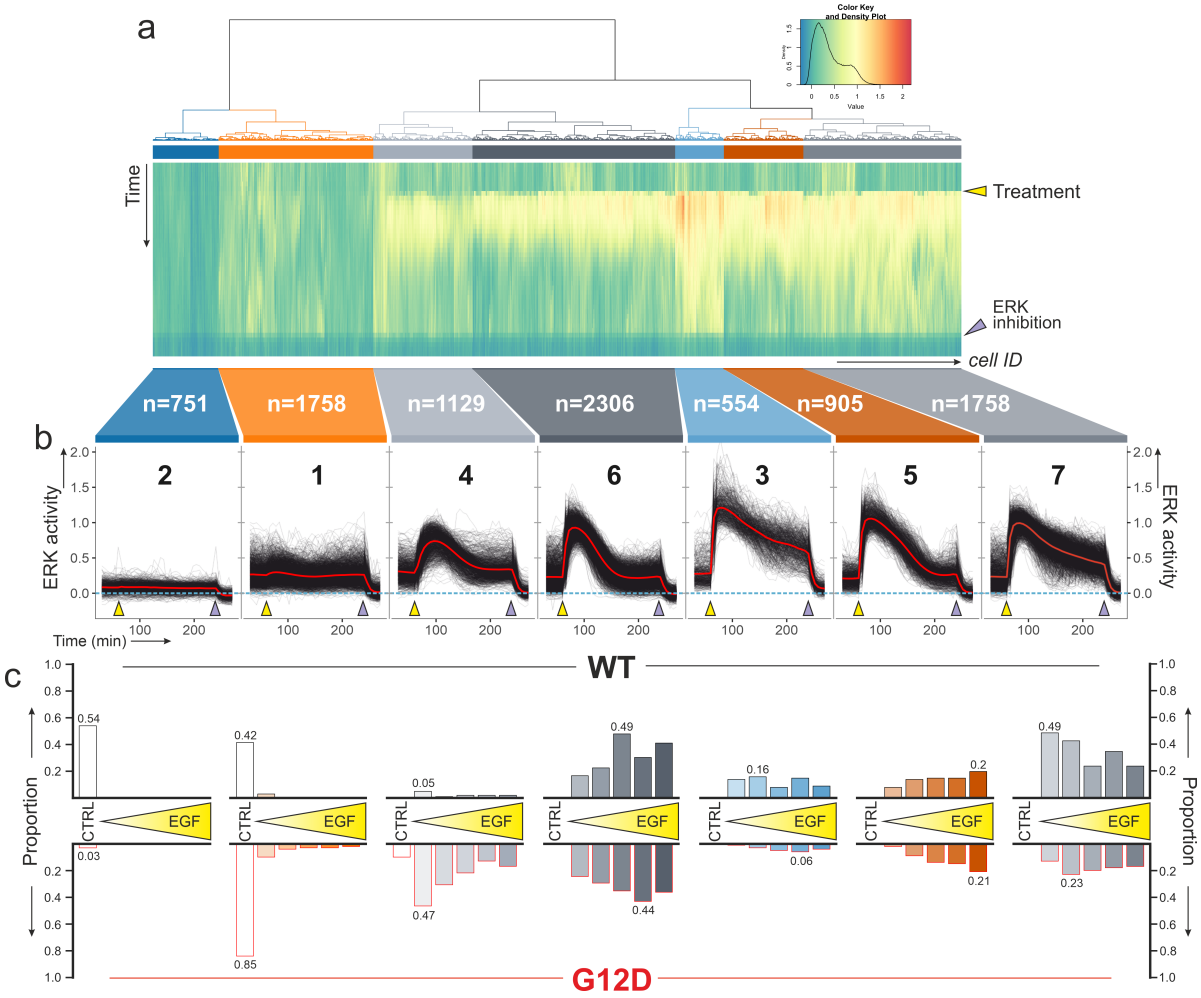

Fig. 2.10 Hierarchical clustering of all curated single-cell tracks are represented as a dendogram (a). Individual clusters are shown as time series plots of single cell curves and the respective mean in red (b). Panel (c) shows the distribution of every cluster for each experimental conditions tested and for each genotype (top: $KRAS^{WT}$, bottom: $KRAS^{G12D}$). The horizontal triangle with a yellow colour gradient is representative of the EGF concentrations tested, namely 0.1, 0.5, 1, 10, and 50 ng/mL. The horizontal line in panel (b) designates an ERK activity of 0. CTRL: control.

2.3 Discussion

Mutant *KRAS* has long been implicated in carcinogenesis and it is a major driver of clinical relevance. We have a good understanding of the GTP and GDP cycling of KRAS and how oncogenic *KRAS* mutations alter KRAS activation. Yet, oncogenic *KRAS* can stimulate proliferation, EMT, stemness but also cell death and senescence; it drives tumorigenesis but it is also found in healthy tissues; as a potent driver of proliferation, it should unbalance homeostasis in any tissue but it does so only in specific ones; all oncogenic mutations increase KRAS activation but the prevalence of different mutations varies across tissues. In fact, we have a rather incomplete understanding of the biochemical mechanisms underpinning KRAS-driven carcinogenesis, limiting our capability to diagnose early and manage effectively KRAS-driven cancers. While studying less characterised aspects of genetic heterogeneity, this work also investigates cell-to-cell variability of non-genetic origin – an aspect increasingly recognised as a key contributor to both tumour maintenance and resistance to chemotherapy although scantly studied.

In this chapter I have shown how MAPK activity is altered by a single *KRAS* point mutation (G12D) establishing a platform for single-cell biochemical imaging that integrates a state-of-the art FRET probe for ERK activity, microfluidics for the tritration of EGF and inhibitors, and image analysis.

In summary, $KRAS^{G12D}$ cells exhibit a higher baseline activity and dampened maximal peak amplitude. Different EGF concentrations affect the amplitude, speed and desensitisation of $KRAS^{G12D}$ and $KRAS^{WT}$ cells differently. Western Blotting analysis shows that cells with a heterozygous mutation in *KRAS* display a rather mild background activation of the MAPK pathway and a robust response to EGF stimulation (see suppl. Fig. 2.19 on page 72). This observation suggests that wild-type and mutant *KRAS* cooperate to maintain cells responsive to environmental cues. However, single-cell data investigated through correlation analysis and hierarchical clustering reveals that mutant cells exhibit milder and slower responses, desensitise faster during prolonged exposure to EGF, and display a strong rebound response after ERK inhibition.

The decreased maximal response amplitude and higher basal activity in mutant cells are signalling features that have been replicated in our laboratory. For example, the panels (a-b) in Figure 2.11 show how several cell lines with wild-type *KRAS* and different *KRAS* mutations (G12A, G12C, G12D and G12V) respond to EGF (100 ng/ml), analysed by flow cytometry by Dr. Suzan Ber. Mutants display differential baseline but also response to EGF. The higher baseline activity in $KRAS^{G12D}$ cells could be directly

attributed to the mutant *KRAS*, which may constitutively activate the MAPK pathway. It is worth pointing out that mutant SW48 cells are heterozygous, meaning they still express wild-type *KRAS* but at half the levels than those in cells carrying homozygous wild-type *KRAS*. The heterozygosity could partially explain the dampened maximal amplitude response observed, since the pool of readily available *KRAS* – and thus the stimulus-response capacity – is much reduced.

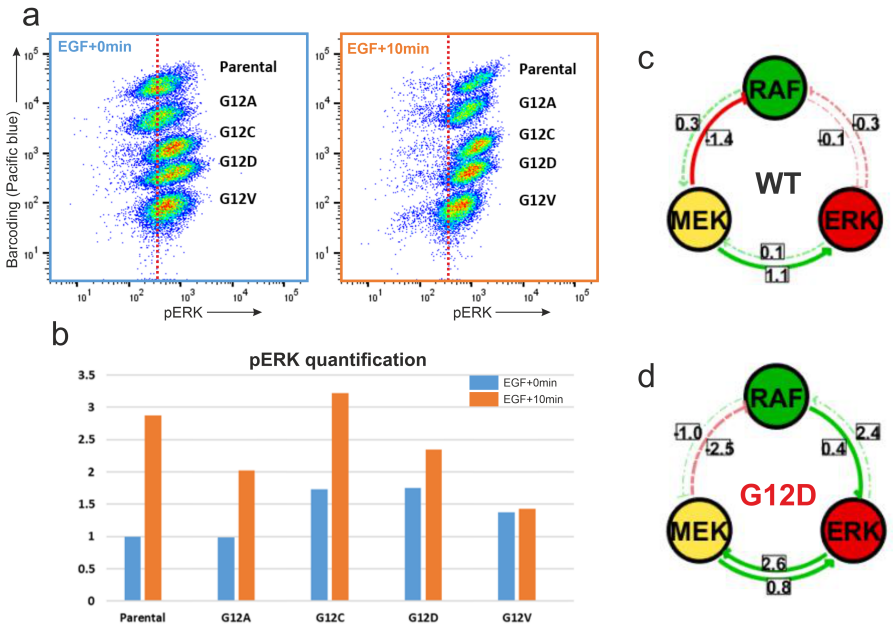

Fig. 2.11 Signalling characteristics of $KRAS^{G12D}$ cells are replicated in other assay types. Parental and mutant SW48 cells are treated in suspension with EGF (100 ng/ml). Barcoding the samples with Pacific Blue dye allows flow cytometry-based analysis (a) of phosphorylated ERK, of which a quantification is also shown (b). Modular Response Analysis (MRA) of SW48 mutant cells show a strong MEK to RAF negative feedback present after 5min treatment with EGF (100 ng/ml). Dashed lines in (a) have been manually drawn to represent parental cell response (as a reference). Flow cytometry data (a, b) was kindly provided by Dr Suzan Ber. MRA data (c, d) was kindly provided by Ms Khushali Patel.

Taken together, it is hypothesised that in the presence of an overactive KRAS, cells trigger negative feedback mechanisms to compensate for the higher basal ERK activity.

It is noted that *KRAS* dependent signalling is indeed highly plastic accounting for the many difficulties of drugging targets downstream of *KRAS*. As a team-wide effort to identify how *KRAS* mutations rewire biochemical networks, another PhD student in the same laboratory – Ms Khushali Patel – has used a population-based systems-biology approach to characterise feedback mechanisms within the MAPK pathway. The use of Modular Response Analysis (MRA) – technique originally developed by Kholodenko et al. (2002) – revealed a mutant-specific negative feedback loop from ERK to RAF (see (c-d) in Fig. 2.11) that might explain the observations previously made. MRA was performed in SW48, LIM1215 and doxycycline-inducible HeLa CCL2 KRAS cells. Although MAPK wiring changes between cell types, *KRAS* mutant cells invariably show the appearance of altered negative feedbacks.

Commonly known proteins involved in the dampening of ERK activity are dual-specificity phosphatases (DUSPS) and sprouty (*SPRY4*). The former directly dephosphorylates ERK after being transcribed by the same protein (Lavoie et al., 2020). DUSP6 in particular has been found to be upregulated in lung tumour cells with *EGFR* or *KRAS* mutations (Unni et al., 2018). Although DUSP6 is found to be upregulated in our mutant cells, its higher expression cannot account for dampened nuclear ERK activity since it resides in the cytoplasm, unlike our nuclear ERK FRET sensor. On the other hand, SPRY4 depletes the pool of active RAS-GTP molecules by stimulating neurofibromin 1 (NF1), a GTPase activating protein (GAP) (Lavoie et al., 2020). Given that the latter is also upregulated in mutant cells, it is plausible that it may play a bigger role in the deactivation kinetics than in wild-type cells as a protective mechanism (to prevent hyperactivity). This could also be due to a loss of the positive feedback loop via protein kinase C (PKC), known to prolong ERK activity (Bhalla et al., 2002).

Although not proven yet, it is speculated that the unexpected ERK activity rebound behaviour is a transient relaxation of this bona fide negative feedback of mutant cells during ERKi treatment. In the absence of MAPK signaling, cells might respond to restore an optimal level of mitogenic signaling. This relaxation is enabled by ERK inhibition which would prevent ERK-induced direct activation of negative feedback regulators and their transcription. Moreover, during the same time period of ERK inhibition, proteases and degradation mechansims may deplete negative regulators of ERK, thus priming cells for temporary overriding of the relatively stringent negative feedback regulation. However, specific DUSPS such as DUSP8 – an ERK phosphatase residing in both cytoplasmic and nuclear compartments – is shown to be downregulated in our SW48 mutant cells (see (b) in Fig. 2.9 on page 51). Therefore, dampened levels of this negative ERK regulator could

have additive effects on the ERK rebound activity behaviour. Curiously, this phenotype is pronounced only in control cells and is rather subtle in mutant cells pre-treated with EGF. A possible explanation to the effects induced by EGF pre-treatment is the ligand-induced internalisation of EGF receptors – another mechanism of ERK deactivation (Bergeron et al., 2016). Control mutant cells may experience much less receptor internalisation and consequently be more sensitive to extracellular stimuli inducing receptor activation.

Although there are currently no treatments specifically targeting *KRAS* G12D mutations, cancer patients suffering the genetic aberration still follow standard treatment strategies for their respective tumour. Because of the difficulty in designing drugs that effectively target mutated *KRAS*, the inhibition of the MAPK pathway has been proposed as an alternative treatment strategy (Moore et al., 2020). Our results indicate that mutant cells transiently treated with ERK inhibiton result in MAPK over-activity which may lead to further cell proliferation, depending on drug administration. Therefore, a temporarily relaxed negative feedback is of significant clinical relevance.

2.3.1 Conclusion

Taken together, the presented data shows that mutant cells have a similar yet subtly different signalling profile to wild-type cells allowing them to potentially better tolerate extreme stimuli (such as chemotherapeutic treatments) and foster high MAPK activity levels that favour a proliferative state.

Assessment of downstream MAPK targets (such as transcript levels of MAPK-regulated genes) and association of the characterised signalling profiles to particular cell fates would further elucidate our understanding of cancer development and better inform current treatment strategies for the management of tumours with G12D mutations in KRAS.

2.3.2 Limitations of this study

Although panels of stable cell lines expressing EKAREN5 and different *KRAS* mutations were prepared, because of the lockdown and faults of the microfluidic setup, experiments could only be executed in SW48 cells, $KRAS^{WT}$ and $KRAS^{G12D}$. The results are therefore, at this stage, very interesting from the perspective of a single-cell system-level characterisation of *KRAS* mutations but not possible to generalise. With the use of the resources I have developed so far, however, it will be possible to investigate the effect of

KRAS mutations in different genetic backgrounds (for example in the colorectal tumour LIM1215 lines, and the non-transformed pancreatic HPNE lines).

The FRET measurements are ratio-based which, although straightforward to compute, entails that probe readings are not necessarily reflective of a cell's absolute ERK activity. In other words, measured FRET data does not linearly correspond to the ERK activity signal. This could partially explain the dissimilarity in ERK activity between the imaging data and the western blot analysis. This limitation was known beforehand and it was decided to follow through with the project since the interest was in comparing MAPK signalling of $KRAS^{G12D}$ cells to those carrying no *KRAS* mutation. Thus, although the measured signal does not represent absolute values, it still provides invaluable information on the signalling dynamics of mutant cells when compared to their wild-type counterpart.

3 identical repeats of low (0.1, 0.5, 1 mg/mL) and 3 identical repeats of high (1, 10, 50 mg/mL) EGF concentration experiments for each $KRAS^{G12D}$ and wild-type SW48 cells were carried out in addition to pilot experiments and experiments that partially failed because of technical issues (for example clogging of individual microfluidic channels). It is to be noted that precise features of biochemical dynamics across different independent experiments exhibit non-negligible variability (see suppl. Fig. 2.17 on page 70 and 2.18 on page 71). Certain results such as the ERK deactivation kinetics in wild-type cells, for example, are particularly variable. Given the high standards taken to execute the experiments as similar as possible, a plausible reason to explain inter-experiment variability has not been found yet. Importantly, the interpretation of the results relies on differences between WT and G12D that are largely unaffected by such variability.

2.4 Materials & Methods

2.4.1 Cell lines and culture conditions

Parental and heterozygous *KRAS* mutant (G12A, G12C, G12D, G12V) SW48 CCL-231 cell lines (derived from colorectal adenocarcinoma) were obtained from Horizon Discovery and cultured in RPMI-1640 medium, supplemented with GlutaMAX^{TM}-I and 10% foetal cow serum (FCS).

Parental and heterozygous *KRAS* mutant (G12A, G12C, G12D, G12V) LIM1215 colorectal cell line (Whitehead et al., 1985) were obtained from ATCC and cultured in RPMI-1640 medium, supplemented with GlutaMAX^{TM}-I, 1 µg/mL insulin (Sigma, cat. no. I9278-5ml), 1 µg/mL hydrocortisone (Sigma, cat. no. H0396-100MG) and 10% FCS.

The pancreatic cell line hPNE E6/E7/st (CRL-4037) was obtained from ATCC. E6 and E7 are human papillomavirus oncogenes that inhibit p53 and Rb tumour suppressor proteins, respectively (Campbell et al., 2007). Moreover, SV40 small t antigen (st) promotes cell growth via the inhibition of protein phosphatase 2A family of Sr/Thr phosphatases (Hahn et al., 2002). This cell line was used to generate a panel of cell lines stably expressing a doxycycline-inducible mutant ($KRAS^{wt/G12A}$, $KRAS^{wt/G12C}$, $KRAS^{wt/G12D}$, $KRAS^{wt/G12V}$,$KRAS^{wt/G12R}$) or wild-type ($KRAS^{wt/wt}$) KRAS.

Cells were cultured in DMEM (1X) medium, phenol red and L-glutamine free, supplemented with 1g/L glucose and pyruvate (Gibco by Life Technologies). Additional medium contents include M3:BaseF^{TM} (1X) (Innovative Life Sciences SolutionTM), 5% FCS, epidermal growth factor (EGF, 10 ng/mL), glutamine (2mM), puromycin (150 ng/mL), 1% penicillin/streptomycin and Hygromycin (150 µg/mL).

All cultured cell lines were stored in an incubator at 37 °C with 5% CO_2, containing a water bath filled with distilled H_2O to control for internal humidity. At 80% confluency, cells were washed with PBS and passaged via trypsinization (Trypsin-EDTA, Gibco).

2.4.2 Molecular cloning

The EKAREN5-NLS plasmid kindly provided by Hugo Snippert and Bas Ponsioen (Utrecht University) contained a puromycin resistance gene. This was unsuitable for our monoclonal cell-line generation needs since all our parental cell lines were already resistant to puromycin. Thus, it was decided to replace puromycin with a blasticidin resistance gene.

To do this, the vector from another similar blasticidin-containing plasmid (EKAREN4) was fused with the sequence expressing the EKAREN5-NLS sensor with 2-way ligation cloning. The restriction enzymes used to digest the vector (from miniTol-EKAREN4-PGK-blasticidin) and insert (from miniTol-EKAREN5-PGK-puromycin) were NheI and PacI. The resulting plasmid (miniTol-EKAREN5-PGK-blasticidin) was confirmed via analytical digest and Sanger sequencing.

2.4.3 Stable cell line generation

Transfection

800,000 (HPNE) or 2 million (SW48, LIM1215) cells were seeded onto T25 flasks. 24h later, cells were transfected with 1.5µg of EKAREN5-NLS plasmid and 1.5µg transposase plasmid using Jetprime (Polyplus transfection) according to the manufacturer's guidelines.

Polyclonal cell lines

HPNE, SW48 and LIM1215 cells with wild-type *KRAS* ($KRAS^{wt/wt}$) and heterozygous mutant *KRAS* ($KRAS^{wt/G12A}$, $KRAS^{wt/G12C}$, $KRAS^{wt/G12D}$, $KRAS^{wt/G12V}$) were used to generate polyclonal cell lines.

72h after transfection, 6µg/mL (LIM1215, HPNE) or 12µg/mL (SW48) of selection agent blasticidin (Invivogen) was added into the growth media. Growth media with blasticidin was replenished every 3-4 days for at least 10 days, after which cells were frozen in freezing media (90% FCS and 10% DMSO) and stored in -180 °C.

Monoclonal cell lines

For the generation of monoclonal cell lines, HPNE, SW48 and LIM1215 cells with $KRAS^{wt/wt}$ (wild-type) and $KRAS^{wt/G12D}$ (mutant) were used.

72h after transfection, cells were trypsinised and single-cell sorted via fluorescence-activated cell sorting (FACS) into 96-well 'feeder' plates pre-seeded 24 hours earlier with non-transfeced cells (250 cells/well for HPNEs, 400 cells/well for SW48 & LIM1215). Each sample (cell line with or without mutation in *KRAS*) submitted for FACS was sorted into three 96-well plate replicates. Once samples were sorted, plates were kept in an incubator at 37°C for 5 days. Then, growth media was replenished every 3-4 days with 6µg/mL (LIM1215, HPNE) or 12µg/mL (SW48) of selection agent blasticidin (Invivogen). 10 days after the addition of blasticidin, single colonies from 96-well plates

were transferred to 24-well plates via trypsinisation and for further expansion. Once confluency was reached, cells were frozen in freezing media (90% FCS and 10% DMSO) and stored in -180 °C.

2.4.4 Microfluidics and sample preparation for EGF titration assays

All microfluidic experiments were carried out using the CellASIC ONIX2 system (Merck Millipore, cat. no. CAX2-S0000), a CellASIC ONIX2 Manifold XT (cat. no. CAX2-MXT20) and CellASIC ONIX plates (cat no. M04S-03-5PK, see Fig. 2.12). Here I describe the preparations and seeding procedures prior to imaging.

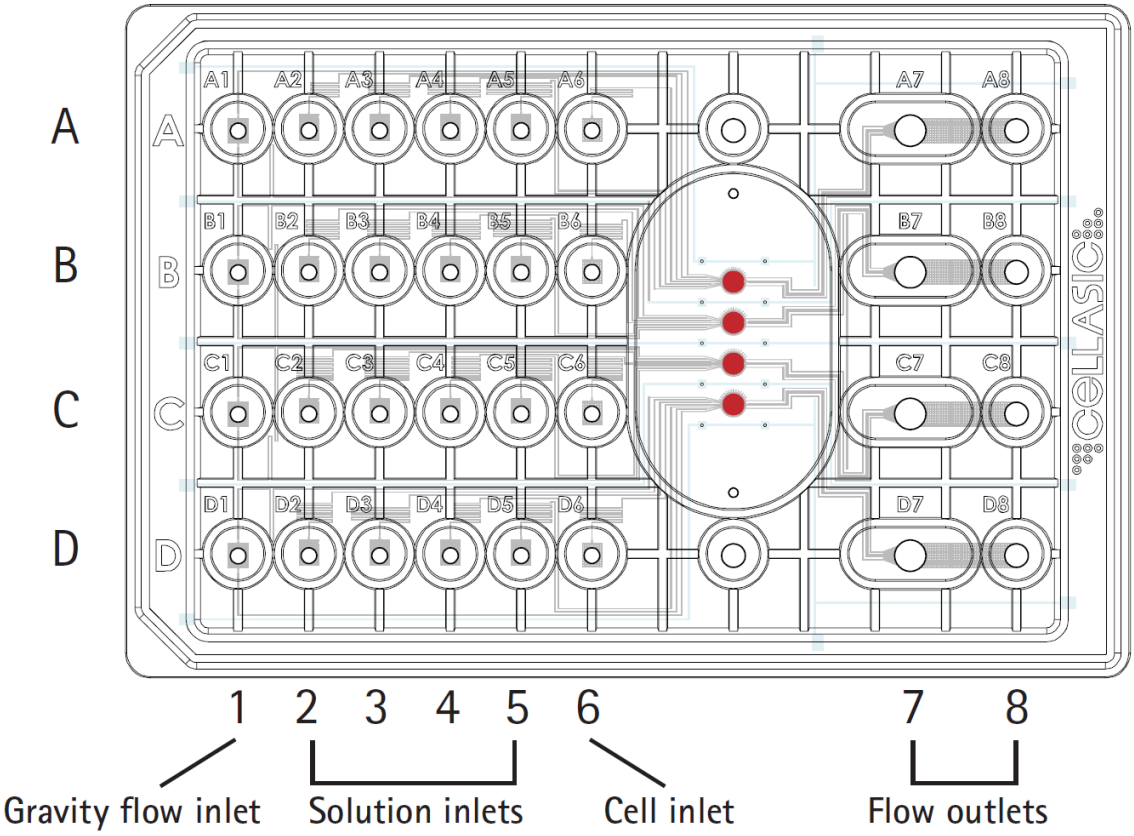

Fig. 2.12 Diagram of a CellASIC plate. Gravity flow inlets (column 1) have a low flow resistance and are typically filled with growth media for cell maintenance. Solution inlets (columns 2-5) have the highest flow resistance and are filled solutions of interest for assay purposes. Cell inlets (column 5) have the least resistance and are used to seed cells onto the cell chambers (coloured red). Flow outlets (columns 7-8) are the wast compartments that accummulate any solution that is perfused through the cell chambers. Figure from the CellASIC ONIX M04S-03 Microfluidic Plate user guide.

Plate priming

At least one hour before seeding, chambers in the CellASIC plate were coated with growth media to facilitate cell attachment and distribution at the time of seeding. Prior to coating, the PBS in the plate's channels (connecting wells with chambers) was replaced with imaging media. The latter consists of RPMI-1640 without phenol red and HEPES (cat no. 11835030) and is supplemented with 1% FCS and 1% penicillin/streptomycin. Whenever solution was aspirated from the CellASIC plate, care was taken not to aspirate solution from the bottom hole of inlets (to prevent air leakage into the plate's internal channel system).

A CellASIC plate was removed from its packaging and PBS was aspirated from all inlets in aseptic conditions. After adding 200µl of imaging media to the solution inlets (2-5, see Fig. 2.12), the CellASIC plate was sealed to the manifold (CellASIC ONIX2 Manifold XT (Temperature Controlled), cat. no. CAX2-MXT20). Then, using the ONX2 software, solution inlets were activated and a pressure of 5psi (34.5kPa) was applied for at least 5 minutes (to allow imaging media to cover all of the chamber surface). Then, pressure was turned off, CellASIC plate was unsealed from the manifold and returned to a microbiological safety cabinet. Media in the waste compartments (7-8) was removed. After aspirating all media (including bottom hole) from cell inlets, 12µL of growth media was added to cell inlets (column 6) to begin chamber coating. Finally, the plate was left in the incubator at 37°C until seeding.

Seeding

Cells were washed with PBS and trypsinised to achieve a solution with cells in suspension. After counting cells with a Countess Automated Cell Counter (Thermo Scientific), a cell solution with a concentration of 1.5-2 cells1/mL was prepared. Then, after removing all growth media (including bottom hole) from the first cell inlet (A6) in the CellASIC plate, 11µL of homogenised cell solution was added. This procedure (media removal & cell loading) was carried out sequentially for each cell inlet. Once completed, media from waste compartments (7-8) was removed to increase the cell solution flow and prevent cell aggregation. Then, using a combination of finger-tapping, strict visual inspection of the chambers and flow control, cells were seeded as evenly as possible.

Once all chambers were seeded with the cells of interest and solution flow was halted (by adding imaging media to waste compartments), the CellASIC plate was stored in the incubator at 37°C for 2-6 hours. Finally, 350µL of imaging media was added to all

gravity flow inlets (column 1) and the CellASIC plate was stored again in the incubator overnight (at least 20h) to allow cellular adaption to the new environment.

On experiment day

At the designated time, solution was aspirated from all inlets, except the cell inlet (6). 300µL of imaging media was added to inlets 2 & 5. The same volume of EGF (sigma-aldrich, cat. no. E9644) and ERK inhibitor (SCH772984, 500 nM, Generon, cat. no. A3805-10mg) solution was added to inlets 3 & 4, respectively. A solution of imaging media and EGF stock buffer was added in inlet A3 for control samples.

To ensure a good fit of the CellASIC plate with the microscope stage, 6 tape strips were attached to the sides of the plate. After adding oil underneath the cell chamber, the plate is returned to the stage and sealed to the manifold. On the ONIX2 software, the perfusion protocol is prepared as in Fig. 2.20 on page 73. Once field of views (FOVs) have been selected on the microscope, the imaging timelapse and microfluidic protocol are synchronously initiated.

2.4.5 Microscopy

All imaging experiments were carried out using a Nikon Eclipse Ti inverted fluorescence widefield microscope controlled by NIS-Elements AR software. Images were captured using a Plan Fluor 40x Oil objective, 200-300ms exposure time and a two-camera system (TuCam, Andor) for the simultaneous detection of FRET acceptor (YFP) and donor (CFP) light emission. The sample is exposed to excitation light – generated by restricting the fluorescence light with a CFP band-pass filter (ET 436/20X). Emission light is then split by a dichroic mirror within the TuCam to capture CFP and YFP emission separately.

Timelapse images of 12 hours duration were captured using an image acquisition frequency of 6 minutes.

2.4.6 FRET measurement

FRET data was measured as described in Chapter 3. Briefly, YFP and CFP channel images undergo smoothing (via median filtering) and background subtraction. Then, a FRET image (YFP/CFP) is generated and average or single-cell FRET data measured using the *regionprops* function from the *sci-kit image* Python package. Measurement data is then saved in .csv file format.

2.4.7 Signal dynamics analysis

Analysis was performed using Python 3.7.6, and plots were generated using Python's *Matplotlib* visualisation package, unless stated otherwise.

Single-cell data from all experimental repeats was collated in a single master .csv file. Data was normalised by subtracting each each cell's FRET data with the median value of minimal ERK activity of all cells of the same treatment condition and biological sample. Minimal ERK activity was calculated (per cell) by averaging FRET data in the 30-48' time window after start of ERK inhibition treatment.

The mean values in section 2.2.1 are reported with the standard error of the mean and number of single cells in brackets.

Derivative values (see (b), (d) and (e) in Fig. 2.5) were calculated using the *gradient* function from the *Numpy* library package.

Peak prominence values of mean FRET data curves (see (c) in Fig. 2.5) were measured using the *find_peaks* function from the *signal* package of the *SciPy* library. Using the same function, peak-related features were calculated on single-cell data.

Pearson correlation plots were generated using the single-cell feature data and the statistical data visualisation library *Seaborn*. Plots were further amended with CorelDRAW 2020 and illustrated as in Fig. 2.6.

2.4.8 Analysis using Time Course Inspector

A .csv file with normalised FRET single-cell data generated with Python was loaded into **Time Course Inspector** (TCI), an *R/Shiny* app developed by Dobrzyński et al. (2019) for the analysis of time series single-cell data. Outlier trajectories – identified by visual inspection of the FRET curves – were removed. Within TCI, data was interpolated with the interval between two points set to 6 (minutes), the image capture frequency. For clustering purposes, X-axis (time) was trimmed to -30min to 3.5 hours since EGF addition. All distribution plots shown were generated with TCI.

Scatter plots

Plotted data was smoothed by calculating the average of the selected timepoint and its two adjacent timepoints. For example, if x axis is set to intensity values at frame 10, the plotted data will represent intensity values averaged over frame 9, 10 and 11.

For scatter plots in Fig. 2.6, baseline ERK activity is the activity at 18min before EGF stimulation. Peak amplitude represents the difference between peak activity (defined as ERK activity at EGF+24min) and baseline activity.

For scatter plots in Fig. 2.7, rebound magnitude is the ERK activity 1h24' after ERK inhibition. Baseline magnitude equates to baseline ERK activity as defined in the previous paragraph. Peak magnitude is the ERK activity at EGF+24'. EGF+3h magnitude is the ERK activity 2h54' after EGF treatment.

Hierarchical clustering

Clustering was performed using the Euclidean distance as a dissimilarity measure, with Ward (Ward.D2) linkage method and a cluster number of $k = 7$.

2.4.9 Western blot

At the indicated time point, samples were immediately placed on ice. Medium was aspirated using a table-top pump, and samples were each then added 3mL of ice-cold PBS. Dishes were angled as vertically as possible for maximal extraction of the PBS (aspirated). Then, cells were lysed with 40uL of RIPA solution containing 50mM TRIS pH7.4, 150mM NaCl, 0.5% sodium deoxychelate, 0.1% SDS, 1% NP-40 (IGEPAL), ultrapure water, 1mM PMSF, 1x protease inhibitor cocktail (PIC) and 1x phosphatase inhibitor (PhosphoSTOP). Cells were harvested using a cell scraper. RIPA solution containing lysed cells was pipetted into 1.5mL Eppendorf tubes and placed immediately on ice under blue light. Once all samples were harvested, samples were vortexed for 10 seconds and followed by a 30-minute incubation at 4°C and in the dark (tubes were covered in foil). Samples were then placed in a centrifuge and spun at 13,000 rpm for 10min and at 4 degrees. The supernatant was transferred into a new Eppendorf tube and the former tube with the pellet (cell debris) discarded. Finally, samples were stored at -80°C, if not assayed directly.

Protein concentration of cell lysates was determined by BCA assay. 30µg of lysate was denatured with 1x sample loading buffer (with 50mM dithioltheitol or DTT) at 70°C for 10min. Samples were loaded onto a NuPAGE Novex 4-12% Bis-Tris protein gel (Life Technologies) and transferred onto a PVDF membrane using wet transfer (tansfer buffer with 20% methanol) at 20V, overnight and at 4°C. Once transferred, the membrane was stained with Ponceau S to confirm successful protein transfer. The membrane was blocked for 1 hour using 5% milk (unless stated otherwise) in TBS-T (0.05% Tween 20).

The membrane was washed (3 x 5min) with TBS-T and incubated with primary antibody solution overnight at 4°C. The following day the membrane was washed again (3 x 5min) with TBS-T and incubated for 1 hour at room temperature with fluorescently-labelled secondary anti-mouse or anti-rabbit antibodies (IRDye-680 anti-rabbit, IRDye-680 anti-mouse, IRDye-800 anti-rabbit, IRDye-800 anti-mouse; LI-COR) diluted 1:5,000 in odyssey blocking buffer (PBS). Finally, the membrane is washed with TBS-T and scanned using the Licor Odyssey CLx imaging system.

Primary antibodies

Primary antibodies and dilutions used: mouse P-p44/p42 MAPK (T202/Y204) (E10) (1:1,000; Cell Signalling, cat. no. 4695S), p44/p42 MAPK (Erk1/2) (137F5) Rabbit (1:1,000, Cell Signalling, cat. no. 9106L), p-CDC25C (T48, Rabbit 1:1,000, cat. no. 9527S), CDC25C (H-6, Santa Cruz, Mouse 1:500, cat no. sc-13138), Hsp90 Rabbit mAb (C45G5, 1:1,000, Cell Signalling, cat. no. 4877S).

2.4.10 RNA sequencing sample preparation and analysis

SW48 cells with heterozygous knock-in mutations for *KRAS* G12A, G12C, G12D, G12V and WT were thawed and cultured for 3 passages before sample preparation. 5 replicates from 3 different batches of each cell line were used for the RNAseq experiment. Briefly, 1.5 million cells were seeded on a 6cm dish. 48h later cells were placed on ice, washed 1x with cold PBS, and collected by scraping with 1ml PBS into 1.5ml Eppendorf tubes. Samples were centrifuged for 3min 1000rpm at 4 °C and pellets kept in −80 °C until shipment. Total RNA isolation, library preparation and sequencing (with 20M reads per sample) was performed by BGI in Hong Kong.

Differential expression data was generated by Dr Shamith Samarajiwa. Gene set enrichment analysis was performed using enrichR (v3.0) using default settings on all differentially expressed genes (FDR < 0.001 & $|\text{logFC}| > 1$). Genes were tested for enrichments in gene sets defined by KEGG pathways or MSigDB. Gene sets with an adjusted p-value < 0.05 were highlighted in the figure.

2.5 Supplementary Figures

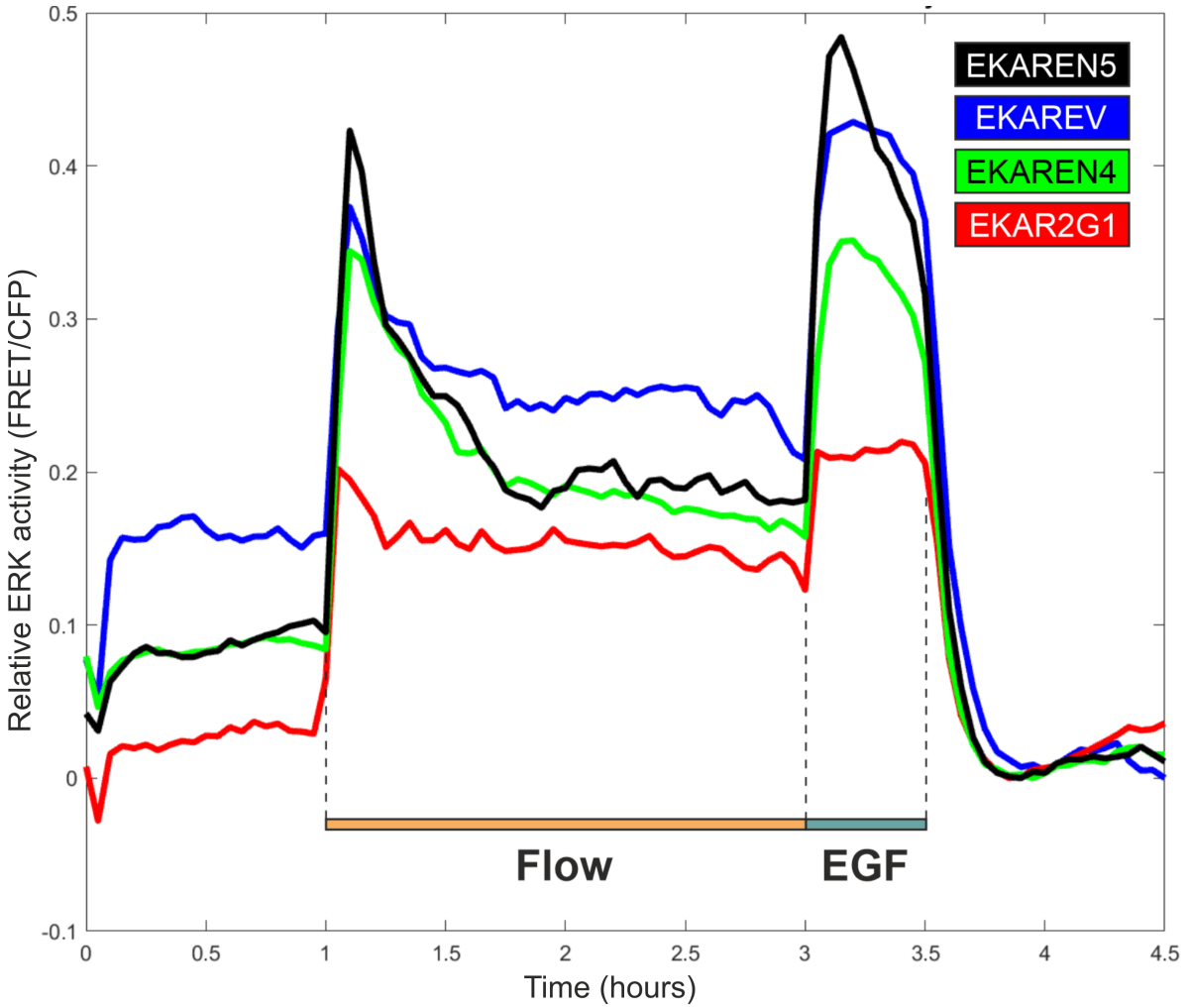

Fig. 2.13 Comparison of various ERK sensors. SW48 cells are treated with EGF (100 ng/ml) for 30min. EKAREN5-NLS was chosen for stable cell line generation as it displays the highest dynamic range, is the least saturable and has been modified to have insensitivity to CDK1 (not shown).

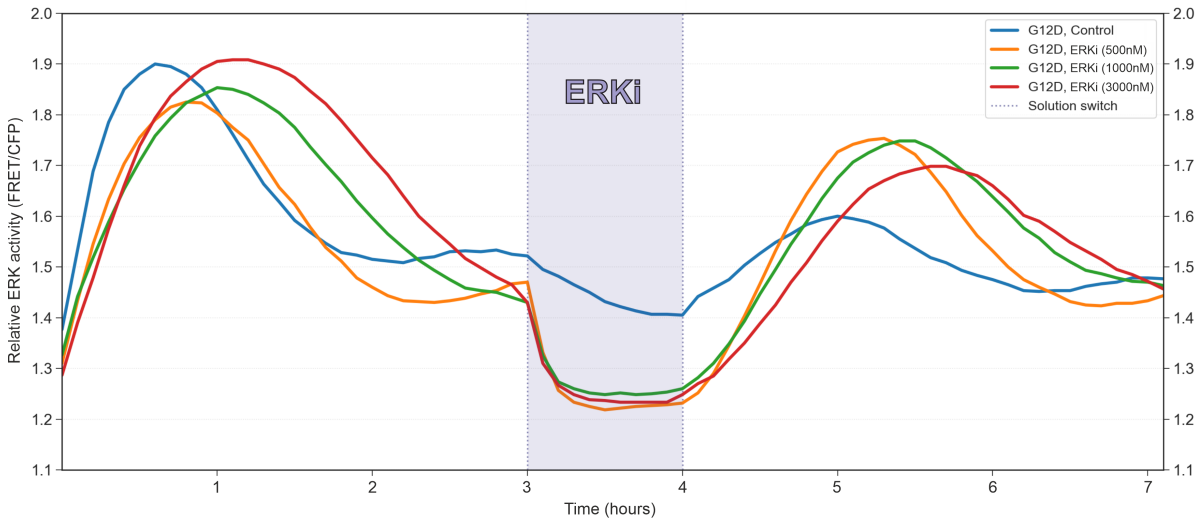

Fig. 2.14 Titration of ERK inhibitor SCH772984. Solution flow starts at t=0 and is maintained constant throughout the whole experiment. Dashed lines designate a change in solution. Non-shaded areas represent imaging media flow.

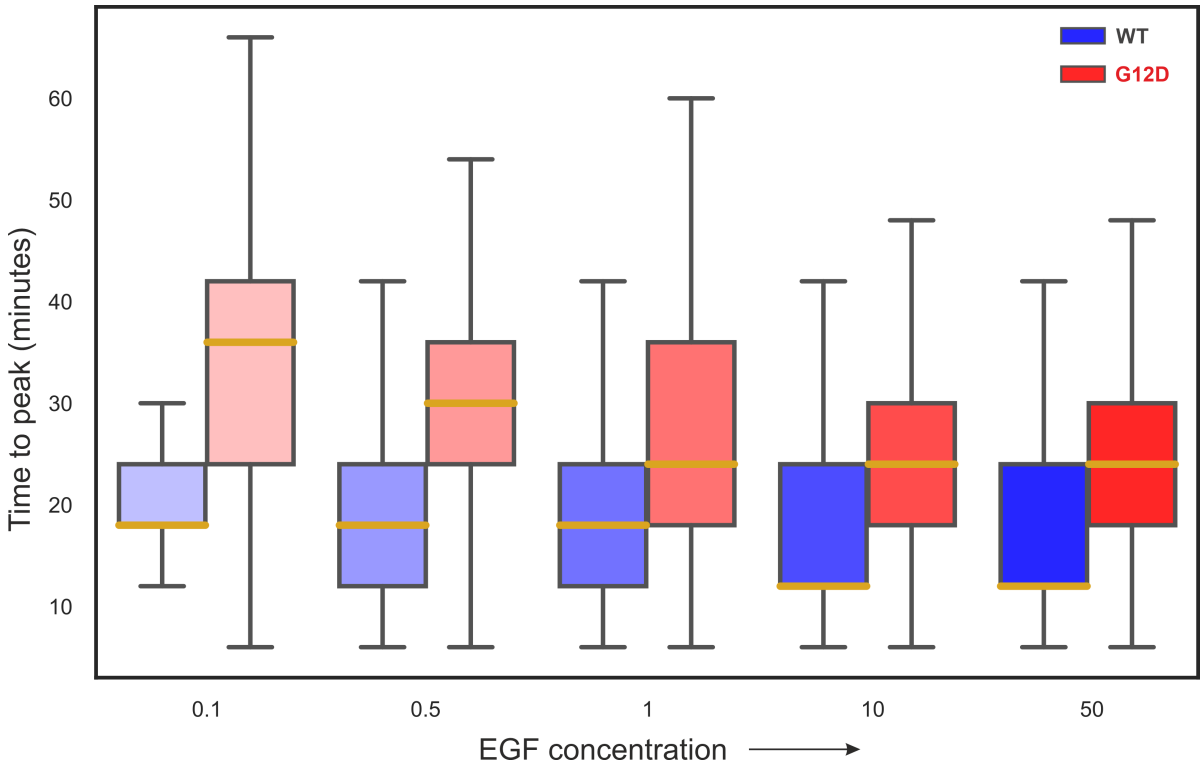

Fig. 2.15 Time to response peak activity. The shades of colour are representative of the EGF concentration.

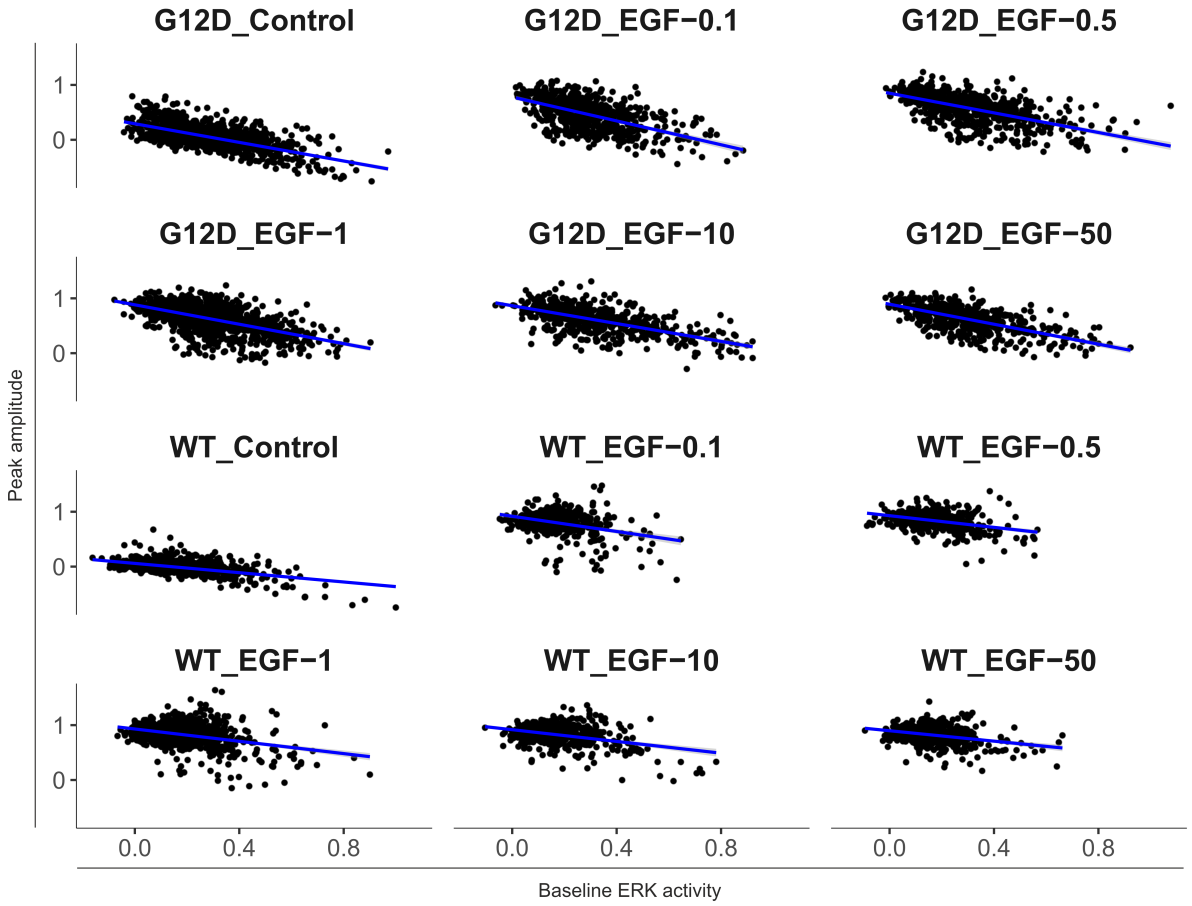

Fig. 2.16 Correlation of baseline ERK activity to response amplitude of all tested conditions in both $KRAS^{G12D}$ (G12D) and $KRAS^{WT}$ (WT) cells.

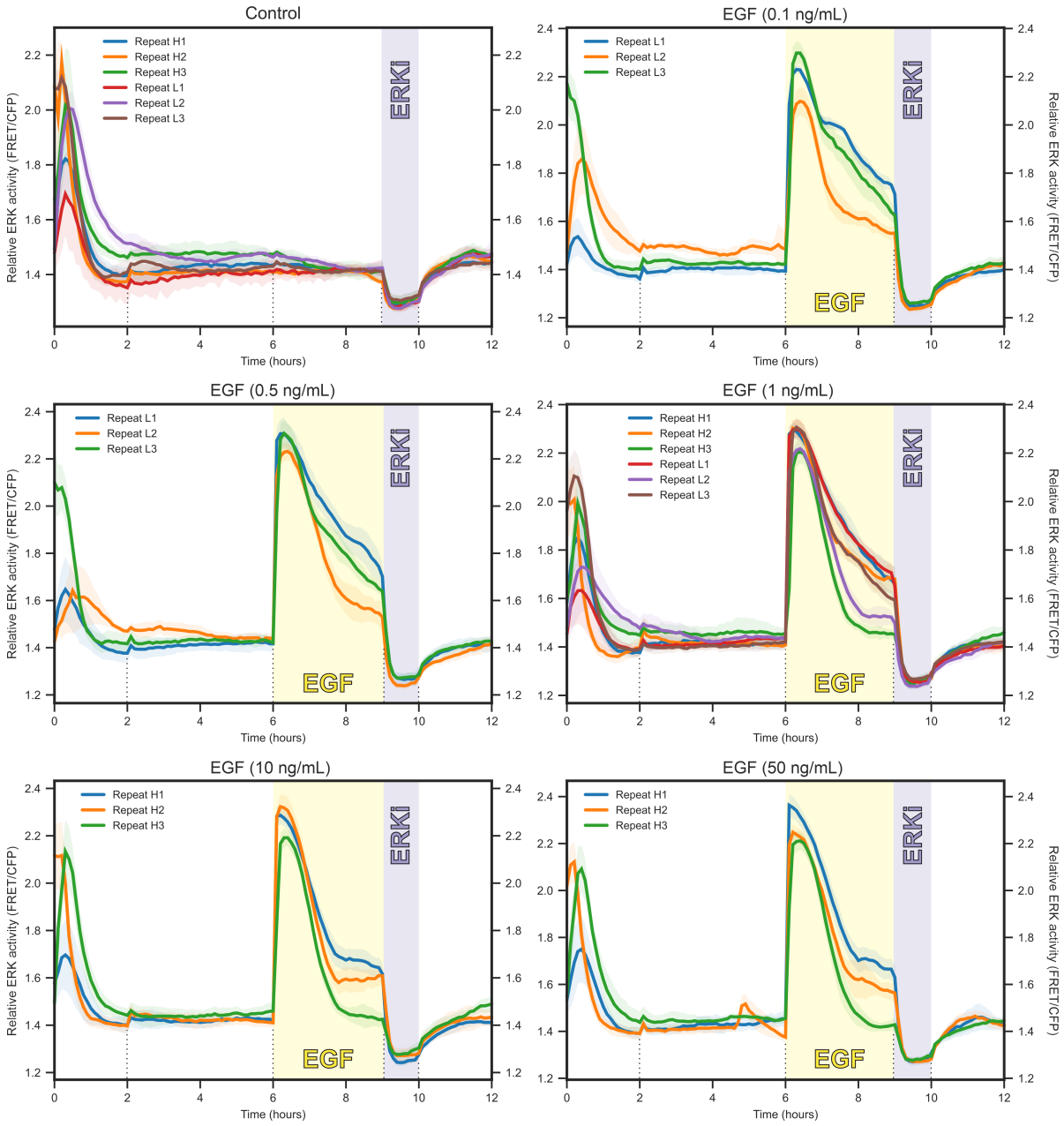

Fig. 2.17 Experimental repeats of EGF titration in cells with $KRAS^{WT}$. Mean FRET data and standard deviation are plotted for each condition tested in each repeat. Following 3 hours of EGF treatment (yellow) cells are treated with SCH772984 (conc.?, purple). The repeats are codenamed according to their experiment type (H = high EGF titration experiment, L = low EGF titration experiment) and replicate number. Thus, 'Repeat H1' refers to the first repeat of high EGF titration experiment (includes Control, EGF-1, EGF-10 and EGF-50 ng/mL). The dashed lines represent a change in solution administration (change of inlet activation in the microfluidic plate). Non-shaded areas represent sections of the experiment where cells are perfused with imaging media

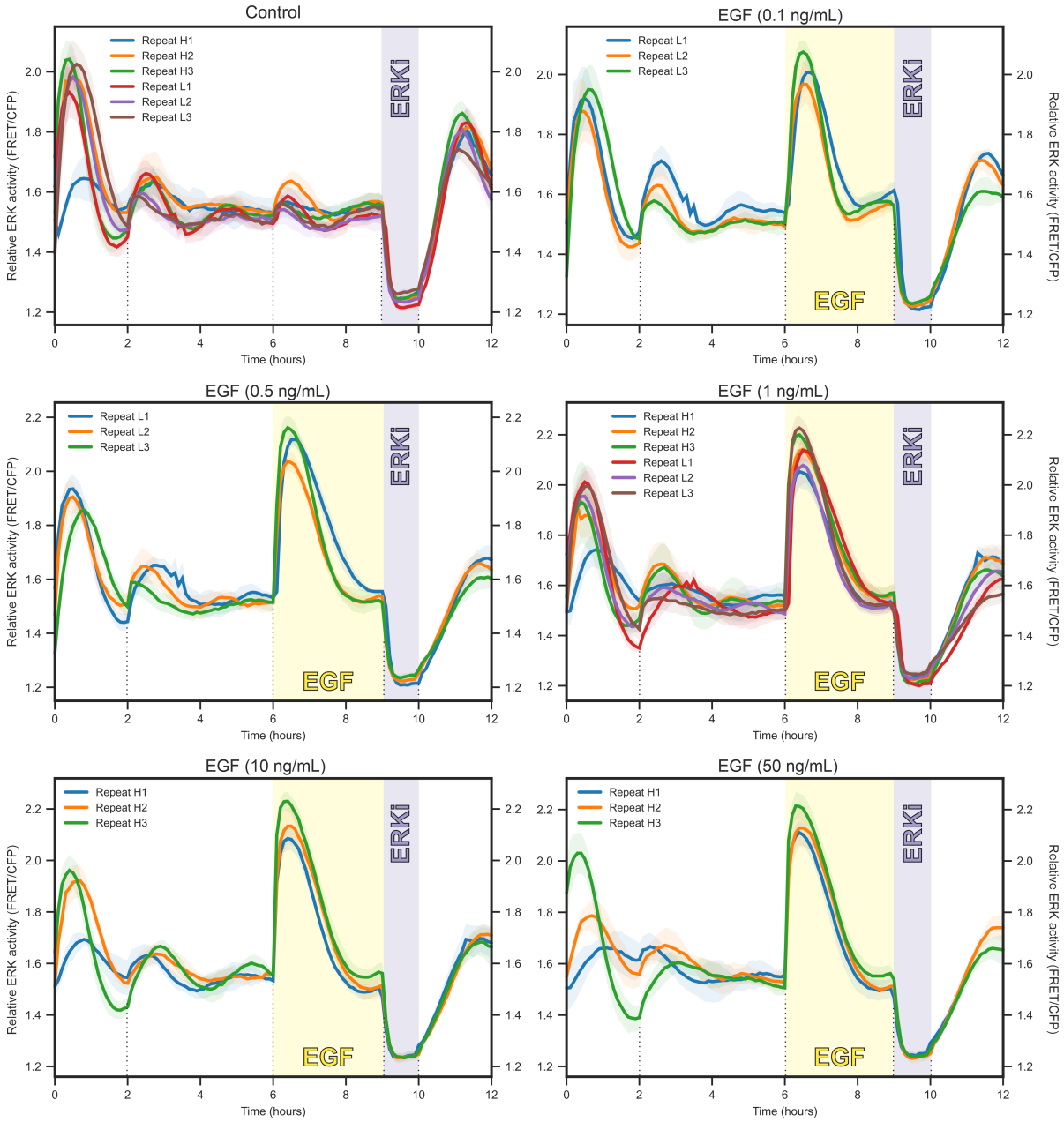

Fig. 2.18 Experimental repeats of EGF titration in cells with $KRAS^{G12D}$. Mean FRET data and standard deviation are plotted for each condition tested in each repeat. Following 3 hours of EGF treatment (yellow) cells are treated with SCH772984 (conc.?, purple). The repeats are codenamed according to their experiment type (H = high EGF titration experiment, L = low EGF titration experiment) and replicate number. Thus, 'Repeat H1' refers to the first repeat of high EGF titration experiment (includes Control, EGF-1, EGF-10 and EGF-50 ng/mL). The dashed lines represent a change in solution administration (change of inlet activation in the microfluidic plate). Non-shaded areas represent sections of the experiment where cells are perfused with imaging media

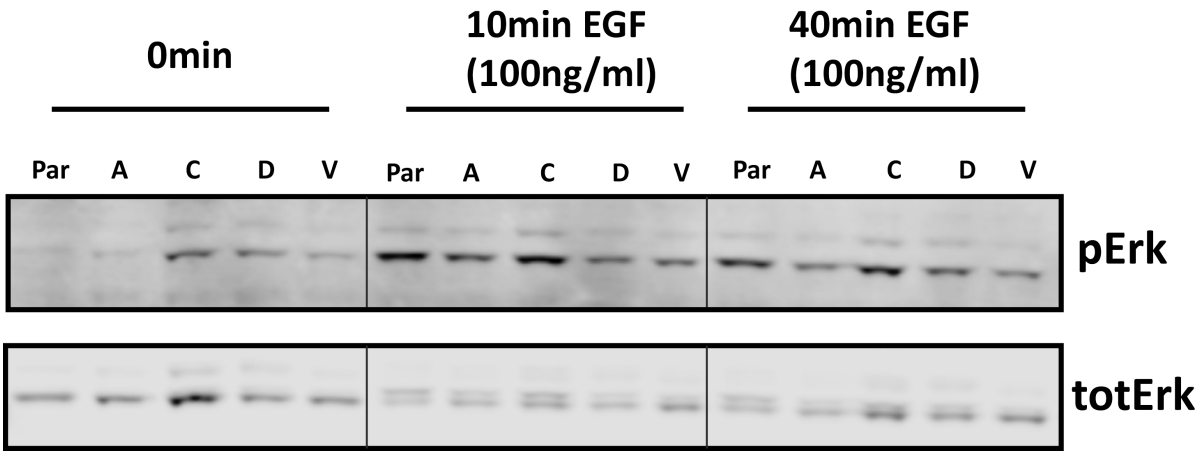

Fig. 2.19 EGF treatment (100ng/mL) of SW48 cell line panel, including parental (Par), $KRAS^{G12A}$ (A), $KRAS^{G12C}$ (C), $KRAS^{G12D}$ (D) and $KRAS^{G12V}$ (V). Figure kindly provided by Dr. Suzan Ber.

LAYOUT								
	1	2	3	4	5	6	7	8
A		SIM	SIM + egf stock buffer	SIM + ERKi 500nM	SIM	SW48wt-N5mc H3B		
B		SIM	SIM + EGF 1ng/mL	SIM + ERKi 500nM	SIM	SW48wt-N5mc H3B		
C		SIM	SIM + EGF 10ng/mL	SIM + ERKi 500nM	SIM	SW48wt-N5mc H3B		
D		SIM	SIM + EGF 50ng/mL	SIM + ERKi 500nM	SIM	SW48wt-N5mc H3B		

PROTOCOL					
Step	Repeat count	Duration (d:hh:mm:ss)	Type	Parameters	Comments
1			Gas	Off	Setup gas flow if needed
2			Temperature	On, 37.0 C	Setup temperature if needed
3		0:02:00:00	Perfusion	X=31.0kPa: WG(5)	
4		0:04:00:00	Perfusion	X=31.0kPa: WG(2)	SIM
5		0:03:00:00	Perfusion	X=31.0kPa: WG(3)	SIM + EGF (0, 1, 10, 50 ng/ml)
6		0:01:00:00	Perfusion	X=31.0kPa: WG(4)	SIM + ERKi
7		0:02:00:00	Perfusion	X=31.0kPa: WG(5)	SIM

Total Protocol Duration: 12 hours

Fig. 2.20 Microfluidic plate layout (top table) and protocol (bottom table) example. The top table shows the arrangement of solutions and samples according to inlet position of the CellASIC plate. SIM in the top table refers to Starvation Imaging Media and column 6 labels are that of the specific cell line used. In the protocol table, the parameters column shows pressure (in kPa) and inlet (number) information. Pressure can only be applied to inlets vertically (per plate column, see top table).

Chapter 3

Optogenetic Tool Development for Novel Insights

3.1 Introduction

Traditional biochemical assays (e.g. Western Blot and proteomics) often provide only population measurements thus masking cell-to-cell variability. Since the 17th century, microscopy permits scientists to describe single cells within a population. Microscopy is then an invaluable tool to describe the structure and morphology of the cell and its compartments, and their variability. In the 90s, however, the ground breaking innovations of digital microscopy, laser systems and molecular cloning, together enabled scientists to utilize high resolution fluorescence microscopy to characterise living specimens genetically tagged with fluorescent proteins. These innovations transformed the study of cell biochemistry and made fluorescence microscopy an essential tool not only for structural but also functional studies. By permitting to map proteins, protein-protein interaction and enzymatic activities in the living cells and tissues, biochemical imaging enables us to study signalling dynamics and heterogeneity of biochemical events within cellular populations. However, the investigation of biochemical networks – the main focus of this thesis – is constrained by the limited capability of microscopy in quantifying several biochemical event at once on the same sample. Therefore, population-based assays are still the main tool applied for the system-level understanding of the cell. To better complement these assays, I have optimised an imaging platform that permits us to quantify at least three FRET reporters simultaneously. The capability to directly monitor the dynamics and variability of small biochemical networks in living cells could provide a deeper and more accurate understanding of cell biochemistry.

3.1.1 Fluorescent Probes for Monitoring Single-Cells

Genetically encoded fluorescent probes enables the readout of a biochemical event of interest when expressed in cells either through transient expression or stable genomic integration. Fluorescent reporters typically consist of a sensing element fused to a reporting unit. The former is an endogenous peptide involved in a biochemical reaction of interest. Whereas the latter radiates a fluorescent signal used as a proxy for the activity of the protein (or molecule) acting on the sensing element (Sample et al., 2014).

The design of these reporters is not trivial; one has to ensure that FP brightness, stability, maturation, quantum yield (φ) and extinction coefficient (ε) are optimally selected to be measurable. Moreover, pKa, redox sensitivity, unspecific sensitivity to analytes (e.g. halides), as well as the propensity for oligomerisation can also have detrimental effects on quantitative measurements. However, years of efforts on the improvement of these factors have resulted in a library of high quality fluorescent proteins.

FRET sensors are probably the most commonly used among the research community. FRET, originally described by Theodor Förster in the 1940's (Forster, 1946), consists in the transfer of non-radiative energy from an excited 'donor' FP (F_D) to an 'acceptor' FP (F_A) (see Fig. 3.1 on the facing page). Thus, like dimerisation sensors, FRET probes consist of two different FPs. In this case, however, they are both functional FPs, and under an activation event, are brought close to each other effectively resulting in fluorescence intensity changes via FRET. As a result, the former's fluorescence decreases (energy loss) whereas the latter's increases (energy gained) (see (a) in Fig. 3.1). For FRET to occur it is vital to ensure that both F_D and F_A spectrally overlap, i.e. the emission spectrum of F_D coincides with the excitation spectrum of F_A (see (a) in Fig. 3.1). Other crucial requirements for FRET are appropriate angle and close proximity between both FPs (see (b) and (c) in Fig. 3.1).

In the case of intramolecular FRET sensors – i.e. when both F_D and F_A are connected forming a single protein unit – approximation between both FPs is enabled by the presence of two specialised domains. First, an interaction domain to which a protein or ligand of interest binds. Second, a binding domain to which the 'activated' interaction domain binds to, resulting in the sensor's conformational change; bringing both F_D and F_A in close proximity. Thus, genetically encoded intramolecular FRET sensors consist of 1) spectrally overlapping FPs, 2) specialised domains (for sensing & conformational change), and 3) linkers connecting all components (see (d) in Fig. 3.1). The popularity of FRET

sensors is partially due to their modular components; switching an FP for another one, for example, is a relatively straightforward and simple task.

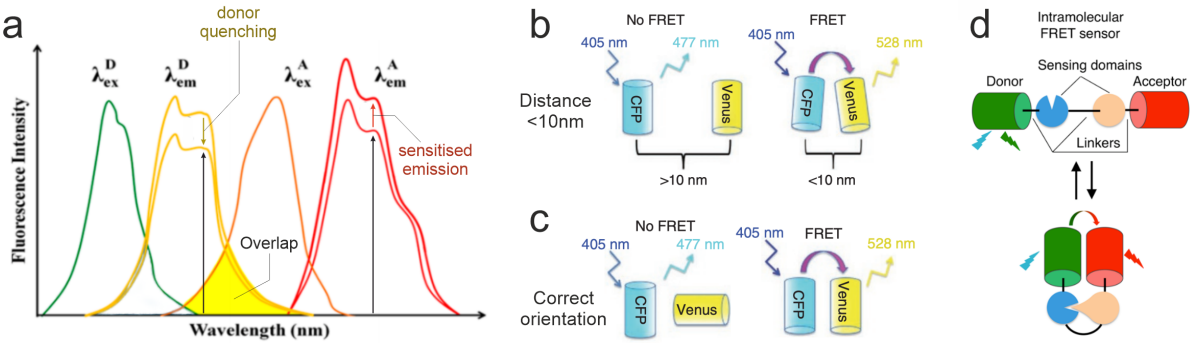

Fig. 3.1 A donor-acceptor fluorescent protein (FP) needs to satisfy a number of conditions in order to undergo energy transger. These include an overlap between the donor emission (λ^D_{em}) and acceptor excitation (λ^A_{ex}) wavelengths (a, adapted from Shrestha et al. (2015)), close proximity (b) and appropiate orientation (c) between both FPs (both adapted from Broussard et al. (2013)). An intramolecular FRET sensor comprises of a donor and acceptor fluorophore bound by protein linkers and reaction-sensitive sensor domains (d, from Bajar et al. (2016))

FRET can be measured in a variety of ways, including via spectral imaging (siFRET), acceptor photobleaching (apFRET), polarisation-resolved (prFRET), sensitised emission (seFRET) and fluorescence lifetime imaging (FLIM-FRET) (Bajar et al., 2016; Shrestha et al., 2015). For the scope of this thesis however, the focus will be on the intensity- and lifetime-based approaches, namely seFRET and FLIM-FRET, respectively.

3.1.2 Sensitised emission FRET

The optical changes occurring when two FPs undergo FRET are that of decreased donor emission (F_D) and sensitized acceptor emission (F_A) (see (a) in Fig. 3.1). The dependency of F_D and F_A on FRET permits FRET to be quantified from intensity measurements. Sensitised acceptor emission is based only off of the energy transfer from a F_D, and it can be measured in a variety of ways. The main concept involves the measurement of the FRET signal by measuring F_A emission when only exciting F_D. However, FRET efficiency cannot be accurately quantified in a straightforward manner due to the presence of spectral bleed-through. More precisely, F_A can be directly but mildly excited by F_D excitation light, and some F_D emission may bleed into the acquired acceptor's emission. This results in an uncorrected FRET image (uFRET) containing, sensitised and directly-excited F_A and F_D emission. Thus, to accurately

calculate FRET efficiency, researchers employ rather complex imaging protocols involving three- or four-channel imaging as well as single-FP imaging for spectral bleed-through corrections (Bajar et al., 2016; Pietraszewska-Bogiel and Gadella, 2011; Sun et al., 2011).

A more straightforward approach to seFRET particularly useful when using intramolecular FRET reporters is two-channel imaging. Using appropriate band pass filters; under direct F_D excitation light both a quenched donor (qD) image (F_D emission channel) and a uFRET image (sensitised emission channel) are captured. One can then achieve a *relative* FRET efficiency (rE) with a simple ratiometric calculation:

$$rE = \frac{uFRET}{qD}$$

Due to the inherent fixed stoichiometry of intramolecular FRET reporters (ie equal protein expression of F_A and F_D), spectral bleed-through in uFRET remains constant meaning that it does not differentially affect rE. Contrarily, single-FP sensors can be confounded by biological variables – such as cell morphology (cell thickness and shrinkage) – affecting their intracellular concentration and ensuing intensiometric quantification. Moreover, a ratiometric-based measurement means FRET sensors display added sensitivity; small FRET changes are amplified. Although accurate FRET efficiency cannot be measured, this ratiometric-based seFRET approach provides a simpler way of measuring signalling activity changes in single living cells.

3.1.3 Measuring FRET with FLIM

When a fluorescent molecule absorbs a photon it transitions to an excited state, due to the increase in energy (see (a) in Fig. 3.2 on the next page). Excited states are unstable and a fluorophore tends to fall back to a ground (stable) state. The time spent in the excited state (in the nanosecond range for the fluorophores most commonly used in biology) is called the fluorescence lifetime (FLT) (Lakowicz, 2006). Returning to a ground state requires releasing energy in a number of ways, including heat and light (photon) emission, among others (Lakowicz, 2006). There are several ways to measure FLT, but methodologies can be broadly categorised as frequency-domain or time-domain Fluorescence Lifetime Imaging Microscopy FLIM). With the latter method, we quantify the number of photons that are emitted when a fluorophore goes from an excited state to a ground state (see (b) in Fig. 3.2). To do this, the sample is exposed to very short laser pulses that excite the fluorophore. Over time, photons are collected and eventually one obtains a fluorescence decay function. This graph is the distribution of

delay times for each photons from the excitation pulse, and the decay constant that can be inferred by fitting exponential curves is a measurement of the fluorescence lifetime. FLIM requires specialist instrumentation and expertise, thus FLIM is not as widespread as other imaging techniques but provides a quantitative and robust measure of physico-chemical characteristic that alters the fluorescence lifetime of a fluorophores, for example FRET.

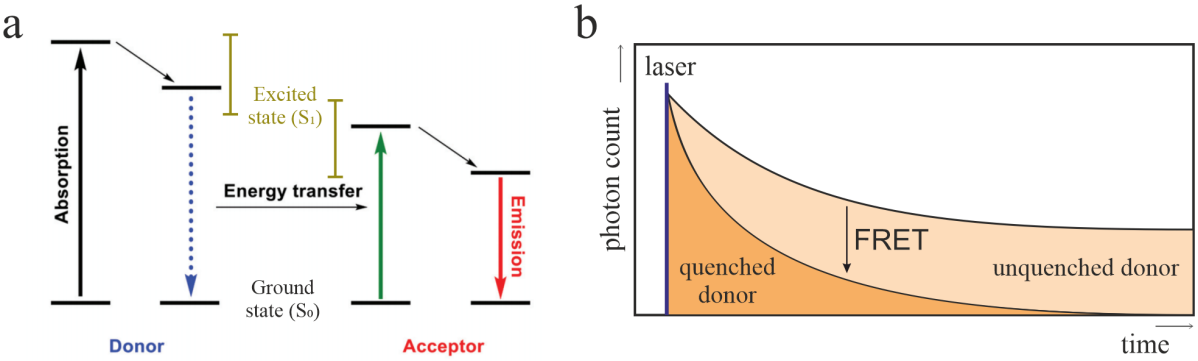

Fig. 3.2 The lifetime of a fluorophore designates the time a fluorophore is in an excited state S_1, as shown in the simplified Jablonski diagram (a, adapted from Huang et al. (2020)). Fluorescence lifetime determined by the photon decay rate is decreased when a donor FP is quenched by undergoing FRET (b, adapted from Becker (2012))

FLIM can be used to investigate a wide range of features such as local viscosity, fluorescence quenching by molecules (oxygen) or ions (Ca^{2+} and Cl^-), binding to specific biological targets or even nanoparticle localisation (Becker, 2012). Its most common use however is for the measurement of FRET. A donor fluorophore's lifetime changes when it undergoes FRET. This is due to the acceptor fluorophore quenching the donor fluorescence, resulting in a more pronounced photon decay rate and thus shorter lifetime (see (a) in Fig. 3.2). Once we have two FLT values, for example the FLT of a donor FP in the presence (τ_{DA}) or absence (τ_D) of an acceptor FP, FRET efficiency (E, the energy transferred from donor to acceptor) can be measured as follows:

$$E = 1 - \frac{\tau_{DA}}{\tau_D}$$

There are various advantages to using FLIM when measuring FRET, the main one being accuracy. The FLT of a fluorophore is not affected by intracellular sensor concentration, but sensitive to the molecular interactions with its environment. This supposes an additonal advantage, as often the precise sensor concentration is not known. Moreover, spectral bleed-through – often present when measuring more than one FP – is not an issue as only F_D is measured.

Multiplexing with FLIM probes

Because FLIM measures just the donor fluorescence, the fluorescence emission of the acceptor molecule (F_A) is redundant. Therefore, the acceptor can be a chromoprotein (a dark FP), i.e. a molecule that can sink energy from the donor without emission of fluorescence. This in turn opens up the possibilities for mutliplexing various probes simultaneously, since there is double the spectral room than that with standard (non-dark acceptor) FRET sensors. FLIM has been used in conjunction with intensity-based FRET measurements to monitor drug delivery and metabolic activity *in vivo* (Rudkouskaya et al., 2020). Another study uses the same combination of techniques for the characterisation of RAS GTPase and calcium activity within single cells after exposure to epidermal growth factor (Grant et al., 2008). Although these and other non-FLIM studies (Galperin et al., 2004; Piljic and Schultz, 2008; Su et al., 2013) demonstrate the use of more than one FRET probe, they are often limited by spectral bleed-through and/or multiple excitation lines (meaning sequential acquisition) to excite all the donor fluorophores.

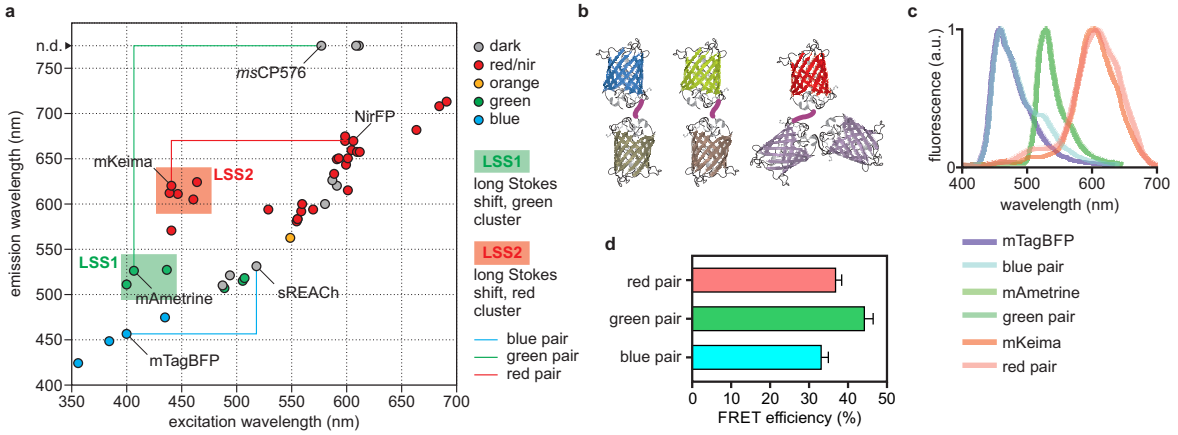

Fig. 3.3 The NyxBits reporters are excitable at the same wavelength yet have spectrally separated emission wavelengths (a). Because they all contain dim/dark acceptor fluorophores (b), blue (mTagBFP), green (mAmetrine) and red (mKeima) donor emission can be measured with low spectral bleed-through (c). These reporters exhibit a good dynamic range granted by their relatively high FRET efficiencies (d). Figure from Fries et al. (2018)

To overcome such limitations, Dr. Fries (previous PhD student in same research group) spear-headed the design of novel reporter system (*NyxBits*) consisting of three spectrally separated FLIM-FRET pairs, excitable with a single laser (Fries et al., 2018). *NyxBits* reporters consist of a bright donor fluorophore (mTagBFP (Subach et al., 2008), mAmetrine (Ai et al., 2008) and mKeima (Kogure et al., 2006)) and a dim/dark

acceptor fluorophore (sREACh (Murakoshi et al., 2008), msCP756 and tdNirFP). These reporters, together with fast photon-counting hardware and custom spectral unmixing software (*NyxSense*), were used to simultaneously monitor the activity of death-inducing proteases caspase 2, 3 and 9 in single living cells. Importantly, this novel optical platform unveiled previously unidentified single-cell non-genetic heterogeneity of caspase activation dynamics and ensuing survival or death (Fries et al., 2018). Despite *NyxBits* reporters providing useful new insights in signal transduction dynamics, their FRET efficiencies are optical features that could be further improved for wider dynamic range purposes.

3.1.4 Image Analysis Tools

For every image that is generated by a microscope, there needs to be a software to handle the image files. In a first instance, to allow the user to view an image but also to quantify the pixel's intensity values. Such task can vary in complexity depending on many factors, including the following non-exhaustive list:

- Image dimensions: these can be 2D or 3D single image or timelapse movies
- Channel number: cells can be imaged for morphology using brightfield or differential interference contrast (DIC), for example, but also for endogenous information reported by one or more fluorescent sensors
- Signal shape: nuclear stains are simpler to measure than 'dots' or non-uniform stain
- Background noise: depending both on instrumentation and signal strength, background pixel intensity can confound measurements of regions of interest. This is specially important if we are to compare different images together, as background levels may vary from image to image.

These are but a few considerations to take when analysing images. Unmentioned, but related and equally important to image dimensionality, is the question of whether cells need to be tracked over time. To the human eye, tracking is a relatively straighforward task, but computers cannot intuitively perform such task since it requires a superior level of visual recognition. Programmatically speaking, cells of one frame – of a 2D timelapse – are pre-assigned an ID (number) which ought to be linked to the same cell in the following frames. Tracking (ID assignment) can be performed manually by a user. However, manual tracking can very quickly become incredibly time-consuming as the

number of objects to measure and track over time will tend to be high to achieve robust statistical power. Hence the importance of automation in this scenario.

Fortunately, there are many tools available to make necessary image corrections, measure intensity and a plethora of other features. With the advent of machine learning, computers can significantly improve performance of crucial image analysis methods such as segmentation and tracking. Nevertheless, machine learning based tracking still does not warrant close to 100% accuracy and remains a challenge even with the best available methods. Therefore, it is crucial to also have access to software that enables the curation of tracking data. Curation - usually performed by the user - requires a tool that enables correction of track trajectories but also allows a user to verify other tracks that may result in measurement of irrelevant objects (such as image artefacts or dead cells).

3.1.5 Optogenetic systems enable dynamic perturbation

In addition to visualisation, perturbation methods are required in order to decode and rewire the vast information network of molecular topologies. Traditional techniques include cellular stimulation by growth factors or insertion of mutant protein-coding DNA (see Fig. 3.4) (W. D. Mühlhäuser et al., 2017). Although such perturbations have furthered our understanding of signalling networks by elucidating on protein-protein interactions, they lack the spatial and temporal resolution to decipher networks crosstalks and more elaborate signalling subtleties such as negative or positive feedback-loops.

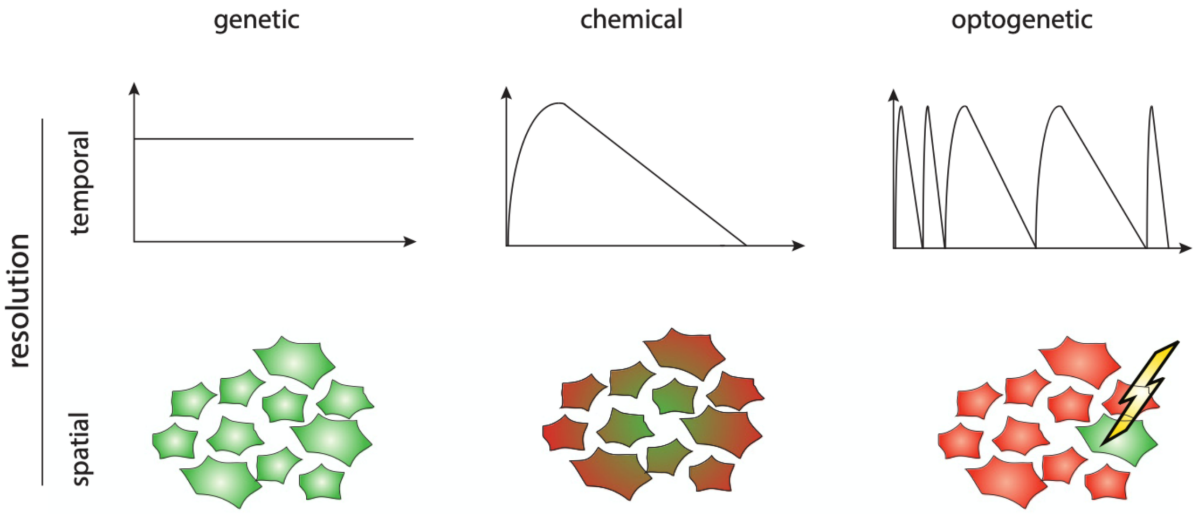

Fig. 3.4 Optogenetics provides perturbations of highly spatiotemporal resolution, in comparison to genetic or chemical stimulations. Figure from W. D. Mühlhäuser et al. (2017)

Optogenetics provides excellent control of biochemical networks (see Fig. 3.4) by using optically active protein domains. In addition to the inherent low invasiveness, optogenetics grants high spatiotemporal control and specificity of target proteins in single living cells or organisms. Optogenetic systems based on photosensitive proteins such as light-oxygen-voltage 2, cryptochrome and phytochrome have been used for plasma membrane recruitment of proteins in order to induce activation of signal transduction pathways (Aoki et al., 2013; Johnson et al., 2017; Toettcher et al., 2013). Such tools should enable us to directly activate oncogenic stimuli, study non-linearity features of signal transduction pathways and address non-genetic heterogeneity.

3.1.6 Concluding Remarks

In this chapter, I present a series of methodological developments, some of which have directly had a crucial role in biological projects (see Chapter 2). Specifically, I describe 1) the optimisations of blue- and green-based FLIM-FRET *NyxBits* reporters with recently developed 'dark' FPs (Murakoshi and Shibata, 2017; Murakoshi et al., 2015) 2) the construction of a custom-made software pipeline for the analysis of two-channel microscopy images for ratiomatric-based seFRET single-cell measurements and 3) the development of phytochrome and LOV-based optogenetic systems.

3.2 Results

3.2.1 Enhancing NyxBits FLIM-FRET pairs

To improve the original *NyxBits* reporters developed in-house, it was decided to pair the donors to recently engineered 'dark' acceptor proteins with low quantum yield (the number of photons emitted over those absorbed).

Improvement of the Blue FLIM-FRET pair

The optical properties of the original blue sensor (namely mTagBFP-sREACh) were already satisfactory and readily functional for experimental purposes. However, the residual fluorescence of sREACh caused by direct donor excitation light presents a complication for accurate FRET efficiency determination. Indeed, mTagBFP-sREACh displays a suboptimal FRET efficiency of 34%. Thus, it was decided to replace sREACh with ShadowG (Murakoshi et al., 2015) and ShadowY (Murakoshi and Shibata, 2017) dark acceptor proteins. With excitation wavelengths peaking at 486nm (ShadowG) and 519nm (ShadowY), these proteins were chosen due to their optical compatibility – higher molar exctinction coefficients and less spectral overlap – with mTagBFP (emission at 457nm) and particularly low quantum yield (φ). Both single and tandem dimer (abbreviated as TD) sensor configurations were tested.

The original sensor exhibits a lifetime value of approximately 1300ps; effectively a FRET efficiency of 34%. Pairing mTagBFP with single and TD-ShadowG further decreases fluorescence lifetime values to 1200ps and 1100ps, respectively (see Figure 3.5 on the facing page). However, mTagBFP-TDshadowG displays significant spectral bleed-through, as suggested by the osberved 'shoulder' at 490-560nm. Although consistent with ShadowG's emission spectra, this finding is surprising as the protein's quantum yield of 0.005 is far inferior to sREACh's of 0.07. mTagBFP-sREACh on the other hand also suffers from bleed-through ('shoulder' visible at 530nm) but to a much lesser extent than with mTagBFP-TDshadowG. Finally, with a single ShadowG, this FRET-FLIM pair shows perhaps the best – although barely – spectral profile; no 'shoulder' is apparent but a slightly increased intensity within ShadowG's emission range when compared to mTagBFP alone. Thus, although mTagBFP-ShadowG has a minimally improved FRET efficiency (from 34% to 38%) and spectral profile, these enhancements do not warrant the consideration of this pair for the further development with a sensor domain.

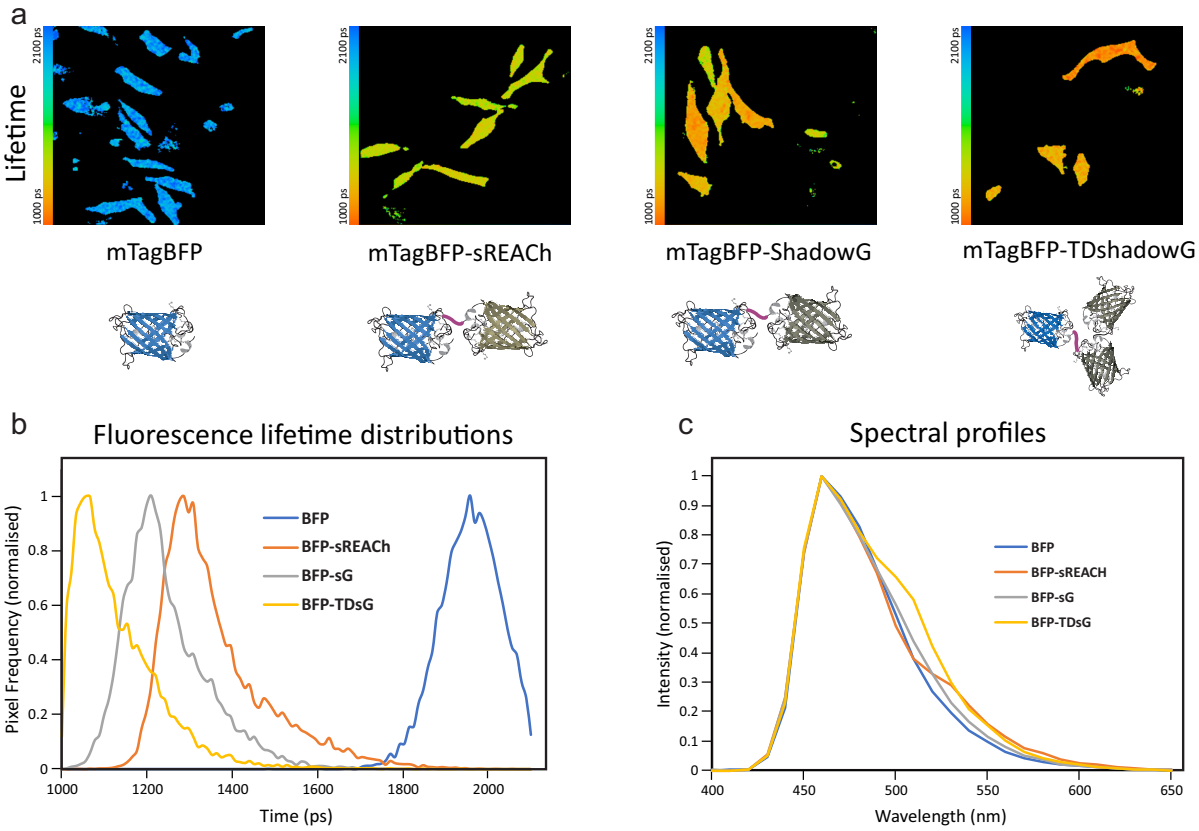

Fig. 3.5 Substitution of sREACh with two dark yellow ShadowG proteins results in lowest fluorescent lifetime, suggesting the highest FRET efficiency. However, both sensor versions with ShadowG display overall a high spectral bleed-through.

Fluorescence lifetime values of the ShadowY-containing pairs proved to be either the same (mTagBFP-TDshadowY, 1300ps) or shorter (mTagBFP-ShadowY, 1100ps) than the original blue sensor (see Figure 3.6). The aforementioned 'shoulder' at 530nm displayed due to residual sREACh emission is quite apparent when compared to both ShadowY-containing pairs which show practically an identical spectral profile to mTagBFP alone. The fluorescence lifetime of 1100ps of mTagBFP-ShadowY effectively results in a FRET efficiency of 43%. The increaed FRET efficiency and reduced residual fluorescenece of the accept makes of mTagBFP-ShadowY an more efficient FRET-FLIM pair for multiplexed detection.

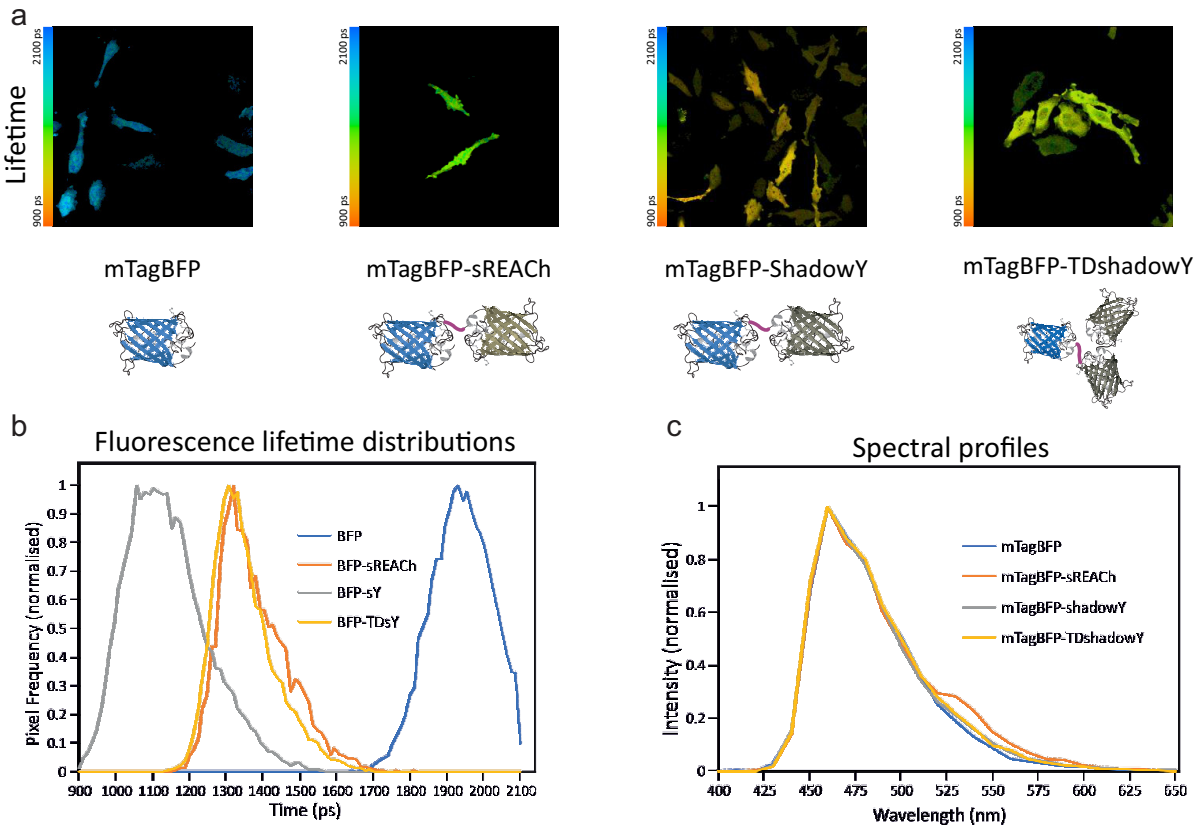

Fig. 3.6 Substitution of sREACh with a single dark yellow ShadowY protein produces a blue FRET pair with enhanced fluorescence lifetime and negligible bleed-through

ShadowY as a dark acceptor for mAmetrine

The original green FLIM-FRET pair (namely mAme-msCP576h) already shows excellent optical properties; with a FRET efficiency of 44% and no spectral bleed-though, it is the best pair of the NyxBits platform. Although msCP576h did not exhibit apparent

issues in aggregation, msCP576h was not monomerized. Therefore, it was considered to pair mAmetrine with ShadowY because ShadowY might remove concerns related to potential aggregation and still exhibits a better spectal overlap with mAmetrine. This overlap suggests that FRET efficiency may be further improved, without affecting spectral bleed-through as ShadowY has a low quantum yield of 0.01. Fluorescence lifetime measurements show that mAme-msCP576h exhibit a higher FRET efficiency (see Figure 3.7) when compared to both single and tandem-dimer ShadowY configurations (both with a lifetime of approximately 1800ps, or around 35% FRET).

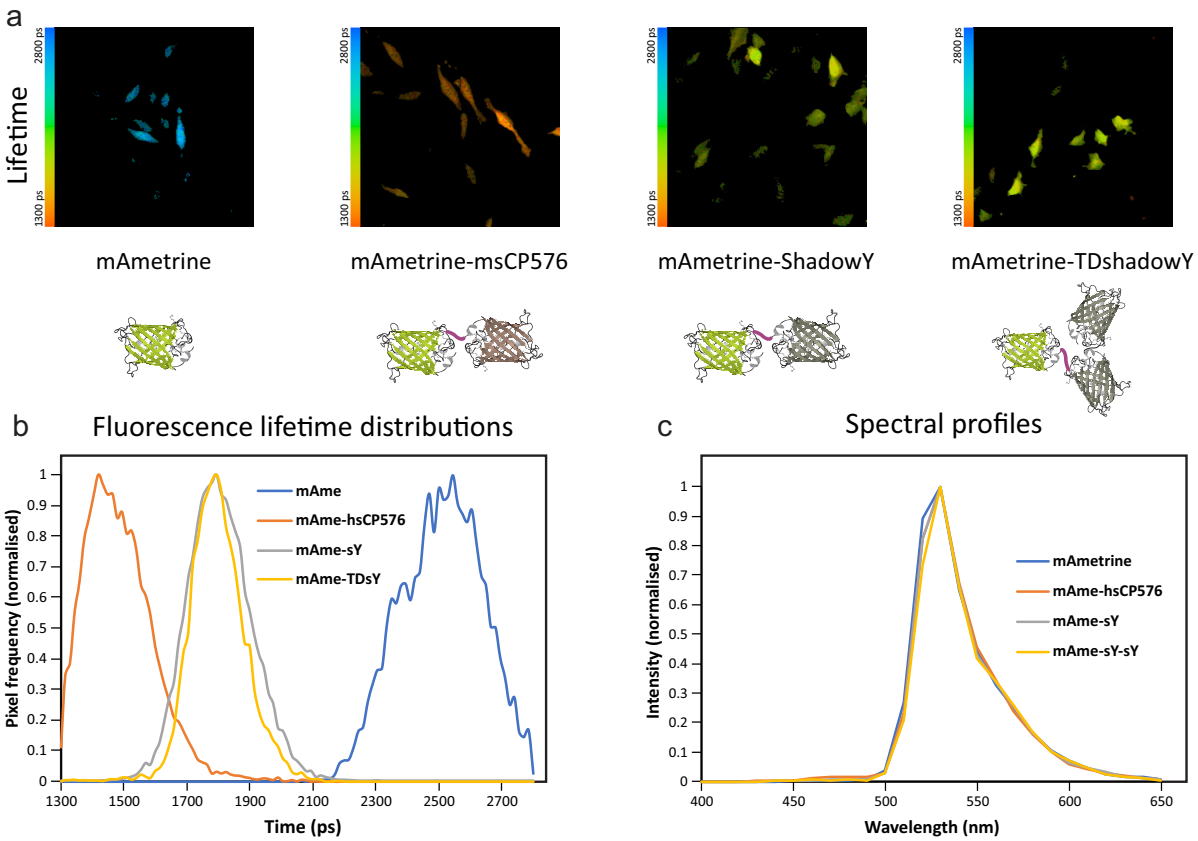

Fig. 3.7 mAmetrine-hsCP576 remains optically superior when compared to new sensors using ShadowY as a dark acceptor.

mAmetrine-ShadowY is thus a viable alternative to mAmetrine-msCP576h for sensors where msCP576h might induce aggregation although for the specific backbone that was attempted (direct fusion) a partial loss of FRET efficiency is observed.

3.2.2 Design of an Image Analysis Pipeline for Single-cell FRET Measurements

Althouth the laboratory has several toolboxes programemed in Matlab that are dedicated to the analysis of seFRET data, segmentation and tracking of SW48 cells has posed specific challenges. Compared to parental SW48, mutant cells are often of irregular shape and adhere more to each other. Analysis of SW48 data required intensive manual curation of the data. Hence, I opted to code a dedicated analysis workflow with the aims of:

1. Improve the quality of the segmentation and tracking using machine learning algorithms
2. Renovate the analysis workflow utilizing Python (departing from Matlab) to further open up our data infrastructure to the broader community
3. Provide a semi-supervised workflow to provide high quality single-cell analysis of biochemical traces and statistical description

The tool I have developped is named PyFRET and it will be available to the community as a GitHub public repository. I opted for Python as the primary programming language for a several reasons. First, Python is among the 'easy-to-learn' programming languages and its open-source nature means that its usage is free of charge to anyone, thus displaying attractive economic and learning accessability. This fosters the exchange of useful software as well as skill by the improvement of software by other interested parties. Second, In addition to its growing worldwide popularity, there is an extensive number of libraries available that facilitate useful functions. Lastly, Python's access to powerful machine and deep learning libraries – such as Keras and Tensorflow – that can be harnessed to dramatically improve traditional image analysis techniques such as segmentation.

Before an image is analysed in any way, it needs to be imported first. Image file selection occurs once executing the main *PyFRET* script. Importantly, the user is asked (via the Command Prompt/Terminal) a series of queries in relation to the imaging experiment (see suppl. Fig. 3.22 on page 123). User input, together with other basic image metadata, is then saved as experiment metadata and later used for automatic plotting. Data from the first field of view (FOV) is then loaded and ready for processing.

Segmentation

Segmentation is the classification of the image's pixels to enable the measurement of objects of interest. Among the various segmentation methods, the most common and simple is thresholding; setting a minimum intensity value above which pixels are considered as the 'foreground'. Such calculation can be performed manually by a user, but certain algorithms such as Otsu's method have been developed to enable automatic optimised thresholding. Although useful, thresholding typically requires a clear bimodal distribution of an image's intensity values. This requirement can be problematic when segmenting noisy images (high background signal and/or low signal intensity of objects). In addition, thresholding does not take into account the spatial context of regions of interest; different objects may be part of a same mask (a 'foreground' region in the image) due to their spatial proximity and similar intensity values.

Indeed, in the example image shown in Figure 3.8 on the following page, thresholding performs well only when nuclei are well separated from one another (see Fig. 3.8A). However, when cells adhere to one another (a hallmark of the SW48 cells, particularly those with a mutation in KRAS) simple thresholding results in segmentation of cell 'clusters' as opposed to single cells (see (B) in Fig. 3.8).

Threshold-induced undersegmentation is most prominent when a FOV experiences focus drift (see (C) in Fig. 3.8), resulting in higher intensity values between cells and thus less contrast. FOVs with many cells (ie 'crowded' FOVs) (see (D) in Fig.3.8) are commonly acquired due to the potentially higher quantity of information (more cells) as well as the cellular behaviour (cluster-like growth). Yet again in this scenario, threshold-based segmentation provides a poor separation of individual cells. To further improve threshold-based segmentation it is common (and necessary) to make additional image operations such as watershedding. Although the watershed manipulation results in more regions being defined (see (D) in Fig. 3.8), false merges (masks overlaying more than one cell) are still clearly visible (see (C) in Fig. 3.8).

With the advent of machine learning, new tools leverage this technology with the aim of dramatically increasing segmentation performance and accuracy. Such tools were considered due to the complex images requiring better performance than traditional threshold-based segmentation. These include StarDist, ilastik and Cellpose. The latter is a generalist, deep-learning based algorithm developed to segment a wide variety of biological objects of interest without the need to adjust parameters or re-train the

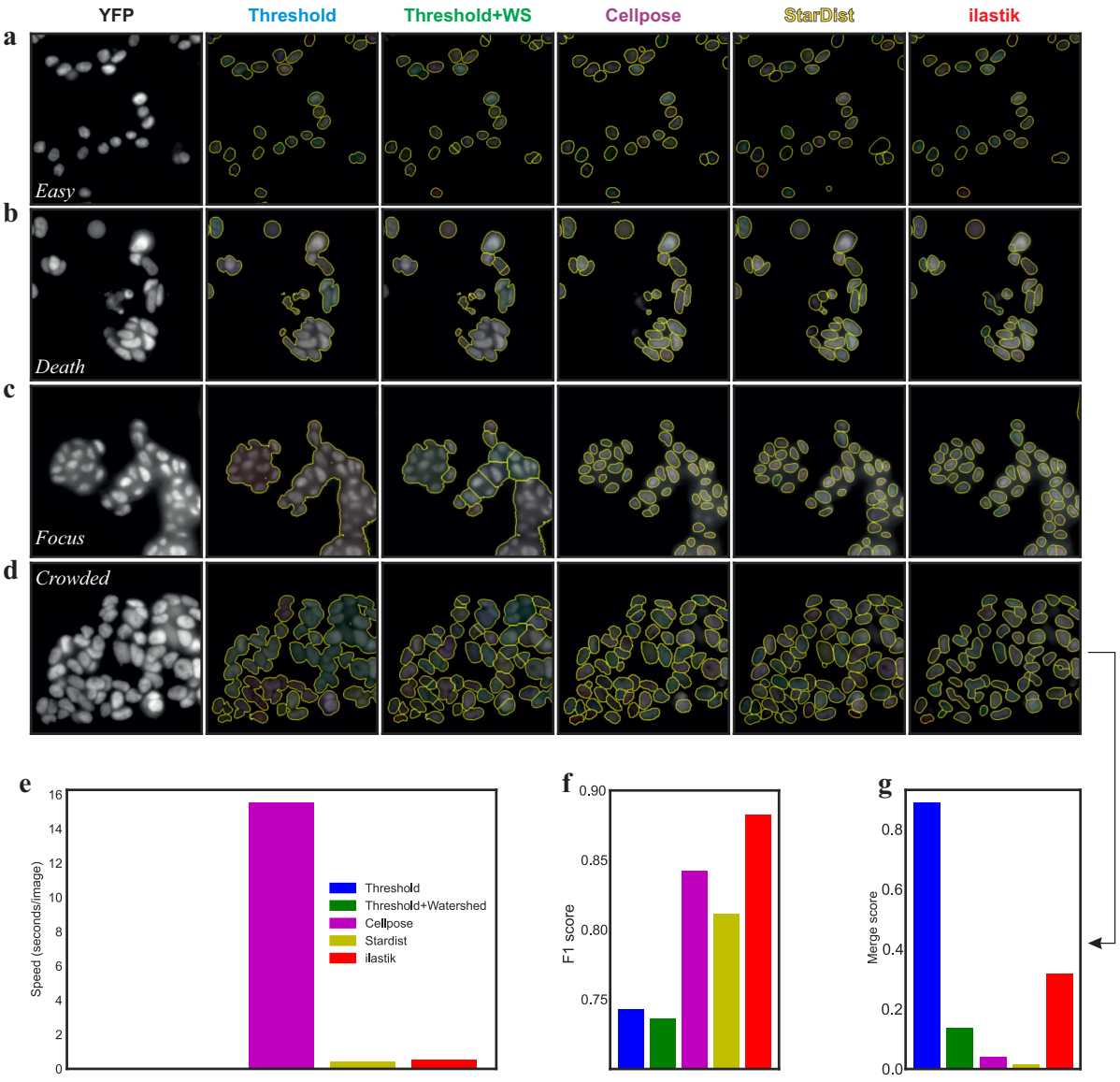

Fig. 3.8 Comparison of several segmentation methods with different image case scenarios. Various segmentation results are visually displayed for the easy (a), death (b), focus (c) and crowded (d) scenarios. All segmentation methods were compared by speed of execution (e), F1 score (f, a measure of both accuracy and precision) and merge score (g) which designates the number of true objects that have been merged. For both (f) and (g), a higher score indicates higher precision/accuracy and higher number of merged objects, respectively. Graph (g) only relates to the crowded (d) scenario.

algorithm (Stringer et al., 2020). StarDist makes use of star-convex polygons and a U-net (Ronneberger et al., 2015) based lightweight neural network. The developers state that StarDist addresses problematic scenarios such as crowded field of views (FOVs) where many 'foreground' masks may overlap with one another (Schmidt et al., 2018). Finally, ilastik is a tool designed to facilitate several machine learning based image processing techniques (including segmentation) by training a non-linear classifier in an intuitive (ie no programming required) and interactive manner (Berg et al., 2019).

In our tests, all the machine learning based tools provide significantly improved segmentation performance over threshold-based operations. Notably, the biggest improvement is observed in the FOV with focus drift (see (C) in Fig. 3.8) where 'smart' software successfully detects slightly-out-of-focus cells. However, not all tools perform identically. Although the F1 score (metric for overall accuracy) indicates ilastik as the best performer (see (F) in Fig. 3.8), the measure does not account this tool's poor performance in false splits (where a nucleus has been assigned more than one mask) or false merges. Overall, these tools display very low rates of such inaccuracies in all scenarios (see suppl. Fig. 3.23 on page 124). However, ilastik performs relatively low in the 'crowded' scenario, where it has a false merge score comparable to threshold-based methods (see (G) in Fig. 3.8). Both StarDist and Cellpose perform well in all cases, including in the difficult crowded and focus drift scenarios, showing very low levels of false splits or false mergers. The major limitation of Cellpose is the speed at which each images are processed (see (E) in Fig. 3.8). The iteration time of 15s/image is drastically longer than the other 'smart' tools (approximately 0.5s/image each) and thresholding-based operations (<200ms/image). Due to the large number of frames in a multi-position timelapse acquisition, such a slow speed causes unsustainably large processing times.

Therefore, I selected StarDist for integration within PyFRET.

Tracking

Tracking is the extension of segmentation in the time dimension where objects are not just separated in each frame, but their identity preserved over the entire timelapse. Briefly, segmentation provides masks (binary images) used to assign a unique label (an id number) to each cell within a field of view. At each subsiquent time point, cell IDs are then propagated to the new masks, and so on and so forth until the last frame of the timelapse. This procedure results in the tracking of individual cells in space and time.

After an extensive literature review, I selected ilastik, a tool developed by Haubold et al. (2016). Ilastik demonstrated high performance and was designed to enable non-

programmers the ability to use machine learning-based image analysis operations. The tool includes a number of workflows, of which *Object Classification [Inputs: Raw Data, Segmentation]* is used.

First, a machine learning model needs to be trained in order to yield successful single-cell tracks. I used a set of 10 images representative of the breadth of scenarios captured on a fluorescence widefield microscope and using nuclear ERK FRET-expressing SW48 colorectal cells. The training consists in the user interactively assigning (via the user interface (UI)) true and false detections, as well as the number of objects (cells) of an inaccurate mask. Once satisfactorily trained, a project file generated by ilastik can be used for tracking analyses of similar-looking images. Although ilastik is meant to be mainly used through its UI, it can also be used programmatically.

Therefore, ilastik can be summoned from Python (using *headless* mode). In short, the segmentation masks generated from Stardist (see section 3.2.2 on page 89) together with YFP-channel images are 'fed' to ilastik, which then uses the assigned trained model to generate an image file containing masks with cell-specific labels across space and time. Thus, this machine learning-based tracking approach enables effective artefact discrimination, sensitive segmentation and high performance tracking.

The analysis performed by ilastik is relatively accurate. However, our final analysis is carried out on fully curated datasets to avoid possible artefacts that might occur because of missegmentation (e.g., in clustered cells) or mistracking (e.g., due to mitosis; see (a) in Fig. 3.9 on the next page). When a field of view (FOV) contains a high number of cells, a significant number of these tend to either stay at the border or come in and out of the FOV. ilastik does not discriminate cell detection at specific locations such as the border. However, these cells should be discarded from (single-cell) analysis since they cannot provide accurate FRET quantifications, if at all (ie not in frame). Thus, masks touching any FOV border are automatically removed via Python.

Moreover, mitotic events are commonly observed in our typical 12-hour imaging experiments. When a cell divides, its daughter cells should be assigned new labels. In ilastik, the option to train a model to detect mitotic events is available. However, the imaging conditions needed to train the model are too simplistic and restrictive; mitosis can be detected mostly if it occurs between two consecutive frames. In our timelapse experiments, the high frequency capture and seemingly long mitotic events of SW48 cells means that cell division can be observed over a long period of time (up to 10 frames or 60 minutes). For this reason, I did not enable mitotic detection in ilastik and

instead use a custom method to automatically detect cell divisions and amend cell tracks accordingly. To do this, the cell area is measured to infer divisions; generally dividing cells are relatively large in size, but cell area is greatly reduced when daughter cells appear on the focal plane. If such area reduction is detected in a tracked cell, its label will be terminated 10 frames prior to the inferred mitotic event (this is to prevent inaccurate measurements of actively dividing cells), after which a new label will be assigned to the daughter cell (see suppl. Fig. 3.24 on page 125).

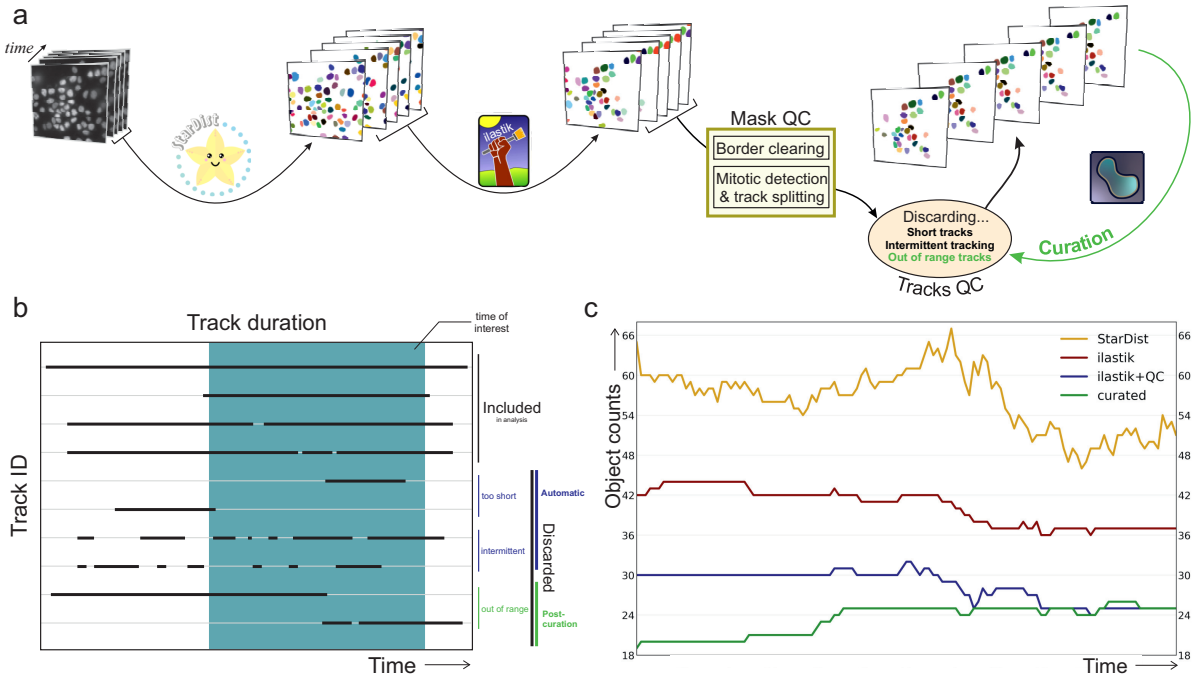

Fig. 3.9 After an image file is segmented with StarDist, ilastik is used to enable machine learning-based cell tracking and further prune data with quality control procedures (a). Cell tracks are discarded if they do not meet specific requirements (b). The number of objects decreases with each analysis step after segmentation in favour of higher accuracy, as shown in the example graph (c)

In addition to these categorical (border clearing) and morphological (mitosis) 'filters', quality control checks were also perofmed on track lengths.

Cells ought to be tracked during the whole duration of the imaging experiment. Whole-experiment or long tracks are preferred as the interest lies in monitoring sensor information (in this case ERK activity) during and across treatments. However, ilastik tends to yield tracks of varying length as well as frequency (see (b) in Fig. 3.9). What determines the length of a track is the detection or loss of a cell-label assignment by

ilastik. The start of a track may represent the appearance of a cell via mitosis or by entering the FOV. Track termination however may represent cells that disappear by death, division or exiting the FOV or the focal plane. Thus short tracks result from appearance and disappearance events that occur in a short window of time. If this occurs on repeated occasions, it can lead to tracks with many 'gaps', as shown in (b) in Figure 3.9 and named as intermittent tracks. A real world scenario are cells remaining close to the edge of a FOV and often entering and exiting the FOV over time. Thus, these tracks are likely to represent cells that cannot be tracked in a reliable way and so are considered unsuitable for analysis. Labels of short and intermittent tracks are assigned *false detection* labels which will be later ignored during measurements.

It is noteworthy to indicate that ilastik can, on occasion, assign more than one label to a same cell. This can happen due to movement and/or focus-induced complexity and the trained algorithm not being able to successfully infer cell-specific events over time. Such tracking misinterpretation can result in multi-labelled cells and ensuing tracks that are not within a time range of interest (treatment time, for example). In other words, an out-of-range track might represent a fraction of a cell's true trajectory. Out-of-range tracks are only discarded after curation (see (b) in Fig. 3.9) since they 1) might be useful for curation purposes (further explained in *Curation* section) and 2) are more likely to represent a true short track after human assessment.

There is a great difference between the number of objects (cells) detected with StarDist only and after tracking and all the quality controls implemented (see (c) in Fig. 3.9). However, using a machine learning-based approach and programmatically filtering tracking data based on cell type-specific characteristics provides us with accurate results and eases the burden on the manual-intensive curation process.

Measurement

After segmentation, tracking and data pruning by unsupervised quality control, an image file and tracking masks are obtained. Next, data is prepared for single-cell analysis of the FRET ratio.

First, both individual channel images (ie YFP and CFP) are denoised by median filtering and background substracted. A non-zero background is always present because of camera noise, stray light and unspecific fluorescence emission from media. Then, I generate an acceptor:donor FRET ratio image (see Fig. 3.10 on the next page), representative of the FRET activity of the expressed sensor. This is the image used to make intensity-based measurements. Finally, the tracking masks are *eroded* to minimise inaccurate

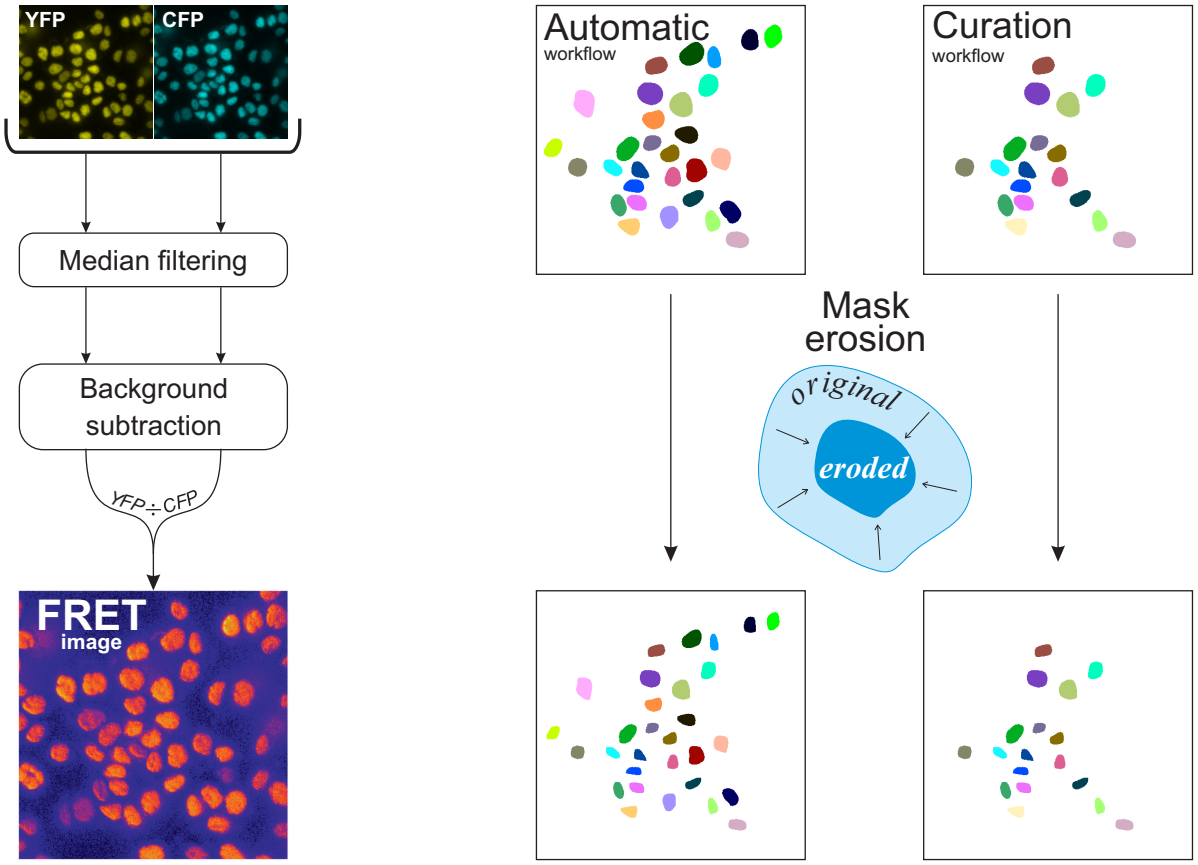

frame	*median*	*mean*	*stdev*	*variance*	*IQR*	*FOV*	...
1	2.08	2.01	0.21	0.05	0.24	10	···
2	2.01	2.01	0.14	0.02	0.22	10	···
3	2.15	1.07	0.16	0.03	0.32	10	···
4	1.94	1.93	0.19	0.04	0.3	10	···
5	1.54	1.68	0.17	0.03	0.23	10	···
6	1.47	1.55	0.14	0.02	0.18	10	···
7	1.38	1.45	0.10	0.01	0.1	10	···
8	1.35	1.39	0.07	0.01	0.09	10	···
9	1.31	1.34	0.06	0.0	0.07	10	···
···	···	···	···	···	···	···	···

frame	*FOV*	*ID*	*intensity*	*area*	*centroid-y*	*centroid-x*	...
1	10	6	2.07971	729	114	227	···
1	10	8	2.18095	863	152	326	···
1	10	14	1.88851	1178	167	216	···
1	10	23	2.16944	1169	188	275	···
···	···	···	···	···	···	···	···
2	10	6	2.12244	903	110	233	···
2	10	8	2.14144	963	146	326	···
2	10	14	1.83314	1152	170	222	···
2	10	23	2.10481	1280	180	283	···
···	···	···	···	···	···	···	···

Fig. 3.10 The intensity image and tracking mask undergo simple operations to ensure accurate and reliable measurements.

boundary measurements resulting from slight image misalignment, for example. Once the intensity image and tracking masks have undergone the aforementioned operations, intensity properties are measured for all frames of a timelapse.

Depending on whether tracking masks are curated or not, the script will generate one or two tables (see Fig. 3.10). When an image file is analysed for the first time, fully automated analysis will only yield a whole FOV database (hereon referred to as DB^{FOV}_{whole}). In other words, the *automatic workflow* in the analysis pipeline only records the mean values of all the single-cell intensity features that are measured. Contrarily, when curated masks are available, a table with single-cell properties (hereon referred to as DB^{FOV}_{s-c}) is saved in addition to DB^{FOV}_{whole}. The pipeline is designed in this manner since non-curated tracking masks are not reliable enough to provide truly accurate single-cell data. Hence, only after visual inspection and correction the script can record single-cell measurements (for full list see suppl. Table 3.1 on page 127) as the assumption after curation is that cell tracks are the true representation of the cells' spatial trajectories.

Last but not least, collected data is used to automatically plot an FOV-specific mean FRET values, as well as raw cell-specific and background signal intensity of both individual channels. This allows fast inspection of the technical and biological signal, which may inform the viewer of potential artefacts and warrant further investigation. Once all FOVs of an imaging experiment have been automatically measured, a master database containing whole FOV properties of all FOVs is saved (hereon referred to as DB^{master}_{whole}). If curation data is available, a master database containing all single-cell data of all FOVs (hereon referred to as DB^{master}_{s-c}) is saved in addition to DB^{master}_{whole}. These rich databases are then used to generate basic plots and further processing (see section *Analysis – Dynamics & Clustering*).

Curation

Automatic analysis of image files allows the harvesting of imaging data in a time-efficient manner and without any input from the user. However, too often automatic measurements fall short of high levels of accuracy, despite the use of AI-aided tools and the ensuing increased performance. It is no different in this analysis pipeline, where ilastik tracks do not yield the accuracy required to reliably analyse single-cell data. Even after applying quality control steps, tracking events such as inaccurate splits, disappearances and appearances remain in the data. Thus, manual curation of cell tracks is still required if one is to yield highly precise data. Although averages of experiments are unaffected by

residual error, highly accurate single-cell analysis always requires manual curation aimed to furher prune data from misegmented or mistracked objects.

The key aspect of curation software is the ability of a user to navigate the raw data (intensity images) compare it with the tracking data and iteratively amend tracking in a time efficient manner. Supervised curations requires significant resources and several graphical tools. I have tested bespoke software available in *Matlab* in the laboratory, and tools available in the community including *ImageJ*, *CellProfiler*, *Omero* and others. *ImageJ* and *CellProfiler* did not seem to be as intuitive and *Omero* does not provide a good range of tools for manual curation.

Therefore, I decided to integrate napari – an open source *Python* image viewer – into my imaging pipeline. napari provides a range of intuitive tools with full GUI support. Being open source, I was able to build and integrate additional custom functions on top of napari's original framework. In this section I will describe napari's viewer, its native features and my own implementations designed to further facilitate manual curation (as illustrated in Fig. 3.11 on the next page).

When napari is instantiated from a custom *python* script, a GUI with several sections appears (see (a) in Fig. 3.11). First, the viewer section displays any image files added to napari. Different types of data can be loaded to napari, including images, masks, points and shapes, among others. When each data type is added, it is displayed as a layer in the *Layer list* section of (see (c) in Fig. 3.11). In this case, I have facilitated a specific button function '*Load materials*' (see (d) in Fig. 3.11) which automatically adds all the necessary data to enable cell track corrections. The essential layers are added (see (c) in Fig. 3.11, namely an intensity image (to assess the raw data) and the corresponding cell masks (for correction) obtained from filtering ilastik's tracking masks. Above the *Layer List* is the *Layer Controls* (see (b) in Fig. 3.11; this section displays layer viewing information as well as access to important mask editing tools allow a user to pick a label (colour), paint, fill and effortlessly fix track mislabelling by activating the n-dimensional function.

These are useful tools to amend cell masks in the current (and contiguous) frame of the viewer. However napari is yet to natively display tracking data. This is a necessary feature as it allows the user to better assess any potential corrections to be made. For this reason, I integrated a *Tracks Graph* that displays single-cell tracks over the course of the entire experiment and with matching colours to the mask layer (see (e) in Fig. 3.11).

Moreover, with the aim of minimising manual curation effort, the *Tracks Graph* displays the time of interest (determined by user input).

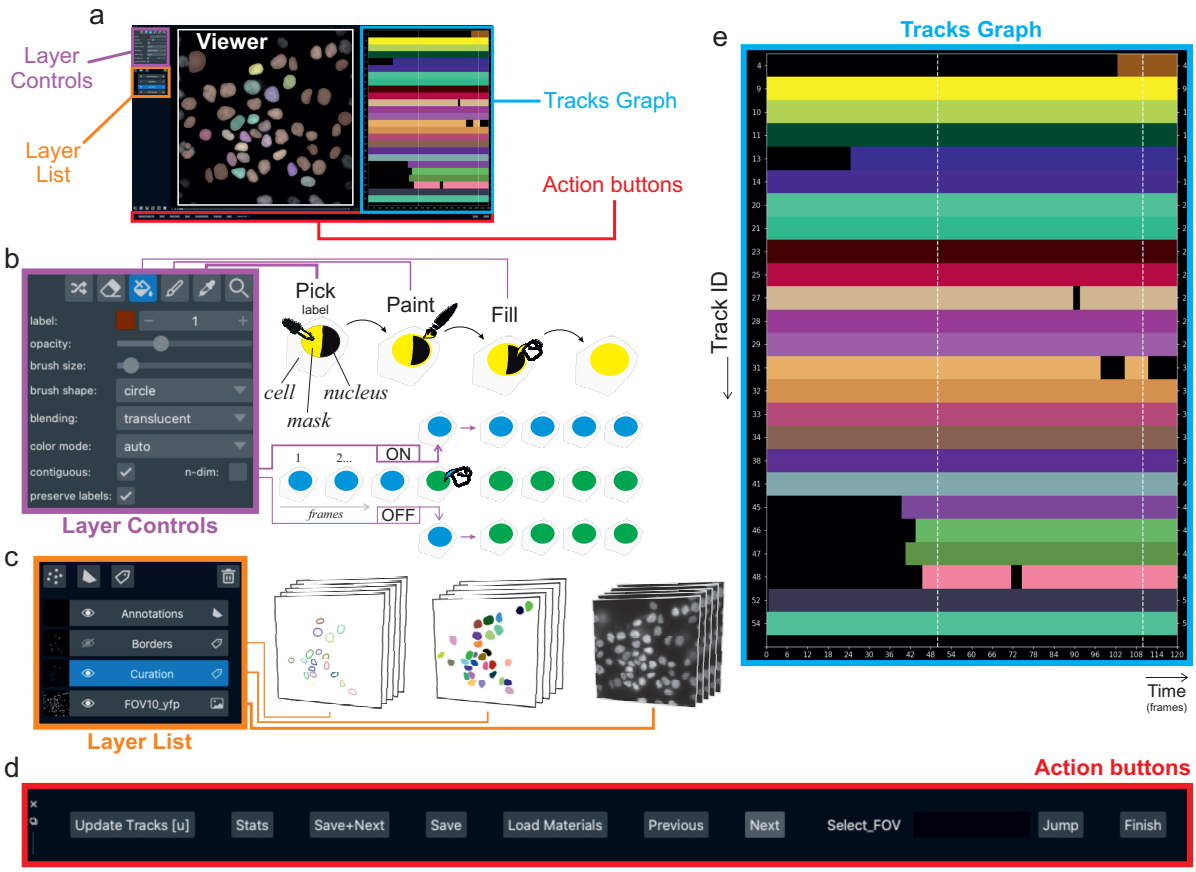

Fig. 3.11 napari provides a useful platform to curate single-cell mask data as well as enabling the integration of custom functionality to achieve a more comprehensive curation experience. napari mainly constitutes a viewer window (a), including a Layer Controls panel (b) to amend and access layer-specific features and a Layer list panel (c) containing layers of different data types. Moreover, custom-made panels such as an Action buttons bar (d) and a Tracks graph (e) has been added to facilitate the curation of image files.

Finally, because napari is still rather in its infancy stages as a standalone image viewer, it requires the use of *Python* to add and retrieve layer data. These and other operations are frequently repeated over the course of curation of a whole imaging experiment. Thus, to maximise efficiency, I have integrated an *Action Buttons* widget containing practical buttons. These provide easily accessible and click-executable functions as follows:

- *Update Tracks [u]*: updates the tracks displayed in the *Tracks Graph* and the *Borders* layer (mask contours). In brackets is the keyboard's letter shortcut.

- *Stats*: displays time information, as well as the number of merged masks in the tracking data
- *Save+next*: saves current curation data and replaces all layer data with that of the next FOV
- *Save*: saves current curation data
- *Load Materials*: loads all the layer data required for curation of cell tracks of currently displayed FOV
- *Previous*: Removes all layer data and displays the previous FOV intensity image
- *Next*: Removes all layer data and displays the next FOV intensity image
- *Select FOV – Jump*: Allows user to view the intensity image of a specific FOV by typing the desired FOV number and consequently clicking on the *Jump* button
- *Finish*: initiates single-cell measurement of all FOVs in an imaging experiment

Analysis – Dynamics & Clustering

Upon curation of tracking masks, re-analysis yields FOV-specific single-cell (DB^{FOV}_{s-c}) and population (DB^{FOV}_{whole}) databases saved in each FOV analysis folder. Moreover, all FOV-specific databases are collated together to produce DB^{master}_{whole} and DB^{master}_{s-c} (see 3.25 on page 126). This is to enable access to experiment-wide population and single-cell information. These databases are then used to automatically generate appropriately labelled plots of various biological insights.

With DB^{master}_{whole}, mean FRET data is plotted according to treatment group (up to 4 groups supported), either separately (with treatment labelling) or in the same graph (see (a) in Fig. 3.12 on the next page). With DB^{master}_{s-c}, probability density function graphs are generated, providing a better view of the data distribution across time (see (b) in Fig. 3.12). Moreover, signalling activity over time comprises a wealth of information in addition to the FRET value. Features, such as signal amplitude, number and frequency of peaks, basal activity (see (c) in Fig. 3.12) and many others can be used to make further biological inferences. These signal characteristics are measured from DB^{master}_{s-c} and stored in a new 'single-cell features database' (hereon referred to as $DB^{s-c}_{features}$). These signalling features are automatically visualised as a matrix (see (d) in Fig. 3.12).

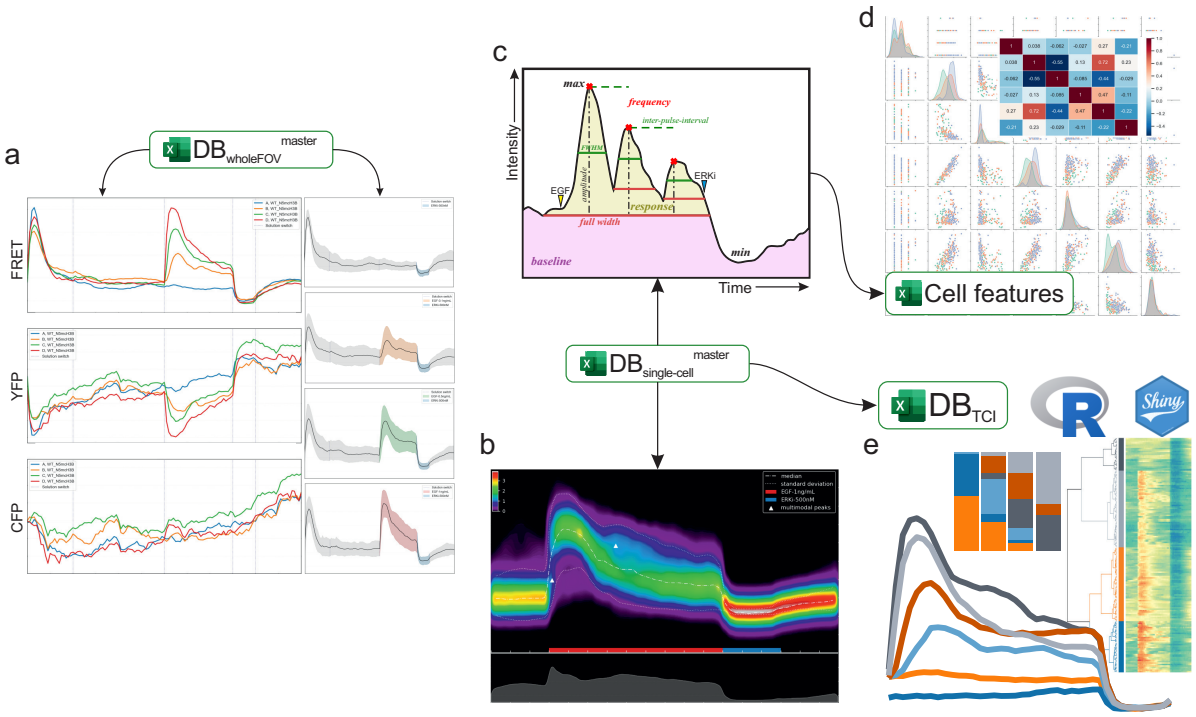

Fig. 3.12 Whole FOV measurements allow the visualisation of average FRET activity (among others) according to pre-defined treatment groups (a). Curated data yields single-cell FRET measurements enabling new types of visualisation (b), further analysis via cluster (e), the quantification of signal features (c) and the ensuing potential correlations (d). Data shown is for illustration purposes only *FWHM*: full width half maximum

Similar types of signalling analyses are carried out by other researchers. In fact, Dobrzyński et al. (2019) made an *R* and *Shiny*-based app (Time Course Inspector or TCI) built to provide exploratory and clustering data analysis capabilities specifically for sensor readout activity in single cells. The only requirement is that single-cell data needs to be provided in a specific format. Thus, a TCI-specific database is also automatically generated from the DB_{s-c}^{master}, mainly to take advantage of the clustering capability of TCI (see (e) in Fig. 3.12).

Overview

The presented ***Python***-based pipeline (*PyFRET*) integrates multiple open-source projects designed for specific image analysis purposes (see Fig. 3.13 on the following page). **StarDist** uses R-Convoluted Neural Networks (Schmidt et al., 2018; Weigert et al., 2020) for precise and accurate nuclear segmentation. **ilastik** (Berg et al., 2019) enables interactive single-cell tracking using machine learning algorithms. **napari** (Contributors, 2019) is an image multi-viewer for python with built-in tools to modify tracking masks generated by ilastik. Masks are used to measure properties including signal intensity. Finally, data is visualised in the form of automatically-generated 'signal activity' graphs or clustered using **Time Course Inspector** (Dobrzyński et al., 2019).

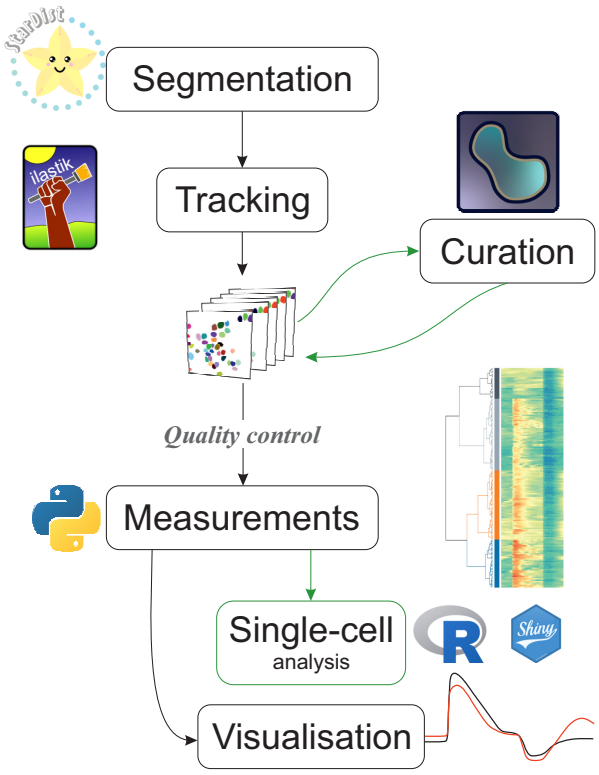

Fig. 3.13 Schematic representation of *PyFRET*. StarDist and ilastik are open-source projects, here used for image segmentation and tracking, respectively. Tracking masks are used for intensity-based measurements. Finally, data is plotted for visualisation of signalling actvity. Green arrows indicate the additional steps required to achieve single-cell information. napari is used for the curation of tracking masks, cells are re-measured and single-cell data is undergoes hierarchical clustering in the Time Course Inspector R/Shiny app.

3.2.3 Development of photo-inducible RAS systems

Optogenetic tools can provide significant advantages compared to the use of growth factors. Such advantages include i) interrogation of single cells, ii) light mediated fast, non-invasive and quantitative titration of biological signals, iii) perturbation by means of direct activation of oncogenic proteins, rather than through growth factors, iv) the possibility to automate experiments, including targeted activation of oncogenic signalling, and v) enables the study of cell-to-cell communication and oncogenic signalling.

In this section I describe my efforts to establish optogenetic tools to induce light-activated oncogenic mutant *KRAS* signalling using a selection of optogenetic systems.

PhyB-PIF6

Toettcher et al. (2013) have used phytochrome B (PhyB) and phytochrome interacting factor 6 (PIF6) to recruit Son of Sevenless (SOS, a guanosine exchange factor) to the plasma membrane by light. The resulting optogenetic system – OptoSOS – activates the MAPK signalling pathway (see (A) in Fig. 3.14 on the next page). A similar strategy to OptoSOS is adopted, whereby instead of SOS, mutant KRAS is bound to PIF6. Such optogenetic system would enable us to probe cellular signalling behaviour in the context of acute oncogene activation.

The development of optogenetic tools for the activation of oncogenic RAS started with Dr. Fries, PhD student in the same research group. The system did not exhibit sufficient reproducibility and, therefore, it was deprioritized until I was able to take over the project. I will briefly describe the work previously carried out in order to better understand my work. I will show and discuss only the data I acquired, but I acknowledge the significant contribution from Dr. Fries.

The plasmid designed to express OptoRAS underwent a number of optimizations in order to guarantee controlled expression of the two elements constituting OptoRAS (i.e. the CAAX anchor and the RAS cargo) to establish stable cell lines suitable both for western blotting and imaging quantitative analysis. An optogenetic plasmid was designed under the control of a pTetOne plasmid with 1) a doxycycline-inducible promoter coding for the CAAX plasma membrane anchor domain (K-Ras CVIM amino acids) fused with PhyB and mCherry and 2) an IRES sequence for the quantitative co-expression of the second element coding for PIF6 and $KRAS^{G12D\Delta CVIM}$ (oncogenic *KRAS* lacking the CAAX domain) fused with YPet. PhyB/PIF6 interact upon red light illumination and

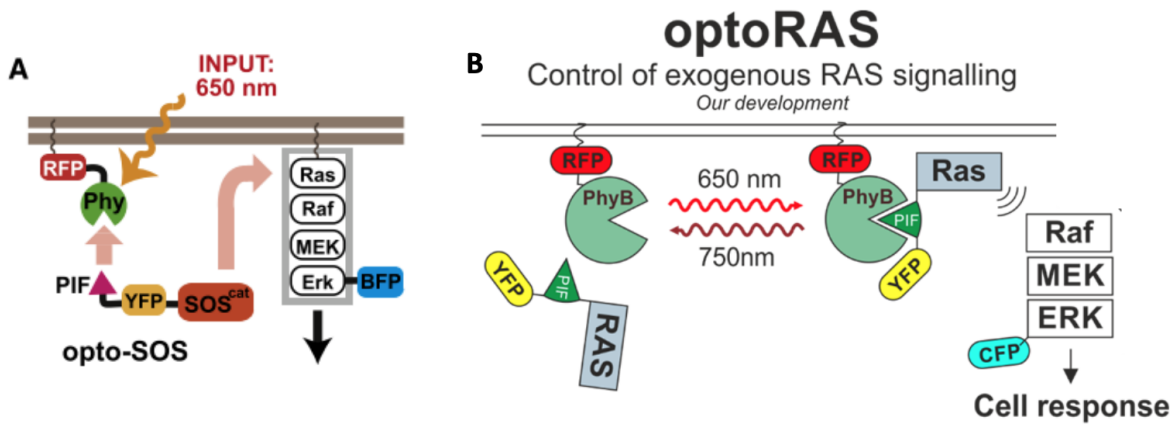

Fig. 3.14 PIF6 component bound to catalytic domain of guanosine nucleotide exchange factor (GEFs) SOS (A, from Toettcher et al. (2013)). The system can be activated by exposing the photoreceptive proteins to red light (650nm). Exposure to infrared light (750nm) induces PhyB/PIF6 dissociation. Putative model of our development: oncogenic RAS-bound PIF6 component is recruited to the plasma membrane upon red light stimulation and induces MAPK signalling (B, provided by Dr. Fries)

reconstitutes KRAS$^{G12D\Delta CVIM}$ to the plasma membrane. The mCherry/YPet fluorescent markers are utilized to quantify translocation/activation.

This particular optogenetic system, ie expression of PhyB-mCherry-CAAX and Ypet-PIF6-KRAS^{G12D} will now be referred to as OptoRAS (see (B) in Fig. 3.14). The order of the two protein coding regions and the IRES sequence were tested (data not shown) to ensure optimal expression levels of the two components (i.e. PhyB-mCherry-Caax and YPet-PIF6-KRAS$^{G12D\Delta CVIM}$).

During pilot experiments utilizing a double promoter plasmid encoding both constructs during transient expressions, effective translocation of the cytoplasmic component (i.e. YPet-PIF6-KRAS$^{G12D\Delta CVIM}$) was first demonstrated in HeLa cells. Cytoplasmic depletion of fluorescently tagged KRAS^{G12D} is observable. Equally, upon exposure to infrared light, the PIF6 component dissociates from PhyB as KRAS^{G12D} re-locates to the cytoplasm. This reversible translocation is reproducible and occurring in the 1 second time scale demonstrating the potential for these constructs to work as a fast acting, reversible and reliable optogenetic 'switch' mechanism for an oncogene.

Translocation to plasma membrane does not guarantee biological activity of OptoRAS. Therefore, the activation of MAPK and PI3K RAS-dependent signal transduction pathways were tested. HeLa cells transiently expressing OptoRAS were stimulated with red light (660nm) for one minute and different samples were prepared for Western Blot

analysis at different times (0, 5, 10, 20, 30 and 40 minutes) post-stimulation. Quantitative analysis of Western blots utilizing the LI-COR gel imaging systems demonstrated the activation of MAPK and PI3K signalling, as shown by increased levels of phospho-Erk and phospho-Akt peaking at 40 and 30 minutes, respectively (see suppl. Fig. 3.26 on page 126). These initial results suggested that light-inducible recruitment of mutant KRAS to the plasma membrane does activate RAS dependent signal transduction pathways. However, independent experiments resulted in different results and occasional phosphorylation of ERK and AKT in response to light in parental HeLa cells (data not shown).

To address the issue of reproducibility, it was decided to engineer a dedicated incubator (designated as OptoFarm, see Fig. 3.15) that permits us to control temperature and CO2 also during photostimulation. Moreover, OptoFarm provides quantitative and computer controlled implementation of light protocols with light at 480nm, 630nm and 735nm and the possibility to execute three experiments in parallel. OptoFarm was designed to ameliorate possible variations in experimental conditions caused by the optical stimulation.

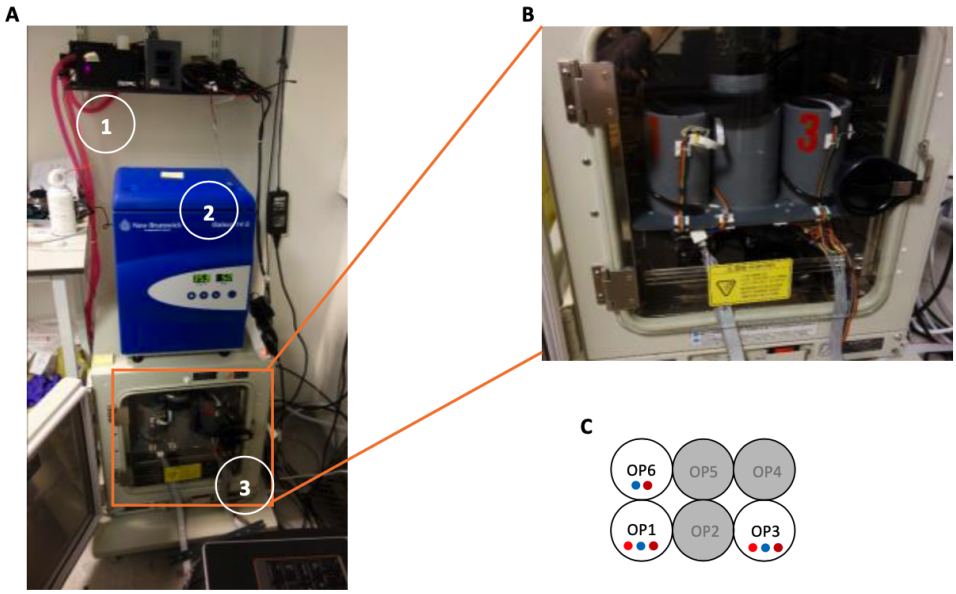

Fig. 3.15 A) The *OptoFarm* includes a water-cooling system (1) for the electronics, a small incubator (2) and a medium-sized incubator (3) containing 'optoPODs' (B), with LED ights installed at the bottom. C) Schematic of the optoPOD setup inside the incubator. Only three optoPODs are operational (coloured) with the shown lights (as dots), ie blue, red and infrared.

Aiming to eliminate the possibility that variability across experiments was caused by transient transfection, the preliminary results on HeLa cells and published work on OptoSOS, motivated us to continue the work. Therefore, it was decided to test the system on a non-transformed cell line capable to transform upon expression of oncogenic KRAS. This PhyB/PIF6-based cell line – generated by using hPNEs E6E7 st (human pancreatic cell line) and OptoRAS – could represent an ideal system to study *KRAS*-driven oncogenesis in a *KRAS*-driven (pancreatic) tumour setting.

Here I will illustrate preliminary characterisation of these cell lines. First I tested optoRAS hPNE cells with a simple protocol involving a deactivation phase – used to ensure optoRAS is not basally stimulated – and a 5min red light activation phase, after which cells where harvested at several sub-1h timepoints. Cells showed a significant decrease in the activity of Erk just after light stimulation (see suppl. Fig. 3.27 on page 128). This led us to question whether phycocyanobilin (PCB) – a cofactor critical for optoRAS to function, added prior to light stimulation – may be affected by exposure to either infrared or red light.

To test this hypothesis, the protocol was amended to allow an additional step (25 minutes rest time prior to 'ON' light) for the PCB-loaded cells to regain a basal state after exposure to 'OFF' light (see Fig. 3.16).

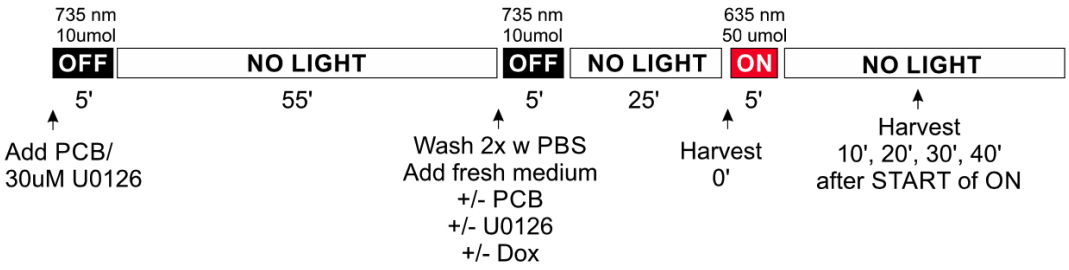

Fig. 3.16 Light protocol for testing the optoRAS system. U0126 is a MEK inhibitor. PCB: phycocyanobilin.

In the western blot analysis (see Fig. 3.17 on the facing page), doxycycline-untreated cells in the presence of PCB do not show significant initial decrease in ERK activation, thus resolving the issue observed in previous experiments (see suppl. Fig. 3.27 on page 128)). However, this phenomenon is yet again seen in conditions where cells are administered with doxycycline. Treated cells without PCB or with the addition of a MEK inhibitor experience a minor decrease in ERK activity, when compared to treated cells in presence of PCB (see Fig. 3.17). This suggests that such unexpected event is partially dependent on PCB (when optoRAS is expressed) and MEK activity.

The assumption that an oncogene would activate the MAPK/ERK pathway in a similar manner to growth factors (ie activation at 5-10 minutes post GF induction) is the rationale as to why all previous experiments were designed to assay cells in the first hour time frame post- light stimulation.

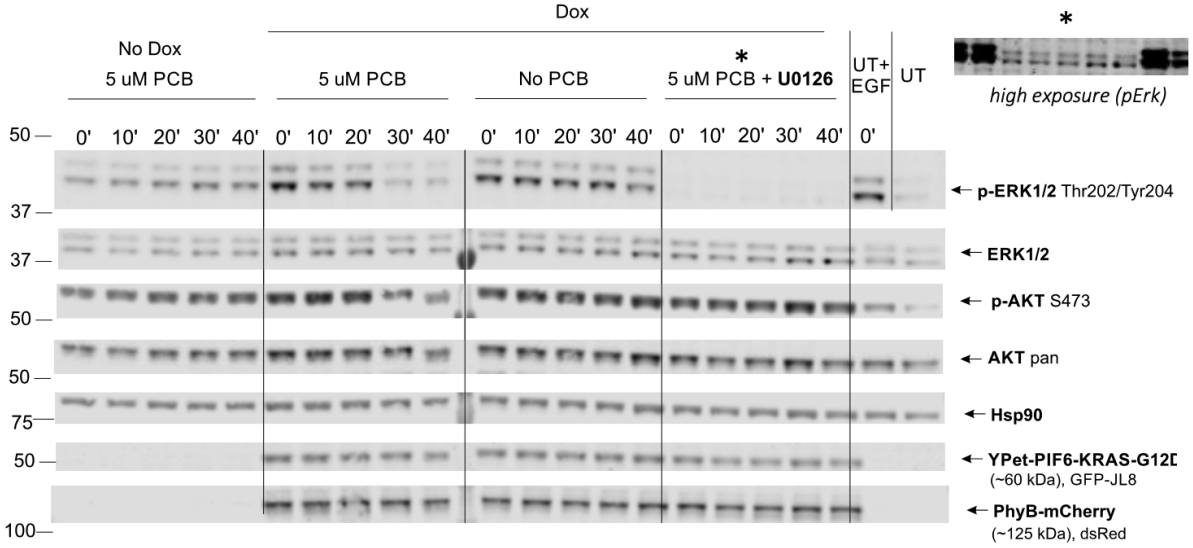

Fig. 3.17 Four different conditions were tested; untreated cells with PCB, treated (with doxycycline) cells with PCB or no PCB or PCB and U0126 (MEK inhibitor). PCB: phycocyanobilin; EGF: epidermal growth factor; UT: untreated

Therefore, it was hypothesised that oncogene-induced activation of MAPK/ERK might behave in a different manner to GFs, by displaying an initial decrease in ERK activity but potentially increased in later time points. To test this hypothesis, cells need to be assayed at longer time points, and this might provide a more insightful representation of the signalling behaviour orchestrated by acute activation of $KRAS^{G12D}$. It was thus decided to assess cells at such time points.

Pre-'ON' light stimulation procedures were carried out in a similar fashion to the aforementioned protocol (see Fig. 3.16 on the facing page), using PCB and doxycycline only as additional supplements. Cells were harvested at 0min, 30min, 24h and 48h after red light (635nm) exposure. Samples overexpressing $KRAS^{G12D}$ were harvested 24h and 48h (including a mock sample) post-transfection (plasmids used for transfection: pcDNA3.1-Myc-$KRAS^{G12D}$ & pcDNA3.1), together with the other samples at their respective time points.

Most notably, this experiment shows more than a two-fold increase of p-ERK levels at 24 hours post red-light stimulation, followed by a decrease at the 48-hour time point

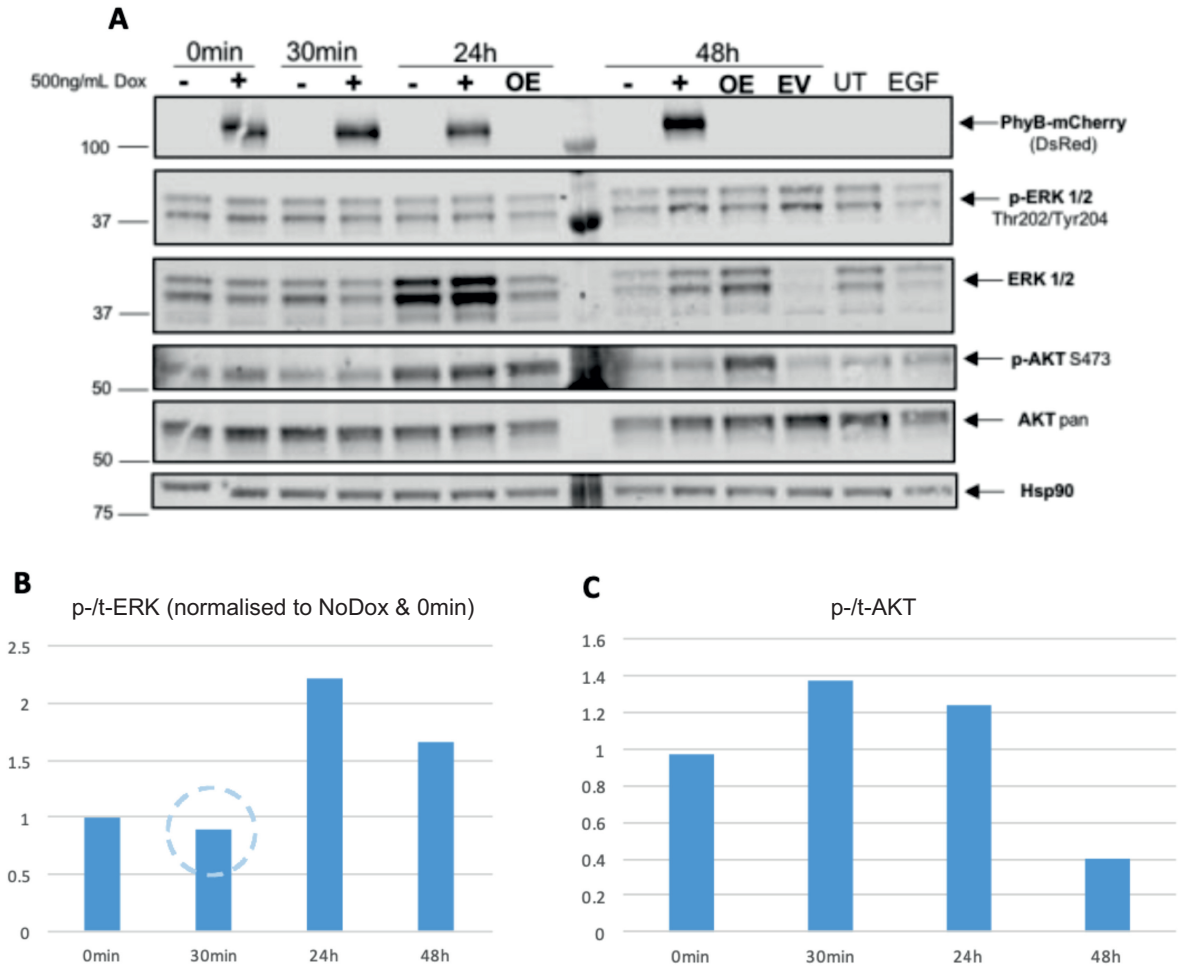

Fig. 3.18 Western blot of a 48-hour long optogenetic experiment (a) to assess the long term performace of OptoRAS. p-ERK (b) and p-AKT (c) activity were quantified and plotted for improved visualisation purposes. OE: overexpression of a mutant KRAS containing plasmid, EV: overexpression of empty vector (pcDNA3.1).

(see (a) in Fig. 3.18 on the preceding page). It is to be noted, however, that an initial decrease in ERK activity can be observed (as seen in (b) in Fig. 3.18), as experienced in previous experiments. In the case of the overexpression samples, ERK is activated at 24 as well as 48 hours post-transfection, as expected. Interestingly, pAKT levels initially increase by 40% but decrease down to 40% at the latest time point. Although ERK activity at 24 hours is considerably higher than basal levels, this is a single experiment and more than one repeat would be necessary to prove that it is a true biological effect. However, if this hypothesis were to be proven correct, it could explain the initial decrease in pERK levels observed in all previous experiments.

CIBN-CRY2

As issues of reproducibility of the original OptoRAS design could not be resolved, it was decided to test a set of different light-indudible domains, the proteins CIBN and CRY2 instead. A plasma membrane-bound CIBN-EGFP-CAAX protein that dimerises with cytoplasmic cryptochrome 2 (CRY2)-bound $KRAS^{G12D}$ upon blue light (488nm) exposure was designed.

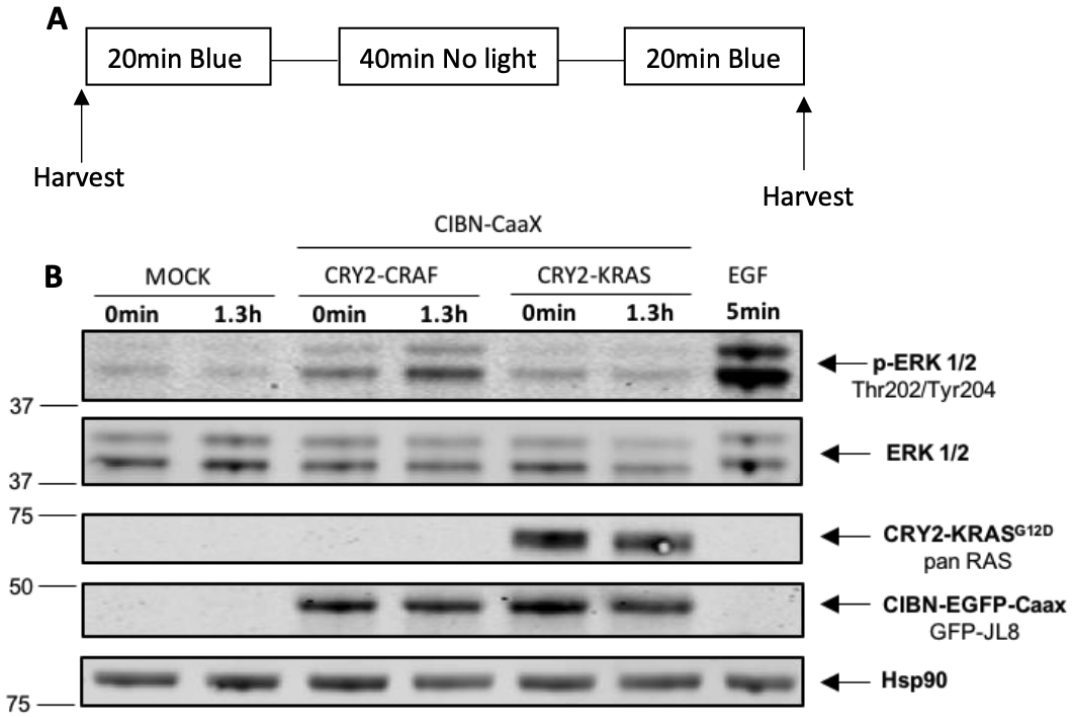

Fig. 3.19 Testing CIBN/CRY2 for the photo activation of KRASG12D. A) Light protocol design performed on cells. Blue light was used to induce dimerization of CRY2 component to CIBN. B) Western blot probing for various proteins.

MCF7 cells transfected with two separate plasmids containing the optogenetic transgenes (i.e. CIBN-EGFP-CAAX and CRY2-KRAS^{G12D} or CRY2-CRAF), or empty vector plasmid (pcDNA3.1), were used for a first pilot experiment. Design of the light protocol was based on previous studies by Aoki et al. (2013) where activation of the CIBN-CAAX/CRY2-CRAF system induces ERK activity 20min after blue light stimulation, on repeated occasions. In our experiment, samples were harvested prior to light illumination and after two 20min-long phases of blue light exposure, separated by a 40min no-light phase (see (A) in Fig. 3.19 on the preceding page).

CRY2-CRAF expressing cells show increased levels of pERK after the second light stimulation (see (B) in Fig. 3.19 on the previous page), confirming that this optogenetic system induces photoactivation of CRAF, resulting in the activation of MAPK signalling. In contrast, no response is observed in the CRY2- KRAS^{G12D} expressing sample after exposure to light. Transgene expression levels (probed with pan RAS and GFP-JL8) are clearly observable, indicating that the optogenetic components are present in the cells.

It was therefore hypothesised, similarly to the PhyB/PIF6 development, that acute activation of KRAS^{G12D} may result in signalling patterns activated at longer time points. As such, it was decided to carry out an experiment where cells would undergo repeated cycles of the previously described light protocol (see (A) in Fig. 3.19 on the preceding page) and harvested at 0min, 2h20min, 6h20min and 24h20min. Once again, photostimulation of CRAF induces ERK activation at 2h20min and most notably at 6h20min (see Fig. 3.20). Light-stimulated cells with CRY2-KRAS^{G12D} does not induce ERK activation at any of the time points.

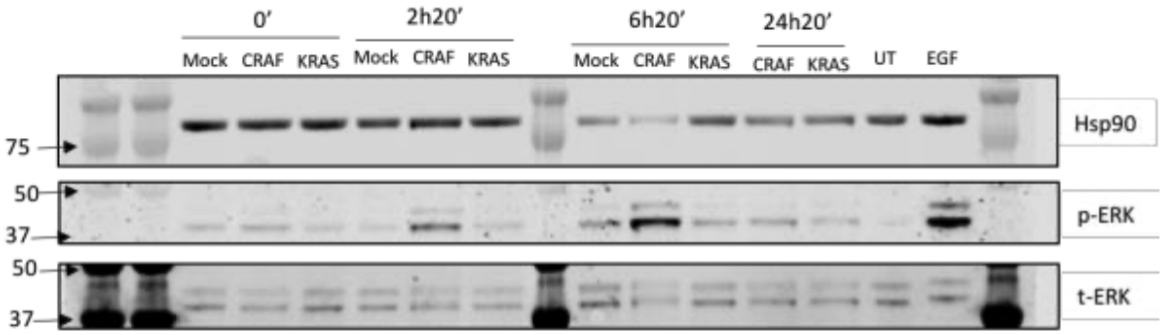

Fig. 3.20 Western blot analysis shows that long term blue light stimulation induces ERK activation in CRY2-CRAF only

In summary, the effective mechanism of CIBN/CRY2-CRAF optogenetic tool was confirmed by observing blue light mediated activation of ERK at different time points.

This phenotype was not observable in CIBN/CRY2-KRAS^{G12D} expressing cells. With no indication of biological activity, the development of this system was abandoned.

Before derisking my project in favour of more established yet powerful assay techniques such as microfluidics, I briefly tested an alternative optogenetic system; improved light-induced dimer (iLID). The advantage of this system is that its optogenetic components were designed to be small and modular (to minimise biochemical interference) and enable fast light-induced association kinetics (Guntas et al., 2015).

With the same objectives as described in the previous two sections, it was decided to construct our model based on iLID photosensitive proteins. Although the development state is at very preliminary stages, a proof of concept experiment was performed, showing the translocation of the cytoplasmic SSBP-tgRFPt protein to the plasma membrane (see Fig. 3.21).

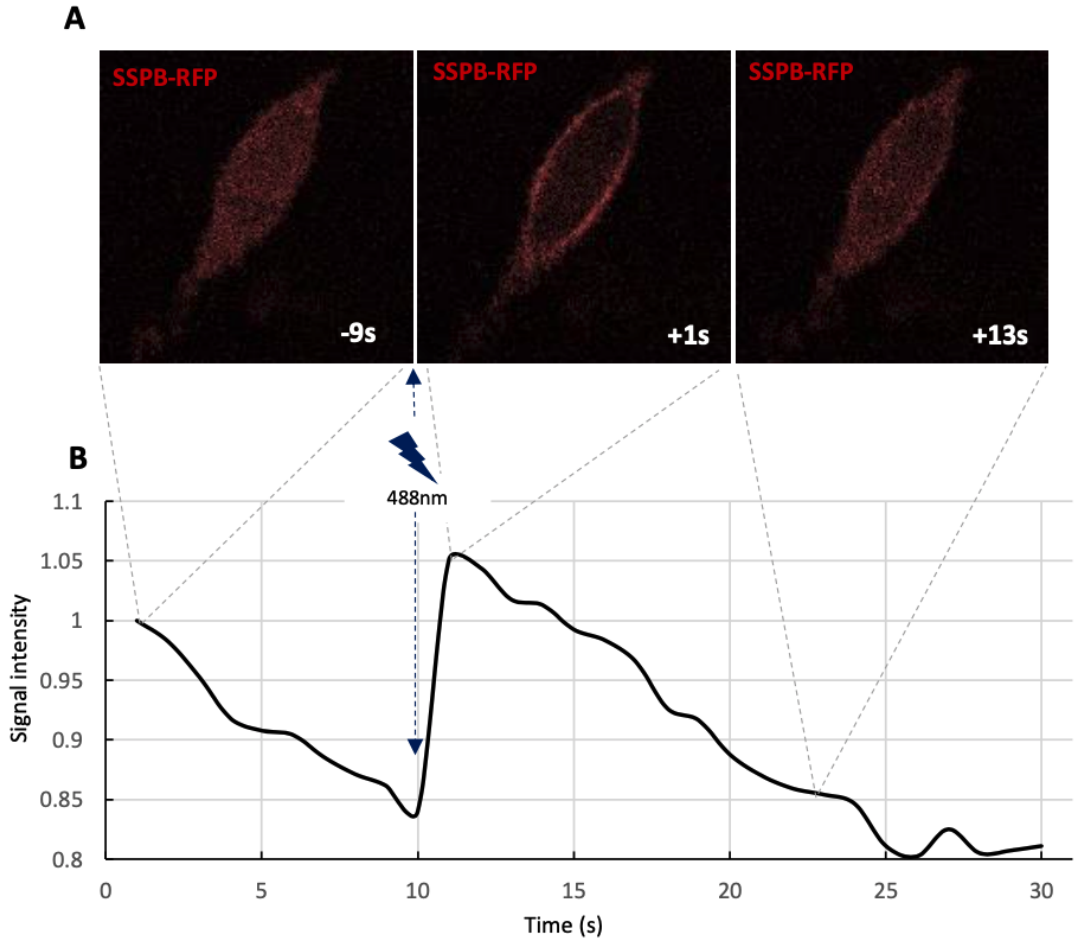

Fig. 3.21 Translocation of iLID optogenetic system. A) Cytoplasmic SSPB-RFP was imaged at 561nm laser excitation pre- and post- 10 second exposure to blue light (488nm). B) Plasma membrane signal intensity quantification (normalised to t0 time point) of the above images.

3.3 Discussion

3.3.1 NyxBits reporters

One of the limitations of FRET sensors is their dynamic range, ie the range of values a sensor can provide reporting for a biological event. Moreover, residual emission fluorescence of dark acceptors of FLIM-FRET pairs is also a common complication that requires custom unmixing software to resolve lifetime images. Thus, there is a preference for FRET-FLIM reporters to show a large dynamic range and low sprectal bleed-through to have more precise biochemical measurements.

In this Chapter I showed the assessment of the optical features of blue (mTagBFP) and green (mAmetrine) *NyxBits* reporters paired with new dark acceptors ShadowY and ShadowG. I report an improvement of approximately 10% in FRET efficiency and a practically absent bleed-through when combining mTagBFP with ShadowY. This improvement further enhances the biochemical resolution of *NyxBits*' blue FLIM-FRET pair.

The green reporter's donor fluorophore – mAmetrine – was tested with ShadowY only. The worse performance of the ShadowY pairs was unexpected, since it boasts a notably superior molar extinction of coefficient to msCP576 (136,000 vs 64,000 M^{-1} cm^{-1}) (Kogure et al., 2006). Moreover, the differences in maximal excitation wavelengths led us to hypothesise that spectral crossover with mAmetrine emission (526nm) should – in theory – be higher with ShadowY (519nm) than with msCP576 (576nm). The reduced FRET observed with ShadowY as acceptor could be due to FRET properties that are largely difficult to control such as chromoprotein orientation or spatial proximity. The latter can be somewhat addressed by reducing the linker size, however at the same time it may further negatively affect the donor-acceptor orientation.

NyxBits reporters have previously been effectively used to study caspase biology. In line with the group's long-term focus on *KRAS* biology, the aim is to now use these improved reporters to multiplex activity of two major signalling pathways regulated by *KRAS*, namely the MAPK and PI3K signalling cascades. It is thus desirable to integrate sensor domains that would detect phosphorylation activity of two relevant and key proteins; ERK and AKT.

3.3.2 Image Analysis Pipeline Improvements

Usually investigators make use of already existing popular (and powerful) imaging softwares, such as Cellprofiler. However, self-contained 'jack-of-all-trades' programs rarely result in excellent performance for all imaging scenarios. In addition to the learning curve, users may be limited by the features offered and find that they need to look elsewhere to meet their analysis needs.

I have devised an analysis workflow (*PyFRET*) that yields accurate single-cell seFRET data of difficult-to-track SW48 colorectal cells. The main advantages of *PyFRET* is that it harnesses the performance of different image processing open-source software projects and provides a framework upon which other users can expand the feature set. *PyFRET* is also an open-source project, freely available for anyone to download from Github (clickable link **here**) and use. However, several areas require further improvements.

Ease of use

First, installation and simple script execution is not as straightforward as a mouse click. Although an installation guide has been written to facilitate the process, the user may encounter installation issues, in which case troubleshooting will be required. Moreover, software package installation (as well as execution of *Python* scripts) is done through an unintuitive interface; the Terminal/Command prompt. Thus, *PyFRET* would greatly increase its ease of use by reducing the number and complexity of the steps required for installation.

The other aspect where ease of use may be affected is at the Curation stage. Curation is performed in napari, a *Python* multi-dimensional image viewer. Just as with any new software tool, there are functions the user needs to learn in order to use the software efficiently. Thus, simple yet effective documentation on napari's features, as well as general guidelines (installation and tool use) are planned to be included in *PyFRET*'s Github homepage.

Finally, pre-analysis user input enquiries for metadata purposes is relatively unintuitive and complex (see suppl. Fig. 3.22). Using a custom graphical user interface (GUI) – for example building on top of napari by using developer-facilitated addition of graphical elements – with a straightforward design would facilitate this process.

Performance

PyFRET's use of custom-trained models for the 2D segmentation and tracking of SW48 cell-specific fluorescent nuclei is rather limiting. This means that any other data with dissimilar image properties would require training new models for effective analysis. Moreover, *PyFRET* currently exclusively handles 2-channel image files captured with a Nikon widefield fluorescence microscope. Thus, adapting *PyFRET* to accept image files and formats from a wide range of microscopes would increase the pipeline's flexibility.

The advantage of using ilastik's intuitive interface lies in that a tracking algorithm can be trained by manually annotating false/true positive masks as well as the the number of objects in an under-segmented mask, for example. Thus trained models tend to perform well when it comes to ignoring artefacts. However, tracking of cell masks, although effective, still requires improvements to minimise manual curation effort (which requires a significant amount of time). Complicated scenarios where cells move behind one another, leaving the focus plane in the process and later re-entering it, add to the overall tracking error burden.

An alternative option of seemingly equal or better performance would be Bayesian Tracker (btrack); a tool specialised in cell (nuclei) tracking and reconstructing trajectories based on a probability network (Bove et al., 2017; Ulicna et al., 2020). Moreover, the tool's developers have already built a btrack-based plugin (named arboretum) for use in napari, which could be benefitial for single FOV image analysis.

3.3.3 Light induced activation of KRAS

PhyB-PIF6

A potential oncogene-induced activation of ERK 24 hours after red-light induced stimulation of our optoRAS model is reported. Initial reproducibility issues with HeLa cells led to significant methodological changes (creation of hPNEs OptoG12D and development of an OptoFARM) and later deprioritisation of the project. Once taken over again in October 2016, further complications were observed and optimisations performed. Therefore, in order to ensure that there is a real biological effect at 24 hours post-stimulation, additional similar optogenetic experiments are necessary.

In the early stages of development, it was already shown that our optoRAS model is capable of inducing reliable, fast and reversible translocation of cytoplasmic KRAS^{G12D} to the plasma membrane. Doxycycline-induced transgene expression levels have been

confirmed via western blot analysis. Most of the variables affecting OptoRAS experiments have been controlled for and/or optimised in order to ensure correct function of the system. However, biological activity remains to be proven.

In the possible case that this line of work does not eventually result in a successful tool capable of acute oncogene-induced MAPK/ERK activation, there are other available and validated tools that can allow us to probe signalling dynamics using different perturbation methods. Remaining within the same methodology; PhyB/PIF6-based optoSOS stimulation is another optogenetic system that has already been successfully used by other research groups (Toettcher et al., 2013). Moreover, the use of growth factors such as EGF is a simple and effective way to induce MAPK stimulation in cells. The use of microfluidic devices coupled with GFs allow for sophisticated probing of signalling modules. Thus, there are a number of other working methodologies that can substitute our OptoRAS model, and that can be readily used in order to address the bigger questions of non-genetic heterogeneity in the context of genetic heterogeneity.

CIBN-CRY2 & iLID

Light induction of CIBN/CRY2-KRAS^{G12D} resulted in unsuccessful activation of the MAPK cascade, contrarily to blue light-mediated stimulation of CIBN/CRY2-CRAF which did show MAPK activation. The latter system was successfully used in previous studies to analyse cell-to-cell signal propagation (Aoki et al., 2013). Here the reliability of CIBN/CRY2-CRAF and its potential use in the study signalling dynamics is confirmed.

Effective translocation of the iLID cytoplasmic component to the plasma membrane is reported. These initial successful results encourage the further development of this optogenetic system. Steps planned to be undertaken for further proof of concept purposes involve the cloning and testing of single empty vector plasmids containing this system and a protein of interest (SOS or KRAS^{G12D}) involved in MAPK signalling. Longer term objectives implicate the generation of an inducible iLID system capable of effective plasma membrane recruitment of a KRAS-derived mutant protein resulting in functional downstream biological activity.

3.3.4 Conclusion

In this chapter, I have presented a number of technological advancements that lay the foundations for the next generation of technology-led biological research. I have improved the dynamic range of a FLIM-FRET reporter, an optimisation which – in conjunction with

another *NyxBit* reporter – could lead to the multiplexing of *KRAS*-regulated signalling pathway activity with superior biochemical resolution. Moreover, I have assessed and explored optogenetic methods that enable the non-invasive stimulation of *KRAS*, with high temporal control. Finally, I have described the development of an analytical tool (*PyFRET*) that facilitates the accurate measurement of single-cell FRET data from cells presenting morphological and movement challenges.

Alongside my focus on biology shown in Chapter 2, I was involved in methodological developments that could expand the toolbox available to the community for direct imaging of small networks of biochemical reactions. To do so, the following improvements were desired: i) a light based stimulation of KRAS signalling, ii) a multiplexing platform that could – in the future – enable the study of signalling up to 3 downstream signals in KRAS-regulated networks (e.g. MAPK, PI3K and Hippo signalling pathways) and iii) provide high quality single cell data analysis. I completed all of these, but as optogenetics and NyxBits are still insufficiently mature to feedback into my biology research, I derisked my project by i) using established sensors in isogenic lines and ii) microfluidics for perfusion-based assays.

3.4 Materials & Methods

3.4.1 Molecular cloning

All reagents used for cloning were from New England Biolabs LTD. Except the mTagBFP-ShadowG pair, all the other *NyxBits* reporters paired with ShadowG & ShadowY were cloned. All plasmids generated were verified via Sanger sequencing.

mAmetrine-shadowY & mAmetrine-TDshadowY

ShadowY was synthesised via GeneArt Gene synthesis, provided by ThermoFisher Scientific. An AgeI restriction site was added to a *NyxBit* reporter plasmid (mAmetrine-UCL-hsCP576) already available. More specifically, it was added prior to the N-terminus of hsCP576. This was done by amplifying the KpnI-stuffer-AgeI-hCp576-PmeI sequence with the following primers:

- 046-AgeI-hCP576fwd (forward): AGCTGGTACCAGCACCGGTATGG TGTCCGTGATCGCCAAG
- 047-AgeI-hCP576rev (reverse): AGCTGTTTAAACTCATCCCAGCAG GCTGTGCCG

The amplicon was then digested with restriction enzymes KpnI and PmeI and re-ligated with (digested) mAmetrine-UCL-hsCP576. Using a ShadowY-containing plasmid, AgeI-ShadowY-PmeI (1), AgeI-ShadowY-AscI (2) and AscI-linker-ShadowY-PmeI (3) were PCR amplified with the following primers:

- (1, forward) 048-AgeI-sYfwd: AGCTACCGGTATGGTGTCCAAGGGCGAAGAA
- (1, reverse) 049-PmeI-sYrev: AGCTGTTTAAACCTATTTGTACAG
- (2, forward) 048-AgeI-sYfwd (see first item)
- (2, reverse) 050-AscI-sYrev: AGCTGGCGCGCCTTTTGTACAGCTCGTCCATGCC
- (3, forward) 051-AscI-**linker**-sYfwd, FWD): AGCTGGCGCGCC**GGGCATGG CACCGGCAGCACCGGCAGCGGCAGCTCCGGCACC**ATGGTGTCCAA GGGCGAAGAA
- (2, reverse) 049-PmeI-sYrev (see second item)

For the mAmetrine-shadowY construct, AgeI-containing vector mAmetrine-hsCP576 and amplicon from reaction (1) were digested with restriction enzymes AgeI and PmeI. Digested products were then ligated. For mAmetrine-TDshadowY, the same vector and amplicons from reactions (2) and (3) were digested with restriction enzymes AgeI, AscI and PmeI. Digested products underwent a 3-way ligation to yield mAmetrine-TDshadowY.

mTagBFP-TDshadowG

First, in order to introduce an additional ShadowG in mTagBFP-ShadowG, an AgeI restriction site was inserted at the C-terminus of ShadowG (and prior to PmeI restricition site). This was done by PCR amplifying the NotI-UCL-ShadowG-AgeI-PmeI sequence from mTagBFP-ShadowG with the following primers:

- 042-NotI-UCLfwd (forward): AGCTGCGGCCGCcCTGGGAGGCACCG
- 043-PmeI-AgeI-sGrev (reverse): AGCTGTTTAAACCATAACCGGTCT TGTACAGCTCGTCC

The amplicon was then digested with restriction enzymes NotI and PmeI, and re-ligated with digested mTagBFP-ShadowG. Then, a second PCR amplification was performed to yield an AgeI-linker-ShadowG-PmeI sequence with the following primers:

- 044-AgeI-sGfwd (forward): AGCTACCGGT**GGGCATGGCACCGGC AGCACCGGCAGCGGCAGCTCCGGCACC**ATGGTGAGCAAGGGCGAGGAG
- 045-PmeI-sGrev (reverse): AGCTGTTTAAACCTTGTACAGCTCGTCC

Note the forward primer contains a linker (in bold), previously used by for the design of the red *NyxBit* reporter pair mKeima-tdNirFP. The amplicon AgeI-linker-ShadowG-PmeI, together with the AgeI-containing mTagBFP-ShadowG plasmid were then digested and ligated, resulting in a plasmid containing tandem dimer ShadowG paired with mTagBFP.

mTagBFP-shadowY & mTagBFP-TDshadowY

I digested mTagBFP-TDshadowG (insert), mAmetrine-shadowY (vector) and mAmetrine-TDshadowY (vector) with restriction enzymes BmtI and NotI-HF. Then I ligated mTagBFP with each vector separately to obtain mTagBFP-shadowY and mTagBFP-TDshadowY.

3.4.2 Cell lines and culture conditions

Maximilian Fries, a PhD student, used the pancreatic cell line hPNE E6/E7/st (CRL-4037) to make a stable cell line expressing a pTetOne doxycycline inducible plasmid (ClonTech Laboratories, Inc) containing the following transgene: PhyB-mCherry-CaaX-IRESwt-YPet-PIF6-KRasG12D. This cell line is referred to as hPNEs OptoG12D.

All used cell lines were cultured as described in Chapter 2 (see section 2.4.1).

3.4.3 Sample preparation for FLIM

55,000 HeLa cells were plated in each well of a 4-well LabTek chamber slide (cat. no. 155383). 24 hours later, cells were transfected using Jetprime (Polyplus transfection) according to the manufacturer's guidelines and using a total of 500 ng of plasmid DNA (*NyxBit* reporter or single donor fluorophore) per well. Transfection medium was replaced with DMEM+10% FBS growth medium 4 hours later. 24 hours later and two hours prior to imaging, samples' medium was replaced with Leibovitz L-15 (Gibco) imaging medium, phenol red free, supplemented with L-Glutamine and 10% FCS.

3.4.4 FLIM measurement & Spectral scanning

All *NyxBits*-related imaging was performed on an SP5 multi-photon confocal laser scanning microscope.

To measure FLIM, light emission was filtered according to the donor proteins to be quantified (mTagBFP: 467-499 nm; mAmetrine: 506-545 nm). Photons were counted using a hybrid photomultiplier tube connected to a module allowing for time correlated single-photon-counting. The images were acquired with a 40x objective, 60 seconds of photon-acquisition time, image resolution of 256x256 and 400 Hz scanning speed. The SPCImage V4.9 (Becker & Hickl) software was used to calculate lifetimes and fit the photon monoexponential decay profiles. Both lifetime and intensity images were exported from SPCImage. Lifetime data was exported to Microsoft Excel, where the raw data of several FOV repeats (n>=4) was averaged for each different sample and subsequently plotted (as shown in Fig. 3.7, 3.5, 3.6).

Emission spectra were capture with a 40x objective, an image format of 256x256, a scan line speed of 400 Hz and an 'open' pinhole (nominal size of 600 µm). The total detection range was 250 nm (400-650um) and the bandwidth and step size was of 10 nm. Analysis was performed by transferring the emission data in the .lif files generated from

the Leica LAS lite software, into Microsoft Excel. The latter was used to generate the shown graphs.

3.4.5 Evaluation metrics

Segmentation performance was assessed by quantifiying the precision (a measure of specificity), recall (a measure of sensitivity) and accuracy of each compared tool.

$$Precision = \frac{TP}{TP+FP}$$

$$Recall = \frac{TP}{TP+FN}$$

$$Accuracy = \frac{TP+TN}{TP+TN+FP+FN}$$

where TP is True Positive, TN is True Negative, FP is False Positive and FN is False Negative. To measure these, the shown images in Fig. 3.8 on page 90 where manually assessed. These measures were used to yield an F1 score; a better representation of both precision and recall, since it's their harmonic mean and defined as follows:

$$F1 = \frac{2*Precision*Recall}{Precision+Recall}$$

Split and merge scores were quantified using the $variation_of_information$ function from the *Python* package sci-kit image, under the metrics module. The function returns two values representatinf the amount of under- (merges) and over-segmentation (splits).

Finally, execution speed of segmentation methods was assessed using an in-cell timer in a Jupyter Notebook. Several iterations were performed and the average value was reported.

3.4.6 Western blotting of optogenetic experiments

Western blot assay was carried out as described in Chapter 2 (see section 2.4.9). 20 µg or 15 µg (48-hour experiment) of lysate were used and further processed as in section 2.4.9.

Primary antibodies

Primary antibodies and dilutions used: alpha-GFP (1:1000; JL-8, Clontech), mouse P-p44/p42 MAPK (T202/Y204) (E10) (1:1,000; Cell Signalling, cat. no. 4695S), p44/p42 MAPK (Erk1/2) (137F5) Rabbit (1:1,000, Cell Signalling, cat. no. 9106L), alpha-pAKT (Ser473) (1:1000; Cell Signalling), alpha-AKT (1:1000; Cell Signalling), alpha-DsRed (1:1000, Clontech), alpha-pan RAS (1:2000, Clone-10, Millipore), Hsp90 Rabbit mAb (C45G5, 1:1,000, Cell Signalling, cat. no. 4877S).

3.4.7 Confocal imaging for iLID translocation

150,000 HeLa cells were seeded in 35mm glass bottom culture dishes (MaTek #1.5) in full medium and transfected (24 hours after plating) using JETPRIME and 1 µg of DNA per lentiviral plasmid; pLL7.0: Venus-iLID-CAAX (from KRas4B) (Addgene #60411) and pLL7.0: tgRFPt-SSPB WT (Addgene #60415). Samples were added L-15 medium (+10% FCS) 48 hours after transfection and prior to imaging.

Imaging was performed on a Leica SP5 multi-photon confocal microscope (Leica Microsystems) equipped, amongst others, with a stage incubator at 37C for optimal imaging conditions. Images were acquired using the 40x oil objective, using an image size 256 px x 256 px and sequential scanning. Cells were first imaged with 561nm (tgRFP-t) laser excitation for 10 seconds, followed by 10-30s of 488nm (mVenus, optogenetic activation) laser excitation, and finally re-imaged with 561nm wavelength for a period of 30s-1minute. Saved images were analysed using FIJI/ImageJ.

3.5 Supplementary Figures

```
Is this a cellASICs experiment? [y/n] y

Name of samples in each chamber (eg. WT/WT/G12D/G12D):  SW48-G12D-H11A/SW48-G12D-H11A/SW48-G12D-H11A/SW48-G12D-H11A

Capture frequency detected: 6min, i.e. 10 frames per hour


Frames where solutions are switched (change of flow).
Separate frames by comma (eg 20,50,100):  21,61,91,101


For treatment input, add data as following example EGF_15-25,ERKi_40-60
i.e. treatment-name_frames-treated.


Treatments performed in chamber A:
 ERKi-500nM_91-101

Treatments performed in chamber B:
 EGF-1ng/mL_61-91,ERKi-500nM_91-101

Treatments performed in chamber C:
 EGF-10ng/mL_61-91,ERKi-500nM_91-101

Treatments performed in chamber D:
 EGF-50ng/mL_61-91,ERKi-500nM_91-101

Provide group details (eg Control_1/EGF_2/Control_3/EGF_4):  Control_1/EGF-1_2/EGF-10_3/EGF-50_4
```

Fig. 3.22 Example of user input log before starting image processing.

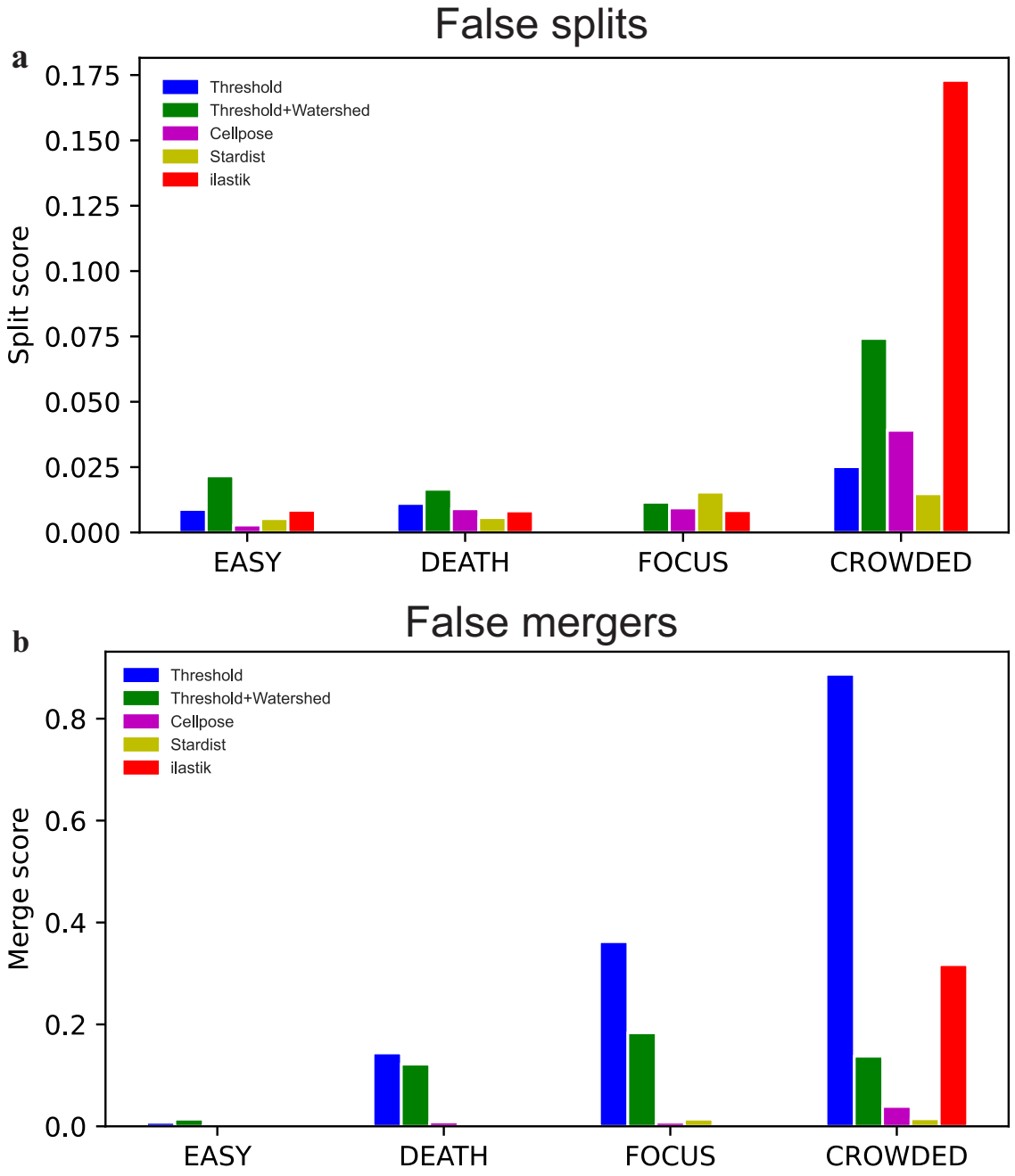

Fig. 3.23 All segmentation methods have similar false splits (a) error rates, except in a 'crowded' scenario where best and worst performers are StarDist and ilastik, respectively. Contrarily, false merges (b) become more frequent with increasing imaging complexity, especially for simple thresholding.

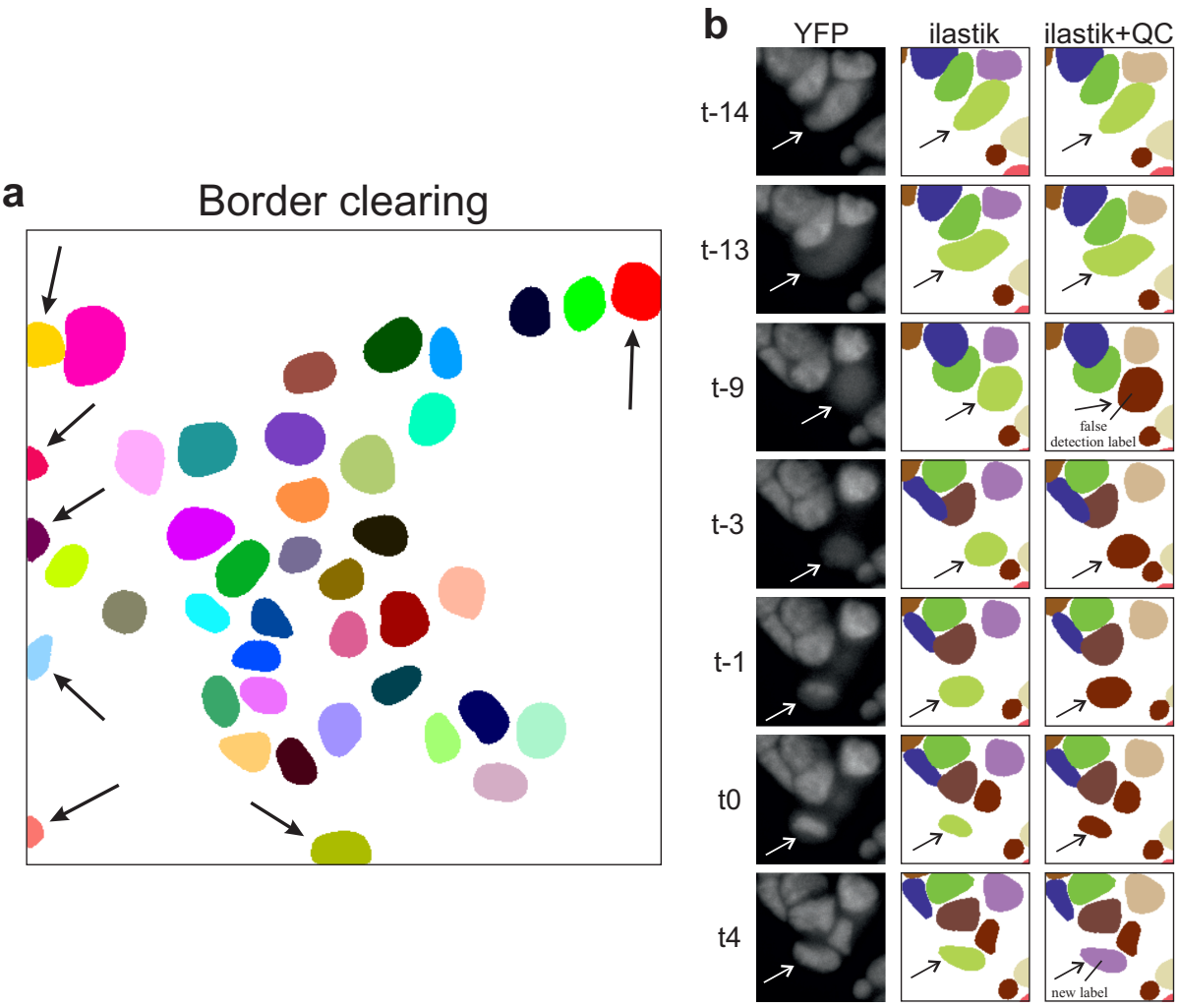

Fig. 3.24 Cells touching the edge of a field of view (FOV) are removed (a). Custom area-based mitotic detection corrects ilastik cell tracks (b).

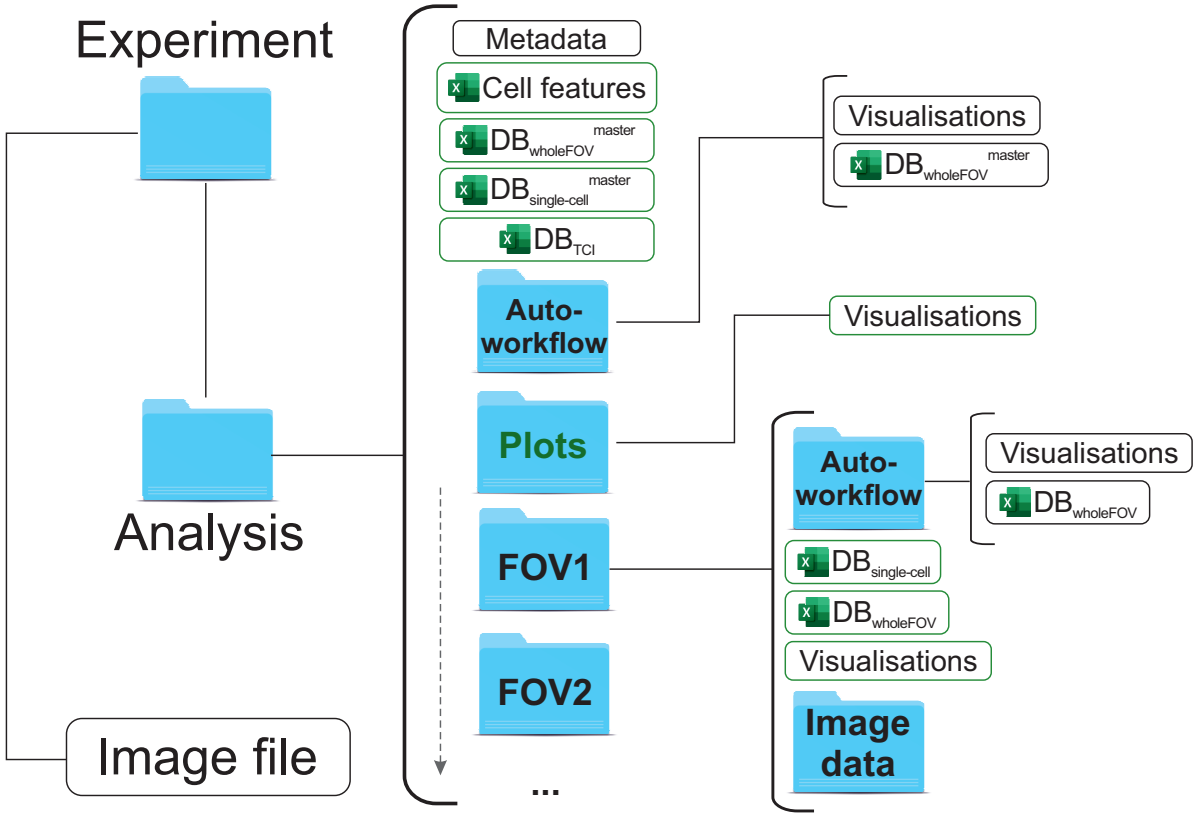

Fig. 3.25 Data is stored in a structured manner, with curated data (in green) being most accessible.

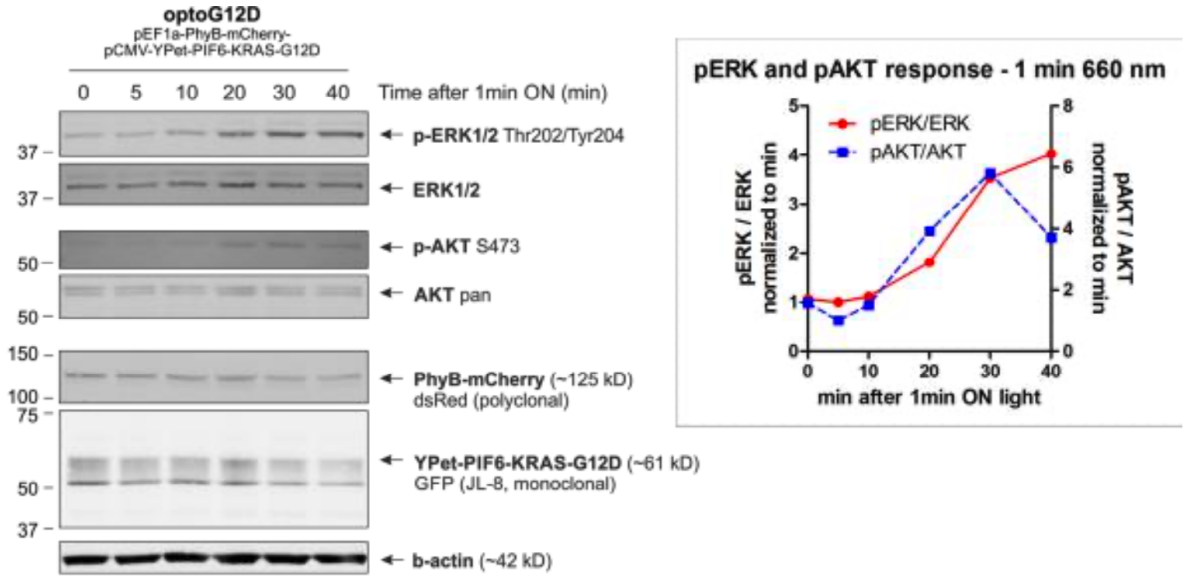

Fig. 3.26 Light induction of ERK and AKT in HeLa cells (kindly provided by Dr. Fries)

		Database	
		whole FOV	single-cell
FRET	Median	x	
	Mean	x	x
	Standart deviation	x	
	Variance	x	
	Mode	x	
	Mean – median	x	
	IQR	x	
	Mad	x	
	Skew	x	
	Kurtosis	x	
	Minimum		x
	Maximum		x
Other	CFP mean	x	
	CFP background	x	
	YFP mean	x	
	YFP background	x	
Mask	Label		x
	Area		x
	Diameter		x
	Centroid-Y		x
	Centroid-X		x
Categorical	FOV	x	x
	Frame	x	x
	Chamber	x	x
	Group name	x	x
	Group number	x	x
	Sample name	x	x
	Treatment	x	x

Table 3.1 Image properties measured in an automatic worklow (whole FOV only) or when curation data is available (single-cell & whole FOV)

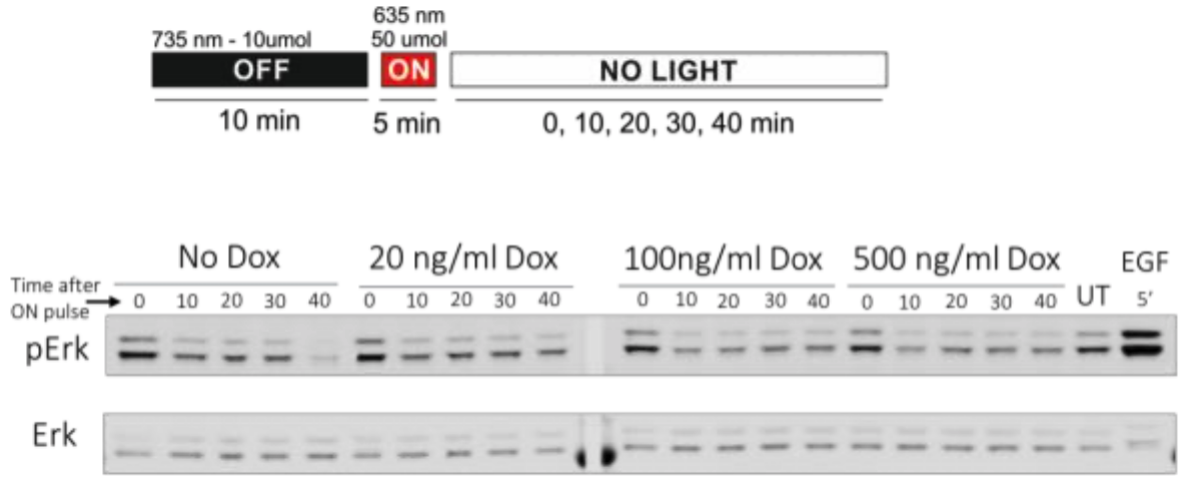

Fig. 3.27 Doxycycline titration experiment reveals high basal pERK levels (kindly provided by Dr. Fries)

Chapter 4

Discussion

In this thesis, I have studied the impact of heterogeneity of genetic and non-genetic origin in oncogenesis and tumour maintenance through the study of protein signalling activity in single cells. Heterogeneity has long been observed in tumours and today supposes one of the major challenges to treat cancer effectively. Genetic heterogeneity has been characterised relatively thoroughly, but the continuous evolution of tumour clones contributes to the rise of therapy resistance and a tumour's metastatic potential. Non-genetic heterogeneity, on the other hand, is less well characterised and thus our understanding of its contribution to oncogenic development is rather poor. However, various studies demonstrating cells' phenotypic plasticity in face of environmental stressors (such as therapy) suggest cell-to-cell variability is a force to be reckoned with. In order to best define variability among cells, one must be able to accurately measure output information on a single-cell basis. Although microscopy has enabled researchers to image live cells for days, technologies allowing us to efficiently yield single-cell protein activity are only beginning to bear its fruits. As a result, my efforts to address heterogeneity have focused on two main areas that have shaped my doctoral project.

In Chapter 2, I describe the characterisation of colorectal tumour single cells with or without a heterozygous G12D mutation in the *KRAS* oncogene. First, mutant cells in a basal state have a higher MAPK activity than its wild-type counterpart. Then, by performing an extended EGF titration assay, $KRAS^{G12D}$ cells are observed to have a lower amplitude response (when compared to $KRAS^{WT}$) and unanimous desensitisation kinetics irrespective of the EGF concentration. Single-cell ERK activity profile analyses further demonstrate that $KRAS^{G12D}$ cells have, overall, a diminished responsive capacity. Moreover and surprisingly, mutant cells show a 'rebound' higher than basal ERK activity shortly after the release of an ERK inhibitor. RNA sequencing analysis reveals the

upregulation of a number of genes known to be involved in MAPK negative feedback mechanisms. Finally, hierarchical clustering of all acquired single-cell signalling activity profiles uncovers the presence of a mutant-exclusive population.

In Chapter 3, I give and account of the optogenetic tool developments derived from the need to obtain higher quality single-cell FRET data, higher biochemical resolution and novel stimulation methods. The ERK FRET reporter cell lines generated for the signalling assays outlined in Chapter 2 presented a set of challenges that prevented the acquisition of accurate single-cell data with the available in-house software. Because of this, I developed from the ground up an image analysis pipeline – called *PyFRET* – that better performs image processing tasks and enables curation of cell tracks. This software proved invaluable in obtaining and analysing accurate single-cell ERK activity profiles in cells expressing a nuclear ERK FRET reporter. Moreover, I present the optimisation of the optical properties of the blue FLIM-FRET reporter of *NyxBits* – a multiplexing platform developed in-house for the simultaneous detection of three biochemical events. Finally, this chapter also outlines efforts in developing *OptoRAS*; the concept of light-induced *KRAS* mutant-specific stimulation of the MAPK pathway. Translocation of two optogenetic systems (PhyB-PIF6 and iLID) are demonstrated and the potential long-term activation of ERK is observed with the PhyB-PIF6 system. However, due to reproducibility issues, the development of *OptoRAS* was deprioritised in favour of more reliable yet still dynamic stimulation methods (growth factor based stimulation via microfluidics).

In this chapter, I will discuss my results in the context of the literature, as well as propose future experiments and/or avenues to pursue in order to harness but also extend my work.

4.1 Mutant *KRAS* and MAPK signalling

The high mutation rate of KRAS in tumours prompted the investigation of its role in oncogenesis and tumour progression. To address such question, numerous *in vivo* and *in vitro* models have been used to assess the tumorigenic potential of various RAS isoforms and mutations. Many such studies usually involved the assessment of cell morphology in tissues (*in vivo*) and/or the quantification of RAS-regulated signalling networks via whole cell lysate protein immunoblotting.

Early studies observed that mutant RAS induced high MAPK activity, as well as showing independence from growth factor receptor activation (Gallego et al., 1992). Thus,

plain hyperactivation of the MAPK pathway (and concomitant high proliferative capacity) was thought to be the net effect of the expression of oncogenic RAS (Koeffler et al., 1991). Additional observations whereby mutant RAS is concomitantly expressed with other mutant MAPK cascade components, such as BRAF (Davies et al., 2002), further reinforced the concept of RAS-induced MAPK hyperactivation and its addiction to high MAPK activity. More recently, specific mutations such as $KRAS^{G12D}$ in hematopoitic stem cells (Van Meter et al., 2007) and lung tumour cells (Ihle et al., 2012) have shown upregulated activity of the MAPK pathway in basal conditions. Highly phoshorylated ERK has also been found in mouse lung tissue expressing mutant $KRAS^{G12C}$ (more so than $KRAS^{G12D}$) (Li et al., 2018b). Lastly, single-cell studies characterising MAPK signalling in mutant KRAS expressing cells also observed higher baseline ERK activity when compared to non-mutant cells (Gillies et al., 2020; Ponsioen et al., 2021).

In line with these observations, in this thesis SW48 colorectal cancer cells with a heterozygous $KRAS^{G12D}$ mutation show subtle yet visibly higher ERK activity than cells with non-mutated KRAS. It is worth noting that this observation is derived from cells under constant and high perfusion flow of 1% FCS-containing imaging media. In a pilot experiment (data not shown) assessing ERK activity over a duration of 12 hours and under various non-perfusion, basal conditions (including starved and non-starved), both $KRAS^{G12D}$ and $KRAS^{WT}$ cells exhibited similar levels of (stable) ERK activity. This suggests that mutant cells' higher MAPK activity observed in the EGF titration assays is achieved via constant flow of media and mechanically induced stress. Indeed, on multiple occasions, the MAPK pathway has been shown to be stimulated via mechanosensorial mechanisms (Chien et al., 1998; Plotkin et al., 2005; Reusch et al., 1997; Tseng et al., 1995; Weyts et al., 2002; Yan et al., 2012). The requirement for upstream signalling activation agrees with previous studies stipulating that a preliminary stimulation is necessary to kickstart oncogenic signalling. In the context of oncogenic KRAS, it is only after treatment with a growth factor (such as EGF) that mutant KRAS cells display the 'expected' high MAPK activity as well as a more sustained signalling response (Hood et al., 2019; Huang et al., 2014; Kruspig et al., 2018). In the absence of growth factor stimulation (i.e. in basal conditions), cells expressing mutant KRAS have been found to display similar (Stolze et al., 2014) or even attenuated (Haigis et al., 2008; Tuveson et al., 2004) MAPK activity when compared to cells with $KRAS^{WT}$.

It is important to stress that MAPK activity is highly dependent on RAS isoform (Hobbs et al., 2016) and mutation (Hammond et al., 2015). For example, primary hepatocytes expressing consitutively active HRAS or KRAS with a G12V mutation

resulted in growth factor induced proliferation. However, survival was mediated differently depending on the isoform that was mutated; cells with $HRAS^{G12V}$ exhibited high ERK & PI3K signalling, whereas cells with $KRAS^{G12V}$ displayed high PI3K signalling only (Rosseland et al., 2008). Similarly, *in vivo* work by Céspedes et al. (2006) showed that high ERK activity in murine tumours was caused only by a G12V mutation in KRAS, whereas tumours with a G12D mutation had higher PI3K signalling. Tissue context is also highly influential in cells' ability to activate the MAPK pathway. When staining for pERK in colonic epithelium tissue comprising of cells expressing $KRAS^{G12D}$, Haigis et al. (2008) observed that phospho-ERK levels were high only in differentiated cells of the upper region of colonic crypts, and not in the bottom region where stem cells usually reside (Testa et al., 2018). Finally, there is also evidence showing that mutant RAS-induced MAPK activation is also cell-type dependent (Brandt et al., 2019).

The aforementioned studies were designed and carried out in order to broaden our knowledge on the effects of mutant RAS as well as its role in oncogenesis and cancer maintenance, broadly speaking. Despite providing crucial information, most of these fail to assess MAPK signalling at the single-cell level with superior temporal resolution. Such quantification is vital to assess heterogeneity – undeniably present in tumours – as well as for the characterisation of the cellular information processing that drives cells to carry out (or not) cell fate decisions.

Oncogenic MAPK signalling dynamics

Numerous studies have strived to characterise how cells encode and decode information transmitted through the MAPK pathway (Aoki et al., 2011; Blum et al., 2019; Cohen-Saidon et al., 2009; Davies et al., 2020; Gillies et al., 2017; Shindo et al., 2016; Wilson et al., 2017), and how it translates into cellular behaviour (Albeck et al., 2013; Goglia et al., 2020; Herrero et al., 2016; Marshall, 1995; Ryu et al., 2015). However, the literature is scarce on how a mutation in an oncogene such as KRAS may affect cells. Given that KRAS regulates several vital signalling pathways, the dynamics of which determine cellular behaviour, how might a mutation alter such pathway signalling in a way that the end result is a fitter phenotype conducive to cancer development? Do individual mutant KRAS expressing cells perceive and process external information differently than non-mutant cells? It is only in the last few years that oncogene-induced MAPK signalling dynamics have started to be described at a single-cell level.

In a recent study aimed at investigating the effects of different KRAS mutations on MAPK signalling, Gillies et al. (2020) found that cells with or without mutant

KRAS (including KRAS^{G12D}), upon EGF stimulation, reached peak ERK activity and desensitised to steady state activity around 15 minutes and 1.5-2 hours after treatment, respectively. Mutant cells' EGF-induced peak ERK activity, however, was either equal or lower than that of cells with wild-type KRAS.

The characterisation of MAPK signalling in KRAS^{G12D} SW48 cells in response to EGF performed in this thesis broadly replicates the aforementioned observations made by Gillies et al. (2020). In addition to the elevated baseline ERK activity and attenuated response to EGF in mutant cells, both KRAS^{WT} and KRAS^{G12D} expressing cells respond to EGF rather fast and desensitise within the same time period of 1.5-2 hours post-EGF. However, SW48 cells with KRAS^{G12D} showed slightly delayed or 'sluggish' kinetics in comparison to KRAS^{WT} cells; mutant cells take more time to reach peak ERK activity from EGF stimulus (also observed by Gillies et al. (2020), see suppl. Fig. 2.15 on page 68) and take slightly more time to desensitise to a steady state activity for EGF 10ng/mL (see Fig. 2.4 on page 43 and (d-e) in Fig. 2.5 on page 44). In fact, the observed delayed kinetics are reminiscent to the ERK signalling activity displayed by a lung cancer cell line with mutant BRAF when stimulated with an optogenetic system (Bugaj et al., 2018). The decreased responsive capacity of KRAS^{G12D} cells demonstrated by single-cell analysis supports the findings of Gillies et al. (2020) whereby cells with a KRAS mutation overall had a lower probability of response (40-75%) when compared to KRAS^{WT} cells (90%). Although ERK baseline activity negatively correlated with response amplitude more so in SW48 KRAS^{G12D} than in KRAS^{WT} cells, such correlation was not found by Gillies et al. (2020). Such discrepancy could be due to a multitude of factors, one of which is the genetic background of cell lines in both studies and the potentially ensuing signalling rewiring. Gillies et al. (2020) use mouse embryonic fibroblasts (MEFs) expressing a single RAS allele (wild-type or mutant) whereas SW48 mutant KRAS cells are heterozygous (i.e. both mutant and wild-type KRAS are endogenously expressed). Gillies et al. (2020) argue that mutant MEFs' surprising (supposedly there is no inactive mutant KRAS expressed) ability to respond to EGF is due to a weakened negative feedback. It is possible that SW48 cells retain the capacity to respond to EGF due to the wild-type (activatable) KRAS, but have a stronger negative feedback that prevents cells from signalling above a certain level (resulting in cells with higher baseline ERK having a lower response amplitude).

Taken together, the characterisation of MAPK signalling in SW48 cells expressing KRAS^{G12D} is consistent with the scarce literature available that has addressed similar questions. Overall, mutant KRAS cells display analogous signalling MAPK dynamics

yet are subtly more sluggish (or incapable) in their capacity to respond to growth factor mediated stimulation.

Negative feedback regulation

Duration, frequency and amplitude are signalling features that heavily influence signalling (Kholodenko et al., 2010), and thus control the activation of specific transcriptional programmes. Because of their importance, it is vital that cells are able to regulate signalling in order to prevent hyperactivation of a pathway, for example. Cells have evolved regulatory mechanisms that either enhance (positive feedback) or diminish (negative feedack) signalling. The MAPK pathway hosts a range of feeback motifs, most of which stem from ERK – known to negatively regulate upstream MAPK components (Buday et al., 1995; Heisermann et al., 1990; Lehr et al., 2004; Matallanas et al., 2011). Feedback mechanisms can be differentially activated in a ligand-dependent manner. A classic example of signalling dynamics is that of the differential ERK activity when cells are treated with EGF or NGF (Marshall, 1995; Ryu et al., 2015; Santos et al., 2007). Underlying these dynamics however, are different feedback mechanisms controlling signal activity. Whilst NGF-induced sustained ERK activity is driven by a PKC positive feedback loop, readaptation (to basal-like levels) following EGF-induced ERK activity results from activation of negative feedback motifs; 1) the upregulation of RAF-1 Kinase Inhibitor Protein (RKIP) (Santos et al., 2007) and 2) ERK-mediated inhibiton of guanosine exchange factor Son of Sevenless (SOS) (Purvis and Lahav, 2013).

In this thesis, colorectal cancer cells with a G12D mutation in *KRAS* display the same readaptation kinetics (akin to KRAS^{WT} cells treated with high EGF concentrations) irrespective of the EGF concentration. Such concentration-independent dynamics alludes to cells' inability to activate PKC for a more sustained ERK activity (typically induced with lower EGF concentrations). Moreover, and contrarily to KRAS^{WT} cells, KRAS^{G12D} cells 'overshoot' ERK activity shortly after one hour of ERK inhibition, especially those that have not been pre-treated with EGF. These results, together with the RNAseq data revelation of the upregulated mRNA expression of negative regulators of the MAPK pathway, suggest that mutant cells have a stronger negative feedback activity. As explained in Discussion 2.3 on page 54, the higher than basal-like ERK activity following ERK inhibition may result from the temporal relaxation of the hypothesised stronger negative feedback in mutant cells.

In line with this hypothesis, using melanoma (A375) cells with mutant BRAF^{V600E} (i.e. resulting in upregulated MAPK activity), Gerosa et al. (2020) observed that

various negative regulators (including EGFR, SPRY, DUSP4/6) of ERK activity were substantially downregulated (protein and gene expression) following ablation of MAPK activity. Similarly, Pratilas et al. (2009) observed downregulation of relevant genes in mRNA expression data. Moreover, RNA sequencing of pancreatic ductal adenocarcinoma (PDAC) cell lines treated with various durations of SCH772984 (same ERK inhibitor used in this thesis) also revealed the significant downregulation of negative regulators DUSP6 & SPRY4, even just after 1 hour of ERK inhbition (Bryant et al., 2019; Klomp et al., 2021). Not so surprisingly, in another study, following 4 and 24 hours of MAPK inhibition (also using SCH772984), PDAC derived cell lines expressing mutant KRAS showed increased levels of MEK and RAF, suggesting a loss of (SCH772984-induced) ERK-mediated negative feedback (Hayes et al., 2016). Despite the genotypic disparity between SW48 and the mentioned cell lines, all display high MAPK activity, which when inhibited results in significant downregulation of several negative regulators involved in MAPK and RTK signalling, as well as the activation of upstream MAPK proteins usually inhibited by ERK.

4.2 Optogenetic tool developments

Live cell signalling studies typically involve the measurement of a single key protein of a signalling network. However, years of research have provided us with the knowledge of signalling transduction network (STN) topology and the fact that they are interconnected between one another. In other words, activity in one STN may affect one or more other STNs, the sum of which may result in an observed cellular decision and/or transcriptional programme activation. Thus, to gain significant insight in cellular information processing there is a need to survey multiple key signalling nodes of pathways known to be closely interlinked. Moreover, the methods used to probe said STNs provide low control when it comes to localisation and timing. Hence the need to develop unobtrusive yet highly precise tools – such as optogenetics – to stimulate cells. Finally, a higher degree of imaging complexity (more than one fluorescent reporter combined with light-based perturbation methods) requires superior tools to unmix the additional information in an image. Machine learning-based high-performing algorithms are useful tools to aid in the endeavour to maximise efficiency in image processing operations and biological activity quantification.

NyxBits

To harness the potential insight of monitoring mutliple signalling networks, developments prior to this PhD led to the creation of a multiplexing platform – *Nyxbits*. Said platform consists of three spectrally separated FLIM-FRET pairs designed to be co-expressed for the simultaneous detection of three biochemical events, as previously used to study caspase biology (Fries et al., 2018). In this thesis is shown the optimisation of two *Nyxbits* reporters (blue and green pair), from which the blue pair's FRET efficiency was significantly improved by pairing mTagBFP with the dark acceptor fluorophore ShadowY, whilst reducing the spectral bleed-through from the donor. With this new and improved FLIM-FRET pair, *Nyxbits* provides the first most advanced FLIM-FRET-based multiplexing platform for the simultaneous measurement of three biochemical events.

The scientific community's attempts at multiplexing biochemical readouts have resulted in similar yet different approaches to our *Nyxbits* platform. First, many have made use of typically two spectrally distinguishable FRET sensors to measure protein activity. Often, sequential image acquisition together with blue/green and yellow/orange FRET sensors are co-expressed in cells. Such combinations have commonly been used to image calcium and another protein of interest (Ding et al., 2011; Grant et al., 2008; Su et al., 2013). For example, Su et al. (2013) used mTagBFP/sfGFP (B/G) & mVenus/mKOk (Y/O) ratiometric biosensors with no additional image correction to monitor tyrosine-protein kinase Src and Ca^{2+} upon EGF treatment. The reason red and near-infrared (NIR) fluorescent proteins are not used to develop red FRET sensors is due to the typical low FRET efficiencies achieved and the likelihood for protein aggregation (an issue encountered when developing the red *Nyxbits* pair mKeima-tdNiRFP). However, variants of the red fluorescent protein (RFP) can be used as acceptors of CFP and YFP for dual FRET sensor co-imaging (Nwe-Nwe Aye-Han et al., 2012). Recent improvements in the optical properties of NIR FPs have given rise to effective NIR FRET sensors such as miRFP670-miRFP720, which Shcherbakova et al. (2018) developed and used together with a CFP-YFP RhoA biosensor and blue-based optogenetic system for Rac1 activation. Similarly, RFP enhancements led by Mo et al. (2020) enabled the multiplexing of three different kinases (Src, Akt & ERK) using ratiometric measurements. More advantageous however, is the excitation of expressed sensors using a single laser line (as opposed to sequential excitation of FPs), since it allows the simultaneous measurement of biochemical activities – technique used to image up two FLIM-FRET sensors Demeautis et al. (2017); Ringer et al. (2017). Finally, the use of homo-FRET sensors (Ross et al., 2018; Snell et al., 2018) and alternative FRET measurement methodology – such as photochromism

(Roebroek et al., 2021) or phosphorescence (Conway et al., 2018) – provide advantageous properties that are harnessed to achieve a higher multiplexing capacity. Although various useful multiplexing platforms have emerged, *Nyxbits* represents a unique system in that it enables truly simultaneous FLIM-FRET measurements (using a single laser line) of three biochemical reactions.

Using light to activate oncogene-induced MAPK signalling

Single-cell assays often require high-level control that traditional stimulation methods (chemical or genetic-induced) cannot provide. Alternative methods that enable a much higher spatiotemporal stimulation control are therefore preferred, especially in experiments involving cell-to-cell communication where ideally individual cells of a population are stimulated. Optogenetics provides such control and it – specifically rhodopsins (Boyden et al., 2005; Zhang et al., 2011) – has been developed and extensively used for neuronal stimulation and the study of brain diseases since the beginning of the 20^{th} century (Deisseroth, 2015). More recently, optogenetics has been used to dynamically stimulate signal transduction networks such as the MAPK pathway. In this thesis, I've shown efforts toward the development of *OptoRAS*; a light-inducible mutant RAS activation system.

Early developments of *OptoRAS* (a phytochrome-based system (PhyB-PIF6)) by a previous PhD student demonstrated the reversible translocation of one of the photoreceptive components (YFP-PIF6-KRAS^{G12D}); from the cytoplasm to the plasma membrane (to which PhyB-CAAX is bound). Because the system was demonstrated to successfully work mechanically and due to complications in preliminary experiments with Helas, it was decided to assess biological activity in a more relevant cell line (pancreatic hPNE). Using such cell line stably expressing a doxycycline-inducible *OptoRAS* and a custom-built optical illumination platform (OptoFarm) to improve the control of experimental variables, I took over the project by carrying out experiments assessing whether light induction of oncogenic *KRAS* activated the MAPK pathway. Long-term (i.e. 24 hours post-light induction) ERK activation was reported, and unexpectedly not within the first 30 minutes after stimulation – the latter is a phenotype observed with growth factor induced stimulation (Ryu et al., 2015). Using a different optogenetic (cryptochrome-based) system, long-term ERK activation was not observed, despite the same system working effectively for C-RAF mediated MAPK activation (see Fig. 3.20 on page 110).

Despite the use of optogenetics to light-activate the MAPK pathway via SOS (Toettcher et al., 2013), RAF (Aoki et al., 2013) & MEK (Patel et al., 2019), to date no system to directly light-induce (oncogenic) KRAS has been developed (Kramer et al., 2021). Thus, although the explained *OptoRAS* system is completely novel in the field, the lack of published research and the importance of *KRAS* in oncogenesis hints at the fact that light-induced MAPK activation via KRAS is not as straightforward as with other MAPK components. Two main reasons might explain the inconsistent results achieved with *OptoRAS*. First, protein conformation at the plasma membrane is crucial for signalling to occur (Prakash and Gorfe, 2019; Prakash et al., 2019, 2016). It is likely that the fused photoreceptive protein complex (YFP-PIF6-KRAS^{G12D} or CRY2-KRAS^{G12D}) prevents KRAS from reaching an optimal protein conformation, consequently preventing it from effectively binding to RAS binding domains of downstream proteins. Just as the placement of the membrane anchor on the photoreceptive protein can affect recruitment (Natwick and Collins, 2021), similarly, how the oncogene is bound to the photoreceptive protein might affect the oncogene's protein conformation. Second, the mutant KRAS^{G12D} that is translocated to the plasma membrane upon light exposure is thought to be GTP-bound (i.e. active KRAS). The GTP/GDP state of the mutant KRAS has not been verified and so it is plausible that the translocated mutant oncogene is in an inactive state, resulting in no activation of the MAPK pathway. This speculation is not unlikely, given the fact that oncogenic KRAS has been shown to require preliminary growth factor stimulation to confer sustained high MAPK activity (Huang et al., 2014). Moreover, the potential steric hindrance caused by the fusion to another (photosensitive) protein may prevent KRAS from dimerising and forming nanoclusters – naturally occurring membrane formations that significantly amplify signalling (Muratcioglu et al., 2020; Nan et al., 2015; Sarkar-Banerjee et al., 2017; Zhou et al., 2017) or are even required for oncogenic signalling (Ambrogio et al., 2018).

4.3 Conclusion

I have shown the effects of mutant *KRAS*^{G12D} on the the MAPK signalling cascade in colorectal cell lines stably expressing a novel ERK sensor using microfluidics and a custom-made image analysis pipeline. Cells with mutant *KRAS* are still responsive to growth factor stimulation, however their acute-like deactivation kinetics are homogeneous, independent of input strength (growth factor concentration). Supporting previous observations in the literature, overall, mutant cells display a rather subdued response to EGF. Such response is potentially due to a speculated stronger negative feedback

as hinted by a high 'rebound' activation following ERK inhibition and the upregulated mRNA expression of negative feedback regulators. Rewiring of feedback mechanisms has high implications on cell information processing and consequentially any regimen that aims to manipulate the MAPK pathway for cancer management purposes. More work aiming at accurately describing relevant feedback mechanisms may not only enlighten our insight on oncogenic signalling but also reveal potential new drug targets with possibly less toxic effects than MAPK ablating treatments.

To enable present (Chapter 2) and future biological projects aimed at characterising oncogene signalling with superior biochemical resolution and stimulation control, in addition to generating numerous monoclonal cell lines of different origins (colorectal and pancreatic) stably expressing EKAREN5 – a novel & enhanced ERK sensor (Ponsioen et al., 2021) – I developed and optimised optical tools. By enhancing a FLIM-FRET pair of the *Nyxbits* reporters, these heavily optimised sensors can be used to multiplex three different proteins involved in key RAS-regulated signal transduction networks. Moreover, although more work is needed to ensure reliability, promising optogenetic developments whereby light mediated activation of mutant KRAS may result in subsequent MAPK stimulation could become an instrumental tool to dynamically decode cellular signal processing.

4.4 Future work

A number of aspects mentioned in the above discussion can be adressed experimentally to further elucidate the effects of mutant KRAS on MAPK signalling. First, despite our interpretations being consistent from experiment to experiment, replicating the performed EGF titration assays and observed results using alternate methodologies or sensors would further strengthen our interpretations and hypotheses. To perform more robust FRET measurements, the ERK CDC25C substrate sequence could be integrated within one of the *Nyxbits* reporters to measure FLIM-FRET (as opposed to ratiometric sensitised emission FRET). Alternatively, although more challenging image analysis wise, common ERK sensors such as ERK-Kinase Translocation Reporter (ERK-KTR) (Regot et al., 2014) could also be directly used to monitor ERK.

Second, further characterisaiton of negative feedback regulation in mutant *KRAS* cells would likely elucidate causes of the 'rebound' signalling effect shortly after ERK inhibition. The results shown here indicate that negative feedback regulation in cells with mutant *KRAS* is distinctively different from KRAS wild-type cells. However, it is not

clear whether this is attributable to a single deregulated feedback motif or whether it is the cumulative sum of multiple dysregulations. To address this, an shRNA/siRNA screen of known negative and positive regulators of the MAPK pathway and subjecting both mutant and wild-type KRAS cells to the same stimulation protocol as used in this thesis would help characterising the effects of individual feedback regulators. If the wild-type phenotype is achieved (or conversely $KRAS^{WT}$ cells behave as $KRAS^{G12D}$ cells), the screen is likely to indicate the particular feedback motif involved. Additionally, using the siRNA screen data together with the SW48 RNAseq data (i.e. to take into account gene up-/down-regulation) is useful information that may be harnessed to build *in silico* models and assess the combined effects of multiple feedback regulators. Moreover, replacing the ERK inhibitor (SCH772984) – which prevents ERK activity on downstream proteins as well as ERK activation by MEK (Chaikuad et al., 2014) – with a MEK inhibitor (such as Selumetinib, which would enable phosphorylation of ERK downstream targets but prevent further activation of ERK) would elucidate whether the mutant-specific 'rebound' phenotype is solely due to direct ERK-induced activity. In the latter case scenario, treatment of mutant cells with a MEKi would result in a similar phenotype to wild-type KRAS cells (i.e. regaining basal-like levels of ERK activity following ERK inhibition). ERK inhibition is known to activate AKT due to loss of ERK negative feedback on EGFR (Chen et al., 2017, 2012). If AKT is probed during ERK inhibition and is found to be phosphorylated (more so than in KRAS wild-type cells), this would suggest that negative feedback regulation strongly signals through AKT, which could in turn enhance ERK-induced transcription via phosphorylation of PEA-15 and subsequent nuclear translocation (Lavoie et al., 2020; Traverse et al., 1992; von Kriegsheim et al., 2009). Yet another feedback mechanism that could be explored involves EGFR; its internalisation – an event that occurs upon EGFR activation (Madshus and Stang, 2009) – and ERK-induced inhibitory phosphorylation at threonine 693 (Lavoie et al., 2020), which can be probed by Western Blot. Although SW48 cells harbour an activating G719S mutation, they still retain EGF response capacity, as observed by the clear ERK peak shortly after EGF treatment (see Fig. 2.4 on page 43). Thus, exposing cells to EGFR inhibition after ERK inhibition – i.e. when cells are usually subjected only to low-nutrient (1% FCS) imaging media – would be a useful intervention to understand to which extent the 'rebound' ERK activity observed post-ERK inhibition in mutant cells is dependent on externally-induced stimulation. Although there are many tyrosine kinase inhibitors (TKIs) used clinically and commercially available, previous studies suggest that afatinib is rather advantageous in that it is more effective at inhibiting mutated EGFR (Kobayashi et al., 2015; Yang et al., 2015) than other standard TKIs such as

gefitinib (Kobayashi et al., 2005). Another method to test whether EGFR internalisation plays a role is by inhibiting such process using a dynamin inhibitor (Henriksen et al., 2013).

Third, signalling dynamics characterisation is another aspect on which further efforts may result in useful insights. For example, the lowest EGF concentration condition in the titration assays shows that $KRAS^{wt}$ cells are ultrasensitive to the growth factor whereas mutant cells visibly display a milder response amplitude (see (c) in Fig. 2.5 on page 44). This observation is an indication that there might be a low EGF concentration that mutant cells cannot sense (and KRAS wild-type cells might). Therefore treating both genotypes with lower EGF concentrations might aid in defining a minimum concentration threshold below which mutant cells cannot sense growth factor induced stimuli.

Fourth and finally, already available RNAseq and imaging data can be harnessed to gain further insight on network dynamics. Due to the known correlation of ERK pulsatile dynamics with proliferation (Goglia et al., 2020), quantification of the percentage of pulsating cells could indicate whether one genotype is more likely to proliferate. RNA expression data can be used to interrogate the effect of chronic expression of mutant KRAS in cells by surveying the relative expression of ERK-response genes according to their known stimulation-response times (i.e. immediate early genes or IEGs, delayed early genes or DEGs and secondary response genes or SRGs) (Avraham and Yarden, 2011).

References

Abraham, S. J., Nolet, R. P., Calvert, R. J., Anderson, L. M., and Gaponenko, V. (2009). The hypervariable region of K-Ras4B is responsible for its specific interactions with calmodulin. *Biochemistry*, 48(32):7575–7583.

Ahearn, I. M., Haigis, K., Bar-Sagi, D., and Philips, M. R. (2011). Regulating the regulator: post-translational modification of RAS. *Nature Reviews Molecular Cell Biology*, 13(1):39–51.

Ai, H. W., Hazelwood, K. L., Davidson, M. W., and Campbell, R. E. (2008). Fluorescent protein FRET pairs for ratiometric imaging of dual biosensors. *Nat Methods*, 5(5):401–403.

Aikin, T. J., Peterson, A. F., Pokrass, M. J., Clark, H. R., and Regot, S. (2019). Collective MAPK Signaling Dynamics Coordinates Epithelial Homeostasis. *bioRxiv*, page 826917.

Albeck, J. G., Mills, G. B., and Brugge, J. S. (2013). Frequency-Modulated Pulses of ERK Activity Transmit Quantitative Proliferation Signals.

Alexandrov, L. B., Kim, J., Haradhvala, N. J., Huang, M. N., Wei, A., Ng, T., Wu, Y., Boot, A., Covington, K. R., Gordenin, D. A., Bergstrom, E. N., Islam, S. M. A., Lopez-Bigas, N., Klimczak, L. J., Mcpherson, J. R., Morganella, S., Sabarinathan, R., Wheeler, D. A., Rozen, S. G., Stratton, M. R., and Consortium, P. (2020). The repertoire of mutational signatures in human cancer. *Nature*, 578:94–101.

Alexandrov, L. B., Nik-Zainal, S., Wedge, D. C., Aparicio, S. A., Behjati, S., Biankin, A. V., Bignell, G. R., Bolli, N., Borg, A., Børresen-Dale, A. L., Boyault, S., Burkhardt, B., Butler, A. P., Caldas, C., Davies, H. R., Desmedt, C., Eils, R., Eyfjörd, J. E., Foekens, J. A., Greaves, M., Hosoda, F., Hutter, B., Ilicic, T., Imbeaud, S., Imielinsk, M., Jäger, N., Jones, D. T., Jonas, D., Knappskog, S., Koo, M., Lakhani, S. R., López-Otín, C., Martin, S., Munshi, N. C., Nakamura, H., Northcott, P. A., Pajic, M., Papaemmanuil, E., Paradiso, A., Pearson, J. V., Puente, X. S., Raine, K., Ramakrishna, M., Richardson, A. L., Richter, J., Rosenstiel, P., Schlesner, M., Schumacher, T. N., Span, P. N., Teague, J. W., Totoki, Y., Tutt, A. N., Valdés-Mas, R., Van Buuren, M. M., Van 'T Veer, L., Vincent-Salomon, A., Waddell, N., Yates, L. R., Zucman-Rossi, J., Andrew Futreal, P., McDermott, U., Lichter, P., Meyerson, M., Grimmond, S. M., Siebert, R., Campo, E., Shibata, T., Pfister, S. M., Campbell, P. J., and Stratton, M. R. (2013). Signatures of mutational processes in human cancer. *Nature*, 500(7463):415–421.

Alon, U. (2007). Network motifs: theory and experimental approaches. *Nature Reviews Genetics*, 8(6):450–461.

Altschuler, S. J. and Wu, L. F. (2010). Cellular Heterogeneity: Do Differences Make a Difference? *Cell*, 141(4):559–563.

Ambrogio, C., Köhler, J., Zhou, Z. W., Wang, H., Paranal, R., Li, J., Capelletti, M., Caffarra, C., Li, S., Lv, Q., Gondi, S., Hunter, J. C., Lu, J., Chiarle, R., Santamaría, D., Westover, K. D., and Jänne, P. A. (2018). KRAS Dimerization Impacts MEK Inhibitor Sensitivity and Oncogenic Activity of Mutant KRAS. *Cell*, pages 857–868.

Anderson, A. R., Weaver, A. M., Cummings, P. T., and Quaranta, V. (2006). Tumor Morphology and Phenotypic Evolution Driven by Selective Pressure from the Microenvironment.

Andor, N., Graham, T. A., Jansen, M., Xia, L. C., Aktipis, C. A., Petritsch, C., Ji, H. P., and Maley, C. C. (2016). Pan-cancer analysis of the extent and consequences of intratumor heterogeneity. *Nature Medicine*, 22(1):105–113.

Aoki, K., Kondo, Y., Naoki, H., Hiratsuka, T., Itoh, R. E., and Matsuda, M. (2017). Propagating Wave of ERK Activation Orients Collective Cell Migration.

Aoki, K., Kumagai, Y., Sakurai, A., Komatsu, N., Fujita, Y., Shionyu, C., and Matsuda, M. (2013). Stochastic ERK activation induced by noise and cell-to-cell propagation regulates cell density-dependent proliferation. *Molecular Cell*, 52(4):529–540.

Aoki, K., Yamada, M., Kunida, K., Yasuda, S., and Matsuda, M. (2011). Processive phosphorylation of ERK MAP kinase in mammalian cells. *Proceedings of the National Academy of Sciences*, 108(31):12675–12680.

Ardito, C. M., Grüner, B. M., Takeuchi, K. K., Lubeseder-Martellato, C., Teichmann, N., Mazur, P. K., DelGiorno, K. E., Carpenter, E. S., Halbrook, C. J., Hall, J. C., Pal, D., Briel, T., Herner, A., Trajkovic-Arsic, M., Sipos, B., Liou, G. Y., Storz, P., Murray, N. R., Threadgill, D. W., Sibilia, M., Washington, M. K., Wilson, C. L., Schmid, R. M., Raines, E. W., Crawford, H. C., and Siveke, J. T. (2012). EGF Receptor Is Required for KRAS-Induced Pancreatic Tumorigenesis. *Cancer Cell*, 22(3):304–317.

Augsten, M., Pusch, R., Biskup, C., Rennert, K., Wittig, U., Beyer, K., Blume, A., Wetzker, R., Friedrich, K., and Rubio, I. (2006). Live-cell imaging of endogenous Ras-GTP illustrates predominant Ras activation at the plasma membrane. *EMBO Rep*, 7(1):46–51.

Avraham, R. and Yarden, Y. (2011). Feedback regulation of EGFR signalling: decision making by early and delayed loops. *Nature Reviews Molecular Cell Biology*, 12:104–117.

Azeloglu, E. U. and Iyengar, R. (2015). Signaling networks: Information flow, computation, and decision making. *Cold Spring Harbor Perspectives in Biology*, 7(4):1–14.

Bajar, B. T., Wang, E. S., Zhang, S., Lin, M. Z., and Chu, J. (2016). A guide to fluorescent protein FRET pairs. *Sensors (Switzerland)*, 16(9):1–24.

Balaban, N. Q., Merrin, J., Chait, R., Kowalik, L., and Leibler, S. (2004). Bacterial persistence as a phenotypic switch. *Science*, 305(5690):1622–1625.

Balázsi, G., Van Oudenaarden, A., and Collins, J. J. (2011). Cellular decision making and biological noise: From microbes to mammals.

Becker, W. (2012). Fluorescence lifetime imaging - techniques and applications. *Journal of Microscopy*, 247(2):119–136.

Bell, C. C. and Gilan, O. (2020). Principles and mechanisms of non-genetic resistance in cancer. *British Journal of Cancer*, 122:465–472.

Bennecke, M., Kriegl, L., Bajbouj, M., Retzlaff, K., Robine, S., Jung, A., Arkan, M. C., Kirchner, T., and Greten, F. R. (2010). Ink4a/Arf and oncogene-induced senescence prevent tumor progression during alternative colorectal tumorigenesis. *Cancer Cell*, 18(2):135–146.

Berg, S., Kutra, D., Kroeger, T., Straehle, C. N., Kausler, B. X., Haubold, C., Schiegg, M., Ales, J., Beier, T., Rudy, M., Eren, K., Cervantes, J. I., Xu, B., Beuttenmueller, F., Wolny, A., Zhang, C., Koethe, U., Hamprecht, F. A., and Kreshuk, A. (2019). ilastik: interactive machine learning for (bio)image analysis. *Nature Methods*, 16(12):1226–1232.

Bergeron, J. J., Di Guglielmo, G. M., Dahan, S., Dominguez, M., and Posner, B. I. (2016). Spatial and temporal regulation of receptor tyrosine kinase activation and intracellular signal transduction. *Annual review of biochemistry*, 85:573–597.

Bhalla, U. S., Ram, P. T., and Iyengar, R. (2002). Map kinase phosphatase as a locus of flexibility in a mitogen-activated protein kinase signaling network. *Science*, 297(5583):1018–1023.

Biggs, N. L., Lloyd, E. K., and Wilson, R. J. (1986). *Graph Theory 1736-1936*. Clarendon Press.

Birkbak, N. J., Eklund, A. C., Li, Q., McClelland, S. E., Endesfelder, D., Tan, P., Tan, I. B., Richardson, A. L., Szallasi, Z., and Swanton, C. (2011). Paradoxical relationship between chromosomal instability and survival outcome in cancer. *Cancer Research*, 71(10):3447–3452.

Birkbak, N. J., Wang, Z. C., Kim, J. Y., Eklund, A. C., Li, Q., Tian, R., Bowman-Colin, C., Li, Y., Greene-Colozzi, A., Dirk Iglehart, J., Tung, N., Ryan, P. D., Garber, J. E., Silver, D. P., Szallasi, Z., and Richardson, A. L. (2012). Telomeric allelic imbalance indicates defective DNA repair and sensitivity to DNA-damaging agents. *Cancer Discovery*, 2(4):366–375.

Blum, Y., Mikelson, J., Dobrzyński, M., Ryu, H., Jacques, M.-A., Jeon, N. L., Khammash, M., and Pertz, O. (2019). Temporal perturbation of Erk dynamics reveals network architecture of FGF2-MAPK signaling. *Molecular Systems Biology*, 15(e8947):1–17.

Bove, A., Gradeci, D., Fujita, Y., Banerjee, S., Charras, G., and Lowe, A. R. (2017). Local cellular neighborhood controls proliferation in cell competition. *Molecular Biology of the Cell*, 28(23):3215–3228.

Boveri, T. (1914). Zur Frage der Entstehung maligner Tumoren. *Science*, 40(1041):857–859.

Boyden, E. S., Zhang, F., Bamberg, E., Nagel, G., and Deisseroth, K. (2005). Millisecond-timescale, genetically targeted optical control of neural activity. *Nature neuroscience*, 8(9):1263–1268.

Brandt, R., Sell, T., Lüthen, M., Uhlitz, F., Klinger, B., Riemer, P., Giesecke-Thiel, C., Schulze, S., El-Shimy, I. A., Kunkel, D., Fauler, B., Mielke, T., Mages, N., Herrmann, B. G., Sers, C., Blüthgen, N., and Morkel, M. (2019). Cell type-dependent differential activation of ERK by oncogenic KRAS in colon cancer and intestinal epithelium. *Nature Communications*, 10(1).

Brightman, F. A. and Fell, D. A. (2000). Differential feedback regulation of the MAPK cascade underlies the quantitative differences in EGF and NGF signalling in PC12 cells. *FEBS Letters*, 482(3):169–174.

Brock, A., Chang, H., and Huang, S. (2009). Non-genetic heterogeneity a mutation-independent driving force for the somatic evolution of tumours. *Nature Reviews Genetics*, 10(5):336–342.

Broussard, J. A., Rappaz, B., Webb, D. J., and Brown, C. M. (2013). Fluorescence resonance energy transfer microscopy as demonstrated by measuring the activation of the serine/threonine kinase Akt. *Nature Protocols*, 8(2):265–281.

Bryant, K. L., Stalnecker, C. A., Zeitouni, D., Klomp, J. E., Peng, S., Tikunov, A. P., Gunda, V., Pierobon, M., Waters, A. M., George, S. D., Tomar, G., Papke, B., Hobbs, G. A., Yan, L., Hayes, T. K., Diehl, J. N., Goode, G. D., Chaika, N. V., Wang, Y., Zhang, G. F., Witkiewicz, A. K., Knudsen, E. S., Petricoin, E. F., Singh, P. K., Macdonald, J. M., Tran, N. L., Lyssiotis, C. A., Ying, H., Kimmelman, A. C., Cox, A. D., and Der, C. J. (2019). Combination of ERK and autophagy inhibition as a treatment approach for pancreatic cancer. *Nature Medicine*, 25(4):628–640.

Buday, L., Warne, P. H., and Downward, J. (1995). Downregulation of the ras activation pathway by map kinase phosphorylation of sos. *Oncogene*, 11(7):1327–1331.

Buettner, F., Natarajan, K. N., Casale, F. P., Proserpio, V., Scialdone, A., Theis, F. J., Teichmann, S. A., Marioni, J. C., and Stegle, O. (2015). Computational analysis of cell-to-cell heterogeneity in single-cell RNA-sequencing data reveals hidden subpopulations of cells. *Nature Biotechnology*, 33(2):155–160.

Bugaj, L. J., Sabnis, A. J., Mitchell, A., Garbarino, J. E., Toettcher, J. E., Bivona, T. G., and Lim, W. A. (2018). Cancer mutations and targeted drugs can disrupt dynamic signal encoding by the Ras-Erk pathway. *Science*, 361(6405).

Burrell, R. A., McGranahan, N., Bartek, J., and Swanton, C. (2013). The causes and consequences of genetic heterogeneity in cancer evolution.

Caignard, A., Martin, M. S., Michel, M. F., and Martin, F. (1985). Interaction between two cellular subpopulations of a rat colonic carcinoma when inoculated to the syngeneic host. *Int J Cancer*, 36(2):273–279.

Campbell, P. M., Groehler, A. L., Lee, K. M., Ouellette, M. M., Khazak, V., and Der, C. J. (2007). K-Ras promotes growth transformation and invasion of immortalized human pancreatic cells by raf and phosphatidylinositol 3-kinase signaling. *Cancer Research*, 67(5):2098–2106.

Campbell, S. L., Khosravi-Far, R., Rossman, K. L., Clark, G. J., and Der, C. J. (1998). Increasing complexity of Ras signaling. *Oncogene*, 17:1395–1413.

Caunt, C. J., Sale, M. J., Smith, P. D., and Cook, S. J. (2015). MEK1 and MEK2 inhibitors and cancer therapy: The long and winding road. *Nature Reviews Cancer*, 15(10):577–592.

Céspedes, M. V., Sancho, F. J., Guerrero, S., Parreño, M., Casanova, I., Pavón, M. A., Marcuello, E., Trias, M., Cascante, M., Capellà, G., et al. (2006). K-ras asp12 mutant neither interacts with raf, nor signals through erk and is less tumorigenic than k-ras val12. *Carcinogenesis*, 27(11):2190–2200.

Chaikuad, A., Tacconi, E. M., Zimmer, J., Liang, Y., Gray, N. S., Tarsounas, M., and Knapp, S. (2014). A unique inhibitor binding site in erk1/2 is associated with slow binding kinetics. *Nature chemical biology*, 10(10):853–860.

Chang, H. H., Hemberg, M., Barahona, M., Ingber, D. E., and Huang, S. (2008). Transcriptome-wide noise controls lineage choice in mammalian progenitor cells. *Nature*, 453(7194):544–547.

Chapman, P. B., Hauschild, A., Robert, C., Haanen, J. B., Ascierto, P., Larkin, J., Dummer, R., Garbe, C., Testori, A., Maio, M., Hogg, D., Lorigan, P., Lebbe, C., Jouary, T., Schadendorf, D., Ribas, A., O'Day, S. J., Sosman, J. A., Kirkwood, J. M., Eggermont, A. M., Dreno, B., Nolop, K., Li, J., Nelson, B., Hou, J., Lee, R. J., Flaherty, K. T., and McArthur, G. A. (2011). Improved Survival with Vemurafenib in Melanoma with BRAF V600E Mutation. *New England Journal of Medicine*, 364(26):2507–2516.

Chatterjee, N. and Walker, G. C. (2017). Mechanisms of DNA damage, repair and mutagenesis. *Environ Mol Mutagen*, 58(5):235–263.

Chen, C.-H., Hsia, T.-C., Yeh, M.-H., Chen, T.-W., Chen, Y.-J., Chen, J.-T., Wei, Y.-L., Tu, C.-Y., and Huang, W.-C. (2017). MEK inhibitors induce Akt activation and drug resistance by suppressing negative feedback ERK-mediated HER2 phosphorylation at Thr701. *Molecular Oncology*, 11(9):1273–1287.

Chen, J.-Y., Lin, J.-R., Cimprich, K. A., and Meyer, T. (2012). A two-dimensional erk-akt signaling code for an ngf-triggered cell-fate decision. *Molecular cell*, 45(2):196–209.

Chiarugi, P. and Cirri, P. (2016). Metabolic exchanges within tumor microenvironment. *Cancer Lett*, 380(1):272–280.

Chien, S., Li, S., and Shyy, J. Y. (1998). Effects of mechanical forces on signal transduction and gene expression in endothelial cells. *Hypertension*, 31(1):162–169.

Chou, J., Provot, S., and Werb, Z. (2010). GATA3 in development and cancer differentiation: Cells GATA have it!

Ciriello, G., Miller, M. L., Arman Aksoy, B., Senbabaoglu, Y., Schultz, N., and Sander, C. (2013). Emerging landscape of oncogenic signatures across human cancers. *Nature Genetics*, 45(10):1127–1133.

Cobleigh, M. A., Vogel, C. L., Tripathy, D., Robert, N. J., Scholl, S., Fehrenbacher, L., Wolter, J. M., Paton, V., Shak, S., Lieberman, G., and Slamon, D. J. (1999). Multinational study of the efficacy and safety of humanized anti-HER2 monoclonal antibody in women who have HER2-overexpressing metastatic breast cancer that has progressed after chemotherapy for metastatic disease. *Journal of Clinical Oncology*, 17(9):2639–2648.

Cohen-Saidon, C., Cohen, A. A., Sigal, A., Liron, Y., and Alon, U. (2009). Dynamics and Variability of ERK2 Response to EGF in Individual Living Cells. *Molecular Cell*, 36(5):885–893.

Contributors, N. (2019). napari: a multi-dimensional image viewer for python.

Conway, J. R., Warren, S. C., Herrmann, D., Murphy, K. J., Cazet, A. S., Vennin, C., Shearer, R. F., Killen, M. J., Magenau, A., Mélénec, P., et al. (2018). Intravital imaging to monitor therapeutic response in moving hypoxic regions resistant to pi3k pathway targeting in pancreatic cancer. *Cell reports*, 23(11):3312–3326.

Cook, J. H., Melloni, G. E., Gulhan, D. C., Park, P. J., and Haigis, K. M. (2021). The origins and genetic interactions of kras mutations are allele-and tissue-specific. *Nature communications*, 12(1):1808.

Cox, A. D. and Der, C. J. (2003). The dark side of ras: regulation of apoptosis. *Oncogene*, 22(56):8999–9006.

Cox, A. D., Fesik, S. W., Kimmelman, A. C., Luo, J., and Der, C. J. (2014). Drugging the undruggable RAS: Mission Possible? *Nature Reviews Drug Discovery*, 13(11):828–851.

Csermely, P., Korcsmáros, T., and Nussinov, R. (2016). Intracellular and intercellular signaling networks in cancer initiation, development and precision anti-cancer therapy: RAS acts as contextual signaling hub. *Seminars in Cell and Developmental Biology*, 58:55–59.

Curtis, C., Shah, S. P., Chin, S. F., Turashvili, G., Rueda, O. M., Dunning, M. J., Speed, D., Lynch, A. G., Samarajiwa, S., Yuan, Y., Gräf, S., Ha, G., Haffari, G., Bashashati, A., Russell, R., McKinney, S., Aparicio, S., Brenton, J. D., Ellis, I., Huntsman, D., Pinder, S., Murphy, L., Bardwell, H., Ding, Z., Jones, L., Liu, B., Papatheodorou, I., Sammut, S. J., Wishart, G., Chia, S., Gelmon, K., Speers, C., Watson, P., Blamey, R., Green, A., MacMillan, D., Rakha, E., Gillett, C., Grigoriadis, A., De Rinaldis, E., Tutt, A., Parisien, M., Troup, S., Chan, D., Fielding, C., Maia, A. T., McGuire, S., Osborne, M., Sayalero, S. M., Spiteri, I., Hadfield, J., Bell, L., Chow, K., Gale, N., Kovalik, M., Ng, Y., Prentice, L., Tavaré, S., Markowetz, F., Langerød, A., Provenzano, E., Purushotham, A., Børresen-Dale, A. L., and Caldas, C. (2012). The genomic and transcriptomic architecture of 2,000 breast tumours reveals novel subgroups. *Nature*, 486(7403):346–352.

Darwin, C. and Kebler, L. (1859). *On the origin of species by means of natural selection, or, The preservation of favoured races in the struggle for life*. London: J. Murray.

Davies, A. E. and Albeck, J. G. (2018). Microenvironmental signals and biochemical information processing: Cooperative determinants of intratumoral plasticity and heterogeneity. *Frontiers in Cell and Developmental Biology*, 6(APR):1–15.

Davies, A. E., Pargett, M., Siebert, S., Gillies, T. E., Choi, Y., Tobin, S. J., Ram, A. R., Murthy, V., Juliano, C., Quon, G., Bissell, M. J., and Albeck, J. G. (2020). Systems-Level Properties of EGFR-RAS-ERK Signaling Amplify Local Signals to Generate Dynamic Gene Expression Heterogeneity. *Cell Systems*, 11(2):161–175.e5.

Davies, H., Bignell, G. R., Cox, C., Stephens, P., Edkins, S., Clegg, S., Teague, J., Woffendin, H., Garnett, M. J., Bottomley, W., et al. (2002). Mutations of the braf gene in human cancer. *Nature*, 417(6892):949–954.

De, S., Campbell, C., Venkitaraman, A. R., and Esposito, A. (2020). Pulsatile mapk signaling modulates p53 activity to control cell fate decisions at the g2 checkpoint for dna damage. *Cell reports*, 30(7):2083–2093.

De Roock, W., Jonker, D. J., Di Nicolantonio, F., Sartore-Bianchi, A., Tu, D., Siena, S., Lamba, S., Arena, S., Frattini, M., Piessevaux, H., Van Cutsem, E., O'Callaghan, C. J., Khambata-Ford, S., Zalcberg, J. R., Simes, J., Karapetis, C. S., Bardelli, A., and Tejpar, S. (2010). Association of KRAS p.G13D mutation with outcome in patients with chemotherapy-refractory metastatic colorectal cancer treated with cetuximab. *JAMA - Journal of the American Medical Association*, 304(16):1812–1820.

Deisseroth, K. (2015). Optogenetics: 10 years of microbial opsins in neuroscience. *Nature neuroscience*, 18(9):1213–1225.

Demeautis, C., Sipieter, F., Roul, J., Chapuis, C., Padilla-Parra, S., Riquet, F. B., and Tramier, M. (2017). Multiplexing PKA and ERK1&2 kinases FRET biosensors in living cells using single excitation wavelength dual colour FLIM. *Scientific Reports*, 7(January):1–14.

Der, C. J., Krontiris, T. G., and Cooper, G. M. (1982). Transforming genes of human bladder and lung carcinoma cell lines are homologous to the ras genes of Harvey and Kirsten sarcoma viruses. *Proceedings of the National Academy of Sciences of the United States of America*, 79(11):3637–40.

Dinarello, C. (2007). Historical insights into cytokines. *European Journal of Immunology*, 37(S1):S34–S45.

Ding, Y., Ai, H.-w., Hoi, H., and Campbell, R. E. (2011). Forster resonance energy transfer-based biosensors for multiparameter ratiometric imaging of ca2+ dynamics and caspase-3 activity in single cells. *Analytical chemistry*, 83(24):9687–9693.

Dobrzyński, M., Jacques, M.-A., and Pertz, O. (2019). Mining single-cell time-series datasets with Time Course Inspector. *Bioinformatics*, 36(6):1968–1969.

Drosten, M., Simon-Carrasco, L., Hernandez-Porras, I., Lechuga, C. G., Blasco, M. T., Jacob, H. K., Fabbiano, S., Potenza, N., Bustelo, X. R., Guerra, C., and Barbacid, M. (2017). H-Ras and K-Ras oncoproteins induce different tumor spectra when driven by the same regulatory sequences. *Cancer Research*, 77(3):707–718.

El-Deiry, W. S., Tokino, T., Velculescu, V. E., Levy, D. B., Parsons, R., Trent, J. M., Lin, D., Mercer, W. E., Kinzler, K. W., and Vogelstein, B. (1993). WAF1, a potential mediator of p53 tumor suppression. *Cell*, 75(4):817–825.

Eling, N., Morgan, M. D., and Marioni, J. C. (2019). Challenges in measuring and understanding biological noise. *Nature Reviews Genetics*, 20(9):536–548.

Elowitz, M. B., Levine, A. J., Siggia, E. D., and Swain, P. S. (2002). Stochastic gene expression in a single cell. *Science*, 297(5584):1183–1186.

Esteban, L. M., Vicario-abejón, C., Fernández-medarde, A., Yienger, K., Lopez, E., Malumbres, M., Mckay, R., Ward, J. M., Pellicer, A., Ferna, P., Vicario-abejo, C., Lopez, E. V. a., and Kay, R. O. N. M. C. (2001). Targeted Genomic Disruption of H- ras and N- ras , Individually or in Combination , Reveals the Dispensability of Both Loci for Mouse Growth and Development. *Molecular and cellular biology*, 21(5):1444–1452.

Faguet, G. B. (2015). A brief history of cancer: Age-old milestones underlying our current knowledge database. *International Journal of Cancer*, 136(9):2022–2036.

Fearon, E. R. and Vogelstein, B. (1990). A genetic model for colorectal tumorigenesis. *Cell*, 61(5):759–767.

Fernández-Medarde, A. and Santos, E. (2011). Ras in cancer and developmental diseases. *Genes & cancer*, 2(3):344–58.

Forster, T. (1946). Energiewanderung und Fluoreszenz. *Die Naturwissenschaften*, 33(6):166–175.

Francis, J. M., Zhang, C. Z., Maire, C. L., Jung, J., Manzo, V. E., Adalsteinsson, V. A., Homer, H., Haidar, S., Blumenstiel, B., Pedamallu, C. S., Ligon, A. H., Love, J. C., Meyerson, M., and Ligon, K. L. (2014). EGFR variant heterogeneity in glioblastoma resolved through single-nucleus sequencing. *Cancer Discov*, 4(8):956–971.

Fries, M. W., Haas, K. T., Ber, S., Saganty, J., Richardson, E. K., Venkitaraman, A. R., and Esposito, A. (2018). Multiplexed biochemical imaging reveals caspase activation patterns underlying single cell fate. *bioRxiv*.

Gagliardi, P. A., Dobrzy, M., Jacques, M.-A., Hughes, R. M., Cohen, A. R., and Correspondence, O. P. (2021). Collective ERK/Akt activity waves orchestrate epithelial homeostasis by driving apoptosis-induced survival. *Developmental Cell*, 56:1712–1726.

Gallego, C., Gupta, S. K., Heasley, L. E., Qian, N.-X., and Johnson, G. L. (1992). Mitogen-activated protein kinase activation resulting from selective oncogene expression in nih 3t3 and rat 1a cells. *Proceedings of the National Academy of Sciences*, 89(16):7355–7359.

Galperin, E., Verkhusha, V. V., and Sorkin, A. (2004). Three-chromophore fret microscopy to analyze multiprotein interactions in living cells. *Nature Methods*, 1(3):209–217.

Gaudet, S. and Miller-Jensen, K. (2016). Redefining Signaling Pathways with an Expanding Single-Cell Toolbox. *Trends in Biotechnology*, 34(6):458–469.

Gerlinger, M., Rowan, A. J., Horswell, S., Larkin, J., Endesfelder, D., Gronroos, E., Martinez, P., Matthews, N., Stewart, A., Tarpey, P., Varela, I., Phillimore, B., Begum, S., McDonald, N. Q., Butler, A., Jones, D., Raine, K., Latimer, C., Santos, C. R., Nohadani, M., Eklund, A. C., Spencer-Dene, B., Clark, G., Pickering, L., Stamp, G., Gore, M., Szallasi, Z., Downward, J., Futreal, P. A., and Swanton, C. (2012). Intratumor Heterogeneity and Branched Evolution Revealed by Multiregion Sequencing. *New England Journal of Medicine*, 366(10):883–892.

Gerosa, L., Chidley, C., Fröhlich, F., Sanchez, G., Lim, S. K., Muhlich, J., Chen, J.-Y., Vallabhaneni, S., Baker, G. J., Schapiro, D., Atanasova, M. I., Chylek, L. A., Shi, T., Yi, L., Nicora, C. D., Claas, A., Ng, T. S., Kohler, R. H., Lauffenburger, D. A., Weissleder, R., Miller, M. A., Qian, W.-J., Wiley, H. S., and Sorger, P. K. (2020). Receptor-Driven ERK Pulses Reconfigure MAPK Signaling and Enable Persistence of Drug-Adapted BRAF-Mutant Melanoma Cells. *Cell Systems*, 11:478–494.

Gillies, T., Pargett, M., Silva, J., Teragawa, C., McCormick, F., and Albeck, J. (2020). Oncogenic mutant RAS signaling activity is rescaled by the ERK/MAPK pathway. *Molecular Systems Biology*, 16(10):1–19.

Gillies, T. E., Pargett, M., Minguet, M., Davies, A. E., and Albeck, J. G. (2017). Linear Integration of ERK Activity Predominates over Persistence Detection in Fra-1 Regulation. *Cell Systems*, 5(6):549–563.e5.

Goglia, A. G., Wilson, M. Z., Jena, S. G., Silbert, J., Basta, L. P., Devenport, D., and Toettcher, J. E. (2020). A Live-Cell Screen for Altered Erk Dynamics Reveals Principles of Proliferative Control. *Cell Systems*, 10(3):240–253.e6.

Golding, I., Paulsson, J., Zawilski, S. M., and Cox, E. C. (2005). Real-time kinetics of gene activity in individual bacteria. *Cell*, 123(6):1025–1036.

Govindan, R., Ding, L., Griffith, M., Subramanian, J., Dees, N. D., Kanchi, K. L., Maher, C. A., Fulton, R., Fulton, L., Wallis, J., Chen, K., Walker, J., McDonald, S., Bose, R., Ornitz, D., Xiong, D., You, M., Dooling, D. J., Watson, M., Mardis, E. R., and Wilson, R. K. (2012). Genomic landscape of non-small cell lung cancer in smokers and never-smokers. *Cell*, 150(6):1121–1134.

Graham, T. A., Temko, D., Tomlinson, I. P. M., Severini, S., and Schuster-Böckler, B. (2018). The effects of mutational processes and selection on driver mutations across cancer types. *Nature Communications*, 9(1).

Grant, D. M., Zhang, W., McGhee, E. J., Bunney, T. D., Talbot, C. B., Kumar, S., Munro, I., Dunsby, C., Neil, M. A., Katan, M., and French, P. M. (2008). Multiplexed FRET to image multiple signaling events in live cells. *Biophysical Journal*, 95(10):L69–L71.

Greaves, M. (2015). Evolutionary determinants of cancer.

Greaves, M. and Maley, C. C. (2012). Clonal evolution in cancer.

Guerra, C., Mijimolle, N., Dhawahir, A., Dubus, P., Barradas, M., Serrano, M., Campuzano, V., and Barbacid, M. (2003). Tumor induction by an endogenous K-ras oncogene is highly dependent on cellular context. *Cancer Cell*, 4(2):111–120.

Guntas, G., Hallett, R. a., Zimmerman, S. P., Williams, T., Yumerefendi, H., Bear, J. E., and Kuhlman, B. (2015). Engineering an improved light-induced dimer (iLID) for controlling the localization and activity of signaling proteins. *Proceedings of the National Academy of Sciences*, 112(1):112–117.

Hahn, W. C., Dessain, S. K., Brooks, M. W., King, E., Elenbaas, B., Sabatini, D. M., James, A., Weinberg, R. A., King, J. E., and Decaprio, J. A. (2002). Enumeration of the Simian Virus 40 Early Region Elements Necessary for Human Cell Transformation. *Molecular and Cellular Biology*, 22(7):2111–2123.

Haigis, K. M., Cichowski, K., and Elledge, S. J. (2019). Tissue-specificity in cancer: The rule, not the exception. 363(6432):1150–1152.

Haigis, K. M., Kendall, K. R., Wang, Y., Cheung, A., Haigis, M. C., Glickman, J. N., Niwa-Kawakita, M., Sweet-Cordero, A., Sebolt-Leopold, J., Shannon, K. M., Settleman, J., Giovannini, M., and Jacks, T. (2008). Differential effects of oncogenic K-Ras and N-Ras on proliferation, differentiation and tumor progression in the colon. *Nature Genetics*, 40(5):600–608.

Hammond, D. E., Mageean, C. J., Rusilowicz, E. V., Wickenden, J. A., Clague, M. J., and Prior, I. A. (2015). Differential reprogramming of isogenic colorectal cancer cells by distinct activating KRAS mutations. *Journal of Proteome Research*, 14(3):1535–1546.

Hanahan, D. and Weinberg, R. A. (2011). Hallmarks of cancer: The next generation. *Cell*, 144(5):646–674.

Handly, L. N., Pilko, A., and Wollman, R. (2015). Paracrine communication maximizes cellular response fidelity in wound signaling. *Elife*, 4:e09652.

Hata, A. N., Niederst, M. J., Archibald, H. L., Gomez-Caraballo, M., Siddiqui, F. M., Mulvey, H. E., Maruvka, Y. E., Ji, F., Bhang, H. E. C., Radhakrishna, V. K., Siravegna, G., Hu, H., Raoof, S., Lockerman, E., Kalsy, A., Lee, D., Keating, C. L., Ruddy, D. A., Damon, L. J., Crystal, A. S., Costa, C., Piotrowska, Z., Bardelli, A., Iafrate, A. J., Sadreyev, R. I., Stegmeier, F., Getz, G., Sequist, L. V., Faber, A. C., and Engelman, J. A. (2016). Tumor cells can follow distinct evolutionary paths to become resistant to epidermal growth factor receptor inhibition. *Nature Medicine*, 22(3):262–269.

Haubold, C., Schiegg, M., Kreshuk, A., Berg, S., Koethe, U., and Hamprecht, F. A. (2016). Segmenting and Tracking Multiple Dividing Targets Using ilastik. In De Vos, W. H., Munck, S., and Timmermans, J.-P., editors, *Focus on Bio-Image Informatics*, chapter 8, pages 199–229. Springer, Cham.

Hayes, T. K., Neel, N. F., Hu, C., Gautam, P., Chenard, M., Long, B., Aziz, M., and Kassner, M. (2016). Long-Term ERK Inhibition in KRAS Mutant Pancreatic Cancer Is Associated with MYC Degradation and Senescence like Growth Suppression. *Cell Press*, 6108(15):1–2.

Heisermann, G. J., Wiley, H., Walsh, B., Ingraham, H., Fiol, C., and Gill, G. (1990). Mutational removal of the thr669 and ser671 phosphorylation sites alters substrate specificity and ligand-induced internalization of the epidermal growth factor receptor. *Journal of Biological Chemistry*, 265(22):12820–12827.

Helleday, T., Eshtad, S., and Nik-Zainal, S. (2014). Mechanisms underlying mutational signatures in human cancers.

Henriksen, L., Grandal, M. V., Knudsen, S. L. J., van Deurs, B., and Grøvdal, L. M. (2013). Internalization mechanisms of the epidermal growth factor receptor after activation with different ligands. *PloS one*, 8(3):e58148.

Herrero, A., Casar, B., Colón-Bolea, P., Agudo-Ibáñez, L., and Crespo, P. (2016). Defined spatiotemporal features of RAS-ERK signals dictate cell fate in MCF-7 mammary epithelial cells. *Molecular biology of the cell*, 27:1958–1968.

Hino, N., Rossetti, L., Marín-Llauradó, A., Aoki, K., Trepat, X., Matsuda, M., and Hirashima, T. (2020). ERK-mediated mechanochemical waves direct collective cell polarization. *Developmental Cell*, 53(6):646–660.E8.

Hiratsuka, T., Fujita, Y., Naoki, H., Aoki, K., Kamioka, Y., and Matsuda, M. (2015). Intercellular propagation of extracellular signal-regulated kinase activation revealed by in vivo imaging of mouse skin. *eLife*, 2015(4):1–18.

Hobbs, G. A., Der, C. J., and Rossman, K. L. (2016). RAS isoforms and mutations in cancer at a glance. *Journal of cell science*, 129(7):1287–92.

Hoek, K. S. and Goding, C. R. (2010). Cancer stem cells versus phenotype-switching in melanoma. *Pigment Cell and Melanoma Research*, 23(6):746–759.

Holohan, C., Van Schaeybroeck, S., Longley, D. B., and Johnston, P. G. (2013). Cancer drug resistance: An evolving paradigm.

Hood, F. E., Klinger, B., Newlaczyl, A. U., Sieber, A., Dorel, M., Oliver, S. P., Coulson, J. M., Blüthgen, N., and Prior, I. A. (2019). Isoform-specific Ras signaling is growth factor dependent. *Molecular Biology of the Cell*, 30(9):1108–1117.

Huang, C., Tian, H., Yoon, J., Sessler, J. L., James, T. D., Wu, L., Emery, B. P., Sedgwick, A. C., Bull, S. D., and He, X.-P. (2020). Förster resonance energy transfer (FRET)-based small-molecule sensors and imaging agents. *Chem. Soc. Rev*, 49:5110.

Huang, H., Daniluk, J., Liu, Y., Chu, J., Li, Z., Ji, B., and Logsdon, C. D. (2014). Oncogenic K-Ras requires activation for enhanced activity. *Oncogene*, 33(4):532–535.

Huang, S. (2009). Non-genetic heterogeneity of cells in development: more than just noise. *Development*, 136(23):3853–3862.

Huang, S. (2014). The war on cancer: Lessons from the war on terror. *Frontiers in Oncology*, 4(OCT):1–4.

Huh, D. and Paulsson, J. (2011). Non-genetic heterogeneity from stochastic partitioning at cell division.

Hyman, D. M., Puzanov, I., Subbiah, V., Faris, J. E., Chau, I., Blay, J. Y., Wolf, J., Raje, N. S., Diamond, E. L., Hollebecque, A., Gervais, R., Fernandez, M. E. E., Italiano, A., Hofheinz, R. D., Hidalgo, M., Chan, E., Schuler, M., Lasserre, S. F., Makrutzki, M., Sirzen, F., Veronese, M. L., Tabernero, J., and Baselga, J. (2015). Vemurafenib in multiple nonmelanoma cancers with BRAF V600 mutations. *New England Journal of Medicine*, 373(8):726–736.

Ihle, N. T., Byers, L. A., Kim, E. S., Saintigny, P., Lee, J. J., Blumenschein, G. R., Tsao, A., Liu, S., Larsen, J. E., Wang, J., Diao, L., Coombes, K. R., Chen, L., Zhang, S., Abdelmelek, M. F., Tang, X., Papadimitrakopoulou, V., Minna, J. D., Lippman, S. M., Hong, W. K., Herbst, R. S., Wistuba, I. I., Heymach, J. V., and Powis, G. (2012). Effect of KRAS oncogene substitutions on protein behavior: Implications for signaling and clinical outcome. *Journal of the National Cancer Institute*, 104(3):228–239.

Iwamoto, K., Shindo, Y., and Takahashi, K. (2016). Modeling Cellular Noise Underlying Heterogeneous Cell Responses in the Epidermal Growth Factor Signaling Pathway. *PLOS Computational Biology*, 12(11):e1005222.

Jackson, M., Marks, L., May, G. H. W., and Wilson, J. B. (2018). The genetic basis of disease. *Essays in Biochemistry*, 62:643–723.

Jeong, W. J., Yoon, J., Park, J. C., Lee, S. H., Lee, S. H., Kaduwal, S., Kim, H., Yoon, J. B., and Choi, K. Y. (2012). Ras stabilization through aberrant activation of Wnt/β-catenin signaling promotes intestinal tumorigenesis. *Science Signaling*, 5(219):1–13.

John, S., Sabo, P. J., Thurman, R. E., Sung, M. H., Biddie, S. C., Johnson, T. A., Hager, G. L., and Stamatoyannopoulos, J. A. (2011). Chromatin accessibility pre-determines glucocorticoid receptor binding patterns.

Johnson, B. E., Mazor, T., Hong, C., Barnes, M., Aihara, K., McLean, C. Y., Fouse, S. D., Yamamoto, S., Ueda, H., Tatsuno, K., Asthana, S., Jalbert, L. E., Nelson, S. J., Bollen, A. W., Gustafson, W. C., Charron, E., Weiss, W. A., Smirnov, I. V., Song, J. S., Olshen, A. B., Cha, S., Zhao, Y., Moore, R. A., Mungall, A. J., Jones, S. J., Hirst, M., Marra, M. A., Saito, N., Aburatani, H., Mukasa, A., Berger, M. S., Chang, S. M., Taylor, B. S., and Costello, J. F. (2014). Mutational analysis reveals the origin and therapy-driven evolution of recurrent glioma. *Science*, 343(6167):189–193.

Johnson, H. E., Goyal, Y., Pannucci, N. L., Schüpbach, T., Shvartsman, S. Y., and Toettcher, J. E. (2017). The Spatiotemporal Limits of Developmental Erk Signaling. *Developmental Cell*, 40(2):185–192.

Kandoth, C., Mclellan, M. D., Vandin, F., Ye, K., Niu, B., Lu, C., Xie, M., Zhang, Q., Mcmichael, J. F., Wyczalkowski, M. A., Leiserson, M. D. M., Miller, C. A., Welch, J. S., Walter, M. J., Wendl, M. C., Ley, T. J., Wilson, R. K., Raphael, B. J., and Ding, L. (2013). Mutational landscape and significance across 12 major cancer types. *Nature*, 502:333–339.

Karaayvaz, M., Cristea, S., Gillespie, S. M., Patel, A. P., Mylvaganam, R., Luo, C. C., Specht, M. C., Bernstein, B. E., Michor, F., and Ellisen, L. W. (2018). Unravelling

subclonal heterogeneity and aggressive disease states in TNBC through single-cell RNA-seq. *Nature Communications*, 9(1):1–10.

Kaufman, B., Shapira-Frommer, R., Schmutzler, R. K., Audeh, M. W., Friedlander, M., Balmaña, J., Mitchell, G., Fried, G., Stemmer, S. M., Hubert, A., Rosengarten, O., Steiner, M., Loman, N., Bowen, K., Fielding, A., and Domchek, S. M. (2015). Olaparib monotherapy in patients with advanced cancer and a germline BRCA1/2 mutation. *Journal of Clinical Oncology*, 33(3):244–250.

Kempe, H., Schwabe, A., Crémazy, F., Verschure, P. J., and Bruggeman, F. J. (2015). The volumes and transcript counts of single cells reveal concentration homeostasis and capture biological noise. *Molecular Biology of the Cell*, 26(4):797–804.

Kholodenko, B. N. (2000). Negative feedback and ultrasensitivity can bring about oscillations in the mitogen-activated protein kinase cascades. *European journal of biochemistry*, 267(6):1583–1588.

Kholodenko, B. N., Hancock, J. F., and Kolch, W. (2010). Signalling ballet in space and time. *Nature Reviews Molecular Cell Biology*, 11(6):414–426.

Kholodenko, B. N., Kiyatkin, A., Bruggeman, F. J., Sontag, E., Westerhoff, H. V., and Hoek, J. B. (2002). Untangling the wires: a strategy to trace functional interactions in signaling and gene networks. *Proceedings of the National Academy of Sciences*, 99(20):12841–12846.

Kidger, A. M. and Keyse, S. M. (2016). The regulation of oncogenic Ras/ERK signalling by dual-specificity mitogen activated protein kinase phosphatases (MKPs). *Seminars in Cell and Developmental Biology*, 50:125–132.

Killoran, R. C. and Smith, M. J. (2019). Conformational resolution of nucleotide cycling and effector interactions for multiple small GTPases determined in parallel. *Journal of Biological Chemistry*, 294(25):9937–9948.

Kiviet, D. J., Nghe, P., Walker, N., Boulineau, S., Sunderlikova, V., and Tans, S. J. (2014). Stochasticity of metabolism and growth at the single-cell level. *Nature*, 514(7522):376–379.

Kiyatkin, A., Aksamitiene, E., Markevich, N. I., Borisov, N. M., Hoek, J. B., and Kholodenko, B. N. (2006). Scaffolding Protein Grb2-associated Binder 1 Sustains Epidermal Growth Factor-induced Mitogenic and Survival Signaling by Multiple Positive Feedback Loops. *The Journal of Biological Chemistry*, 281(29):19925–19938.

Klomp, J. E., Klomp, J. A., and Der, C. J. (2021). The ERK mitogen-activated protein kinase signaling network: The final frontier in RAS signal transduction. *Biochemical Society Transactions*, 49(1):253–267.

Knudson, A. G. (1971). Mutation and Cancer: Statistical Study of Retinoblastoma. 68(4):820–823.

Kobayashi, S., Boggon, T. J., Dayaram, T., Jänne, P. A., Kocher, O., Meyerson, M., Johnson, B. E., Eck, M. J., Tenen, D. G., and Halmos, B. (2005). Egfr mutation and resistance of non–small-cell lung cancer to gefitinib. *New England Journal of Medicine*, 352(8):786–792.

Kobayashi, Y., Togashi, Y., Yatabe, Y., Mizuuchi, H., Jangchul, P., Kondo, C., Shimoji, M., Sato, K., Suda, K., Tomizawa, K., et al. (2015). Egfr exon 18 mutations in lung cancer: molecular predictors of augmented sensitivity to afatinib or neratinib as compared with first-or third-generation tkis. *Clinical cancer research*, 21(23):5305–5313.

Koeffler, H., McCormick, F., and Denny, C. (1991). Molecular mechanisms of cancer. *Western Journal of Medicine*, 155(5):505.

Koera, K., Nakamura, K., Nakao, K., Miyoshi, J., Toyoshima, K., Hatta, T., Otani, H., Aiba, A., and Katsuki, M. (1997). K-Ras is essential for the development of the mouse embryo. *Oncogene*, 15(10):1151–1159.

Kogure, T., Karasawa, S., Araki, T., Saito, K., Kinjo, M., and Miyawaki, A. (2006). A fluorescent variant of a protein from the stony coral Montipora facilitates dual-color single-laser fluorescence cross-correlation spectroscopy. *Nature Biotechnology*, 24(5):577–581.

Komatsu, N., Aoki, K., Yamada, M., Yukinaga, H., Fujita, Y., Kamioka, Y., and Matsuda, M. (2011). Development of an optimized backbone of FRET biosensors for kinases and GTPases. *Molecular biology of the cell*, 22(23):4647–56.

Konieczkowski, D. J., Johannessen, C. M., Abudayyeh, O., Kim, J. W., Cooper, Z. A., Piris, A., Frederick, D. T., Barzily-Rokni, M., Straussman, R., Haq, R., Fisher, D. E., Mesirov, J. P., Hahn, W. C., Flaherty, K. T., Wargo, J. A., Tamayo, P., and Garraway, L. A. (2014). A melanoma cell state distinction influences sensitivity to MAPK pathway inhibitors. *Cancer Discovery*, 4(7):816–827.

Konishi, H., Karakas, B., Abukhdeir, A. M., Lauring, J., Gustin, J. P., Garay, J. P., Konishi, Y., Gallmeier, E., Bachman, K. E., and Ben, H. P. (2007). Knock-in of mutant K-ras in nontumorigenic human epithelial cells as a new model for studying K-ras-mediated transformation. *Cancer Research*, 67(18):8460–8467.

Kramer, M. M., Lataster, L., Weber, W., and Radziwill, G. (2021). Molecular Sciences Optogenetic Approaches for the Spatiotemporal Control of Signal Transduction Pathways. *International Journal of Molecular Sciences*, 22(5300).

Kreso, A., O'Brien, C. A., van Galen, P., Gan, O. I., Notta, F., Brown, A. M. K., Ng, K., Ma, J., Wienholds, E., Dunant, C., Pollett, A., Gallinger, S., McPherson, J., Mullighan, C. G., Shibata, D., and Dick, J. E. (2013). Variable Clonal Repopulation Dynamics Influence Chemotherapy Response in Colorectal Cancer. *Science*, 339(6119):543–548.

Kruspig, B., Monteverde, T., Neidler, S., Hock, A., Kerr, E., Nixon, C., Clark, W., Hedley, A., Laing, S., Coffelt, S. B., Le Quesne, J., Dick, C., Vousden, K., Martins, C. P., and Murphy, D. J. (2018). The ERBB network facilitates KRAS-driven lung tumorigenesis. *Science Translational Medicine*, 10(44).

Lakowicz, J. R. (2006). *Principles of fluorescence spectroscopy*. Springer science & business media.

Lamarck, J.-B. (1802). *Recherches sur l'organisation des corps vivans et particulièrement sur son origine, sur la cause de ses développemens et des progrès de sa composition, et sur celle qui, tendant continuellement à la détruire dans chaque individu, amène nécessairement sa mort; précédé du discours d'ouverture du course de zoologie, donné dans le Muséum national d'Histoire Naturelle*. Maillard, Paris.

Lamarck, J.-B. (1809). *Philosophie zoologique, ou exposition des considérations relatives à l'histoire naturelle des animaux; à la diversité de leur organisation et des facultés qu'ils en obtiennent; aux causes physiques qui maintiennent en eux la vie et donnent lieu aux mouvemens qu'ils exécutent; enfin, à celles qui produisent les unes le sentiment, et les autres l'intelligence de ceux qui en sont doués*. Baillière, Paris.

Lampson, B. L., Pershing, N. L., Prinz, J. A., Lacsina, J. R., Marzluff, W. F., Nicchitta, C. V., MacAlpine, D. M., and Counter, C. M. (2013). Rare codons regulate KRas oncogenesis. *Current Biology*, 23(1):70–75.

Lane, D. P. and Crawford, L. V. (1979). T antigen is bound to a host protein in SV40-transformed cells. *Nature*, 278(5701):261–263.

Lavoie, H., Gagnon, J., and Therrien, M. (2020). ERK signalling: a master regulator of cell behaviour, life and fate. *Nature Reviews Molecular Cell Biology*, 21(10):607–632.

Lehr, S., Kotzka, J., Avci, H., Sickmann, A., Meyer, H. E., Herkner, A., and Muller-Wieland, D. (2004). Identification of major erk-related phosphorylation sites in gab1. *Biochemistry*, 43(38):12133–12140.

Lengauer, C., Kinzler, K. W., and Vogelstein, B. (1997). Genetic instability in colorectal cancers. *Nature*, 386(6625):623–627.

Leung, G. P., Feng, T., Sigoillot, F. D., Geyer, F. C., Shirley, M. D., Ruddy, D. A., Rakiec, D. P., Freeman, A. K., Engelman, J. A., Jaskelioff, M., and Stuart, D. D. (2019). Hyperactivation of MAPK Signaling Is Deleterious to RAS/RAF-mutant Melanoma. *Molecular Cancer Research*, 17(1):199–211.

Li, S., Balmain, A., and Counter, C. M. (2018a). A model for RAS mutation patterns in cancers: finding the sweet spot.

Li, S., Jang, H., Zhang, J., and Nussinov, R. (2018b). Raf-1 Cysteine-Rich Domain Increases the Affinity of K-Ras/Raf at the Membrane, Promoting MAPK Signaling. *Structure*, 26(3):513–525.e2.

Lloyd, M. C., Cunningham, J. J., Bui, M. M., Gillies, R. J., Brown, J. S., and Gatenby, R. A. (2016). Darwinian dynamics of intratumoral heterogeneity: Not solely random mutations but also variable environmental selection forces. *Cancer Research*, 76(11):3136–3144.

Loewer, A., Batchelor, E., Gaglia, G., and Lahav, G. (2010). Basal Dynamics of p53 Reveal Transcriptionally Attenuated Pulses in Cycling Cells. *Cell*, 142(1):89–100.

Losick, R. and Desplan, C. (2008). Stochasticity and cell fate.

Lyon, M. F. (1961). Gene action in the X-chromosome of the mouse (mus musculus L.). *Nature*, 190(4773):372–373.

Macheret, M. and Halazonetis, T. D. (2015). DNA Replication Stress as a Hallmark of Cancer. *Annual Review of Pathology: Mechanisms of Disease*, 10(1):425–448.

Madshus, I. H. and Stang, E. (2009). Internalization and intracellular sorting of the egf receptor: a model for understanding the mechanisms of receptor trafficking. *Journal of cell science*, 122(19):3433–3439.

Makadia, H. K., Schwaber, J. S., and Vadigepalli, R. (2015). Intracellular Information Processing through Encoding and Decoding of Dynamic Signaling Features. *PLoS Computational Biology*, 11(10).

Makena, M. R., Ranjan, A., Thirumala, V., and Reddy, A. P. (2020). Cancer stem cells: Road to therapeutic resistance and strategies to overcome resistance.

Maki, C. G. and Howley, P. M. (1997). Ubiquitination of p53 and p21 Is Differentially Affected by Ionizing and UV Radiation. *Molecular and Cellular Biology*, 17(1):355–363.

Maley, C. C., Aktipis, A., Graham, T. A., Sottoriva, A., Boddy, A. M., Janiszewska, M., Silva, A. S., Gerlinger, M., Yuan, Y., Pienta, K. J., Anderson, K. S., Gatenby, R., Swanton, C., Posada, D., Wu, C. I., Schiffman, J. D., Hwang, E. S., Polyak, K., Anderson, A. R., Brown, J. S., Greaves, M., and Shibata, D. (2017). Classifying the evolutionary and ecological features of neoplasms.

Maley, C. C., Galipeau, P. C., Li, X., Sanchez, C. A., Paulson, T. G., and Reid, B. J. (2004). Selectively advantageous mutations and hitchhikers in neoplasms: p16 lesions are selected in Barrett's esophagus. *Cancer Research*, 64(10):3414–3427.

Marine, J. C., Dawson, S. J., and Dawson, M. A. (2020). Non-genetic mechanisms of therapeutic resistance in cancer.

Marshall, C. J. (1995). Specificity of receptor tyrosine kinase signaling: Transient versus sustained extracellular signal-regulated kinase activation.

Marusyk, A., Almendro, V., and Polyak, K. (2012). Intra-tumour heterogeneity: a looking glass for cancer? *Nature Reviews Cancer*, 12(5):323–334.

Matallanas, D., Romano, D., Al-Mulla, F., O'Neill, E., Al-Ali, W., Crespo, P., Doyle, B., Nixon, C., Sansom, O., Drosten, M., Barbacid, M., and Kolch, W. (2011). Mutant K-Ras Activation of the Proapoptotic MST2 Pathway Is Antagonized by Wild-Type K-Ras. *Molecular Cell*, 44(6):893–906.

Maynard, J. and Haigh, J. (1974). The hitch-hiking effect of a favourable gene. *Genet. Res., Camb*, 23:23–35.

Mayr, C. (2017). Regulation by 3-Untranslated Regions.

McCubrey, J. A., Steelman, L. S., Chappell, W. H., Abrams, S. L., Wong, E. W., Chang, F., Lehmann, B., Terrian, D. M., Milella, M., Tafuri, A., Stivala, F., Libra, M., Basecke, J., Evangelisti, C., Martelli, A. M., and Franklin, R. A. (2007). Roles of the Raf/MEK/ERK pathway in cell growth, malignant transformation and drug resistance.

McGranahan, N., Burrell, R. A., Endesfelder, D., Novelli, M. R., and Swanton, C. (2012). Cancer chromosomal instability: therapeutic and diagnostic challenges. *EMBO reports*, 13(6):528–538.

Mebratu, Y. and Tesfaigzi, Y. (2009). How ERK1/2 activation controls cell proliferation and cell death is subcellular localization the answer?

Medema, J. P. (2013). Cancer stem cells: The challenges ahead. *Nature Cell Biology*, 15(4):338–344.

Mo, G. C. H., Posner, C., Rodriguez, E. A., Sun, T., and Zhang, J. (2020). A rationally enhanced red fluorescent protein expands the utility of FRET biosensors. *Nature Communications*, 11(1848).

Moodie, S. A., Willumsen, B. M., Weber, M. J., and Wolfrnan, A. (1993). Complexes of Ras . GTP with Raf-1 and Mitogen-Activated Protein Kinase Kinase. *Science*, 260(14):1658–1661.

Moore, A. R., Rosenberg, S. C., McCormick, F., and Malek, S. (2020). RAS-targeted therapies: is the undruggable drugged? *Nature Reviews Drug Discovery*, 19(8):533–552.

Moran, U., Phillips, R., and Milo, R. (2010). SnapShot: Key numbers in biology.

Murakoshi, H., Lee, S. J., and Yasuda, R. (2008). Highly sensitive and quantitative FRET-FLIM imaging in single dendritic spines using improved non-radiative YFP. *Brain Cell Biology*, 36(1-4):31–42.

Murakoshi, H. and Shibata, A. C. E. (2017). ShadowY: a dark yellow fluorescent protein for FLIM-based FRET measurement. *Scientific Reports*, 7(1):6791.

Murakoshi, H., Shibata, A. C. E., Nakahata, Y., and Nabekura, J. (2015). A dark green fluorescent protein as an acceptor for measurement of Förster resonance energy transfer. *Scientific Reports*, 5:15334.

Muratcioglu, S., Aydin, C., Odabasi, E., Ozdemir, E. S., Firat-Karalar, E. N., Jang, H., Tsai, C. J., Nussinov, R., Kavakli, I. H., Gursoy, A., and Keskin, O. (2020). Oncogenic K-Ras4B Dimerization Enhances Downstream Mitogen-activated Protein Kinase Signaling. *Journal of Molecular Biology*, 432(4):1199–1215.

Muñoz-García, J., Neufeld, Z., and Kholodenko, B. N. (2009). Positional information generated by spatially distributed signaling cascades. *PLoS Comput Biol*, 5(3):e1000330.

Nagy, J. D. (2004). Competition and natural selection in a mathematical model of cancer. *Bulletin of Mathematical Biology*, 66(4):663–687.

Nakamura, H., Arai, Y., Totoki, Y., Shirota, T., Elzawahry, A., Kato, M., Hama, N., Hosoda, F., Urushidate, T., Ohashi, S., Hiraoka, N., Ojima, H., Shimada, K., Okusaka, T., Kosuge, T., Miyagawa, S., and Shibata, T. (2015). Genomic spectra of biliary tract cancer. *Nature Genetics*, 47(9):1003–1010.

Nakayama, K., Satoh, T., Igari, A., Kageyama, R., and Nishida, E. (2008). FGF induces oscillations of Hes1 expression and Ras/ERK activation.

Nan, X., Tamgüney, T. M., Collisson, E. A., Lin, L.-j., Pitt, C., and Galeas, J. (2015). Ras-GTP dimers activate the Mitogen-Activated Protein Kinase (MAPK) pathway. 112(26).

Natwick, D. E. and Collins, S. R. (2021). Optimized iLID Membrane Anchors for Local Optogenetic Protein Recruitment. *ACS Synthetic Biology*, 10(5):1009–1023.

Newlaczyl, A. U., Coulson, J. M., and Prior, I. A. (2017). Quantification of spatiotemporal patterns of Ras isoform expression during development. *Scientific Reports*, 7(December 2016):1–7.

Ng, K. P., Hillmer, A. M., Chuah, C. T., Juan, W. C., Ko, T. K., Teo, A. S., Ariyaratne, P. N., Takahashi, N., Sawada, K., Fei, Y., Soh, S., Lee, W. H., Huang, J. W., Allen, J. C., Woo, X. Y., Nagarajan, N., Kumar, V., Thalamuthu, A., Poh, W. T., Ang, A. L., Mya, H. T., How, G. F., Yang, L. Y., Koh, L. P., Chowbay, B., Chang, C. T., Nadarajan, V. S., Chng, W. J., Than, H., Lim, L. C., Goh, Y. T., Zhang, S., Poh, D., Tan, P., Seet, J. E., Ang, M. K., Chau, N. M., Ng, Q. S., Tan, D. S., Soda, M., Isobe, K., Nöthen, M. M., Wong, T. Y., Shahab, A., Ruan, X., Cacheux-Rataboul, V., Sung, W. K., Tan, E. H., Yatabe, Y., Mano, H., Soo, R. A., Chin, T. M., Lim, W. T., Ruan, Y., and Ong, S. T. (2012). A common BIM deletion polymorphism mediates intrinsic resistance and inferior responses to tyrosine kinase inhibitors in cancer. *Nature Medicine*, 18(4):521–528.

Nicotra, A. B., Atkin, O. K., Bonser, S. P., Davidson, A. M., Finnegan, E. J., Mathesius, U., Poot, P., Purugganan, M. D., Richards, C. L., Valladares, F., and van Kleunen, M. (2010). Plant phenotypic plasticity in a changing climate.

Nik-Zainal, S., Van Loo, P., Wedge, D. C., Alexandrov, L. B., Greenman, C. D., Lau, K. W., Raine, K., Jones, D., Marshall, J., Ramakrishna, M., Shlien, A., Cooke, S. L., Hinton, J., Menzies, A., Stebbings, L. A., Leroy, C., Jia, M., Rance, R., Mudie, L. J., Gamble, S. J., Stephens, P. J., McLaren, S., Tarpey, P. S., Papaemmanuil, E., Davies, H. R., Varela, I., McBride, D. J., Bignell, G. R., Leung, K., Butler, A. P., Teague, J. W., Martin, S., Jönsson, G., Mariani, O., Boyault, S., Miron, P., Fatima, A., Langerod, A., Aparicio, S. A., Tutt, A., Sieuwerts, A. M., Borg, Å., Thomas, G., Salomon, A. V., Richardson, A. L., Borresen-Dale, A. L., Futreal, P. A., Stratton, M. R., and Campbell, P. J. (2012). The life history of 21 breast cancers. *Cell*, 149(5):994–1007.

Norman, T. M., Lord, N. D., Paulsson, J., and Losick, R. (2015). Stochastic Switching of Cell Fate in Microbes. *Annual Review of Microbiology*, 69(1):381–403.

Novick, A. and Weiner, M. (1957). Enzyme induction as an all-or-none phenomenon. *Proceedings of the National Academy of Sciences of the United States of America*, 43(7):553.

Nowell, P. C. (1976). The clonal evolution of tumor cell populations. *Science*, 194(4260):23–28.

Nussey, D. H., Postma, E., Gienapp, P., and Visser, M. E. (2005). Evolution: Selection on heritable phenotypic plasticity in a wild bird population. *Science*, 310(5746):304–306.

Nwe-Nwe Aye-Han, D. Allen, M., Qiang Ni, and Jin Zhang (2012). Parallel tracking of cAMP and PKA signaling dynamics in living cells with FRET-based fluorescent biosensors. *Molecular BioSystems*, 8(5):1435–1440.

Ostrow, S. L. and Hershberg, R. (2016). The Somatic Nature of Cancer Allows It to Affect Highly Constrained Genes. *Genome Biol. Evol.*, 5(5):1614–1620.

Ostrow, S. L., Simon, E., Prinz, E., Bick, T., Shentzer, T., Nagawkar, S. S., Sabo, E., Ben-Izhak, O., Hershberg, R., and Hershkovitz, D. (2016). Variation in KRAS driver substitution distributions between tumor types is determined by both mutation and natural selection. *Scientific Reports*, 6(1):21927.

Paez, J. G., Jänne, P. A., Lee, J. C., Tracy, S., Greulich, H., Gabriel, S., Herman, P., Kaye, F. J., Lindeman, N., Boggon, T. J., Naoki, K., Sasaki, H., Fujii, Y., Eck, M. J., Sellers, W. R., Johnson, B. E., and Meyerson, M. (2004). EGFR mutations in lung, cancer: Correlation with clinical response to gefitinib therapy. *Science*, 304(5676):1497–1500.

Parada, L. F., Tabin, C. J., Shih, C., and Weinberg, R. A. (1982). Human EJ bladder carcinoma oncogene is homologue of Harvey sarcoma virus ras gene. *Nature*, 297:474–478.

Park, J.-I., Strock, C. J., Ball, D. W., and Nelkin, B. D. (2003). The ras/raf/mek/extracellular signal-regulated kinase pathway induces autocrine-paracrine growth inhibition via the leukemia inhibitory factor/jak/stat pathway. *Molecular and cellular biology*, 23(2):543–554.

Parker, J. J., Canoll, P., Niswander, L., Kleinschmidt-DeMasters, B. K., Foshay, K., and Waziri, A. (2018). Intratumoral heterogeneity of endogenous tumor cell invasive behavior in human glioblastoma. *Scientific Reports*, 8(1):1–10.

Patel, A. L., Yeung, E., McGuire, S. E., Wu, A. Y., Toettcher, J. E., Burdine, R. D., and Shvartsman, S. Y. (2019). Optimizing photoswitchable mek. *Proceedings of the National Academy of Sciences*, 116(51):25756–25763.

Paudel, B. B., Harris, L. A., Hardeman, K. N., Abugable, A. A., Hayford, C. E., Tyson, D. R., and Quaranta, V. (2018). A Nonquiescent "Idling" Population State in Drug-Treated, BRAF-Mutated Melanoma. *Biophysical Journal*, 114(6):1499–1511.

Paz, A., Haklai, R., Elad-Sfadia, G., Ballan, E., and Kloog, Y. (2001). Galectin-1 binds oncogenic H-Ras to mediate Ras membrane anchorage and cell transformation. *Oncogene*, 20(51):7486–7493.

Pietraszewska-Bogiel, A. and Gadella, T. W. (2011). FRET microscopy: from principle to routine technology in cell biology. *Journal of Microscopy*, 241(2):111–118.

Piljic, A. and Schultz, C. (2008). Simultaneous recording of multiple cellular events by FRET. *ACS Chemical Biology*, 3(3):156–160.

Pisco, A. O., Brock, A., Zhou, J., Moor, A., Mojtahedi, M., Jackson, D., and Huang, S. (2013). Non-Darwinian dynamics in therapy-induced cancer drug resistance - Supplementary Figures. *Nature Communications*, 4:1–11.

Pisco, A. O. and Huang, S. (2015). Non-genetic cancer cell plasticity and therapy-induced stemness in tumour relapse: 'What does not kill me strengthens me'. *British Journal of Cancer*, 112(11):1725–1732.

Plotkin, L. I., Mathov, I., Aguirre, J. I., Parfitt, A. M., Manolagas, S. C., and Bellido, T. (2005). Mechanical stimulation prevents osteocyte apoptosis: requirement of integrins, src kinases, and erks. *American Journal of Physiology-Cell Physiology*, 289(3):C633–C643.

Plowman, S. J., Williamson, D. J., O'sullivan, M. J., Doig, J., Ritchie, A.-M., Harrison, D. J., Melton, D. W., Arends, M. J., Hooper, M. L., and Patek, C. E. (2003). While K-ras Is Essential for Mouse Development, Expression of the K-ras 4A Splice Variant Is Dispensable. *MOLECULAR AND CELLULAR BIOLOGY*, 23(24):9245–9250.

Ponsioen, B., Post, J. B., Buissant des Amorie, J. R., Laskaris, D., van Ineveld, R. L., Kersten, S., Bertotti, A., Sassi, F., Sipieter, F., Cappe, B., Mertens, S., Verlaan-Klink, I., Boj, S. F., Vries, R. G. J., Rehmann, H., Vandenabeele, P., Riquet, F. B., Trusolino, L., Bos, J. L., and Snippert, H. J. G. (2021). Quantifying single-cell ERK dynamics in colorectal cancer organoids reveals EGFR as an amplifier of oncogenic MAPK pathway signalling. *Nature Cell Biology*, 23(4):377–390.

Prakash, P. and Gorfe, A. A. (2019). Probing the conformational and energy landscapes of kras membrane orientation. *The Journal of Physical Chemistry B*, 123(41):8644–8652.

Prakash, P., Litwin, D., Liang, H., Sarkar-Banerjee, S., Dolino, D., Zhou, Y., Hancock, J. F., Jayaraman, V., and Gorfe, A. A. (2019). Dynamics of Membrane-Bound G12V-KRAS from Simulations and Single-Molecule FRET in Native Nanodiscs.

Prakash, P., Zhou, Y., Liang, H., Hancock, J. F., and Gorfe, A. A. (2016). Oncogenic K-Ras Binds to an Anionic Membrane in Two Distinct Orientations : A Molecular Dynamics Analysis. *Biophysical Journal*, 110(March):1125–1138.

Pratilas, C. A., Taylor, B. S., Ye, Q., Viale, A., Sander, C., Solit, D. B., and Rosen, N. (2009). V600ebraf is associated with disabled feedback inhibition of raf–mek signaling and elevated transcriptional output of the pathway. *Proceedings of the National Academy of Sciences*, 106(11):4519–4524.

Pribluda, A., De La Cruz, C. C., and Jackson, E. L. (2015). Intratumoral heterogeneity: From diversity comes resistance. *Clinical Cancer Research*, 21(13):2916–2923.

Prior, I. A., Hood, F. E., and Hartley, J. L. (2020). The Frequency of Ras Mutations in Cancer.

Purvis, J. E. and Lahav, G. (2013). Encoding and decoding cellular information through signaling dynamics. *Cell*, 152(5):945–956.

Pylayeva-Gupta, Y., Grabocka, E., and Bar-Sagi, D. (2011). RAS oncogenes: weaving a tumorigenic web. *Nature reviews. Cancer*, 11(11):761–74.

Radhakrishna, V. K., Siravegna, G., Hu, H., Lockerman, E., Kalsy, A., Lee, D., Keating, C. L., and David, A. (2016). Tumor cells can follow distinct evolutionary paths to become resistant to epidermal growth factor receptor inhibition. 22(3):262–269.

Raser, J. M. and O'Shea, E. K. (2004). Control of stochasticity in eukaryotic gene expression. *Science*, 304(5678):1811–1814.

Regot, S., Hughey, J. J., Bajar, B. T., Carrasco, S., and Covert, M. W. (2014). High-sensitivity measurements of multiple kinase activities in live single cells. *Cell*, 157(7):1724–1734.

Reid, B. (1996). Barrett's esophagus: ordering the events that lead to cancer. *European Journal of Cancer Prevention*, 5(2):57–65.

Reiter, J. G., Baretti, M., Gerold, J. M., Makohon-Moore, A. P., Daud, A., Iacobuzio-Donahue, C. A., Azad, N. S., Kinzler, K. W., Nowak, M. A., and Vogelstein, B. (2019). An analysis of genetic heterogeneity in untreated cancers. *Nature Reviews Cancer*, 19(11):639–650.

Reusch, H. P., Chan, G., Ives, H. E., and Nemenoff, R. A. (1997). Activation of jnk/sapk and erk by mechanical strain in vascular smooth muscle cells depends on extracellular matrix composition. *Biochemical and biophysical research communications*, 237(2):239–244.

Ringer, P., Weißl, A., Cost, A.-L., Freikamp, A., Sabass, B., Mehlich, A., Tramier, M., Rief, M., and Grashoff, C. (2017). Multiplexing molecular tension sensors reveals piconewton force gradient across talin-1. *Nature methods*, 14(11):1090–1096.

Rodgers, K. and Mcvey, M. (2016). Error-prone repair of DNA double-strand breaks HHS Public Access. *J Cell Physiol*, 231(1):15–24.

Roebroek, T., Vandenberg, W., Sipieter, F., Hugelier, S., Stove, C., Zhang, J., and Dedecker, P. (2021). Simultaneous readout of multiple fret pairs using photochromism. *Nature communications*, 12(1):1–12.

Ronneberger, O., Fischer, P., and Brox, T. (2015). U-net: Convolutional networks for biomedical image segmentation. In *Lecture Notes in Computer Science (including subseries Lecture Notes in Artificial Intelligence and Lecture Notes in Bioinformatics)*, volume 9351, pages 234–241. Springer Verlag.

Ross, B. L., Tenner, B., Markwardt, M. L., Zviman, A., Shi, G., Kerr, J. P., Snell, N. E., McFarland, J. J., Mauban, J. R., Ward, C. W., et al. (2018). Single-color, ratiometric biosensors for detecting signaling activities in live cells. *Elife*, 7:e35458.

Rosseland, C. M., Wierød, L., Flinder, L. I., Oksvold, M. P., Skarpen, E., and Huitfeldt, H. S. (2008). Distinct functions of h-ras and k-ras in proliferation and survival of primary hepatocytes due to selective activation of erk and pi3k. *Journal of cellular physiology*, 215(3):818–826.

Rudkouskaya, A., Sinsuebphon, N., Ochoa, M., Chen, S. J., Mazurkiewicz, J. E., Intes, X., and Barroso, M. (2020). Multiplexed non-invasive tumor imaging of glucose metabolism and receptor-ligand engagement using dark quencher FRET acceptor. *Theranostics*, 10(22):10309–10325.

Ryu, H., Chung, M., Dobrzyński, M., Fey, D., Blum, Y., Sik Lee, S., Peter, M., Kholodenko, B. N., Li Jeon, N., and Pertz, O. (2015). Frequency modulation of ERK activation dynamics rewires cell fate. *Molecular Systems Biology*, 12(4):866.

Sack, L. M., Davoli, T., Li, M. Z., Westbrook, T. F., Wong, K.-K., and Correspondence, S. J. E. (2018). Profound Tissue Specificity in Proliferation Control Underlies Cancer Drivers and Aneuploidy Patterns. *Cell*, 173:499–514.

Salgia, R. and Kulkarni, P. (2018). The Genetic/Non-genetic Duality of Drug 'Resistance' in Cancer. *Trends in Cancer*, 4(2):110–118.

Sample, V., Mehta, S., and Zhang, J. (2014). Genetically encoded molecular probes to visualize and perturb signaling dynamics in living biological systems. *J Cell Sci*, 127(Pt 6):1151–1160.

Santo-Domingo, J., Galindo, A. N., Cominetti, O., De Marchi, U., Cutillas, P., Dayon, L., and Wiederkehr, A. (2019). Glucose-dependent phosphorylation signaling pathways and crosstalk to mitochondrial respiration in insulin secreting cells. *Cell Commun Signal*, 17(1):14.

Santos, E., Tronick, S. R., Aaronson, S. A., Pulciani, S., and Barbacid, M. (1982). T24 human bladder carcinoma oncogene is an activated form of the normal human homologue of BALB- and Harvey-MSV transforming genes. *Nature*, 298(5872):343–347.

Santos, S. D. M., Verveer, P. J., and Bastiaens, P. I. H. (2007). Growth factor-induced MAPK network topology shapes Erk response determining PC-12 cell fate. *Nature Cell Biology*, 9(3):324–330.

Sarkar-Banerjee, S., Sayyed-Ahmad, A., Prakash, P., Cho, K. J., Waxham, M. N., Hancock, J. F., and Gorfe, A. A. (2017). Spatiotemporal Analysis of K-Ras Plasma Membrane Interactions Reveals Multiple High Order Homo-oligomeric Complexes. *Journal of the American Chemical Society*, 139(38):13466–13475.

Schmidt, U., Weigert, M., Broaddus, C., and Myers, G. (2018). Cell detection with star-convex polygons. In *Medical Image Computing and Computer Assisted Intervention - MICCAI 2018 - 21st International Conference, Granada, Spain, September 16-20, 2018, Proceedings, Part II*, pages 265–273.

Schneider, G., Schmidt-Supprian, M., Rad, R., and Saur, D. (2017). Tissue-specific tumorigenesis: Context matters.

Scott, J. and Marusyk, A. (2017). Somatic clonal evolution: A selection-centric perspective. *Biochimica et Biophysica Acta - Reviews on Cancer*, 1867(2):139–150.

Sender, R., Fuchs, S., and Milo, R. (2016). Revised Estimates for the Number of Human and Bacteria Cells in the Body. *PLoS Biology*, 14(8):1–14.

Senft, D., Leiserson, M. D., Ruppin, E., and Ronai, Z. A. (2017). Precision Oncology: The Road Ahead. *Trends in Molecular Medicine*, 23(10):874–898.

Seo, K. Y., Jelinsky, S. A., and Loechler, E. L. (2000). Factors that influence the mutagenic patterns of DNA adducts from chemical carcinogens. *Mutation Research - Reviews in Mutation Research*, 463(3):215–246.

Serrano, M., Lin, A. W., McCurrach, M. E., Beach, D., and Lowe, S. W. (1997). Oncogenic ras provokes premature cell senescence associated with accumulation of p53 and p16(INK4a). *Cell*, 88(5):593–602.

Shankaran, H., Ippolito, D. L., Chrisler, W. B., Resat, H., Bollinger, N., Opresko, L. K., and Wiley, H. S. (2009). Rapid and sustained nuclear-cytoplasmic ERK oscillations induced by epidermal growth factor. *Molecular Systems Biology*, 5(332):1–13.

Sharma, P., Hu-Lieskovan, S., Wargo, J. A., and Ribas, A. (2017). Primary, Adaptive, and Acquired Resistance to Cancer Immunotherapy.

Sharma, S. V., Lee, D. Y., Li, B., Quinlan, M. P., Takahashi, F., Maheswaran, S., McDermott, U., Azizian, N., Zou, L., Fischbach, M. A., Wong, K. K., Brandstetter, K., Wittner, B., Ramaswamy, S., Classon, M., and Settleman, J. (2010). A Chromatin-Mediated Reversible Drug-Tolerant State in Cancer Cell Subpopulations. *Cell*, 141(1):69–80.

Shcherbakova, D. M., Cammer, N. C., Huisman, T. M., Verkhusha, V. V., and Hodgson, L. (2018). Direct multiplex imaging and optogenetics of rho gtpases enabled by near-infrared fret. *Nature chemical biology*, 14(6):591–600.

Sheffels, E., Sealover, N. E., Wang, C., Kim, D. H., Vazirani, I. A., Lee, E., Terrell, E. M., Morrison, D. K., Luo, J., and Kortum, R. L. (2018). Oncogenic RAS isoforms show a hierarchical requirement for the guanine nucleotide exchange factor SOS2 to mediate cell transformation. *Science Signaling*, 11(546):1–16.

Shi, H., Hugo, W., Kong, X., Hong, A., Koya, R. C., Moriceau, G., Chodon, T., Guo, R., Johnson, D. B., Dahlman, K. B., Kelley, M. C., Kefford, R. F., Chmielowski, B., Glaspy, J. A., Sosman, J. A., Van Baren, N., Long, G. V., Ribas, A., and Lo, R. S. (2014). Acquired resistance and clonal evolution in melanoma during BRAF inhibitor therapy. *Cancer Discovery*, 4(1):80–93.

Shima, F., Ijiri, Y., Muraoka, S., Liao, J., Ye, M., Araki, M., Matsumoto, K., Yamamoto, N., Sugimoto, T., Yoshikawa, Y., Kumasaka, T., Yamamoto, M., Tamura, A., and Kataoka, T. (2010). Structural Basis for Conformational Dynamics of GTP-bound Ras Protein. *The Journal of Biological Chemistry*, 285(29):22696–22705.

Shimomura, O., Johnson, F. H., and Saiga, Y. (1962). Extraction, purification and properties of aequorin, a bioluminescent protein from the luminous hydromedusan, Aequorea. *J Cell Comp Physiol*, 59:223–239.

Shindo, Y., Iwamoto, K., Mouri, K., Hibino, K., Tomita, M., Kosako, H., Sako, Y., and Takahashi, K. (2016). Conversion of graded phosphorylation into switch-like nuclear translocation via autoregulatory mechanisms in ERK signalling. *Nature Communications*, 7:1–10.

Shrestha, D., Jenei, A., Nagy, P., Vereb, G., and Szöllősi, J. (2015). Understanding FRET as a Research Tool for Cellular Studies. *Int. J. Mol. Sci*, 16:6718–6756.

Sigal, A., Milo, R., Cohen, A., Geva-Zatorsky, N., Klein, Y., Liron, Y., Rosenfeld, N., Danon, T., Perzov, N., and Alon, U. (2006). Variability and memory of protein levels in human cells. *Nature*, 444(7119):643–646.

Smith, M. J., Neel, B. G., and Ikura, M. (2013). NMR-based functional profiling of RASopathies and oncogenic RAS mutations. *Proceedings of the National Academy of Sciences of the United States of America*, 110(12):4574–4579.

Snell, N. E., Rao, V. P., Seckinger, K. M., Liang, J., Leser, J., Mancini, A. E., and Rizzo, M. A. (2018). Homotransfer FRET reporters for live cell imaging. *Biosensors*, 8(4).

Snijder, B., Sacher, R., Rämö, P., Damm, E. M., Liberali, P., and Pelkmans, L. (2009). Population context determines cell-to-cell variability in endocytosis and virus infection. *Nature*, 461(7263):520–523.

Solopova, A., Van Gestel, J., Weissing, F. J., Bachmann, H., Teusink, B., Kok, J., and Kuipers, O. P. (2014). Bet-hedging during bacterial diauxic shift. *Proceedings of the National Academy of Sciences of the United States of America*, 111(20):7427–7432.

Spencer, S. L., Gaudet, S., Albeck, J. G., Burke, J. M., and Sorger, P. K. (2009). Non-genetic origins of cell-to-cell variability in TRAIL-induced apoptosis. *Nature*, 459(7245):428–432.

Spudich, J. L. and Koshland, D. E. (1976). Non-genetic individuality: Chance in the single cell.

Stephens, P. J., Greenman, C. D., Fu, B., Yang, F., Bignell, G. R., Mudie, L. J., Pleasance, E. D., Lau, K. W., Beare, D., Stebbings, L. A., McLaren, S., Lin, M. L., McBride, D. J., Varela, I., Nik-Zainal, S., Leroy, C., Jia, M., Menzies, A., Butler, A. P., Teague, J. W., Quail, M. A., Burton, J., Swerdlow, H., Carter, N. P., Morsberger, L. A., Iacobuzio-Donahue, C., Follows, G. A., Green, A. R., Flanagan, A. M., Stratton, M. R., Futreal, P. A., and Campbell, P. J. (2011). Massive genomic rearrangement acquired in a single catastrophic event during cancer development. *Cell*, 144(1):27–40.

Stephens, P. J., Tarpey, P. S., Davies, H., Van Loo, P., Greenman, C., Wedge, D. C., Nik-Zainal, S., Martin, S., Varela, I., Bignell, G. R., Yates, L. R., Papaemmanuil, E., Beare, D., Butler, A., Cheverton, A., Gamble, J., Hinton, J., Jia, M., Jayakumar, A., Jones, D., Latimer, C., Lau, K. W., McLaren, S., McBride, D. J., Menzies, A., Mudie, L., Raine, K., Rad, R., Chapman, M. S., Teague, J., Easton, D., Langerød, A., Karesen, R., Schlichting, E., Naume, B., Sauer, T., Ottestad, L., Lee, M. T. M., Shen, C. Y., Tee, B. T. K., Huimin, B. W., Broeks, A., Vargas, A. C., Turashvili, G., Martens, J., Fatima, A., Miron, P., Chin, S. F., Thomas, G., Boyault, S., Mariani, O., Lakhani, S. R., Van De Vijver, M., Van't Veer, L., Foekens, J., Desmedt, C., Sotiriou, C., Tutt, A., Caldas, C., Reis-Filho, J. S., Aparicio, S. A., Salomon, A. V., Børresen-Dale, A. L., Richardson, A. L., Campbell, P. J., Futreal, P. A., and Stratton, M. R. (2012). The landscape of cancer genes and mutational processes in breast cancer. *Nature*, 486(7403):400–404.

Stolze, B., Reinhart, S., Bulllinger, L., Fröhling, S., and Scholl, C. (2014). Comparative analysis of KRAS codon 12, 13, 18, 61, and 117 mutations using human MCF10A isogenic cell lines. *Scientific Reports*, 5:1–9.

Stringer, C., Michaelos, M., and Pachitariu, M. (2020). Cellpose: a generalist algorithm for cellular segmentation. *bioRxiv*.

Su, T., Pan, S., Luo, Q., and Zhang, Z. (2013). Monitoring of dual bio-molecular events using FRET biosensors based on mTagBFP/sfGFP and mVenus/mKOκ fluorescent protein pairs. *Biosensors and Bioelectronics*, 46:97–101.

Subach, O. M., Gundorov, I. S., Yoshimura, M., Subach, F. V., Zhang, J., Grüenwald, D., Souslova, E. A., Chudakov, D. M., and Verkhusha, V. V. (2008). Conversion of red fluorescent protein into a bright blue probe. *Chem Biol*, 15(10):1116–1124.

Sun, C., Hobor, S., Bertotti, A., Zecchin, D., Huang, S., Galimi, F., Cottino, F., Prahallad, A., Grernrum, W., Tzani, A., Schlicker, A., Wessels, L. F. A., Smit, E. F., Thunnissen, E., Halonen, P., Lieftink, C., Beijersbergen, R. L., DiNicolantonio, F., Bardelli, A., Trusolino, L., and Bernards, R. (2014). Intrinsic resistance to MEK inhibition in KRAS mutant lung and colon cancer through transcriptional induction of ERBB3. *Cell Reports*, 7(1):86–93.

Sun, Y., Wallrabe, H., Seo, S. A., and Periasamy, A. (2011). FRET microscopy in 2010: The legacy of Theodor Förster on the 100th anniversary of his birth. *ChemPhysChem*, 12(3):462–474.

Sung, P. and Klein, H. (2006). Mechanism of homologous recombination: Mediators and helicases take on regulatory functions.

Tabassum, D. P. and Polyak, K. (2015). Tumorigenesis: It takes a village. *Nature Reviews Cancer*, 15(8):473–483.

Takahashi, M., Hayashi, K., Yoshida, K., Ohkawa, Y., Komurasaki, T., Kitabatake, A., Ogawa, A., Nishida, W., Yano, M., Monden, M., et al. (2003). Epiregulin as a major autocrine/paracrine factor released from erk-and p38mapk-activated vascular smooth muscle cells. *Circulation*, 108(20):2524–2529.

Tejpar, S., Celik, I., Schlichting, M., Sartorius, U., Bokemeyer, C., and Van Cutsem, E. (2012). Association of KRAS G13D tumor mutations with outcome in patients with metastatic colorectal cancer treated with first-line chemotherapy with or without cetuximab. *Journal of Clinical Oncology*, 30(29):3570–3577.

Temko, D., Tomlinson, I. P., Severini, S., Schuster-Böckler, B., and Graham, T. A. (2018). The effects of mutational processes and selection on driver mutations across cancer types. *Nature communications*, 9(1):1–10.

Terrell, E. M., Durrant, D. E., Ritt, D. A., Sealover, N. E., Sheffels, E., Spencer-Smith, R., Esposito, D., Zhou, Y., Hancock, J. F., Kortum, R. L., and Morrison, D. K. (2019). Distinct Binding Preferences between Ras and Raf Family Members and the Impact on Oncogenic Ras Signaling. *Molecular Cell*, 76(6):872–884.e5.

Testa, U., Pelosi, E., and Castelli, G. (2018). Colorectal cancer: genetic abnormalities, tumor progression, tumor heterogeneity, clonal evolution and tumor-initiating cells. *Medical Sciences*, 6(2):31.

Tischer, D. and Weiner, O. D. (2014). Illuminating cell signalling with optogenetic tools. *Nature reviews. Molecular cell biology*, 15(8):551–8.

Toettcher, J. E., Weiner, O. D., and Lim, W. A. (2013). Using optogenetics to interrogate the dynamic control of signal transmission by the Ras/Erk module. *Cell*, 155(6):1422–1434.

Toshiyuki, M. and Reed, J. C. (1995). Tumor suppressor p53 is a direct transcriptional activator of the human bax gene. *Cell*, 80(2):293–299.

Traverse, S., Gomez, N., Paterson, H., Marshall, C., and Cohen, P. (1992). Sustained activation of the mitogen-activated protein (map) kinase cascade may be required for differentiation of pc12 cells. comparison of the effects of nerve growth factor and epidermal growth factor. *Biochemical Journal*, 288(2):351–355.

Tsai, F. D., Lopes, M. S., Zhou, M., Court, H., Ponce, O., Fiordalisi, J. J., Gierut, J. J., Cox, A. D., Haigis, K. M., and Philips, M. R. (2015). K-Ras4A splice variant is widely expressed in cancer and uses a hybrid membrane-targeting motif. *Proceedings of the National Academy of Sciences*, 112(3):779–784.

Tseng, H., Peterson, T. E., and Berk, B. C. (1995). Fluid shear stress stimulates mitogen-activated protein kinase in endothelial cells. *Circulation research*, 77(5):869–878.

Tuveson, D. A., Shaw, A. T., Willis, N. A., Silver, D. P., Jackson, E. L., Chang, S., Mercer, K. L., Grochow, R., Hock, H., Crowley, D., Hingorani, S. R., Zaks, T., King, C., Jacobetz, M. A., Wang, L., Bronson, R. T., Orkin, S. H., DePinho, R. A., and Jacks, T. (2004). Endogenous oncogenic K-rasG12D stimulates proliferation and widespread neoplastic and developmental defects. *Cancer Cell*, 5(4):375–387.

Ulicna, K., Vallardi, G., Charras, G., and Lowe, A. R. (2020). Automated deep lineage tree analysis using a bayesian single cell tracking approach. *bioRxiv*.

Unni, A. M., Harbourne, B., Oh, M. H., Wild, S., Ferrarone, J. R., Lockwood, W. W., and Varmus, H. (2018). Hyperactivation of ERK by multiple mechanisms is toxic to RTK-RAS mutation-driven lung adenocarcinoma cells. *eLife*, 7:1–24.

Van Boxtel, C., Van Heerden, J. H., Nordholt, N., Schmidt, P., and Bruggeman, F. J. (2017). Taking chances and making mistakes: Non-genetic phenotypic heterogeneity and its consequences for surviving in dynamic environments. *Journal of the Royal Society Interface*, 14(132).

Van Heerden, J. H., Wortel, M. T., Bruggeman, F. J., Heijnen, J. J., Bollen, Y. J., Planqué, R., Hulshof, J., O'Toole, T. G., Wahl, S. A., and Teusink, B. (2014). Lost in transition: Start-up of glycolysis yields subpopulations of nongrowing cells. *Science*, 343(6174).

Van Meter, M. E. M., Díaz-Flores, E., Archard, J. A., Passegué, E., Irish, J. M., Kotecha, N., Nolan, G. P., Shannon, K., and Braun, B. S. (2007). K-Ras G12D expression induces hyperproliferation and aberrant signaling in primary hematopoietic stem/progenitor cells. *Blood*, 109(9):3945–3952.

Venkatesan, S., Birkbak, N. J., and Swanton, C. (2017). Constraints in cancer evolution. *Biochemical Society Transactions*, 45(1):1–13.

Vermeulen, L., Sprick, M. R., Kemper, K., Stassi, G., and Medema, J. P. (2008). Cancer stem cells - Old concepts, new insights.

Via, S. (1993). Adaptive Phenotypic Plasticity: Target or By-Product of Selection in a Variable Environment? Technical Report 2.

Vigil, D., Cherfils, J., Rossman, K. L., and Der, C. J. (2010). Ras superfamily GEFs and GAPs: validated and tractable targets for cancer therapy? *Nature reviews. Cancer*, 10(12):842–57.

Vogelstein, B. and Kinzler, K. W. (1993). The multistep nature of cancer. *Trends in Genetics*, 9(4):138–141.

Vogelstein, B. and Kinzler, K. W. (2004). Cancer genes and the pathways they control.

Vogelstein, B., Papadopoulos, N., Velculescu, V. E., Zhou, S., Diaz, L. A., and Kinzler, K. W. (2013). Cancer Genome Landscapes. *Science*, 339(6127):1546–1558.

Vogt, G. (2015). Stochastic developmental variation, an epigenetic source of phenotypic diversity with far-reaching biological consequences. *Journal of Biosciences*, 40(1):159–204.

Voice, J. K., Klemke, R. L., Le, A., and Jackson, J. H. (1999). Four human ras homologs differ in their abilities to activate raf-1, induce transformation, and stimulate cell motility. *Journal of Biological Chemistry*, 274(24):17164–17170.

von Kriegsheim, A., Baiocchi, D., Birtwistle, M., Sumpton, D., Bienvenut, W., Morrice, N., Yamada, K., Lamond, A., Kalna, G., Orton, R., Gilbert, D., and Kolch, W. (2009). Cell fate decisions are specified by the dynamic ERK interactome. *Nature Cell Biology*, 11(12):1458–1464.

W. D. Mühlhäuser, W., Fischer, A., Weber, W., and Radziwill, G. (2017). Optogenetics - Bringing light into the darkness of mammalian signal transduction. *Biochimica et Biophysica Acta - Molecular Cell Research*, 1864(2):280–292.

Wallace, A. R. (1867). *Mimicry, and Other Protective Resemblances Among Animals*, volume 88. Westminster Review.

Weigert, M., Schmidt, U., Haase, R., Sugawara, K., and Myers, G. (2020). Star-convex polyhedra for 3d object detection and segmentation in microscopy. In *The IEEE Winter Conference on Applications of Computer Vision (WACV)*.

Weyts, F., Li, Y.-S., van Leeuwen, J., Weinans, H., and Chien, S. (2002). Erk activation and $\alpha v\beta 3$ integrin signaling through shc recruitment in response to mechanical stimulation in human osteoblasts. *Journal of cellular biochemistry*, 87(1):85–92.

Whitehead, R. H., Macrae, F. A., St. John, D. J. B., and Ma, J. (1985). A colon cancer cell line (lim1215) derived from a patient with inherited nonpolyposis colorectal cancer. *Journal of the National Cancer Institute*, 74(4):759–765.

Wiederschain, G. Y. (2005). Lab ref. a handbook of recipes, reagents, and other reference tools for use at the bench (roskams, j., and rodgers, l.(eds.), humana press, humana, 2002, 272 p., 35). *Biochemistry*, 70(5):606.

Willumsen, B. M., Christensen, A., Hubbert, N. L., Papageorge, A. G., and Lowy, D. R. (1984). The p21 ras C-terminus is required for transformation and membrane association. *Nature*, 310(5978):583–586.

Wilson, D. M. and Bohr, V. A. (2007). The mechanics of base excision repair, and its relationship to aging and disease. *DNA Repair*, 6(4):544–559.

Wilson, M. Z., Ravindran, P. T., Lim, W. A., Toettcher, J. E., Wilson, M. Z., Ravindran, P. T., Lim, W. A., and Toettcher, J. E. (2017). Tracing Information Flow from Erk to Target Gene Induction Reveals Mechanisms of Dynamic and Combinatorial Control. *Molecular Cell*, pages 1–13.

Wood, L. D., Parsons, D. W., Jones, S., Lin, J., Sjöblom, T., Leary, R. J., Shen, D., Boca, S. M., Barber, T., Ptak, J., Silliman, N., Szabo, S., Dezso, Z., Ustyanksky, V., Nikolskaya, T., Nikolsky, Y., Karchin, R., Wilson, P. A., Kaminker, J. S., Zhang, Z., Croshaw, R., Willis, J., Dawson, D., Shipitsin, M., Willson, J. K., Sukumar, S., Polyak, K., Ben, H. P., Pethiyagoda, C. L., Pant, P. V., Ballinger, D. G., Sparks, A. B., Hartigan, J., Smith, D. R., Suh, E., Papadopoulos, N., Buckhaults, P., Markowitz, S. D., Parmigiani, G., Kinzler, K. W., Velculescu, V. E., and Vogelstein, B. (2007). The genomic landscapes of human breast and colorectal cancers. *Science*, 318(5853):1108–1113.

Wooten, D. J. and Quaranta, V. (2017). Mathematical models of cell phenotype regulation and reprogramming: Make cancer cells sensitive again! *Biochimica et Biophysica Acta - Reviews on Cancer*, 1867(2):167–175.

Yan, J., Roy, S., Apolloni, A., Lane, A., and Hancock, J. F. (1998). Ras isoforms vary in their ability to activate raf-1 and phosphoinositide 3-kinase. *Journal of Biological Chemistry*, 273(37):24052–24056.

Yan, Y.-x., Gong, Y.-w., Guo, Y., Lv, Q., Guo, C., Zhuang, Y., Zhang, Y., Li, R., and Zhang, X.-z. (2012). Mechanical strain regulates osteoblast proliferation through integrin-mediated erk activation. *PloS one*, 7(4):e35709.

Yang, J. C., Sequist, L. V., Geater, S. L., Tsai, C.-M., Mok, T. S. K., Schuler, M., Yamamoto, N., Yu, C.-J., Ou, S.-H. I., Zhou, C., et al. (2015). Clinical activity of afatinib in patients with advanced non-small-cell lung cancer harbouring uncommon egfr mutations: a combined post-hoc analysis of lux-lung 2, lux-lung 3, and lux-lung 6. *The lancet oncology*, 16(7):830–838.

You, J. S. and Jones, P. A. (2012). Cancer Genetics and Epigenetics: Two Sides of the Same Coin?

Zhang, F., Vierock, J., Yizhar, O., Fenno, L. E., Tsunoda, S., Kianianmomeni, A., Prigge, M., Berndt, A., Cushman, J., Polle, J., et al. (2011). The microbial opsin family of optogenetic tools. *Cell*, 147(7):1446–1457.

Zhou, B., Der, C. J., and Cox, A. D. (2016). The role of wild type RAS isoforms in cancer. *Seminars in Cell and Developmental Biology*.

Zhou, Y., Prakash, P., Liang, H., Cho, K.-J., Gorfe, A. A., and Hancock, J. F. (2017). Lipid-Sorting Specificity Encoded in K-Ras Membrane Anchor Regulates Signal Output. *Cell*, 2:239–251.

Zopf, C. J., Quinn, K., Zeidman, J., and Maheshri, N. (2013). Cell-Cycle Dependence of Transcription Dominates Noise in Gene Expression. *PLoS Comput Biol*, 9(7):1003161.

Zwijnenburg, P. J., Meijers-Heijboer, H., and Boomsma, D. I. (2010). Identical but not the same: The value of discordant monozygotic twins in genetic research. *American Journal of Medical Genetics Part B: Neuropsychiatric Genetics*, 153(6):1134–1149.